



Universiteit  
Leiden  
The Netherlands

## **Blood flow dynamics in the total cavopulmonary connection long-term after Fontan completion**

Rijnberg, F.M.

### **Citation**

Rijnberg, F. M. (2023, December 20). *Blood flow dynamics in the total cavopulmonary connection long-term after Fontan completion*. Retrieved from <https://hdl.handle.net/1887/3674148>

Version: Publisher's Version

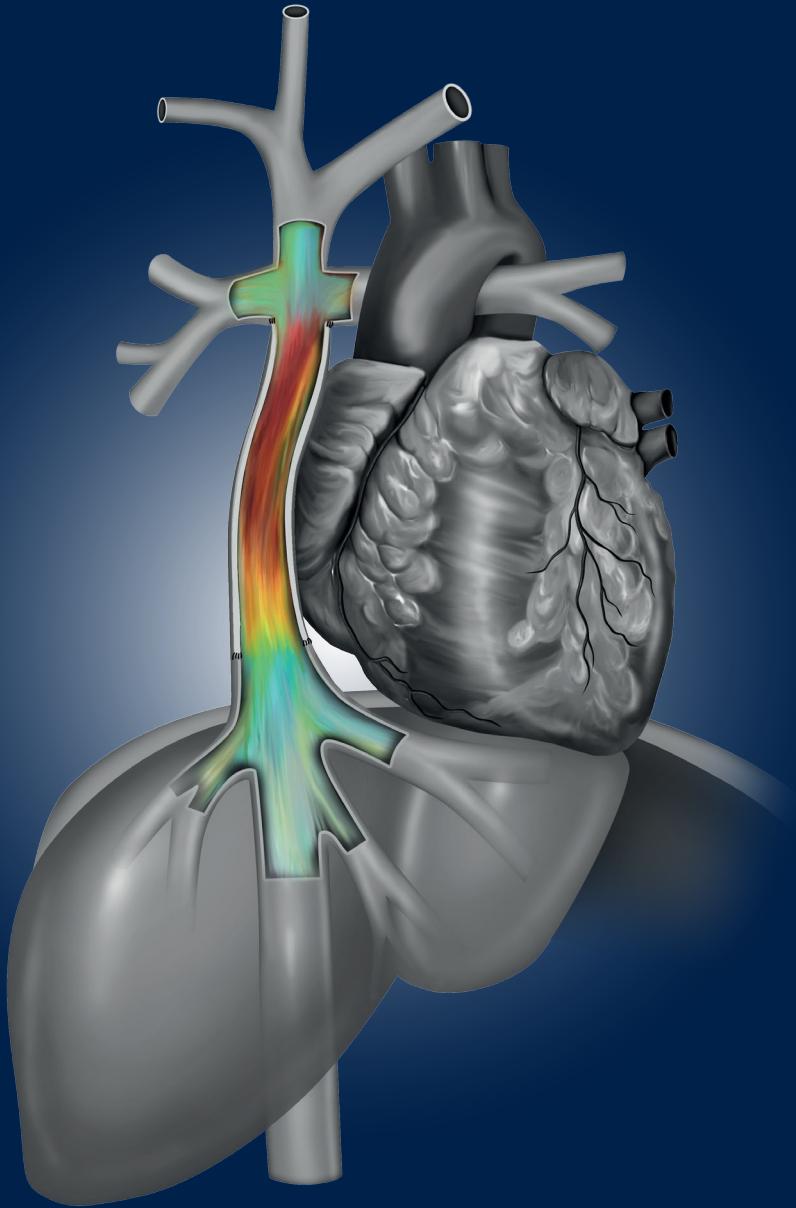
License: [Licence agreement concerning inclusion of doctoral thesis in the Institutional Repository of the University of Leiden](#)

Downloaded from: <https://hdl.handle.net/1887/3674148>

**Note:** To cite this publication please use the final published version (if applicable).

# **Blood flow dynamics in the total cavopulmonary connection**

long-term after Fontan completion



**Friso M. Rijnberg**



**Blood flow dynamics in the  
total cavopulmonary connection**  
long-term after Fontan completion

Friso M. Rijnberg



© copyright Friso Rijnberg, 2023

Cover design: Friso Rijnberg en Minaananda | <https://www.fiverr.com/s/radawy>

Lay-out & printing: ProefschriftMaken || [www.proefschriftmaken.nl](http://www.proefschriftmaken.nl)

ISBN 978-94-6469-658-5

All rights reserved. No part of this publication may be reproduced, stored in a retrieval system or transmitted, in any form or by any means, electronic, mechanical, photocopying, recording or otherwise, without prior permission of the author or the copyright-owning journals for previous published chapters.

**Blood flow dynamics in the  
total cavopulmonary connection**  
long-term after Fontan completion

Proefschrift

ter verkrijging van  
de graad van doctor aan de Universiteit Leiden,  
op gezag van rector magnificus prof.dr.ir. H. Bijl,  
volgens besluit van het college voor promoties  
te verdedigen op woensdag 20 december 2023  
klokke 16.15 uur

door

Friso Matthijs Rijnberg  
geboren te Rotterdam  
in 1990

**Promotor**

Prof. dr. M.G. Hazekamp

**Co-promotores:**

Dr. A.A.W. Roest

Dr. ir. J.J.M. Westenberg

**Promotiecommissie:**

Prof. dr. N.A. Blom

Prof. dr. H.J. Lamb

Dr. ir. J.J. Wentzel (Erasmus Medisch Centrum, Rotterdam)

Prof. dr. K. François (Universitair Ziekenhuis Gent, Gent, België)

Prof. dr. Y.A.C. d'Udekem d'Acoz (Children's National, Washington, USA)

Financial support by the Dutch Heart Foundation for the publication of this thesis is gratefully acknowledged.

The research described in this thesis was supported by a grant from the Dutch Heart Foundation (2018-T083) and by a grant from Stichting Hartekind.

The printing of this thesis was financially supported by Pie Medical Imaging B.V. and Krijnen Medical Innovations B.V.

# Table of contents

<b>Chapter 1</b>	General introduction and thesis outline	11
<b>PART I</b>	<b>LONG-TERM OUTCOME AFTER THE FONTAN PROCEDURE</b>	<b>23</b>
<b>Chapter 2</b>	A 45-year experience with the Fontan procedure: tachyarrhythmia, an important sign for adverse outcome <i>Interactive Journal of Cardiovascular and Thoracic Surgery 2019</i>	25
<b>Chapter 3</b>	Long-term outcome of direct relief of subaortic stenosis in single ventricle patients <i>World Journal for Pediatric and Congenital Heart Surgery 2018</i>	47
<b>PART II</b>	<b>IN VIVO BLOOD FLOW DYNAMICS OF THE FONTAN CIRCULATION</b>	<b>63</b>
<b>Chapter 4</b>	The influence of respiration on blood flow in the Fontan circulation: insights for imaging-based clinical evaluation of the total cavopulmonary connection <i>Frontiers Cardiovascular Imaging 2021</i>	65
<b>Chapter 5</b>	Reduced scan time and superior image quality with 3D flow MRI compared to 4D flow MRI for hemodynamic evaluation of the Fontan pathway <i>Scientific Reports 2021</i>	89
<b>Chapter 6</b>	Segmental analysis of blood flow dynamics in the TCPC	113
	Segmental assessment of blood flow efficiency in the total cavopulmonary connection using 4D flow MRI: vortical flow is associated with increased viscous energy loss <i>European Heart Journal open 2021</i>	115
	Four-dimensional flow magnetic resonance imaging-derived blood flow energetics of the inferior vena cava-to-extracardiac conduit junction in Fontan patients <i>European Journal of CardioThoracic Surgery 2019</i>	135

	Tornado-like flow in the Fontan circulation: insights from quantification and visualization of viscous energy loss rate using 4D flow MRI <i>European Heart Journal</i> 2019	153
<b>Chapter 7</b>	Assessment of extracardiac conduit adequacy	157
	Hemodynamic consequences of an undersized extracardiac conduit in an adult Fontan patient revealed by 4D flow MRI <i>Circulation Cardiovascular Imaging</i> 2021	159
	Extracardiac conduit adequacy along the respiratory cycle in adolescent Fontan patients <i>European Journal of CardioThoracic Surgery</i> 2021	167
<b>Chapter 8</b>	4D flow MRI derived energetics in the Fontan circulation correlate with exercise capacity and cT1 liver mapping <i>Journal of Cardiovascular Magnetic Resonance</i> 2022	193
<b>PART III</b>	<b>COMPUTATIONAL FLUID DYNAMICS OF THE FONTAN CIRCULATION</b>	<b>213</b>
<b>Chapter 9</b>	Energetics of blood flow in cardiovascular disease: concept and clinical implications of adverse energetics in patients with a Fontan circulation <i>Circulation</i> 2018	215
<b>Chapter 10</b>	Non-uniform mixing of hepatic venous flow and inferior vena cava flow in the Fontan conduit <i>Journal of the Royal Society Interface</i> 2021	251
<b>Chapter 11</b>	Hemodynamic performance of 16-20mm extracardiac conduits in adolescent Fontan patients <i>European Journal of CardioThoracic Surgery</i> 2022	273
<b>Chapter 12</b>	Summary and future perspectives	293
<b>Chapter 13</b>	Dutch summary	307

<b>APPENDICES</b>	<b>323</b>
List of publications	325
About the author	329
Acknowledgements	330



*Voor Elise, Emilie en Hugo*



**CHAPTER 1**



# General introduction



## Univentricular heart disease

The normal heart consists of both a right- and left atrium and ventricle. The right side of the heart actively pumps oxygen-poor blood (blue) towards the lungs for oxygenation, while the left side of the heart pumps the oxygen-rich blood (red) towards the rest of the body (**Figure 1, left**). Approximately one percent of children are born with a congenital heart disease, characterized by structural defects in one or multiple parts of the heart and/or great vessels.<sup>1</sup> Patients born with a univentricular heart defect represent the most severe end of the spectrum of congenital heart disease, having only one functional ventricle that excludes a successful biventricular surgical repair. Typical univentricular heart defects include tricuspid atresia, double-inlet left ventricle and hypoplastic left heart syndrome (**Figure 1, right**).

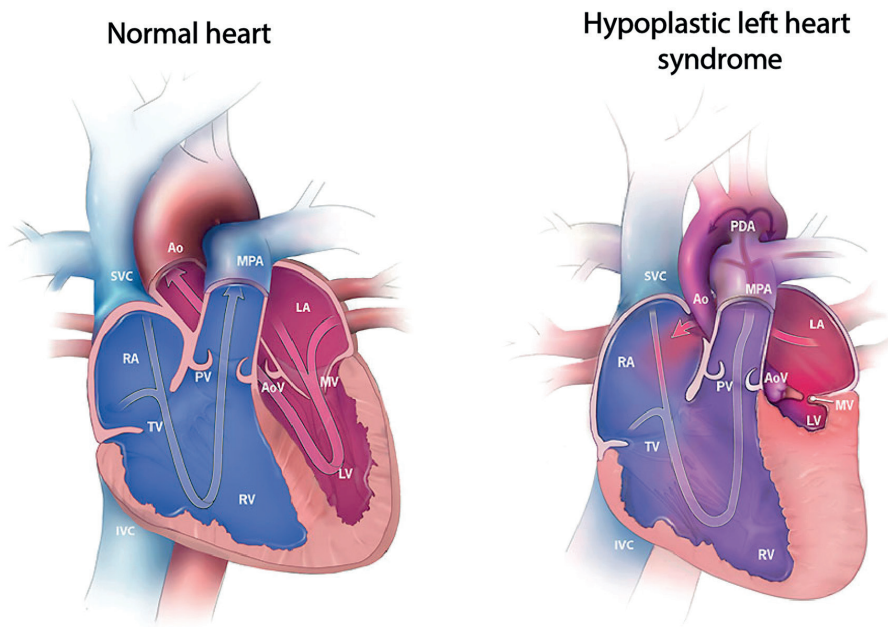


**Figure 1.** Example of a normal heart and a patient with a hypoplastic left heart syndrome. *Reproduced from Centers for Disease Control and Prevention, National Center on Birth Defects and Developmental Disabilities.*

RA/LA; right/left atrium, RV/LV; right/left ventricle, IVC/SVC; inferior/superior vena cava, TV; tricuspid valve, MV; mitral valve, AoV, aortic valve, PV; pulmonary valve, MPA; main pulmonary artery, Ao; aorta, PDA; patent ductus arteriosus

## Fontan procedure

Firstly performed in 1968, the Fontan procedure is the current gold standard palliative approach for patients with a univentricular heart defect.<sup>2</sup> The Fontan procedure nowadays includes a series of operations with the end goal to completely bypass the subpulmonary ventricle from the pulmonary circulation: the Fontan circulation. As a first step, various operations are usually needed in the first weeks of life to obtain a balanced pulmonary and systemic circulation with an unobstructed systemic outflow tract. At the age of 6-12 months, the superior vena cava is disconnected from the right atrium and directly connected with the pulmonary artery (PA), the so-called bidirectional Glenn shunt. When the child is 2-4 years old and approximately 15kg, the Fontan circulation is completed by connecting the inferior vena cava (IVC) with the PA, which can be performed using multiple different surgical techniques that have evolved over time (**Figure 2**)<sup>3</sup>. The atriopulmonary connection technique directly connects the right atrium auricle with the PA, since the inclusion of the right atrial contraction was considered necessary for maintaining adequate pulmonary blood flow (**Figure 2A**). This technique, however, is associated with progressive dilatation of the right atrium leading to arrhythmias, thrombus formation and inefficient blood flow and has now been abandoned.<sup>4</sup> Nowadays, the total cavopulmonary connection (TCPC) technique is used to direct inferior vena cava blood towards the PA and can be performed in two ways: the lateral tunnel and the extracardiac conduit technique. The main goal of these techniques is to exclude (most) of the right atrium from the Fontan circulation and thereby avoid the complications observed in patients with an atriopulmonary Fontan connection (**Figure 2A**). The lateral tunnel technique uses an intra-atrial patch to streamline blood flow from the inferior vena cava towards the PA, thereby excluding part of the atrium from the systemic venous return.<sup>5</sup> The main advantage is the growth potential of the Fontan tunnel, since part of the tunnel is made from atrial tissue. The extracardiac conduit technique uses a synthetic (Gore-Tex) conduit to connect the inferior vena cava with the PA, thereby fully excluding the right atrium from the systemic venous return.<sup>6</sup> This technique is now the preferred approach in most centers worldwide and in Leiden since 2000. However, the lack of growth potential of the synthetic conduit remains concerning, and long-term data regarding conduit size adequacy for older Fontan patients is currently lacking. As a result, the most optimal technique (lateral tunnel or extracardiac conduit) is still a matter of debate.<sup>7</sup>

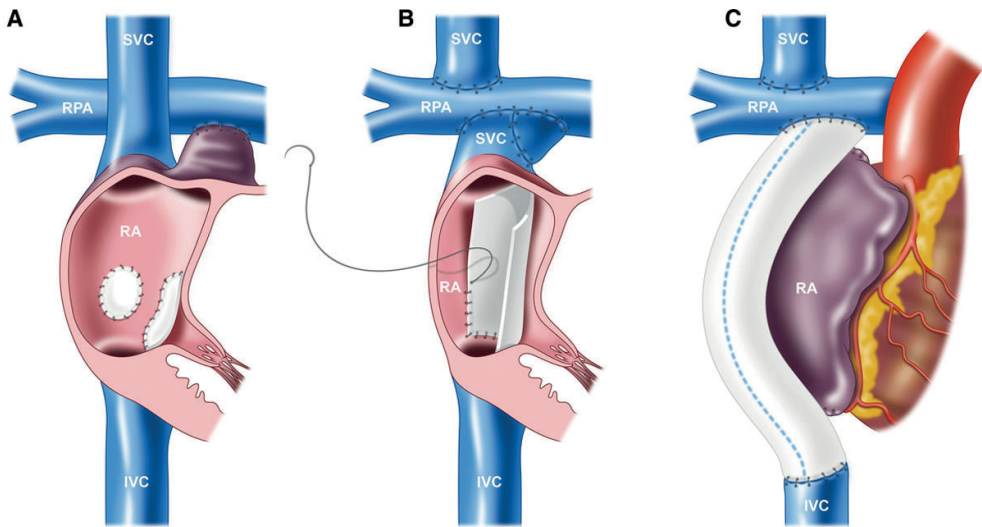


**Figure 2.** The different surgical techniques for completing the Fontan circulation are shown, including the atriopulmonary connection (A), the lateral tunnel technique (B) and the extracardiac conduit technique (C). Reproduced with permission from D'Udekem et al.<sup>3</sup>

RA; right atrium, RPA; right pulmonary artery, IVC/SVC; inferior/superior vena cava.

## Fontan physiology

In a normal biventricular circulation, the right ventricle creates the driving force for pulmonary blood flow to overcome the resistance in the pulmonary vascular bed. During exercise, the right ventricular work increases in order to augment cardiac output.<sup>8</sup> In the Fontan circulation, however, blood flow towards the pulmonary circulation is relatively passive, as no subpulmonary ventricle is present that actively pumps blood towards the lungs. Consequently, a chronically elevated venous pressure (CVP) is required to overcome the resistance and associated pressure drop in the TCPC and the pulmonary vascular bed. During exercise, further increase in CVP is needed to augment cardiac output. However, the chronic elevation of CVP that is clinically tolerated and the subsequent increase in CVP during exercise are both limited<sup>9-11</sup>, resulting in reduced preload towards the single ventricle and thus reduced cardiac output.

## Outcome

The introduction of the Fontan procedure has dramatically improved survival rates for children born with a single ventricle. Nowadays, approximately 70.000 patients worldwide are estimated to be alive and this population is expected to double in the next 20 years. Today, the majority of children with a single ventricle are expected to survive well into adulthood, with an estimated survival of 85% after 30 years for Fontan patients operated in the current era.<sup>12</sup> However, the vulnerable Fontan physiology results in significant morbidity over time, including the occurrence of protein losing enteropathy, liver fibrosis/cirrhosis to even hepatocellular carcinoma, brady- and tachyarrhythmias, systolic and diastolic heart failure, significantly reduced exercise capacity and eventually failure of the Fontan circulation. However, great variability in clinical condition exists between patients and there is an unmet need for a better understanding which patients are prone to worse outcome.<sup>12</sup> Characteristic of the Fontan circulation, the chronically elevated CVP and reduced cardiac output are both important pathophysiologic mechanisms of frequently observed morbidity in Fontan patients. For example, elevated CVP is associated with the formation of liver fibrosis/cirrhosis<sup>13</sup> and reduced stroke volume is one of the most important factors responsible for impaired exercise capacity.<sup>14</sup> Therefore, unobstructed blood flow with minimal resistance from the systemic veins towards the lungs is critical to ensure efficient blood flow with optimal hemodynamics. In this thesis a focus is placed on evaluation of blood flow efficiency in the TCPC, an area that can potentially be optimized at the initial Fontan procedure or during follow-up by reintervention.

## Evaluation of blood flow in the TCPC

### Magnetic resonance imaging

Currently, evaluation of the Fontan circulation using MRI is advised every 2-3 years to early detect (subclinical) complications.<sup>12</sup> Magnetic resonance imaging is a non-invasive technique that can be used to evaluate *in vivo* blood flow using various phase-contrast sequences. Conventionally, 2D flow MRI acquisitions are used to determine unidirectional blood flow velocity at multiple predefined planes within the Fontan circulation.<sup>15</sup> In the recent years, however, 4D flow MRI has emerged as a novel tool able to capture three-directional (3D) velocities in a 3D volume of interest for multiple timesteps along the cardiac cycle (4D= three-directional velocities + time). It not only allows for quantification of flow rates at every position within the acquired volume of interest, but also can be used to obtain 3D flow patterns within the TCPC. Abnormal, helical flow patterns can be present in the TCPC resulting in less efficient blood flow

that may increase risk for future Fontan failure.<sup>16</sup> Besides visualization of flow patterns with 4D flow MRI, novel in vivo hemodynamic markers such as kinetic energy and viscous energy loss rate (kinetic energy lost due to friction within the blood flow) can be quantified from the acquired 3D velocity field.<sup>17</sup> Therefore, 4D flow MRI evaluation of blood flow in the TCPC may identify novel insights into the presence of adverse flow patterns and associated energetic markers which may be related to adverse clinical outcome.

## Computational fluid dynamics

Computational fluid dynamics can be used to simulate in silico blood flow in the TCPC by numerically solving the continuity equation and Navier-Stokes equations for incompressible fluid flows.<sup>18</sup> Using CFD, a three-dimensional time-resolved pressure and velocity field can be obtained based on patient-specific 3D TCPC models coupled with patient-specific MRI-derived boundary conditions. This allows for quantification of high-resolution blood flow patterns and associated hemodynamics including viscous energy loss, pressure gradients and resistance. Furthermore, CFD allows for simulation of different physiologic flow conditions including the effect of respiration and exercise on TCPC flow and energetics. In addition, “virtual surgery” can be performed with CFD models, by adapting the TCPC geometry on the computer and subsequently simulate the effect of the geometry adaptation on flow dynamics.<sup>19</sup>

## Outline thesis

The first goal in this thesis is to assess the outcome of Fontan surgery performed in the LUMC in the past 45 years. In order to improve future outcome in Fontan patients, a better understanding of the Fontan physiology and better characterization of the state of the Fontan circulation during follow-up are important gaps in current knowledge.<sup>12</sup> In this thesis, the main focus was to investigate the role of the TCPC in current Fontan circulations, by prospectively evaluating TCPC flow dynamics in a cohort of teenage and adolescent Fontan patients using advanced flow MRI and computational fluid dynamics and assess its relationship with adverse outcome.

In **part I**, long-term outcome of the 45-year experience with the Fontan procedure at the Leiden University Medical Center is described, one of the longest experiences to date including the first procedures performed by Dr Fontan himself (Chapter 2). In chapter 3, long-term outcome of the direct relief of subaortic stenosis in single ventricle patients is described, as a relatively simple alternative to the most commonly used indirect relief methods (e.g. Norwood or Damus-Kaye-Stansel).



**Part II** of this thesis is focused on the assessment of in vivo flow dynamics in the TCPC using multiple different MRI flow imaging modalities. Chapter 4 reviews the role of the cardiac and respiratory cycle on blood flow in the TCPC and its relevance for interpreting the different imaging modalities. Since no subpulmonary ventricle is present, blood flow pulsatility along the cardiac cycle in the TCPC is minimal. To exploit this fact, in chapter 5 a novel scan technique was developed (cardiac-cycle averaged 3D flow MRI) and compared with cardiac-cycle resolved 2D flow MRI and 4D flow MRI. In chapter 6, 4D flow MRI derived energetics in segments of the TCPC are investigated. While previous studies focused on blood flow in the TCPC from the level of the Fontan conduit, blood flow patterns and energetics at the level where the IVC, hepatic veins and Fontan conduit join (IVC-conduit junction) are evaluated with 4D flow MRI in this study. Finally, a case-report illustrates novel insights that can be derived by evaluating TCPC hemodynamics using 4D flow MRI with possible consequences for clinical care.

In chapter 7, the adequacy of the 16-20mm synthetic extracardiac Gore-Tex conduit along the respiratory cycle is assessed using realtime 2D flow MRI, allowing to separate flow measurements in both inspiration and expiration. A case-report shows the effect of an undersized extracardiac conduit on local flow patterns and associated energetics in the TCPC derived from 4D flow MRI.

Chapter 8 describes the correlation between in vivo 4D flow MRI derived energetics (kinetic energy and viscous energy loss rate) in the TCPC with exercise capacity and iron-corrected liver T1 mapping as a marker of liver fibrosis/venous congestion.

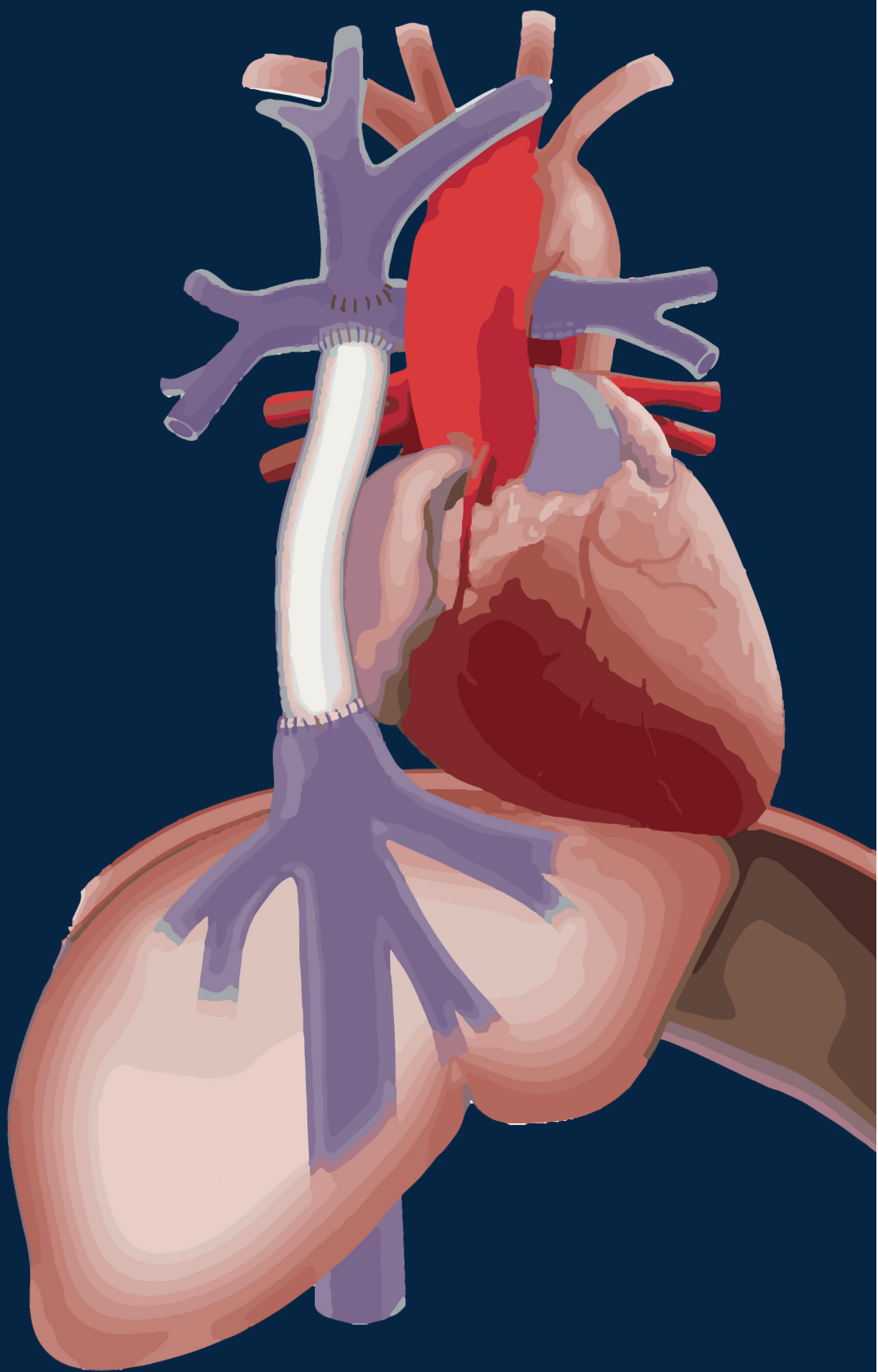
**Part III** is focused on the application of CFD for assessment of TCPC flow dynamics. Chapter 9 reviews the role of flow derived energetics in cardiovascular disease, highlighting the important insights gained using CFD in Fontan patients. In general, the performance of the TCPC as assessed by CFD is evaluated based on power loss and the distribution of hepatic venous flow towards both lungs (hepatic flow distribution). In chapter 10, the assumption of uniform distribution of hepatic venous flow at the level of the Fontan conduit is tested using patient-specific CFD models, for the first time directly including the hepatic veins. In chapter 11, the hemodynamic performance of conventionally used 16-20mm extracardiac conduits is assessed in teenage and adolescent patients using patient-specific CFD models during both rest and simulated exercise conditions, separated into inspiratory and expiratory phases. Finally, in chapter 12 the results of the studies in this thesis are discussed and future perspectives are provided. In chapter 13 a summary in Dutch is provided.

## References

1. Roth GA, Mensah GA, Johnson CO, Addolorato G, Ammirati E, Baddour LM, Barengo NC, Beaton AZ, Benjamin EJ, Benziger CP, Bonny A, Brauer M, Brodmann M, Cahill TJ, Carapetis J, Catapano AL, Chugh SS, Cooper LT, Coresh J, Criqui M, DeCleene N, Eagle KA, Emmons-Bell S, Feigin VL, Fernández-Solà J, Fowkes G, Gakidou E, Grundy SM, He FJ, Howard G, Hu F, Inker L, Karthikeyan G, Kassebaum N, Koroshetz W, Lavie C, Lloyd-Jones D, Lu HS, Mirijello A, Temesgen AM, Mokdad A, Moran AE, Muntner P, Narula J, Neal B, Ntsekhe M, Moraes de Oliveira G, Otto C, Owolabi M, Pratt M, Rajagopalan S, Reitsma M, Ribeiro ALP, Rigotti N, Rodgers A, Sable C, Shakil S, Sliwa-Hahnle K, Stark B, Sundström J, Timpel P, Tleyjeh IM, Valgimigli M, Vos T, Whelton PK, Yacoub M, Zuhlke L, Murray C and Fuster V. Global Burden of Cardiovascular Diseases and Risk Factors, 1990-2019: Update From the GBD 2019 Study. *J Am Coll Cardiol*. 2020;76:2982-3021.
2. Fontan F and Baudet E. Surgical repair of tricuspid atresia. *Thorax*. 1971;26:240-8.
3. d'Udekem Y, Iyengar AJ, Cochrane AD, Grigg LE, Ramsay JM, Wheaton GR, Penny DJ and Brizard CP. The Fontan procedure: contemporary techniques have improved long-term outcomes. *Circulation*. 2007;116:157-64.
4. Poh C, Zannino D, Weintraub RG, Winlaw DS, Grigg LE, Cordina R, Hornung TS, Bullock A, Justo R, Gentles TL, Verrall CE, du Plessis K, Celermajer DS and D'udekem Y. Three decades later: The fate of the population of patients who underwent the Atriopulmonary Fontan procedure. *International journal of cardiology*. 2017;231:99-104.
5. de Leval MR, Kilner P, Gewillig M and Bull C. Total cavopulmonary connection: a logical alternative to atriopulmonary connection for complex Fontan operations. Experimental studies and early clinical experience. *J Thorac Cardiovasc Surg*. 1988;96:682-95.
6. Marcelletti C, Corno A, Giannico S and Marino B. Inferior vena cava-pulmonary artery extracardiac conduit. A new form of right heart bypass. *J Thorac Cardiovasc Surg*. 1990;100:228-32.
7. Daley M and d'Udekem Y. The optimal Fontan operation: Lateral tunnel or extracardiac conduit? *J Thorac Cardiovasc Surg*. 2021;162:1825-1834.
8. Gewillig M and Brown SC. The Fontan circulation after 45 years: update in physiology. *Heart*. 2016;102:1081-6.
9. Van De Bruaene A, La Gerche A, Claessen G, De Meester P, Devroe S, Gillijns H, Bogaert J, Claus P, Heidebuchel H, Gewillig M and Budts W. Sildenafil improves exercise hemodynamics in Fontan patients. *Circ Cardiovasc Imaging*. 2014;7:265-73.
10. Gewillig M and Brown SC. The Fontan circulation after 45 years: update in physiology. *Heart*. 2016;102:1081-6.
11. Schmitt B, Steendijk P, Ovroutski S, Lunze K, Rahmzadeh P, Maarouf N, Ewert P, Berger F and Kuehne T. Pulmonary vascular resistance, collateral flow, and ventricular function in patients with a Fontan circulation at rest and during dobutamine stress. *Circ Cardiovasc Imaging*. 2010;3:623-31.
12. Rychik J, Atz AM, Celermajer DS, Deal BJ, Gatzoulis MA, Gewillig MH, Hsia TY, Hsu DT, Kovacs AH, McCrindle BW, Newburger JW, Pike NA, Rodefeld M, Rosenthal DN, Schumacher KR, Marino BS, Stout K, Veldtman G, Younoszai AK, d'Udekem Y, American Heart Association Council on Cardiovascular Disease in the Y, Council on C and Stroke N. Evaluation and Management of the Child and Adult With Fontan Circulation: A Scientific Statement From the American Heart Association. *Circulation*. 2019.

13. Emamaullee J, Zaidi AN, Schiano T, Kahn J, Valentino PL, Hofer RE, Taner T, Wald JW, Olthoff KM, Bucuvalas J and Fischer R. Fontan-Associated Liver Disease: Screening, Management, and Transplant Considerations. *Circulation*. 2020;142:591-604.
14. Paridon SM, Mitchell PD, Colan SD, Williams RV, Blaufox A, Li JS, Margossian R, Mital S, Russell J and Rhodes J. A cross-sectional study of exercise performance during the first 2 decades of life after the Fontan operation. *J Am Coll Cardiol*. 2008;52:99-107.
15. Fratz S, Chung T, Greil GF, Samyn MM, Taylor AM, Valsangiacomo Buechel ER, Yoo SJ and Powell AJ. Guidelines and protocols for cardiovascular magnetic resonance in children and adults with congenital heart disease: SCMR expert consensus group on congenital heart disease. *J Cardiovasc Magn Reson*. 2013;15:51.
16. Houtzager JH, Westenberg JJ, de Koning PJ, Hazekamp MG and Roest AA. Helical flow pattern in the right pulmonary artery after Fontan palliation. *Eur Heart J Cardiovasc Imaging*. 2014;15:1183.
17. Elbaz MS, van der Geest RJ, Calkoen EE, de Roos A, Lelieveldt BP, Roest AA and Westenberg JJ. Assessment of viscous energy loss and the association with three-dimensional vortex ring formation in left ventricular inflow: In vivo evaluation using four-dimensional flow MRI. *Magn Reson Med*. 2017;77:794-805.
18. Gerrah R and Haller SJ. Computational fluid dynamics: a primer for congenital heart disease clinicians. *Asian Cardiovasc Thorac Ann*. 2020;28:520-532.
19. Trusty PM, Slesnick TC, Wei ZA, Rossignac J, Kanter KR, Fogel MA and Yoganathan AP. Fontan Surgical Planning: Previous Accomplishments, Current Challenges, and Future Directions. *J Cardiovasc Transl Res*. 2018;11:133-144.





# PART I

Long-term outcome after the Fontan procedure



## CHAPTER 2

# 2

# A 45-year experience with the Fontan procedure: tachyarrhythmia, an important sign for adverse outcome

Rijnberg FM, Blom NA, Sojak V, Bruggemans EF, Kuipers IM, Rammeloo LAJ, Jongbloed MRM, Bouma BJ, Hazekamp MG.



# **Abstract**

## **Objectives**

This study aimed to evaluate our 45-year experience with the Fontan procedure and to identify risk factors for late mortality and morbidity.

## **Methods**

Demographic, pre-, peri- and postoperative characteristics were retrospectively collected for all patients who underwent a Fontan procedure in a single-center between 1972-2016.

## **Results**

The study included 277 Fontan procedures (44 atriopulmonary connections [APC], 28 Fontan-Björk, 42 lateral tunnels [LT] and 163 extracardiac conduits [ECC]). Early failure occurred in 17 patients (6.1%). Median follow-up of the study cohort was 11.9 years ( $Q_1$ - $Q_3$ , 7.6-17.5). Longest survival estimates were 31% (95% CI, 18%-44%) at 35 years for APC/Björk, 87% (95% CI, 63%-96%) at 20 years for LT and 99% (95% CI, 96%-100%) at 15 years for ECC. Estimated freedom from Fontan failure (death, heart transplant, take-down, protein losing enteropathy, NYHA III-IV) at 15-years was 65% (95% CI, 52%-76%) for APC/Björk, 90% (95% CI, 73%-97%) for LT and 90% (95% CI, 82%-94%) for ECC. The development of tachyarrhythmia was an important predictor of Fontan failure (HR 2.6, 95% CI 1.2-5.8,  $P=0.017$ ), thromboembolic/neurological events (HR 3.6, 95% CI 1.4-9.4,  $P=0.008$ ) and pacemaker for sinus node dysfunction (HR 3.7, 95% CI 1.4-9.6,  $P=0.008$ ). Prolonged pleural effusion (>21 days) increased risk of experiencing PLE (HR 4.7, 95% CI 2.0-11.1,  $P<0.001$ ).

## **Conclusions**

With modern techniques, survival and freedom from Fontan failure is good. However, Fontan patients remain subject to general attrition. Tachyarrhythmia is an important sign for adverse outcome. Prevention and early treatment of tachyarrhythmia may therefore be paramount for improving long-term outcome.

## Introduction

The Fontan procedure is the current palliative treatment of single ventricle anomalies. The surgical technique has evolved from the atriopulmonary connection (APC) or Fontan-Björk modification (right atrium to right ventricle), via the intracardiac lateral tunnel (LT) to the extracardiac conduit (ECC) procedure, which is nowadays the preferred approach in most centers. Early Fontan failure has reduced from 27% in early experiences<sup>1,2</sup> to 4% in a recent ECC cohort<sup>3</sup>, with low perioperative mortality rates of 0.5-1%<sup>3,4</sup>. Mid-term and long-term outcomes with the newer Fontan techniques are good, with 15-year and 20-year survival rates of 85-96%<sup>4-6</sup> and 76-79%<sup>6,7</sup>, respectively.

As the number of survivors of the Fontan procedure expands, information on long-term outcomes in patients with the various approaches of the Fontan palliation becomes increasingly valuable<sup>8-11</sup>. In this study, we report our 45-year experience with the Fontan procedure and aim to identify factors associated with late mortality and morbidity.

## Materials and Methods

We conducted a retrospective study of 277 consecutive patients who underwent a Fontan procedure (excluding Kawashima procedures) at Leiden University Medical Center, the Netherlands (1972-2016). Fontan procedures consisted of 44 APC, 28 Fontan-Björk, 42 LT and 163 ECC procedures. In further analyses, APC and Fontan-Björk procedures were combined. APC/Fontan-Björk was the preferred technique between 1972-1990 (96%), LT between 1991-1999 (67%) and ECC between 2000-2016 (91%). All data were obtained from (referring) hospital records and were analysed for demographic, pre-, peri- and postoperative characteristics until last follow-up. The Hospital Medical Ethical Committee approved the study.

## Definitions

Early outcomes were defined as events occurring before hospital discharge or within 30 days and late outcomes as events occurring after initial hospital discharge.

Fontan failure was defined as death, heart transplantation, Fontan take-down, protein losing enteropathy (PLE) or plastic bronchitis, or *New York Heart Association* (NYHA) class III-IV. The diagnosis of PLE was based on loss of alpha-1-antitrypsin in the stool or by the combination of low albumin/total protein with generalised edema. The diagnosis of plastic bronchitis was based on the expectoration of bronchial casts. In further analyses, PLE and plastic bronchitis were combined. Prolonged pleural effusion (PE) was defined as an effusion duration needing drains >21 days. First occurrence of a clinically relevant

arrhythmia was defined by the need of antiarrhythmic medication, electrical cardioversion or pacemaker (PM) placement. Tachyarrhythmia included atrial fibrillation, atrial flutter, other supraventricular tachycardias and ventricular tachycardia. Bradyarrhythmia was defined as sinus node dysfunction (SND) or complete atrioventricular block (described separately) requiring PM. Thromboembolic event (TE) was defined as a thrombus in the Fontan pathway (superior vena cava/Fontan tunnel/right atrium) or pulmonary embolism. Neurological event (NE) was defined as a cerebral vascular accident (CVA), ischemic or haemorrhagic. Surgical reinterventions included all Fontan related interventions including first PM implantations but excluding PM replacements. Early re sternotomies (bleeding/tamponade) were excluded. The combined outcome for Fontan-related morbidity consisted of Fontan failure, tachyarrhythmia, bradyarrhythmia or TE/NE. Systolic cardiac function and atrioventricular valve (AVV) regurgitation were assessed qualitatively from echocardiographic reports. Systolic function was graded as good/mildly impaired, moderate or poor. Significant AVV-regurgitation was defined as  $\geq$  moderate-severe. NYHA-class was assessed by review of the medical records. Liver fibrosis/cirrhosis was based on findings of ultrasound, magnetic resonance imaging or computed tomography reports or from autopsy findings.

## Statistical analyses

Continuous data are presented as median (first to third quartile [ $Q_1$ - $Q_3$ ]). Categorical data are presented as number and percentage. Early outcome was described for the whole cohort. Late outcome was reported for hospital survivors with intact Fontan circulation (no take-down) only. Late survival and freedom from late morbidity rates were estimated using the Kaplan-Meier method and reported as percentages with asymmetrical 95% confidence intervals (CI). Kaplan-Meier curves were created for each Fontan group according to the initial Fontan technique and equality of the survival distributions was tested using the log-rank test. Possible predictors of late mortality and morbidity endpoints were tested using univariable and multivariable (enter method) Cox regression models. Analysed endpoints included mortality, Fontan failure, PLE/plastic bronchitis, tachyarrhythmia, bradyarrhythmia, TE/NE and the combined outcome for Fontan-related morbidity. Variables included in the univariable Cox regression models are mentioned in Table 1, with the addition of prolonged PE and first occurrence of the events PLE, tachyarrhythmia, bradyarrhythmia and TE/NE. These possible intermediate events were treated as time-dependent covariates. The LT and ECC groups were combined in the Cox regression analyses due to the limited amount of events in each subgroup. Age was divided into three age groups that were considered clinically relevant:  $<4$  years, 4-8 years and  $>8$  years. Variables with a P-value  $<0.15$  in univariable analyses were included in the multivariable models. The proportional hazards assumption was tested for each variable using time-dependent covariates. For the tachyarrhythmia, bradyarrhythmia, TE/NE and PLE endpoints, a patient was

censored when death, heart transplant or Fontan take-down occurred before the event. The influence of ventricular morphology on late outcome was tested in both the total study cohort and the LT/ECC group only, since the predominance of left ventricular morphology in the APC/Björk group could mask the effect of ventricular morphology on late outcome. Because fenestration was introduced after the introduction of the LT technique, the effect of fenestration on endpoints was tested in the LT/ECC group only. A P-value of <0.05 (two-sided) was considered statistically significant. Data were analysed and displayed with SPSS 24.0 (IBM-SPSS, NY, USA) or Prism 7.0 (GraphPad, CA, USA).

## Results

2

### Study population

The focus of this study was on late events in hospital survivors with intact Fontan circulation (study cohort). Demographics and patient characteristics of the study cohort are detailed in Table 1. Complete follow-up was available for 94% of patients (median, 11.9 years; Q<sub>1</sub>-Q<sub>3</sub>, 7.6-17.5). Fifteen patients were lost to follow-up (median time after Fontan completion, 10 months; Q<sub>1</sub>-Q<sub>3</sub>, 41 days-3.9 years).

### Early outcomes for the whole cohort

Early failure occurred in 17 patients (6.1%, median 3 days, Q<sub>1</sub>-Q<sub>3</sub> 1-26 days): 11 deaths (5 APC/Björk [6.9%], 4 LT [9.5%], 2 ECC [1.2%]) and 7 take-downs (1 LT [2.4%], 6 ECC [3.7%]). One patient died shortly after early take-down. Five patients (1.8%) had an early TE. Sixteen patients (5.8%) had an early NE (15 ischemic, 1 haemorrhagic). Prolonged PE occurred in 46 patients (18%). Since 2000, the year in which the ECC technique was introduced, early failure improved from 9.3% to 4.1%, early mortality from 8.3% to 1.2%, early TE from 3.6% to 1.2% and early NE from 11.6% to 3.0%.

**Table 1.** Patient demographics and characteristics of hospital survivors with intact Fontan circulation

Characteristic	APC/Björk* (n=67)	LT* (n=38)	ECC* (n=155)
Male*, n(%)	39(58)	22(58)	93(60)
Age at Fontan*, years, median(Q <sub>1</sub> -Q <sub>3</sub> )	8.1(4.9-14.2)	4.3(2.8-6.0)	3.5(3.0-4.3)
Dextrocardia*, n(%)	7(10)	9(24)	5(3)
Heterotaxy*, n(%)	0(0)	7(18)	6(4)
Common AVV*, n(%)	1(2)	3(8)	15(10)
TAPVD/PAPVD*, n(%)	0(0)	3(8)	5(3)
Ventricular morphology*, n(%)			
Left ventricle	61(91)	26(68)	77(50)
Right ventricle	4(6)	10(26)	60(39)
Biventricular/indeterminate	2(3)	2(5)	18(12)
Morphological group, n(%)			
DILV	13(19)	9(24)	27(17)
DORV	0(0)	2(5)	17(11)
TA	50(75)	10(26)	31(20)
HLHS*	0(0)	0(0)	35(23)
ccTGA	3(5)	5(13)	11(7)
TGA	1(2)	2(5)	2(1)
PA+IVS	0(0)	5(13)	13(8)
Unbalanced AVSD+DORV	0(0)	1(3)	6(4)
Unbalanced AVSD	0(0)	0(0)	9(6)
Other	0(0)	4(11)	4(3)
Procedures pre-Fontan, n(%)			
Number of surgical procedures, mean(SD)	1.0(0.8)	1.7(0.8)	2.2(0.7)
Systemic-pulmonary shunt*	37(55)	16(42)	94(61)
PA banding*	6(9)	8(21)	42(27)
Prior/concomitant PA stent/reconstruction*	12(18)	4(11)	31(20)
Prior/concomitant AVV repair/replacement*	1(2)	4(11)	27(17)
Glenn shunt*	15(22)	32(84)	155(100)
Age at Glenn, years, median(Q <sub>1</sub> -Q <sub>3</sub> )	2.1(0.8-3.5)	1.9(0.9-3.8)	0.6(0.4-1.1)
Pre-Fontan characteristics			
Oxygen saturation**(%), n=217, median(Q <sub>1</sub> -Q <sub>3</sub> )	82(78-85)	84(78-85)	81(78-84)
Mean PAP** n=229, mmHg, median(Q <sub>1</sub> -Q <sub>3</sub> )	10(9-15)	9(8-12)	11(9-12)
≥moderate systolic dysfunction, n(%)	1(3)	1(3)	0(0)
AVV regurgitation* (≥moderate-severe), n(%)	0(0)	5(15)	13(9)
Fontan characteristics			
CPB time** n=190, minutes, median(Q <sub>1</sub> -Q <sub>3</sub> )	137(106-205)	119(82-214)	95(76-126)
Cross clamp time** n=201, minutes, median(Q <sub>1</sub> -Q <sub>3</sub> )	73(56-124)	67(56-99)	15(0-47)
Age at Fontan*, years, median(Q <sub>1</sub> -Q <sub>3</sub> )	8.1(4.9-14.2)	4.3(2.8-6.0)	3.5(3.0-4.3)
Fenestration*, n(%)	1(2)	26(68)	109(70)
Age at last FU with intact Fontan circulation***, years, median(Q <sub>1</sub> -Q <sub>3</sub> )	29.5(19.3-42.2)	22.9(15.8-25.9)	12.9(10.0-16.2)

\*Variables included in the univariable Cox regression models \*\*not included in the univariable Cox regression models due to missing data. \*\*\*Censored at death, heart transplant or take-down.

AVV, atrioventricular valve; T(P)APVD, total (partial) anomalous pulmonary venous drainage; DILV, double inlet left ventricle; DORV, double outlet right ventricle; TA, tricuspid atresia; HLHS, hypoplastic left heart syndrome; ccTGA, congenital corrected transposition of the great arteries; PA+IVS, pulmonary atresia+intact ventricular septum; AVSD, atrioventricular septal defect; PA(P), pulmonary artery (pressure); CPB, cardiopulmonary bypass

**Table 2.** Modes of late death

<b>Late mortality</b>	<b>43</b>
Fontan failure with preserved systolic ventricular function	16
-Pneumonia	3
-Fontan pathway obstruction/dysfunction	5
-TE	4
-Peri-procedural after reintervention for Fontan failure with preserved systolic ventricular function	4
Fontan failure with poor systolic ventricular function	4
Peri-procedural after other reintervention	2
Sudden death	6
Neurological event	2
Sepsis	3
Other	6
Unknown	4

## Late outcomes in the study cohort

### Survival

There were 43 late deaths (median age 26.8 years,  $Q_1$ - $Q_3$ , 18.5-38.8). Modes of late death are described in Table 2. One patient received a heart transplantation 10 months after Fontan completion. The estimated overall survival rate after the Fontan procedure was 70% (95% CI, 56%-80%), 63% (95% CI, 49%-74%), 52% (95% CI, 38%-64%) and 31% (95% CI, 18%-44%) at 15, 20, 30 and 35 years, respectively, in the APC/Björk group, 97% (95% CI, 79%-100%) and 87% (95% CI, 63%-96%) at 15 and 20 years, respectively, in the LT group and 99% (95% CI, 96%-100%) at 15 years in the ECC group (Figure 1A;  $P<0.001$ ). APC/Björk type of Fontan (HR, 4.6; 95% CI, 1.2-17.5;  $P=0.024$ ) and occurrence of TE/NE (HR, 16.8; 95% CI, 7.7-37.1;  $P=0.002$ ) were independent risk factors for late death (Supplemental table A). Fenestration was not associated with late death or any other analysed endpoints.

### Fontan failure

Late failure of the Fontan circulation occurred in 59 patients. First failure event was death ( $n=28$ ), PLE ( $n=26$ ), NYHA class III/IV ( $n=3$ ), take-down ( $n=1$ ) or heart transplantation ( $n=1$ ). Freedom from Fontan failure rate was 65% (95% CI, 52%-76%), 57% (95% CI, 43%-68%) and 44% (95% CI, 31%-56%) at 15, 20 and 30 years, respectively, in the APC/Björk group, 90% (95% CI, 73%-97%) at 15 and 20 years in the LT group and 90% (95% CI, 82%-94%) at 15 years in the ECC group (Figure 1B;  $P<0.001$ ). APC/Björk type of Fontan (HR 3.4; 95% CI, 1.2-9.4;  $P=0.020$ ), tachyarrhythmia (HR, 2.6; 95% CI, 1.2-5.8;  $P=0.017$ ), TE/NE (HR, 9.3; 95% CI, 4.1-21.2;  $P<0.001$ ) and prolonged PE (HR, 2.7; 95% CI, 1.3-6.0;  $P=0.011$ ) were independent risk factors for late Fontan failure (Supplemental table A). Ventricular

morphology (right (excluding HLHS) versus left functional ventricle) was not associated with late Fontan failure, neither in the total study cohort nor in the LT/ECC group only.

### ***Arrhythmia***

#### ***Tachyarrhythmia***

Three patients had pre-Fontan periods of sustained tachyarrhythmia and were excluded from tachyarrhythmia endpoint analysis. Fifty-nine patients developed a tachyarrhythmia after a median of 10.8 years ( $Q_1$ - $Q_3$ , 4.8-16.9). Freedom from tachyarrhythmia rate was 46% (95% CI, 32%-58%) and 24% (95% CI, 11%-34%) at 15 and 20 years, respectively, in the APC/Björk group, 81% (95% CI, 62%-90%) at 15 and 20 years in the LT group and 94% (95% CI, 87%-98%) at 15 years in the ECC group (Figure 1C;  $P<0.001$ ). Post hoc log-rank analysis between LT and ECC groups showed a significantly lower freedom from tachyarrhythmia in the LT group ( $P=0.022$ ), which occurred predominantly within the first 5 years (all atrial flutter). APC/Björk type of Fontan (HR, 5.1; 95% CI 2.1-12.7;  $P<0.001$ ), age at Fontan  $>8$  years (HR, 3.0; 95% CI, 1.4-6.9;  $P=0.001$ ) and common AVV (HR, 9.0; 95% CI, 3.0-27.3;  $P<0.001$ ) were independent predictors of occurrence of tachyarrhythmia (Supplemental table A).

#### ***Bradyarrhythmia***

Twenty-three patients received a PM for SND, of which 2 at the time of the Fontan procedure and were excluded from the analysis. Freedom from PM for SND rate was 94% (95% CI, 84%-98%), 86% (95% CI, 72%-94%) and 69% (95% CI, 51%-82%) at 10, 20 and 30 years, respectively, in the APC/Björk group; 90% (95% CI, 73%-97%) and 87% (95% CI, 69%-95%) at 10 and 20 years, respectively, in the LT group and 95% (95% CI, 89%-98%) at 10 years in the ECC group (Supplemental figure 1A;  $P=0.600$ ). Tachyarrhythmia was the only risk factor for PM for SND (HR, 6.0; 95% CI, 1.8-19.6;  $P=0.008$ ) (Supplemental table A).

#### ***Complete AV block***

Two patients needed a PM for complete AV block before the Fontan procedure. Eleven patients (4%) needed a PM for complete AV block at a median of 5.5 years ( $Q_1$ - $Q_3$ , 22 days-20.7 years) after the Fontan procedure, which were mostly related to tricuspid valve interventions (3/11) or ablation therapy (3/11).

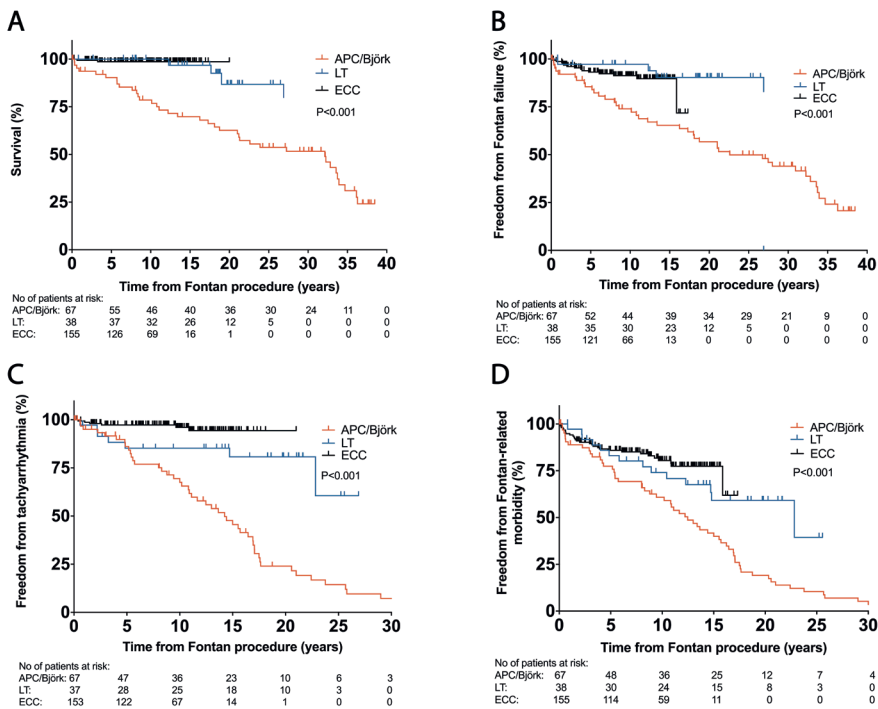


**Figure 1.** Kaplan-Meier curves per Fontan group (hospital survivors) for overall survival (A), freedom from Fontan failure (B), freedom from tachyarrhythmia (C) and combined outcome for Fontan-related morbidity (D). P-values of the log-rank tests between groups are indicated in the graphs.

APC; atriopulmonary connection, LT; lateral tunnel, ECC; extracardiac conduit

### Thromboembolic and neurological events

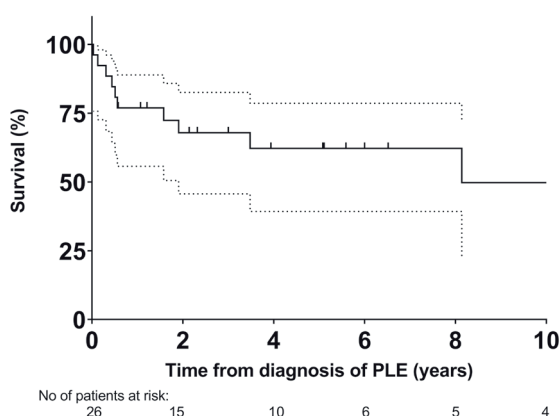
Late TE occurred in 20 patients after a median of 10.4 years ( $Q_1$ - $Q_3$ , 3.6-22.0). Site of thrombus was right atrium (n=10), pulmonary embolism (n=10), Fontan tunnel (n=3) and superior vena cava (n=3). Anticoagulant medication at time of TE was oral anticoagulation (OAC) in 8 patients, platelet inhibitor in 2 or none (n=7). In 3 patients, the event occurred shortly after reintervention. Fifteen patients experienced a late NE (12 ischemic, 3 haemorrhagic). Of the 12 ischemic CVAs, 4 occurred shortly after reintervention and 1 post-partum. The other 7 patients were on OAC (n=1), platelet inhibitors (n=3), no anticoagulation (n=2) or unknown anticoagulation (n=1). All patients with a haemorrhagic CVA were on OAC. Freedom from late TE/NE rate was 81% (95% CI, 68%-89%), 72% (95% CI, 58%-82%) and 60% (95% CI 45%-72%) at 15, 20 and 30 years, respectively, in the APC/Björk group, 89% (95% CI, 70%-96%) at 15 and 20 years in the LT group and 93% (95% CI, 85%-97%) at 15 years in the ECC group (Supplemental



figure 1B;  $P=0.082$ ). Tachyarrhythmia was the only risk factor for TE/NE (HR, 3.6; 95% CI, 1.4-9.4;  $P=0.008$ ) (Supplemental table A).

### PLE

Twenty-six patients developed PLE at a median of 4.4 years ( $Q_1$ - $Q_3$ , 1.5-8.7) after the Fontan procedure (median age at diagnosis of PLE 10.6 years,  $Q_1$ - $Q_3$  6.7-16.8). Freedom from PLE rate was 88% (95% CI, 82%-92%) and 82% (95% CI, 69%-89%) at 20 and 30 years, respectively. Patients were not divided into Fontan subgroups due to low event numbers. Survival after diagnosis of PLE was 60% (95% CI, 37%-77%) at 5 years (Figure 2). The occurrence of PLE appeared to be related to Fontan tunnel obstruction/dysfunction ( $n=8$ ), pulmonary artery stenosis/hypoplasia ( $n=5$ ),  $\geq$ moderate AVV regurgitation ( $n=5$ ), pneumonia episode ( $n=3$ ), bradyarrhythmia ( $n=2$ ) or diaphragm paresis ( $n=1$ ). In 6 patients, no clear contributions could be identified. Prolonged PE was an independent risk factor for occurrence of PLE (HR, 4.7; 95% CI, 2.0-11.1;  $P<0.001$ ) (Supplemental table A).



**Figure 2.** Kaplan-Meier curve for survival after the diagnosis of PLE/plastic bronchitis. Dashed lines indicate 95% confidence intervals.

Thirteen patients with PLE underwent surgical/percutaneous reintervention and 9 patients received conservative treatment. Two patients died early after initial hospital admission and treatment information was missing in 2 patients. (Transient) resolution of PLE occurred in 8 patients (31%). In 2 patients, in whom PLE was triggered by a pneumonia episode, resolution occurred after recovery of the pneumonia but with regular PLE exacerbations during recurrent infectious episodes.

### ***Combined outcome for Fontan-related morbidity***

The combined outcome for Fontan-related morbidity (i.e. Fontan failure, tachyarrhythmia, bradyarrhythmia or TE/NE) occurred in 101 patients. Freedom from the combined outcome rate was 40% (95% CI, 28%-52%) and 19% (95% CI, 10%-30%) at 15 and 20 years, respectively, in the APC/Björk group, 59% (95% CI, 40%-74%) at 15 years in the LT group and 77% (95% CI, 68%-86%) at 15 years in the ECC group (Figure 1D;  $P<0.001$ ). APC/Björk type of Fontan (HR, 2.4; 95% CI, 1.2-4.8;  $P=0.016$ ), common AVV (HR, 3.2; 95% CI, 1.4-7.1;  $P=0.006$ ), total/partial anomalous pulmonary venous drainage (TAPVD/PAPVD) (HR, 5.2; 95% CI, 1.3-20.2;  $P=0.018$ ) and prolonged PE (HR, 1.9; 95% CI, 1.1-3.4;  $P=0.020$ ) were independent risk factors for the combined adverse events (Supplemental table A).

### ***Surgical reinterventions***

Seventy-seven patients underwent 109 surgical reinterventions (Supplemental table B). Freedom from surgical reintervention rate was 54% (95% CI, 40%-66%), 40% (95% CI, 27%-53%) and 25% (95% CI, 14%-38%) at 15, 20 and 25 years, respectively, in the APC/Björk group, 60% (95% CI, 41%-74%) at 15 and 20 years in the LT group and 83% (95% CI, 74%-89%) at 15 years in the ECC group (Supplemental figure 1C;  $P<0.001$ ). The high incidence of surgical reinterventions in the LT group was mainly caused by PM placements ( $n=9$ , 50%).

### ***Percutaneous reinterventions***

Thirty-two patients underwent 52 catheter interventions after a median of 5.9 years ( $Q_1$ - $Q_3$ , 1.8-17.4), excluding routine fenestration closures (Supplemental table C).

### ***Status at last follow-up***

At last follow-up, 200 patients were alive with an intact Fontan circulation (median time after Fontan completion, 11.5 years;  $Q_1$ - $Q_3$ , 7.6-15.6.), with 88% of these patients in NYHA class 1. Medication status at last follow-up ( $n=196$ ) included ACE-inhibitors ( $n=19$ , 10%),  $\geq 1$  antiarrhythmics ( $n=26$ , 13%),  $\geq 1$  diuretics ( $n=21$ , 11%) and pulmonary vasodilator therapy ( $n=6$ , 3%). Of the patients  $<18$  years, 105 (78%) were on platelet inhibitors and 30 were on OAC (22%). In the adult patients, 21 were on platelet inhibitors (34%), 37 were on OAC (61%), 1 patient received NOAC (2%) and 2 patients (3%) received no anticoagulation.

Ventricular systolic function ( $n=199$ ) at last follow-up (median time after Fontan completion, 10.5 years;  $Q_1$ - $Q_3$ , 6.6-14.6) was good-mildly impaired ( $n=188$ ), moderately impaired ( $n=9$ ) or poor ( $n=2$ ). Fourteen out of 195 patients (7.2%) with known neurological status at last follow-up had severe neurological deficits due to prior CVA. In the total study cohort, liver cirrhosis was identified in 16 patients, fibrosis in 3 and

hepatocellular carcinoma in 1 patient (median time after Fontan procedure, 20.5 years; Q<sub>1</sub>-Q<sub>3</sub>, 16.5-26.8).

## Discussion

Early outcomes of the Fontan procedure are nowadays good. We observed a 1.2% perioperative mortality rate and 3.7% early take-down rate in our ECC cohort, in line with the literature<sup>3,4</sup>. However, insight in long-term outcome and risk factors for late adverse events becomes increasingly important for the expanding cohort of adult Fontan patients.

### Late survival and Fontan failure

Late survival in contemporary Fontan cohorts is good, with a reported survival rate of 70-91% after 20 years (LT)<sup>6,8,12</sup> and 93-98% after 15 years (ECC)<sup>4,5</sup>. This is in line with our experience, with a late survival rate in hospital survivors of 87% after 20 years (LT) and 99% after 15 years (ECC). Failure of the Fontan circulation with preserved ventricular systolic function was the predominant mode of death. These patients presented with right heart failure symptoms often unresponsive to diuretics and with good or only mildly impaired systolic ventricular function, in whom increased resistance of the Fontan pathway (e.g. pulmonary embolism, stenosis of a valve(d) conduit) used in some APC patients, compression of RA-RV conduits) seemed to be responsible for the failure of the Fontan circulation. However, we could not exclude diastolic dysfunction as a mode of Fontan failure, as diastolic function was rarely reported.

The APC and Björk-Fontan techniques are nowadays abandoned, as dilatation of the incorporated atrium is known to result in a high incidence of arrhythmias and energy dissipating turbulent flow<sup>13,14</sup>. Thirty-year survival rates after APC Fontan are scarce and vary between 41%-69%<sup>8,11</sup>. We observed a 30-year survival rate of 52% in our APC/Björk cohort, and our data showed a nearly linear survival curve, suggesting that long-term survival >50 years after the Fontan procedure will probably be rare in this group of patients. Of note, the APC/Björk cohort received their Fontan completion at an older age (median, 8.1 years versus 4.3 [LT] and 3.5 [ECC]), which should be kept in mind when comparing the curves. We identified APC/Björk type of Fontan and TE/NE to be risk factors for late death and APC/Björk type of Fontan, tachyarrhythmia, TE/NE and prolonged PE were risk factors for late Fontan failure. The association of tachyarrhythmia and TE/NE with late Fontan failure is in line with others<sup>11,12,15</sup>.

## Late morbidity

### *Arrhythmia*

In our experience, APC/Björk type of Fontan, age >8 years and common AVV were predictors of late tachyarrhythmia. Although the incidence of tachyarrhythmia has reduced with the LT and ECC techniques, these patients are still subject to a gradual increase of tachyarrhythmia over time<sup>12, 15</sup>. The presumed superiority of the ECC over the LT technique in terms of avoiding tachyarrhythmia has been a matter of debate, although a recent meta-analysis supported this assumption<sup>16</sup>. In our experience, LT patients seemed to have a higher risk of tachyarrhythmia compared to ECC patients. However, group and event numbers were relatively small and the higher incidence of heterotaxia (18% [LT], versus 4% [ECC]), which has been associated with an increased risk of tachyarrhythmia<sup>12</sup>, might have influenced outcome. Tachyarrhythmia is not tolerated well and can lead to haemodynamic deterioration, increased venous pressures and increased risk of TE events<sup>12, 17, 18</sup>. With the deleterious effects of tachyarrhythmia on long-term outcome in Fontan patients becoming more clear<sup>11, 12, 15</sup>, avoidance of this complication is important.

To minimize the risk of developing supraventricular tachyarrhythmia, we prefer to use the extracardiac TCPC in order to minimize atrial suture lines, prevent atrial dilatation and minimize the risk of sinus node dysfunction. When tachyarrhythmia occurs, early and aggressive treatment may be paramount to improve long-term outcome for these patients. Treatment can range from medication and ablation therapy, antitachycardia pacemaker therapy to Fontan conversion with concomitant MAZE surgery for selected cases (APC/LT) with therapy resistant tachyarrhythmia.

In our experience, freedom of PM for SND was generally good. Tachyarrhythmia was associated with the need of a PM for SND. This association can be explained by the increased incidence of late SND in our APC/Björk cohort, which appeared to be iatrogenically caused by the need for antiarrhythmic medication.

### *Thromboembolic and neurological events*

The risk of TE/NE has significantly decreased with the introduction of the LT and ECC techniques. In our experience, tachyarrhythmia was a risk factor for TE/NE, an association also recently described by Wilson et al.<sup>12</sup>. This even more emphasises the importance of avoiding tachyarrhythmias in Fontan patients, especially as the occurrence of TE/NE was a strong predictor of death in our cohort. Our anticoagulation protocol in the modern cohort is to start with OAC for the first 3-12 months postoperatively, which is subsequently changed to antiplatelet therapy only. At adult age the majority of patients switch to OAC.

**PLE**

Freedom from PLE rate at 20 years was 88%, similar to the 88-89% observed in previous large cohorts<sup>8, 15</sup>, and 5-year mortality after diagnosis of PLE was 40%. Only 31% of patients had (transient) resolution of PLE symptoms, emphasising the need for better treatment options. While the pathogenesis of PLE is not fully clarified, increased central venous pressure is an important factor<sup>19</sup>, and therefore factors leading to increased resistance may trigger PLE. We had several cases in which PLE (transiently) resolved after Fontan tunnel replacement or after resolution of a pneumonia episode. We speculate that pneumonia can cause increased pulmonary vascular resistance, leading to increased central venous pressure, thereby triggering PLE episodes in some patients. Prolonged PE was strongly associated with occurrence of PLE in our study, in concordance with previous studies<sup>15, 20</sup>. Future focus on these patients with prolonged PE may aid in our understanding of PLE, which is essential to improve treatment and outcome.

***Combined outcome for Fontan-related morbidity***

While the occurrence of the combined outcome for Fontan-related morbidity events (i.e., Fontan failure, arrhythmia or TE/NE) has decreased with modern techniques, our data showed that general attrition remains present, with a nearly linear trend over time. At 15 years, 41% (LT) and 23% (ECC) of patients had experienced one or more adverse events.

***Surgical reinterventions***

Freedom from surgical reintervention for the modern cohort (LT/ECC) has increased significantly compared with our early APC/Björk cohort. Most of these latter patients (57%) were reoperated for compression, severe regurgitation or stenosis of the RA-RV (Björk-Fontan) conduit or for stenotic valves used in some APC patients. Only 4 (3%) ECC patients required conduit replacement/stent placement due to small tunnel size or stenosis. Pacemaker was the most common reintervention in the LT/ECC cohort, accounting for 50% and 25% of the surgical procedures, respectively.

**Limitations and strengths**

This study is limited by its retrospective character. Also, some variables (e.g. pre-operative haemodynamics) could not be included in the analysis due to missing data in the older cohort. Furthermore, our study may have been underpowered to assess the influence of some variables on long-term outcome. Relatively low numbers of events occurred in the modern cohort of LT/ECC patients. Finally, the different Fontan techniques also represent different surgical eras and this should be kept in mind when interpreting the results. Liver examinations were not routinely performed and results therefore do not represent the incidence of liver fibrosis/cirrhosis in Fontan patients.

Strength of our study is its very long-term follow-up with 94% completeness. Additionally, the majority of hospital survivors (86%) received routine follow-up at the Center for Congenital Heart Disease Amsterdam-Leiden, which ensured the inclusiveness of data.

## Conclusion

In the current era, the majority of patients survive into adulthood. Implementation of the LT/ECC techniques has significantly delayed the development of late complications, however, Fontan patients remain subject to gradual attrition. The incidence of PLE remained substantial in our ECC cohort and patients with prolonged pleural effusions carry the highest risk for developing PLE. The occurrence of tachyarrhythmia is an important sign for adverse outcome. Prevention and early treatment may therefore be paramount for improving the long-term outcome of Fontan patients.

## References

1. Gentles TL, Mayer JE, Jr., Gauvreau K, Newburger JW, Lock JE, Kupferschmid JP, Burnett J, Jonas RA, Castaneda AR, Wernovsky G. Fontan operation in five hundred consecutive patients: factors influencing early and late outcome. *J Thorac Cardiovasc Surg* 1997;114(3):376-91.
2. Knott-Craig CJ, Danielson GK, Schaff HV, Puga FJ, Weaver AL, Driscoll DD. The modified Fontan operation. An analysis of risk factors for early postoperative death or takedown in 702 consecutive patients from one institution. *J Thorac Cardiovasc Surg* 1995;109(6):1237-43.
3. Iyengar AJ, Winlaw DS, Galati JC, Celermajer DS, Wheaton GR, Gentles TL, Grigg LE, Weintraub RG, Bullock A, Justo RN, d'Udekem Y. Trends in Fontan surgery and risk factors for early adverse outcomes after Fontan surgery: the Australia and New Zealand Fontan Registry experience. *J Thorac Cardiovasc Surg* 2014;148(2):566-75.
4. Nakano T, Kado H, Tatewaki H, Hinokiyama K, Oda S, Ushinohama H, Sagawa K, Nakamura M, Fusazaki N, Ishikawa S. Results of extracardiac conduit total cavopulmonary connection in 500 patients. *Eur J Cardiothorac Surg* 2015;48(6):825-32; discussion 832.
5. Iyengar AJ, Winlaw DS, Galati JC, Wheaton GR, Gentles TL, Grigg LE, Justo RN, Radford DJ, Weintraub RG, Bullock A, Celermajer DS, d'Udekem Y, Australia, New Zealand Fontan R. The extracardiac conduit Fontan procedure in Australia and New Zealand: hypoplastic left heart syndrome predicts worse early and late outcomes. *Eur J Cardiothorac Surg* 2014;46(3):465-73; discussion 473.
6. Downing TE, Allen KY, Glatz AC, Rogers LS, Ravishankar C, Rychik J, Faerber JA, Fuller S, Montenegro LM, Steven JM, Spray TL, Nicolson SC, Gaynor JW, Goldberg DJ. Long-term survival after the Fontan operation: Twenty years of experience at a single center. *J Thorac Cardiovasc Surg* 2017;154(1):243-253 e2.
7. Dabal RJ, Kirklin JK, Kukreja M, Brown RN, Cleveland DC, Eddins MC, Lau Y. The modern Fontan operation shows no increase in mortality out to 20 years: a new paradigm. *J Thorac Cardiovasc Surg* 2014;148(6):2517-23 e1.
8. Pundi KN, Johnson JN, Dearani JA, Pundi KN, Li Z, Hinck CA, Dahl SH, Cannon BC, O'Leary PW, Driscoll DJ, Cetta F. 40-Year Follow-Up After the Fontan Operation: Long-Term Outcomes of 1,052 Patients. *J Am Coll Cardiol* 2015;66(15):1700-10.
9. Khairy P, Fernandes SM, Mayer JE, Jr., Triedman JK, Walsh EP, Lock JE, Landzberg MJ. Long-term survival, modes of death, and predictors of mortality in patients with Fontan surgery. *Circulation* 2008;117(1):85-92.
10. d'Udekem Y, Iyengar AJ, Galati JC, Forsdick V, Weintraub RG, Wheaton GR, Bullock A, Justo RN, Grigg LE, Sholler GF, Hope S, Radford DJ, Gentles TL, Celermajer DS, Winlaw DS. Redefining expectations of long-term survival after the Fontan procedure: twenty-five years of follow-up from the entire population of Australia and New Zealand. *Circulation* 2014;130(11 Suppl 1):S32-8.
11. Poh CL, Zannino D, Weintraub RG, Winlaw DS, Grigg LE, Cordina R, Hornung T, Bullock A, Justo RN, Gentles TL, Verrall C, du Plessis K, Celermajer DS, d'Udekem Y. Three decades later: The fate of the population of patients who underwent the Atriopulmonary Fontan procedure. *Int J Cardiol* 2017;231:99-104.
12. Wilson TG, Shi WY, Iyengar AJ, Winlaw DS, Cordina RL, Wheaton GR, Bullock A, Gentles TL, Weintraub RG, Justo RN, Grigg LE, Radford DJ, d'Udekem Y, Australia, New Zealand Fontan R. Twenty-Five Year Outcomes of the Lateral Tunnel Fontan Procedure. *Semin Thorac Cardiovasc Surg* 2017;29(3):347-353.

13. Rijnberg FM, Hazekamp MG, Wentzel JJ, de Koning PJH, Westenberg JJM, Jongbloed MRM, Blom NA, Roest AAW. Energetics of Blood Flow in Cardiovascular Disease: Concept and Clinical Implications of Adverse Energetics in Patients With a Fontan Circulation. *Circulation* 2018;137(22):2393-2407.
14. de Leval MR, Kilner P, Gewillig M, Bull C. Total cavopulmonary connection: a logical alternative to atriopulmonary connection for complex Fontan operations. Experimental studies and early clinical experience. *J Thorac Cardiovasc Surg* 1988;96(5):682-95.
15. Allen KY, Downing TE, Glatz AC, Rogers LS, Ravishankar C, Rychik J, Fuller S, Montenegro LM, Steven JM, Spray TL, Nicolson SC, Gaynor JW, Goldberg DJ. Effect of Fontan-Associated Morbidities on Survival With Intact Fontan Circulation. *Am J Cardiol* 2017;119(11):1866-1871.
16. Li D, Fan Q, Hirata Y, Ono M, An Q. Arrhythmias After Fontan Operation with Intra-atrial Lateral Tunnel Versus Extra-cardiac Conduit: A Systematic Review and Meta-analysis. *Pediatr Cardiol* 2017;38(4):873-880.
17. Ohuchi H, Miyazaki A, Watanabe T, Yamada O, Yagihara T, Echigo S. Hemodynamic deterioration during simulated supraventricular tachycardia in patients after the Fontan operation. *Int J Cardiol* 2007;117(3):381-7.
18. Quinton E, Nightingale P, Hudsmith L, Thorne S, Marshall H, Clift P, de Bono J. Prevalence of atrial tachyarrhythmia in adults after Fontan operation. *Heart* 2015;101(20):1672-7.
19. Ohuchi H, Yasuda K, Miyazaki A, Kitano M, Sakaguchi H, Yazaki S, Tsuda E, Yamada O. Haemodynamic characteristics before and after the onset of protein losing enteropathy in patients after the Fontan operation. *Eur J Cardiothorac Surg* 2013;43(3):e49-57.
20. Hirsch JC, Goldberg C, Bove EL, Salehian S, Lee T, Ohye RG, Devaney EJ. Fontan operation in the current era: a 15-year single institution experience. *Ann Surg* 2008;248(3):402-10.



## Supplementary materials

**Supplemental table A.** Results of the multivariable Cox Regression\* analyses for late outcome

Variable	HR	95% CI	P-value
<b>Mortality</b>			
APC/Björk (vs LT/ECC)	4.6	1.2-17.5	<b>0.024</b>
Age at Fontan >8 years (vs <4 years)	1.7	0.5-5.5	0.357
Glenn	0.5	0.2-1.3	0.158
Tachyarrhythmia	1.4	0.5-3.8	0.396
TE/NE	16.8	7.7-37.1	<b>0.002</b>
PLE	2.2	0.9-5.5	0.082
<b>Fontan Failure</b>			
APC/Björk (vs LT/ECC)	3.4	1.2-9.4	<b>0.020</b>
Age at Fontan >8 years (vs <4 years)	1.7	0.7-4.3	0.282
Female sex	0.7	0.4-1.3	0.256
Glenn	1.5	0.7-3.5	0.325
Tachyarrhythmia	2.6	1.2-5.8	<b>0.017</b>
TE/NE	9.3	4.1-21.2	<b>&lt;0.001</b>
Prolonged PE (>21 days)	2.7	1.3-6.0	<b>0.011</b>
<b>Tachyarrhythmia</b>			
APC/Björk (vs LT/ECC)	5.1	2.1-12.7	<b>&lt;0.001</b>
Age at Fontan >8 years (vs <4 years)	4.0	1.8-9.1	<b>0.001</b>
Common AVV	9.0	3.0-27.3	<b>&lt;0.001</b>
Glenn	0.7	0.4-1.4	0.279
<b>Bradyarrhythmia</b>			
Tachyarrhythmia	3.7	1.4-9.6	<b>0.008</b>
<b>TE/NE</b>			
APC/Björk (vs LT/ECC)	1.3	0.5-3.4	0.545
Age fontan >8 years (vs <4 years)	2.0	0.7-5.4	0.177
Dextrocardia	0.2	0.0-1.5	0.126
Tachyarrhythmia	3.6	1.4-9.4	<b>0.008</b>
<b>PLE</b>			
Female sex	0.5	0.2-1.2	0.134
Prolonged PE (>21 days)	4.7	2.0-11.1	<b>&lt;0.001</b>
<b>Combined outcome for Fontan related morbidity</b>			
APC/Björk (vs LT/ECC)	2.4	1.2-4.8	<b>0.016</b>
Age at Fontan >8 years (vs <4 years)	1.8	1.0-3.3	0.061
Heterotaxia	0.8	0.2-2.8	0.759
Common AVV	3.2	1.4-7.1	<b>0.006</b>
TAPVD/PAPVD	5.2	1.3-20.2	<b>0.018</b>
Glenn	0.8	0.4-1.4	0.396
Prolonged PE (>21 days)	1.9	1.1-3.4	<b>0.020</b>

\* Enter method. All variables included in the multivariable Cox regression models are shown.

APC, atriopulmonary connection; ECC, extracardiac conduit; LT, lateral tunnel; PLE, protein losing enteropathy; PE, pleural effusion; TE, thromboembolic; NE, neurological event; AVV, atrioventricular valve.

**Supplemental Table B.** Surgical reinterventions per type of Fontan

<b>APC/Björk (n=43)</b>	<b>69</b>
-Redo Fontan	39
-Conversion to TCPC	15
-PM placement*	16
-Other	7
<b>LT (n=14)</b>	<b>18</b>
-PM placement	9
-Redo Fontan	3
-Conversion to ECC	2
-Other	4
<b>ECC (n=20)</b>	<b>24</b>
-PM placement	6
-LVOTO relief	4
-Take-down	3
-Redo Fontan	3
-PA/Glenn plasty	2
-Other	6

Values are numbers.

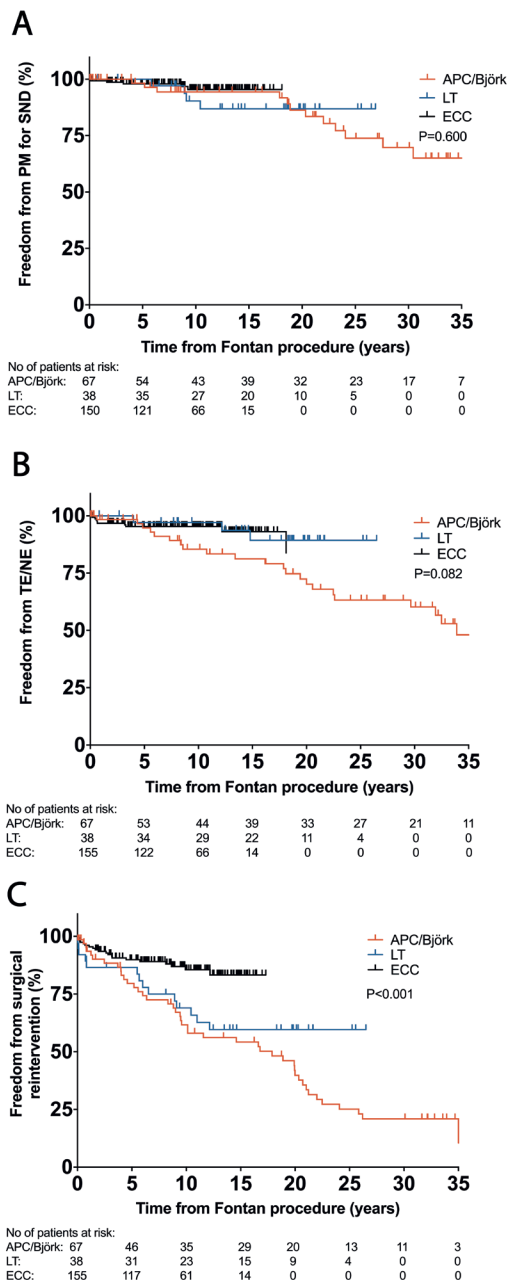
\*Some PM placements were concomitant with a Fontan conversion or redo.

APC, atriopulmonary connection; LT, lateral tunnel; ECC, extracardiac conduit; TCPC, total cavopulmonary connection; PM, pacemaker; LVOTO, left ventricular outflow tract obstruction; PA, pulmonary artery

**Supplemental Table C.** Percutaneous reinterventions

<b>Type of reintervention</b>	<b>52</b>
-Veno-venous collateral coiling	10
-Aorto-pulmonary collateral coiling	6
-Pulmonary artery stent placement	6
-Fontan conduit stent placement	3
-Dilatation of stent	8
-Dilatation of aortic arch	1
-Valve placement in Björk conduit	3
-Ablation	7
-Other	8

Values are numbers.



**Supplemental Figure 1.** Kaplan-Meier curves per Fontan group (hospital survivors) for freedom from PM for SND (A), TE/NE (B) and surgical reinterventions (C). P-values of the log-rank tests between groups are indicated in the graphs.

APC; atriopulmonary connection, LT; lateral tunnel, ECC; extracardiac conduit, PM; pacemaker, SND; sinus node dysfunction, TE/NE; thromboembolic event/neurological event



## CHAPTER 3

# 3

# Long-term outcome of direct relief of subaortic stenosis in single ventricle patients

Rijnberg FM, Sojak V, Blom NA, Hazekamp MG

# **Abstract**

## **Background**

Single ventricle patients with unrestrictive pulmonary blood flow and (potential) subaortic stenosis are challenging to manage and optimal surgical strategy is unknown. Direct relief of subaortic stenosis by enlargement of the VSD and/or subaortic chamber has generally been replaced for a DKS or Norwood procedure due to concerns of iatrogenic heart block, re-obstruction or ventricular dysfunction. Studies reporting long-term outcome after the direct approach are limited. The aim of our study was to describe and analyze our experience with direct relief of subaortic stenosis in single ventricle patients.

## **Methods**

Demographic data, characteristics, (pre)-operative and outcome details were collected for children undergoing direct relief of subaortic stenosis between 1989 and 2016.

## **Results**

Twenty three patients (median age 7.4 months, range 10 days- 5.5 years) underwent direct relief of subaortic stenosis. Complete follow-up was available in all patients (median 15.6 years, range 34 days-26.3 years). Seven patients (30%) had recurrence of subaortic stenosis. One patient developed complete heart block (4%) and 1 patient developed moderate ventricular dysfunction. Five (50%) patients developed a (pseudo) aneurysm at site of the patch and ventriculotomy. There were 2 perioperative deaths. Eighty six percent of patients underwent a successful Fontan procedure.

## **Conclusions**

Direct relief of subaortic stenosis is associated with a substantial risk of re-obstruction and patch (pseudo)aneurysm formation. However, risk of heart block is low and long-term outcome is good with the majority of patients reaching Fontan completion. In our opinion, the direct approach appears to be a good and relatively simple procedure in selected cases for the treatment of subaortic stenosis.

## Introduction

Single ventricle (SV) with unrestrictive pulmonary blood flow and (potential) systemic ventricular outflow tract obstruction remains a rare and challenging anomaly with heterogeneous underlying anatomy.<sup>1</sup> Classical examples are double inlet left ventricle (DILV) or tricuspid atresia (TA) with associated transposition of the great arteries (TGA). In these patients, systemic blood flow needs to pass through a ventricular septal defect (VSD), sometimes called bulboventricular foramen, to a rudimentary subaortic outlet chamber. Such a VSD tends to become restrictive and has been linked to initial pulmonary artery banding (PAB) due to ventricular hypertrophy<sup>2-5</sup>, or after volume-unloading surgery (Glenn or Fontan) due to altered ventricular geometry<sup>6</sup>, particularly when associated with aortic arch obstruction.<sup>7,8</sup> Subaortic or aortic arch (AA) obstruction has been widely recognized as a risk factor for a good Fontan outcome. Therefore, early relief of such obstruction is mandatory. However, initial neonatal management in this patient group is not uniform, varying from an aggressive neonatal Norwood (NW) or Damus-Kaye-Stansel (DKS) approach to a more conservative initial PAB  $\pm$  AA plasty with potential later relief of developed subaortic stenosis (SAS) concomitant with the Glenn or Fontan procedure. SAS can occur because of 1) a restrictive subaortic chamber, 2) a restrictive VSD, 3) subaortic fibrous tissue/membrane or 4) a combination of these causes. SAS can be relieved directly by means of VSD and/or subaortic chamber enlargement, or indirectly by means of a NW or DKS procedure, in which the actual subaortic obstruction is bypassed by connecting the pulmonary trunk with the aorta. In addition, some centers have used a palliative arterial switch procedure for this purpose.<sup>9</sup> The direct approach has been mostly replaced by the DKS/NW procedure because of the risk of heart block, development of recurrent SAS and ventricular dysfunction due to a ventriculotomy, thus making these patients potentially less suitable for a Fontan pathway. However, the DKS/NW procedure can result in left pulmonary artery compression by the neo-aortic root, or in semilunar valve insufficiency due to altered root geometry. Moreover, these operations carry higher mortality and morbidity when performed in a neonatal period.<sup>1,10,11</sup>

There are only few reports on long-term outcomes in SV patients who underwent direct relief of SAS by enlargement of VSD and/or subaortic outflow chamber.<sup>12</sup> In this study we aim to revisit this partially abandoned concept by describing and analyzing our experience with the direct approach for relief of SAS in SV patients.



## Patients and Methods

We conducted a retrospective study in children with SV and unobstructed pulmonary blood flow, in whom initial or later SAS had been relieved directly via VSD and/or subaortic chamber enlargement. The study was approved by the Ethics Committee and individual consent for the study was waived due to its retrospective study design. At our institution, this is the preferred approach in children who do not strictly need a NW or DKS procedure. In subjects with a small aortic valve, ascending aorta or otherwise unsuitable anatomy (e.g. unbalanced AVSD), an initial DKS/NW procedure was considered the only available option. Data from medical records were analyzed for demographic, pre-, peri- and postoperative characteristics (Table 1). Primary endpoints included mortality, achievement of Fontan circulation and adequacy of SAS relief. Secondary endpoints were the incidence of recurrent SAS, heart block, subaortic chamber aneurysm, ventricular function and semilunar valve function.

Data are presented as medians with ranges where appropriate. The presence of SAS was established by means of preoperative echocardiography or catheterization and/or peroperative evaluation of subaortic outflow tract by the surgeon. Any measurable gradient, VSD/aortic valve ratio <1.0 or restriction at level of the subaortic chamber was considered relevant and formed an indication for relief using VSD and/or subaortic chamber enlargement.

**Table 1. General characteristics and demographic data**

Characteristic	Results
Age relief SAS	7.2 months (10 days-4.7 years)
Age first operation	34 days (0 days-11.2 months)
Sex (M/F)	(12/11)
Weight (kg)	3.3 (2.2-4.3)
Left SV morphology	20 (91)
Aortic arch obstruction	12 (55)
Pulmonary artery banding	23 (100)
Glenn	20 (91)
Age Glenn	8.3 months (3.1 months-3.7 years)
Fontan	19 (83)
Age Fontan (years)	3.1 (1.4-5.3)
Mortality	4 (17)
Follow-up	15.6 years (34 days-26.3 years)

Values are reported as median + range or as percentage. SAS; subaortic stenosis

SV; single ventricle

## Surgical technique

All operations were performed via median sternotomy using cardiopulmonary bypass and cold antegrade cardioplegia. The approach of VSD enlargement could be via a right ventricle (RV) ventriculotomy, right atrium, pulmonary valve or via the aorta and was based on surgeon preference. VSD and/or subaortic chamber enlargement was performed according to the technique firstly described by Cheung et al.<sup>13</sup> The VSD was enlarged superiorly or apically towards the obtuse margin of the heart (Figure 1A, dashed line). When a ventricular approach was used, the vertical incision was closed with a patch (Figure 1B). A RV ventriculotomy was the preferred approach in cases in which pre-operative echocardiography showed a small subaortic chamber, thereby allowing thorough inspection and muscle resection in this area.

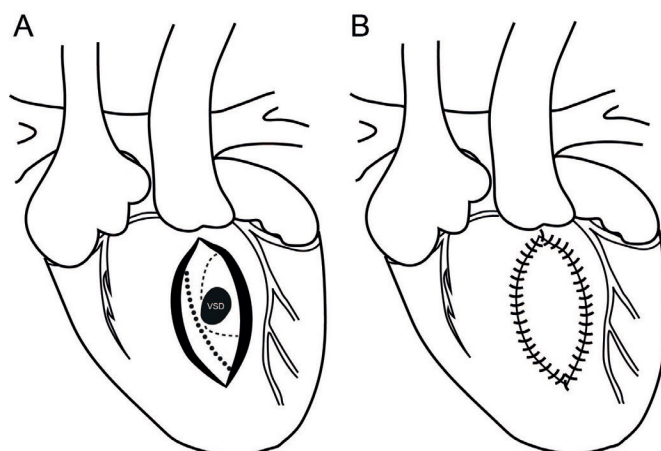


**Figure 1.** (A) View from a patient with DILV+TGA, where systemic blood flow needs to pass the VSD into a rudimentary RV towards the aorta. After a ventriculotomy, the VSD can be enlarged safely into the superior and apical direction towards the obtuse margin. The safe margin (dashed line) and suspected course of the conduction system (circles) are indicated. (B) After enlarging the VSD, the subaortic chamber is enlarged with a patch.

## Results

In the period 1989-2016, 23 children (median age 7.4 months, range 10 days-5.5 years) received direct relief of SAS at our institution. Patient demographics and general characteristics are shown in Table 1. Primary diagnoses are listed in Table 2. All patients underwent staged approach SV palliation with initial PAB  $\pm$  AA repair (n=11, 48%) and required primary relief of SAS at presentation or somewhere down the pathway (Figure 2, Table 3). Nine patients (39%) underwent direct relief of SAS as part of the

first operation (median age 29 days, range 7 days- 9.5 months), 9 patients (39%) at time of Glenn procedure (median age 7.4 months, range 4.4 months- 3.4 years), 1 between Glenn and Fontan procedure (age 3.2 years), 4 (17%) concomitant with Fontan procedure (median age 3.6 years, range 1.4- 4.8 years) and in 1 patient 3.5 years after Fontan completion. Concomitant surgery at time of first stage palliation was AVV repair in 1. Surgical procedures concomitant with the Glenn procedure were BT shunt (n=4), PAB (n=2), AVV repair (n=2), AVV closure (n=1) and a NW procedure (n=1). Management of the pulmonary valve at time of the Glenn procedure was variable and based on surgeon preference. Concomitant surgery at time of Fontan was AVV repair (n=3), AVV closure (n=3), DKS (n=1) and pulmonary artery augmentation (n=1).

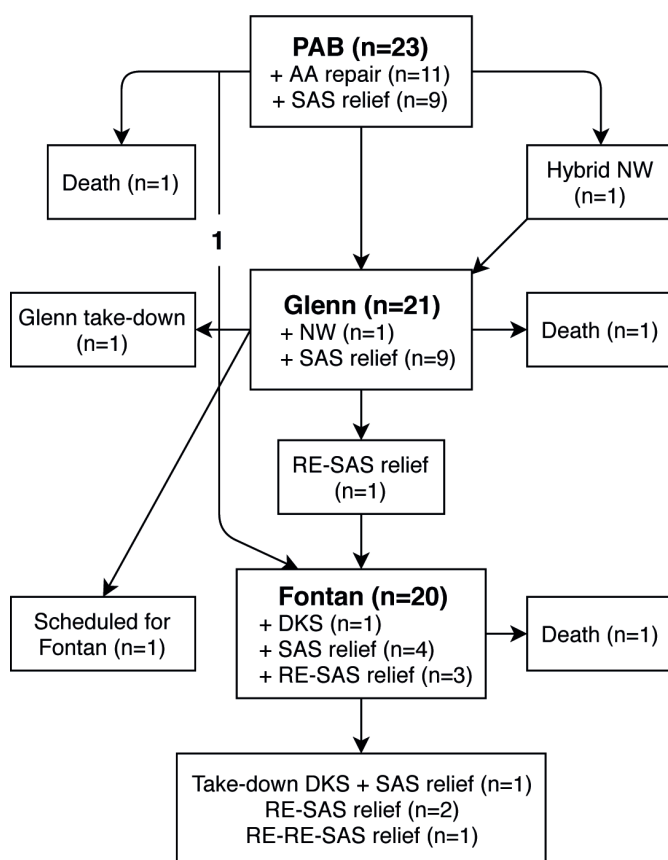


**Figure 2.** Clinical pathway of SV patients.

Approach of VSD enlargement was via a RV ventriculotomy in 11 procedures (42%), right atrium in 4 (15%), pulmonary artery in 1 (4%) and aorta in 10 procedures (38%). In 10 patients, a patch was used to enlarge the subaortic (RV) outlet chamber (6 xenopericard, 1 Gore-Tex®, 2 pulmonic homograft and in 1 unknown).

Two patients underwent both the direct and indirect approach and were excluded from primary endpoint analysis as long-term outcome in these patients was not considered to reflect one particular approach. One patient had DILV + TGA, a severely hypoplastic AA and SAS and underwent primary palliation with a hybrid NW procedure + VSD and subaortic chamber enlargement, thereby successfully deferring the NW procedure to stage II. The other patient received a DKS procedure concomitant with Fontan completion for relief of SAS. After 1.9 years, the DKS was closed and the VSD enlarged due to severe pulmonary regurgitation.

**Table 2. Primary diagnosis**

Diagnosis	Nr
DILV + TGA	17 (9)
TA + TGA	2 (1)
ccTGA +/- TA	3 (1)
DORV	1 (1)

Number of patients with aortic arch obstruction are shown in parenthesis.

DILV, double inlet left ventricle; TGA, transposition of great arteries; TA, tricuspid atresia; ccTGA, congenital corrected transposition of great arteries; DORV, double outlet right ventricle

## Primary outcome

Complete follow up was available in all patients for a median period of 15.6 years (range 34 days-26.3 years). Overall mortality was 17% (4/23), of which were 2 peri-operative deaths. One patient died 2 days after initial PAB + AA repair + subaortic chamber enlargement due to unexpected cardiac arrest without known cause. One patient died 1 day after Fontan completion + VSD enlargement. This patient was reoperated for fenestration creation because of low cardiac output, which was complicated by cardiac arrest with severe neurological damage. One child with DILV+TGA, mitral atresia and dysplastic tricuspid valve underwent 2 tricuspid valve repairs and eventually tricuspid valve replacement with post-operative poor ventricular function. This child died of end stage heart failure at an age of 4.3 years. One late death occurred 16.5 years after Fontan completion after a large cerebral vascular accident. Eighteen out of 21(excluding the 2 patients with both direct and indirect approach) patients underwent Fontan completion and one patient is scheduled for completion (86%).

**Table 3.** Clinical pathway

No.	Diagnosis	First procedure	Timing of SAS relief				Post-Fontan SAS relief	SAS mechanism/ gradient	RE-SAS mechanism/ gradient
			SAS relief Glenn	Interstage II- III SAS relief	SAS relief Fontan				
1	DILV+TGA	PAB	VSD↑+SAC↑	-	-	-	-	VSD ratio <1.0	-
2	DILV+TGA	PAB+VSD↑+SAC↑	-	RE-VSD↑	-	-	-	12mmHg	36mmHg
3	TA+TGA	PAB+AA+R+SAC↑	-	-	VSD↑	-	-	23mmHg	-
4	ccTGA+TA	PAB	VSD↑	-	-	-	-	VSD ratio 0.7	-
5	DILV+TGA	PAB+MVP+AA+R+VSD↑+SAC↑	-	-	RE-VSD↑	-	-	VSD ratio <1.0, 3mm	8mmHg
6	DILV+TGA	PAB+AA+R+SAC↑	-	-	No Fontan	-	-	Restrictive SAC	-
7	DILV+TGA	PAB	-	-	VSD↑	RE-VSD↑	-	20mmHg	40mmHg
8	DILV+TGA	PAB+AA+R+VSD↑	-	-	-	-	-	VSD ratio <1.0, 3mm	-
9	DILV+TGA	PAB	VSD↑	-	RE-VSD↑	RE-RE-VSD↑	-	VSD ratio <1.0	35mmHg, RE-RE 46mmHg
10	TA+TGA	PAB	VSD↑	-	-	-	-	30mmHg	-
11	DILV+TGA+TA	PAB	No Glenn	-	VSD↑	-	-	10mmHg, 9mm	-
12	DILV+TGA	PAB+VSD↑+SAC↑	NW	-	-	-	-	VSD ratio <1.0	-
13	DILV+TGA	PAB	VSD↑	-	-	-	-	5mmHg	-
14	DILV+TGA	PAB+AA+R+VSD↑	-	-	-	-	-	VSD ratio 0.7	-
15	DILV+TGA	PAB+AA+R+VSD↑+SAC↑	-	-	-	RE-VSD↑	-	VSD ratio 0.6	70mmHg
16	ccTGA+TA	PAB	VSD↑	-	-	-	-	VSD ratio <1.0, 6mm	-
17	DILV+TGA	PAB	SAC↑	-	-	-	-	Restrictive SAC	-
18	DILV+TGA+MA	PAB+AA+R	-	VSD↑	No Fontan	-	-	21mmHg	-
19	DILV+TGA	PAB+AA+R	VSD↑+SAC↑	-	Scheduled	-	-	25mmHg	-
20	DILV+TGA	PAB+AA+R+SAC↑	No Glenn	-	No Fontan	-	-	Restrictive SAC	-
21	ccTGA	PAB+AA+R	-	-	VSD↑	fibrous tunnel	-	VSD ratio <1.0	49mmHg
22	DORV	PAB+AA+R	VSD↑	-	-	-	-	20mmHg	-
23	DILV+TGA	PAB	-	-	DKS	VSD↑	-	VSD ratio <1.0	-

DILV; double inlet left ventricle, TA; tricuspid atresia, TGA; transposition of the great arteries, ccTGA; congenital corrected transposition of the great arteries, DORV; double outlet right ventricle, MA; mitral atresia, AA; aortic arch, PAB; pulmonary artery banding, VSD↑; ventricular septal defect enlargement, AAR; aortic arch repair, SAC↑; subaortic chamber enlargement, MVP; mitral valve plasty, SAS; subaortic stenosis, DKS; Damus-Kaye-Stansel. VSD ratio=VSD/Aortic valve diameter ratio

At latest follow up, there was complete relieve of SAS in 17/18 patients. In 1 patient, there was a stable laminar flow with a velocity of 3.0m/s over the VSD and is monitored frequently with echocardiography.

### Secondary outcome

Twenty out of 23 patients received a total of 26 VSD enlargement procedures (including reobstructions), of which 3 were in the neonatal period. Two patients underwent neonatal subaortic chamber enlargement only because of adequately sized VSD. These 5 neonatal patients presented with adequately sized aortic valve and ascending aorta with restriction at the level of the VSD (n=3) and/or subaortic chamber (n=4). One patient (4%) developed iatrogenic complete heart block for which a pacemaker was implanted. Five patients (50%) developed an aneurysm at site of the ventriculotomy, which was a true aneurysm in 1 and false in 4, and were repaired concomitantly during Fontan procedure in 2 and in a separate operation in 3 patients. The patient with a true aneurysm had an aneurysm of the entire subaortic ventricle, not only of the xenopericard patch, and required plication of the subaortic RV at time of Fontan.

At latest follow up, no patients had more than trivial aortic regurgitation. Ventricular function was good in 17, mildly impaired in 1 and moderately impaired in 1 patient (NT-Pro BNP median 151, range 50- 3591 ng/L (n=12) , ASAT 28, range 17-62 U/L, ALAT 27, range 14- 46 U/L [n=15]). All surviving patients are in NYHA class 1-2.

In total 7 patients (30%) developed re-obstruction after direct SAS relief. Six re-obstructions occurred at VSD level and re-obstruction was caused by a fibrous subaortic tunnel in 1 patient. One patient developed a second re-obstruction. These re-obstructions were addressed in 1 patient 19 days after Glenn, in 3 patients during Fontan procedure and in 3 patients 8.9, 4.5 and 5.7 years after the Fontan procedure. The patient with a second re-obstruction underwent VSD enlargement 11.0 years after Fontan completion. The risk of re-obstruction was evident up until 10 years after first direct relief of SAS (Figure 3). We could not identify any risk factors for re-obstruction. There was no association between age at first relief of SAS or presence of AA hypoplasia/coarctation with risk of re-obstruction.

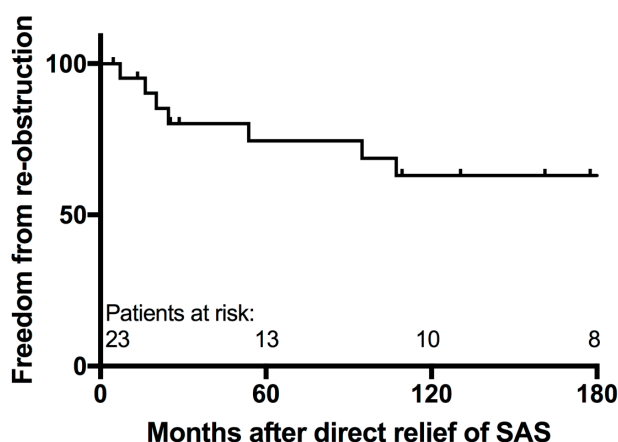


**Figure 3.** Freedom from recurrent SAS after first relief of SAS via the direct approach. The hazard of recurrent SAS is highest in the first few years, but can occur up till 10 years after first relief of SAS.

## Comment

The management of SV patients with (potential) SAS is subjected to different possible strategies. The conservative option is an initial PAB  $\pm$  AA repair. Early and interim results were, however, not optimal with poor candidacy for Fontan palliation.<sup>14,15</sup> Therefore, others use a more aggressive neonatal modified NW/DKS procedure, thereby relieving any (potential) SAS at the first operation. However, this approach is associated with substantial perioperative mortality, reaching up to 27%.<sup>15</sup> Contemporary results of the NW procedure for non-HLHS syndromes report considerable early mortality, with 15.4% in hospital mortality and 14.5% interstage mortality. Although left dominant morphologies (such as DILV+TGA and TA+TGA) have superior results compared with right dominant morphologies, early mortality still approaches 13-20% and can be higher in low-volume centers.<sup>10,11,16</sup>

When SAS occurs early, most surgeons will perform a DKS or NW procedure. Another possible option is direct relief of SAS by enlarging the VSD and/or subaortic outflow chamber, but this method has mainly been reserved for patients with pulmonary regurgitation, pulmonary stenosis or for patients who present late after Fontan palliation in which pulmonary valves are closed and therefore are unsuitable for DKS repair.<sup>1</sup> This is based on relative good experiences with the DKS procedure and the possible disadvantages associated with the direct approach. Because most centers abandoned this technique, there is no study describing the long-term outcome of the direct approach in a relatively contemporary patient cohort.

In a large single center series, Lan et al. described the outcome in 140 patients with DILV/TA + TGA (median FU 7.7 years). Overall survival was 71%, with 24% mortality in patients without relief of SAS and 32% in patients with relief of SAS (n=95). Fifty-one patients received DKS and 44 patients underwent VSD enlargement with a similar cumulative mortality percentage of 33 vs 32%. Overall Fontan completion/suitability was 76%.<sup>12</sup>

Recently, long-term results (median 17 years) of a large cohort of 152 DILV+TGA and 59 TA+TGA patients from the Australia and New Zealand Fontan registry have been reported. In their experience, 5% of DILV patients had SAS at presentation and 44% developed SAS over time. Overall, 91% of DILV patients and 60% of TA patients proceeded to Fontan completion.<sup>17</sup>

In our selected cohort of mainly DILV+TGA patients with (developed) SAS, survival was 83% and the Fontan procedure was achieved or scheduled in 86% of patients. Differences with Lan et al can be explained by an earlier era of that report and the inclusion of a higher amount of TA+TGA patients, which have significant higher mortality than DILV+TGA patients.<sup>12,17</sup> Our results are however comparable to the results of Franken et al, where overall (with and without development of SAS) 91% of DILV+TGA patients proceeded to Fontan completion.<sup>17</sup>

When SAS is present at birth, many centers adopt a strategy of a neonatal NW or DKS procedure to relief SAS and to concomitantly address AA hypoplasia when present. SAS at birth was associated with increased risk of death in the report by Franken et al. Association with a particular neonatal surgical strategy for relief of SAS could however not be established. In our experience, we had 5 patients who underwent neonatal relief of SAS by VSD ± subaortic chamber enlargement (n=3) or by subaortic chamber enlargement only (n=2). One of these latter 2 patients suffered from cardiac arrest 3 days postoperatively without known cause. The other patient underwent VSD enlargement at time of Fontan procedure due to recurrence of SAS at VSD level. The other 3 patients underwent an uncomplicated Fontan procedure and are doing well without re-obstruction at an age of 10.9, 7.5 and 15.6 years.

In one patient with a severely hypoplastic AA and SAS, we used a Hybrid NW + VSD enlargement to delay the NW procedure to the next stage with good result. In our opinion, neonatal VSD enlargement can be an acceptable option in selected patients and can thereby possibly delay DKS or NW surgery to a later stage when necessary with potential better outcome. Furthermore, we used the direct approach in 1 patient after DKS failure because of severe pulmonary regurgitation 1.9 years after Fontan with good outcome.



The risk of complete heart block has been reported to be between 0% and 34%.<sup>12,18-22</sup> In our experience, 1 patient received a pacemaker because of complete heart block out of 26 performed VSD enlargement procedures (4%). Ventricular function was well preserved in all but one of our patients and we did not encounter cases with new aortic valve insufficiency.

The rate of re-obstruction reported in literature varies between 11 and 44%<sup>4,18,20,21,23</sup>, and can occur many years after Fontan completion.<sup>24</sup> This is in line with our experience, where 30% developed recurrent SAS, of which 1 patient had a second re-obstruction. In 4 of these patients, re-obstruction occurred 8.9, 5.7, 4.5 and 11 years after Fontan completion indicating the continuous hazard of re-obstruction. Regular follow-up with echocardiography is therefore important in these patients even many years after Fontan repair.

In our experience, however, re-operation for re-obstruction could be done without associated mortality. To address the high rate of re-obstruction, one option would be to enlarge the VSD more aggressively, which in our opinion can be done without increased risk of heart block when strictly performed in the described direction.<sup>13</sup> Another option would be to always do a DKS at time of Glenn or Fontan procedure. As a large proportion of DILV+TGA patients develop SAS, which is reported to occur in up to 44% of patients over time<sup>17</sup>, some centers have adopted a strategy where every patient receives a DKS procedure, independent of the occurrence of SAS, at stage II or during Fontan.<sup>17,25,26</sup> However, although short- and mid-term outcome of the pulmonary valve (neo-aortic) after DKS is good<sup>25-27</sup>, the long-term 15-20 year outcome is mainly unknown.<sup>28</sup> Whether a universal DKS/NW, and therefore inherently an unnecessary DKS in some patients, is the best option for these patients is not known. To keep the option of future DKS open in these patients, we prefer to spare the pulmonary valve at time of Glenn procedure, especially in patients with previous SAS.

In a series of 23 patients undergoing VSD and subaortic outflow chamber enlargement by Jahangiri et al<sup>18</sup>, no formation of aneurysms were reported. Karl et al reported the formation of an aneurysm in 1 out of 2 patients in which they enlarged the VSD via ventriculotomy.<sup>8</sup> In our experience, 5/10 patients developed an aneurysm, of which 4 were false aneurysms and 1 was a true aneurysm. Two of these patients required a separate operation to address this. We speculate that the reason of these false aneurysms, besides technically, can be the cause of the abnormal blood flow inherent to this technique, where blood has to travel from the LV through the VSD in an abnormal angle. Collision of this blood flow with the patch can be the cause of the increased risk of false aneurysms and is an area for future research with 4D flow magnetic resonance imaging.

## Indications for the direct approach

In our opinion there are 3 groups of SV patients with (potential) SAS: 1) patients with small aortic valve and/or ascending aorta  $\pm$  SAS, for which a NW/DKS procedure is the only available option, 2) patients with an adequately sized subaortic pathway, which undergo primary palliation with PAB  $\pm$  AA repair at our center, and 3) patients with adequately sized aortic valve and ascending aorta but with restriction at the level of the VSD or subaortic chamber. For these patients we prefer to perform PAB  $\pm$  AA repair with direct relief of SAS when present, or perform direct relief of SAS in a later stage when it develops.

## Limitations and strengths

This is a retrospective, single-center study which includes patients over a long time-frame and is limited by its small sample size. Strength of this study is its relative contemporary cohort and long-term follow-up of SV patients who underwent direct relief of SAS.

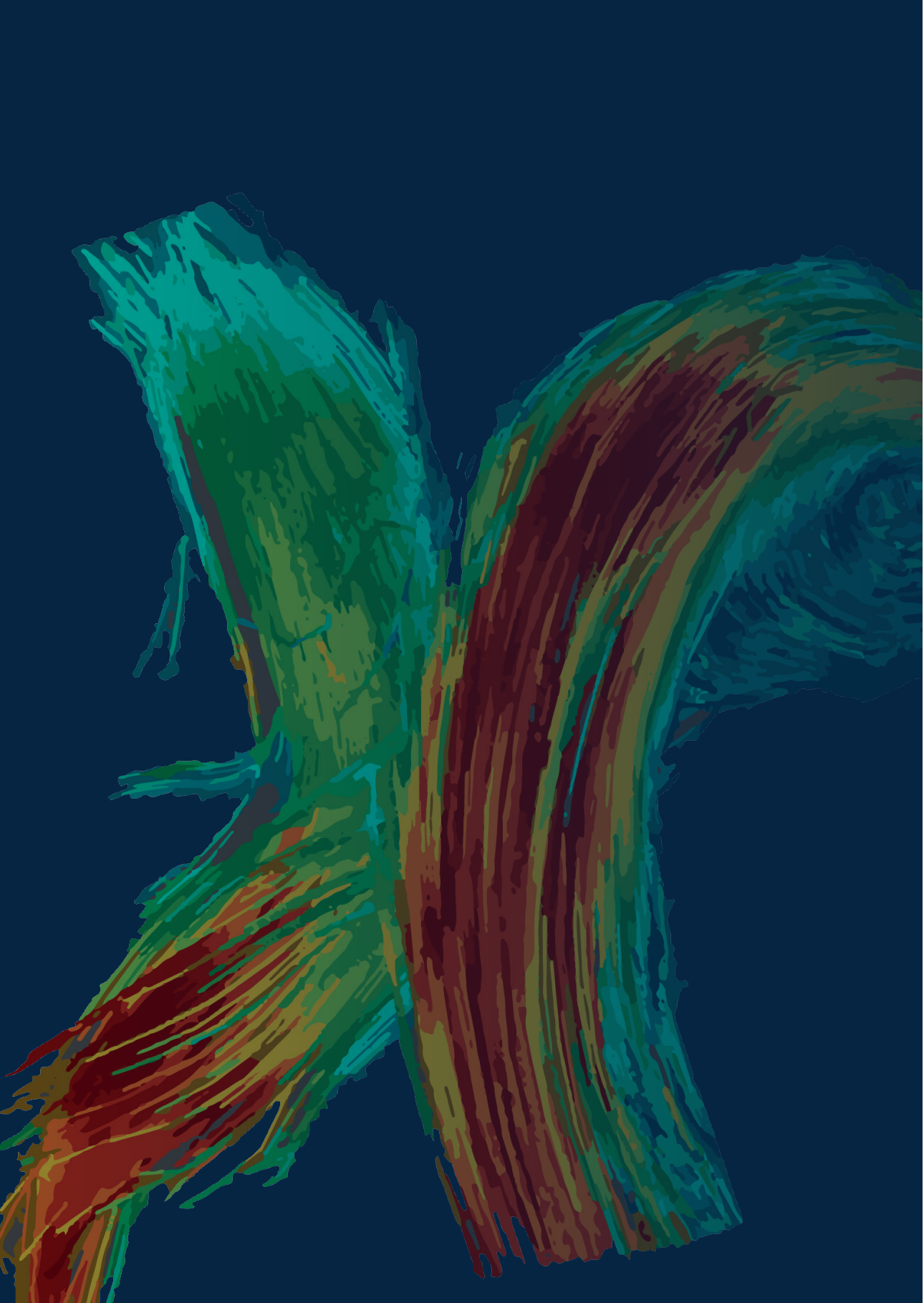
## Conclusion

In our experience, the relief of SAS via the direct approach appears to result in good long-term outcome in terms of survival and Fontan suitability. When enlarging the VSD strictly via the described approach, risk of complete heart block is low. The ventricular function remained well preserved and we did not encounter new aortic valve insufficiencies. However, risk of re-obstruction is high and can occur many years after Fontan completion. Furthermore, we encountered a substantial risk of formation of an aneurysm at site of the patch and the ventriculotomy. In conclusion, direct relief of SAS appears to offer a relatively simple solution for a select group of SV patients with SAS. Although this approach is associated with a substantial risk of patch aneurysms and re-obstruction, this could be treated without associated mortality and long-term results appear to be good. Optimization of our current approach by more aggressive VSD enlargement or prophylactic DKS at time of Glenn or Fontan may reduce the burden of these complications and are subject to future study. The definitive role of VSD and/or subaortic chamber enlargement within the clinical pathway of SV patients with (potential) SAS is in our opinion therefore not limited to patients with pulmonary valve problems and can defer DKS/NW, if necessary, to an older age.

## References

1. Alsoufi B. Management of the single ventricle and potentially obstructive systemic ventricular outflow tract. *J Saudi Heart Assoc.* 2013;25(3):191-202.
2. Miura T, Kishimoto H, Kawata H, Hata M, Hoashi T, Nakajima T. Management of univentricular heart with systemic ventricular outflow obstruction by pulmonary artery banding and Damus-Kaye-Stansel operation. *Ann Thorac Surg.* 2004;77(1):23-28.
3. Odum JN, Laks H, Drinkwater DC, Jr., et al. Staged surgical approach to neonates with aortic obstruction and single-ventricle physiology. *Ann Thorac Surg.* 1999;68(3):962-967; discussion 968.
4. Jensen RA, Jr., Williams RG, Laks H, Drinkwater D, Kaplan S. Usefulness of banding of the pulmonary trunk with single ventricle physiology at risk for subaortic obstruction. *Am J Cardiol.* 1996;77(12):1089-1093.
5. Serraf A, Conte S, Lacour-Gayet F, et al. Systemic obstruction in univentricular hearts: surgical options for neonates. *Ann Thorac Surg.* 1995;60(4):970-976; discussion 976-977.
6. Donofrio MT, Jacobs ML, Norwood WI, Rychik J. Early changes in ventricular septal defect size and ventricular geometry in the single left ventricle after volume-unloading surgery. *J Am Coll Cardiol.* 1995;26(4):1008-1015.
7. Matitiau A, Geva T, Colan SD, et al. Bulboventricular foramen size in infants with double-inlet left ventricle or tricuspid atresia with transposed great arteries: influence on initial palliative operation and rate of growth. *J Am Coll Cardiol.* 1992;19(1):142-148.
8. Karl TR, Watterson KG, Sano S, Mee RB. Operations for subaortic stenosis in univentricular hearts. *Ann Thorac Surg.* 1991;52(3):420-427; discussion 427-428.
9. Lacour-Gayet F, Serraf A, Fermont L, et al. Early palliation of univentricular hearts with subaortic stenosis and ventriculoarterial discordance. The arterial switch option. *J Thorac Cardiovasc Surg.* 1992;104(5):1238-1245.
10. Alsoufi B, McCracken C, Kanter K, Shashidharan S, Kogon B. Current Results of Single Ventricle Palliation of Patients With Double Inlet Left Ventricle. *Ann Thorac Surg.* 2017;104(6):2064-2071.
11. Alsoufi B, Slesnick T, McCracken C, et al. Current outcomes of the Norwood operation in patients with single-ventricle malformations other than hypoplastic left heart syndrome. *World J Pediatr Congenit Heart Surg.* 2015;6(1):46-52.
12. Lan YT, Chang RK, Laks H. Outcome of patients with double-inlet left ventricle or tricuspid atresia with transposed great arteries. *J Am Coll Cardiol.* 2004;43(1):113-119.
13. Cheung HC, Lincoln C, Anderson RH, et al. Options for surgical repair in hearts with univentricular atrioventricular connection and subaortic stenosis. *J Thorac Cardiovasc Surg.* 1990;100(5):672-681.
14. Franklin RC, Sullivan ID, Anderson RH, Shinebourne EA, Deanfield JE. Is banding of the pulmonary trunk obsolete for infants with tricuspid atresia and double inlet ventricle with a discordant ventriculoarterial connection? Role of aortic arch obstruction and subaortic stenosis. *J Am Coll Cardiol.* 1990;16(6):1455-1464.
15. Tchervenkov CI, Shum-Tim D, Beland MJ, Jutras L, Platt R. Single ventricle with systemic obstruction in early life: comparison of initial pulmonary artery banding versus the Norwood operation. *Eur J Cardiothorac Surg.* 2001;19(5):671-677.
16. Hornik CP, He X, Jacobs JP, et al. Relative impact of surgeon and center volume on early mortality after the Norwood operation. *Ann Thorac Surg.* 2012;93(6):1992-1997.

17. Franken LC, Admiraal M, Verrall CE, et al. Improved long-term outcomes in double-inlet left ventricle and tricuspid atresia with transposed great arteries: systemic outflow tract obstruction present at birth defines long-term outcome. *Eur J Cardiothorac Surg.* 2017;51(6):1051-1057.
18. Jahangiri M, Shinebourne EA, Ross DB, Anderson RH, Lincoln C. Long-term results of relief of subaortic stenosis in univentricular atrioventricular connection with discordant ventriculoarterial connections. *Ann Thorac Surg.* 2001;71(3):907-910.
19. Cerillo AG, Murzi B, Giusti S, Crucean A, Redaelli S, Vanini V. Pulmonary artery banding and ventricular septal defect enlargement in patients with univentricular atrioventricular connection and the aorta originating from an incomplete ventricle. *Eur J Cardiothorac Surg.* 2002;22(2):192-199.
20. Hiramatsu T, Imai Y, Kurosawa H, et al. Midterm results of surgical treatment of systemic ventricular outflow obstruction in Fontan patients. *Ann Thorac Surg.* 2002;73(3):855-860; discussion 860-851.
21. Clarke AJ, Kasahara S, Andrews DR, et al. Mid-term results for double inlet left ventricle and similar morphologies: timing of Damus-Kaye-Stansel. *Ann Thorac Surg.* 2004;78(2):650-657; discussion 657.
22. Rodefeld MD, Ruzmetov M, Schamberger MS, Girod DA, Turrentine MW, Brown JW. Staged surgical repair of functional single ventricle in infants with unobstructed pulmonary blood flow. *Eur J Cardiothorac Surg.* 2005;27(6):949-955.
23. Pass RH, Solowiejczyk DE, Quaegebeur JM, et al. Bulboventricular foramen resection: hemodynamic and electrophysiologic results. *Ann Thorac Surg.* 2001;71(4):1251-1254.
24. Finta KM, Beekman RH, Lupinetti FM, Bove EL. Systemic ventricular outflow obstruction progresses after the Fontan operation. *Ann Thorac Surg.* 1994;58(4):1108-1112; discussion 1112-1103.
25. Shimada M, Hoashi T, Kagisaki K, Shiraishi I, Yagihara T, Ichikawa H. Clinical outcomes of prophylactic Damus-Kaye-Stansel anastomosis concomitant with bidirectional Glenn procedure. *J Thorac Cardiovasc Surg.* 2012;143(1):137-143, 143 e131.
26. Alsoufi B, Al-Wadai A, Khan M, et al. Outcomes of Damus-Kaye-Stansel anastomosis at time of cavopulmonary connection in single ventricle patients at risk of developing systemic ventricular outflow tract obstruction. *Eur J Cardiothorac Surg.* 2014;45(1):77-82.
27. Fiore AC, Rodefeld M, Vijay P, et al. Subaortic obstruction in univentricular heart: results using the double barrel Damus-Kaye Stansel operation. *Eur J Cardiothorac Surg.* 2009;35(1):141-146.
28. Yamauchi S, Kawata H, Iwai S, et al. Risk Factors for Semilunar Valve Insufficiency After the Damus-Kaye-Stansel Procedure. *Ann Thorac Surg.* 2015;100(5):1767-1772.



# PART II

*In vivo* blood flow dynamics of the  
Fontan circulation

**CHAPTER 4**

4

# The influence of respiration on blood flow in the Fontan circulation: insights for imaging-based clinical evaluation of the total cavopulmonary connection

Séline F.S. van der Woude, Friso M. Rijnberg (shared first author), Mark G. Hazekamp, Monique R.M. Jongbloed, Sasa Kenjeres, Hildo J. Lamb, Jos J.M. Westenberg, Arno A.W. Roest, Jolanda J. Wentzel.



## Abstract

Congenital heart disease is the most common birth defect and functionally univentricular heart defects represent the most severe end of this spectrum. The Fontan circulation provides a unique solution for single ventricle patients, by connecting both caval veins directly to the pulmonary arteries. As a result, the pulmonary circulation in Fontan palliated patients is characterized by a passive, low-energy circulation that depends on increased systemic venous pressure to drive blood towards the lungs. The absence of a subpulmonary ventricle led to the widely believed concept that respiration, by sucking blood to the pulmonary circulation during inspiration, is of great importance as a driving force for antegrade blood flow in Fontan patients. However, recent studies show that respiration influences pulsatility, but has a limited effect on net forward flow in the Fontan circulation. Importantly, since MRI examination is recommended every 2 years in Fontan patients, clinicians should be aware that most conventional MRI flow sequences do not capture the pulsatility of the blood flow as a result of the respiration. In this review, the unique flow dynamics influenced by the cardiac and respiratory cycle at multiple locations within the Fontan circulation is discussed. The impact of (not) incorporating respiration in different MRI flow sequences on the interpretation of clinical flow parameters will be covered. Finally, the influence of incorporating respiration in advanced computational fluid dynamic modeling will be outlined.

## Introduction

Congenital heart disease is the most common birth defect with an estimated incidence of 1 in 100 live births.(1) Functionally univentricular heart defects represent the most severe end of the spectrum of congenital heart disease, characterized by a severely underdeveloped ventricle that is unable to drive the systemic or pulmonary circulation. Many underlying diagnoses can be present, including patients with a underdeveloped right ventricle (e.g. tricuspid atresia) or an underdeveloped left ventricle (e.g. hypoplastic left heart syndrome). The Fontan operation is the palliative treatment of choice for single ventricle patients, by connecting both caval veins directly to the pulmonary arteries (PAs), also called the total cavopulmonary connection (TCPC).(2) Via this procedure, the venous inflow connections to the heart are rerouted, excluding the hypoplastic ventricle from the circulation, whereas the other ventricle will serve as systemic ventricle. Without the interposition of a subpulmonary ventricle, the pulmonary circulation in Fontan patients is a low-energy, passive circulation that is dependent on elevated systemic venous pressure to drive pulmonary blood flow towards the single ventricle. The Fontan circulation is thus characterized by chronically elevated central venous pressure with reduced cardiac output due to chronic preload deprivation of the single ventricle.(3) Although the Fontan circulation has led to survival into adulthood >90%, significant morbidity is present including a reduced quality of life, exercise capacity and the occurrence of liver fibrosis/cirrhosis or protein losing enteropathy.(4)

Because of the vulnerable state of the Fontan physiology and its dependence on favorable hemodynamics, regular evaluation of flow within the Fontan circulation is recommended for early detection of (subclinical) complications.(4) Currently, echocardiography and magnetic resonance imaging (MRI) are the imaging modalities of choice to evaluate TCPC flow, but differently incorporate the effect of respiration on flow rates. Since respiration importantly influences TCPC flow(5-7), knowledge about the effect of respiration on blood flow and how flow measurements and flow-related clinical parameters are affected by different MRI protocols is therefore important for clinicians taking care of Fontan patients.

In this review, blood flow characteristics as influenced by the cardiac and respiratory cycle at multiple locations within the TCPC are discussed. The effect of not/partially incorporating the influence of the respiratory cycle in conventional MRI flow imaging will be described. Finally, the importance of including respiration-resolved flow measurements in advanced computational fluid dynamic (CFD) modeling of TCPC hemodynamics (e.g. wall shear stress, energy loss) is outlined.

## The total cavopulmonary connection (TCPC): definition of the different vessels

Nowadays, the Fontan circulation is created using two techniques. The lateral tunnel technique connects the IVC to the PA via an intra-atrial patch (thus including part of the right atrium in the Fontan tunnel)(2). The extracardiac conduit technique(14) connects the IVC with the PA via a rigid Goretex conduit outside the heart. Conventionally, the term "TCPC" is considered to cover the area consisting of the Fontan tunnel (both the lateral tunnel and extracardiac conduit technique, above the entry of the HVs), the SVC, and both right- and left PAs. Thus, most papers use the terminology "IVC" when assessing flow in the Fontan tunnel.(12, 15, 16) In this review, as depicted in Figure 1, the term "IVC" is used for the **subhepatic** IVC (below the entry of the HVs), and "Fontan tunnel" for the **suprahepatic** IVC (above the entry of the HVs) to make a clear distinction between these locations within the TCPC.

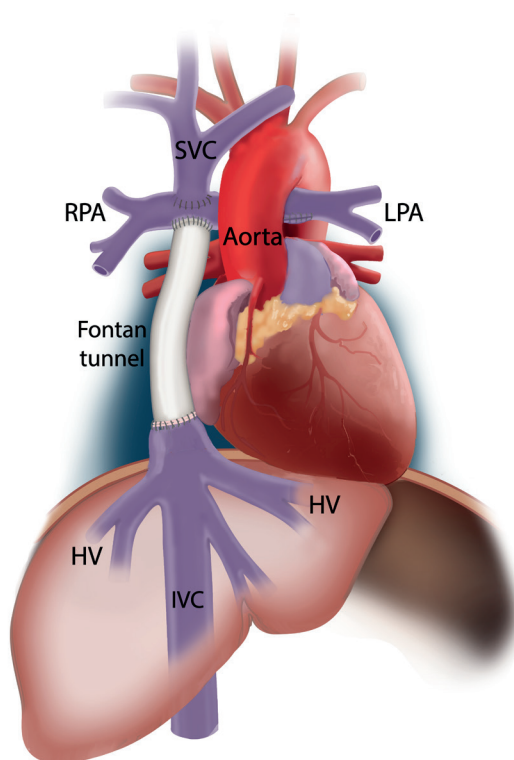


**Figure 1.** A schematic representation of the TCPC is shown. In this example, an extracardiac conduit Fontan circulation is shown. The IVC represents the part inferior to the entry of the hepatic veins. The suprahepatic part of the IVC is indicated as the Fontan tunnel, representing either the extracardiac conduit or lateral intraatrial tunnel.

## Physiology of TCPC flow

In the normal biventricular circulation, systemic venous return towards the right atrium is determined by the ratio of the pressure gradient between 1) the mean systemic filling pressure and right atrial pressure and 2) the venous vascular resistance.(17) Consequently, a change in one of these parameters is needed to affect venous return and, as a consequence of the Frank-Starling mechanism, thereby affects preload leading to altered cardiac output. For example, factors that increase systemic filling pressure (e.g. augmented blood volume or vasomotor tone) can alter systemic venous return by increasing the pressure gradient promoting venous return.(17, 18)

In the Fontan circulation, systemic venous return and thus pulmonary blood flow to the single ventricle is therefore determined by the ratio of 1) the pressure gradient between the mean systemic filling pressure and the atrium, and 2) the venous vascular resistance and the total resistance in the Fontan circuit, constituting of the serial TCPC resistance and pulmonary vascular resistance.(3, 9) In general, four components have been described in literature that can affect flow rates in the TCPC, including alterations in blood flow along the cardiac cycle(19), the respiratory cycle, flow alterations because of peripheral muscular pump activity during lower-leg exercise (8, 9), and by gravitational forces, leading to decreased inferior systemic venous flow rates at the upright versus the supine position.(11) All these factors influence TCPC flow by altering the venous pressure gradient from the systemic veins towards the atrium. For example, central venous pressure has been shown to be raised to 20-30mmHg during lower-leg exercise by the contribution of the peripheral muscle pump, thereby effectively raising the pressure gradient and thus pulmonary blood flow in Fontan patients.(3, 20)

Unique to the Fontan circulation where the systemic venous return and pulmonary circulation are fully bypassed from the single ventricle, only minor alterations in blood flow occur along the cardiac cycle, with in general increased flow during systole and early diastole (early filling), with decreased flow during late diastole (atrial contraction).(19) In Fontan patients, however, the effect of respiration on venous return and pulmonary blood flow pulsatility is much more pronounced. This is predominantly caused by a change in intrathoracic pressures (i.e. intrapleural and pericardial pressures), leading to a change in atrial pressures, and a change in abdominal pressure, thereby effectively changing the pressure gradient from the inferior vena cava and hepatic veins, via the pulmonary arteries and pulmonary vascular bed, to the atrium. For this reason, mechanical ventilation using positive end-expiratory pressure has been shown to reduce cardiac output in Fontan patients (21), with significantly increased pulmonary blood flow and cardiac output when negative pressure ventilation is applied.(21, 22) Additionally, it also explains reduced caval flow rates during the Valsalva maneuver, as

increased intrathoracic pressures during Valsalva lead to a decreased pressure gradient and thus venous return.(10)

Of note, it is currently not known if changes in PVR during respiration also have effect on the change in blood flow during respiration. In healthy persons, PVR is lowest around functional residual capacity, with an increase in PVR at total lung capacity or residual volume.(23) To date, no studies have studied possible changes in PVR during normal respiration in Fontan patients.

The minor effect of the cardiac cycle on blood flow pulsatility is in contrast to a normal biventricular circulation, where a rise in pulmonary artery pressure during systole results in significant pulmonary blood flow alterations during the cardiac cycle, with a much less pronounced influence of respiration. Because of its relevance to blood flow imaging, flow dynamics along the cardiac and respiratory cycle are the subject of this review.

## **Imaging modalities for assessment of TCPC blood flow along cardiac and respiratory cycle**

### ***Doppler echocardiography***

Doppler echocardiography allows for real-time measurement of one-directional blood flow velocity along the direction of the ultrasound beam. Simultaneous recording of the respiratory and electrocardiography (ECG) signal provides insight into the timing of the velocity measurements with respect to the cardiac and respiratory cycle.

### ***Phase contrast-MRI***

Flow quantification using phase contrast MRI (PC-MRI) is based on the fact that changes in the phase of the MR signal along a magnetic field gradient are proportional to the velocity of the blood flow.(35) Subsequently, flow rates can be calculated by multiplying the mean velocity over a cross section with the vessel cross-sectional area. For most PC-MRI techniques, however, the time to acquire these phase (i.e. velocity) images exceeds the length of a single heartbeat. Therefore, to obtain dynamic flow information along an entire cardiac cycle, it requires data acquisition over multiple heartbeats, gated to the ECG signal (ECG-gating). Subsequently, the data from multiple heartbeats is synchronized and retrospectively reconstructed into one single cardiac cycle. Importantly, flow imaging using ECG-gating will therefore not take respiratory effects on flow rates into account, as data from multiple different heartbeats are acquired irrespective of the phase of the respiratory cycle.

***Respiratory motion compensation***

PC-MRI can be performed under breath hold (2D flow MRI only) or free-breathing conditions. Since breathing motion can lead to image artifacts with poor image quality, PC-MRI acquired during free-breathing usually requires some form of respiratory movement compensation. Most commonly, a respiratory abdominal belt or navigator is used to track the level of the diaphragm. Only data acquired within a predefined range around the end-expiratory diaphragm position is accepted to minimize breathing artifacts. Thus, only flow data acquired around the end-expiratory phase of the respiratory cycle will be captured when a respiratory navigator is used, similar to the breath-hold condition.(36) Knowledge about the effect of respiration on blood flow and how flow measurements and flow-related clinical parameters are affected by the different PC-MRI sequences and respiratory compensation strategies is therefore important for clinicians taking care of Fontan patients.

Currently, multiple PC-MRI sequences are used that are mainly focused on flow dynamics during the cardiac cycle with variable degrees of incorporation of the respiratory component.

***2D flow MRI***

2D flow MRI obtains ECG-gated, one-directional (through-plane) velocity at a predefined 2D plane at a vessel of interest, and is the current clinical standard for flow quantification. (13) Scan durations are in the order of 10-15 seconds. 2D flow can be acquired using free-breathing, with or without respiratory motion compensation, or under breath-hold conditions. Thus, 2D flow MRI does not capture respiration induced flow variations.

***2D real-time flow MRI***

Advances in MRI acquisition strategies nowadays allow for 2D real-time (ungated) flow acquisitions without the need for respiratory motion compensation, allowing for assessment of dynamic flow variations (typical temporal resolution 15-20 measurements per second) along both the cardiac and respiratory cycle.(37) The respiratory and electrocardiography (ECG) signals are simultaneously recorded, allowing to synchronize the timing of the flow rate measurements with the phase of the cardiac and respiratory cycle.

***3D flow MRI***

Recently, 3D flow MRI has been introduced for assessment of flow and flow-related parameters in the TCPC in Fontan patients, exploiting the negligible TCPC blood flow pulsatility along the cardiac cycle.(38) With 3D flow MRI, three-directional velocities within a 3D volume of interest are acquired for a single, cardiac-cycle averaged (no ECG-gating) phase. It allows for quantification of cardiac-cycle averaged flow rates and flow

related clinical parameters (e.g. pulmonary flow distribution), within a 1.5 minute scan. 3D flow MRI does not incorporate the effect of respiration on flow characteristics.(38)

#### **4D flow MRI**

4D flow MRI allows for the acquisition of ECG-gated (usually 20-30 phases along the cardiac cycle), three-directional velocities within a 3D volume of interest. Flow rates can be retrospectively quantified at any vessel of interest within the scanned volume. Furthermore, it allows for visualization of three-dimensional flow patterns within the TCPC and quantification of advanced hemodynamic parameters (e.g. viscous energy loss rate). Scan durations are in the order of 8-16 minutes, depending on the application, sequence and use of respiratory motion compensation.(39) Due to the long scan times, 4D flow MRI can only be acquired using free-breathing with or without the use of respiratory motion compensation. Consequently, conventional 4D flow MRI sequences do not incorporate the effect of respiration on flow dynamics.

#### **5D flow MRI**

Most recently, 5D flow MRI has been used to quantify blood flow by obtaining ECG- and respiratory-gated, three-directional velocities within a 3D volume (i.e. 4D flow MRI + respiratory-gating = 5D flow MRI). 5D flow MRI allows for obtaining cardiac-cycle resolved (ECG-gated) flow information from data acquired in four different respiration phases: inspiration, end-inspiration, expiration and end-expiration.(32)

### **The influence of the cardiac and respiratory cycle on net forward flow in the TCPC**

An important differentiation must be made between net forward flow and flow pulsatility within the TCPC. It is a common belief that part of the venous return in Fontan patients is dependent on energy provided by respiration(11, 12).Hsia et al.(11) used doppler echocardiography to define the percentage of respiration-dependent flow as follows:  $\frac{Q_{\text{insp}} - Q_{\text{exp}}}{Q_{\text{insp}} + Q_{\text{exp}}}$ ,

where  $Q_{\text{insp}}$  and  $Q_{\text{exp}}$  are the flow rates during inspiration and expiration, respectively. Based on this parameter, approximately 30%, 14% and 55% of Fontan tunnel flow, subhepatic IVC and HV flow is respiration-dependent, respectively. In comparison, in healthy controls respiration-dependent flow in the subhepatic IVC, HVs and suprahepatic IVC were 11%, 25% and 15%, respectively. Therefore, it has been suggested that a significant percentage of specifically Fontan tunnel and HV net forward flow is dependent on respiration as a driving force. However, although inspiration does actively *increase* flow rates compared to breath-holding conditions due to a decrease in intrathoracic pressure and atrial pressure augmenting the transpulmonary pressure gradient, it must be emphasized that expiration also leads to *decreased* flow rates, thereby mostly

countering the effect of inspiration. Consequently, defining the respiration-dependency of flow using inspiration and expiration flow rates is not ideal. In fact, respiration has only a significant influence on the net forward flow if the increased flow volume during inspiration (i.e. inspiratory flow rate \* duration of inspiration) outweighs the decreased flow volume during expiration, compared to a breath-hold condition. Indeed, Wei *et al* (16) demonstrated that respiration did not significantly affect net forward flow rates (difference on average  $<0.1 \text{ L/min/m}^2$ ) by comparing 2D real-time MRI acquired under both free-breathing and breath-hold conditions in the SVC, Fontan tunnel and aorta. Recently, Gabbert *et al* also stressed the limited influence of respiration on net forward flow in the Fontan tunnel.(7) In line with these findings, net forward flow was not affected by forced breathing conditions or after a 6 week inspiratory muscle training program.(5, 41) Initiation of hyperventilation (representing the ventilatory pump) in addition to zero resistance exercise (representing the muscle pump) did also not result in significantly higher blood flow rates.(8) Thus, it must be concluded that respiration is not an important driving force for net forward flow in the TCPC.

### **The influence of the cardiac and respiratory cycle on blood flow pulsatility in the TCPC**

However, these studies clearly showed a significant increase in *pulsatility* (flow variations along the cardiac and/or respiratory cycle) caused by respiration, with high variability between the different vessels of the TCPC.(5, 7, 16) Various parameters have been used to assess blood flow pulsatility along the respiratory cycle, of which the *inspiratory-to-expiratory flow ratio* (mean inspiratory flow rate divided by mean expiratory flow rate,  $Q_{\text{insp}}/Q_{\text{exp}}$ ) is most commonly used.

Fontan tunnel flow represents approximately 65-70% of total systemic venous return. (12, 43) Many studies consistently show the pronounced effect of respiration on Fontan tunnel flow rates (5, 12, 15, 16, 31, 40), with a 70-90% higher flow rate during inspiration compared to the entire respiratory cycle, significantly more pronounced compared to a 20% increase observed in healthy controls.(5, 12) Other studies demonstrate similar findings by reporting a  $Q_{\text{insp}}/Q_{\text{exp}}$  of 1.6-3.0.(16, 24, 28) By dividing 2D real-time flow MRI measurements of the Fontan tunnel into components along the respiratory and cardiac cycle, it was shown that respiration-derived pulsatility was 2.8-times the pulsatility along the cardiac cycle. This was the opposite in healthy controls, where pulsatility along the cardiac cycle was 2.5-times the pulsatility along the respiratory cycle at the level of the suprahepatic IVC (Figure 2).(7) As opposed to its effect on net forward flow, normal and forced breathing significantly increases blood flow pulsatility in Fontan patients, further illustrating that respiration rather than the cardiac cycle is the major contributor of flow pulsatility in the Fontan tunnel (Figure 2). (5, 7, 16)



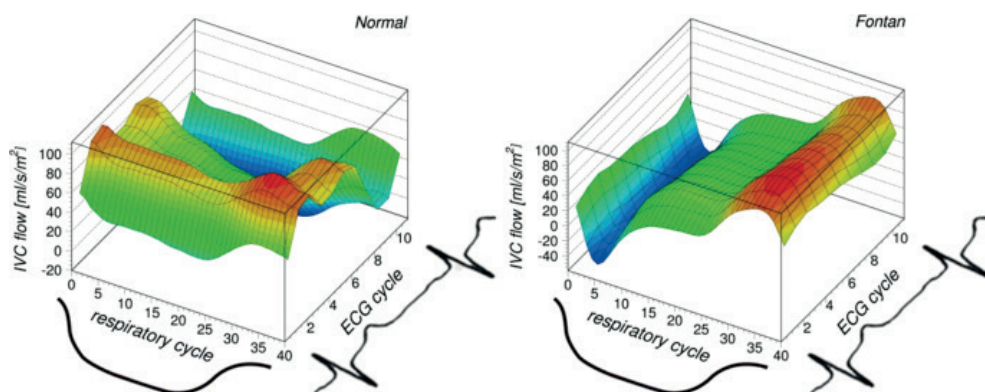


**Figure 2.** Figure 2 shows the blood flow profile in the suprahepatic IVC (healthy control, left image) and Fontan tunnel (right image), separated along the respiratory and cardiac cycle. Flow rates are indicated in color, with red indicating higher flow rates and blue indicating lower/negative flow rates. In healthy controls, pulsatility is almost exclusively observed along the cardiac cycle with retrograde flow observed during atrial contraction. In complete contrast, in Fontan patients pulsatility is almost exclusively observed along the respiratory cycle, with minimal or negative flow rates observed during expiration and maximal flow rates during inspiration. Along the cardiac cycle, negligible pulsatility is present.

**Reproduced from Gabbert et al.**(7) <https://www.nature.com/articles/s41598-019-38848-5/figures/2>

The Fontan tunnel receives blood from both the subhepatic IVC and HVs, which contribute on average 62% and 38%, respectively, to total Fontan tunnel flow.(6, 11, 25, 26, 28, 29) The study of flow dynamics in this area is of great importance, as the splanchnic venous return plays an important role in the pathophysiology of liver cirrhosis and protein-losing enteropathy. Using (invasive) doppler echocardiography,  $Q_{\text{insp}}/Q_{\text{exp}}$  in the subhepatic IVC was 1.3-1.6 (11, 28), not significantly different from healthy controls ( $Q_{\text{insp}}/Q_{\text{exp}}$  1.2).(6, 11, 25, 26) Thus, respiration has a much less pronounced influence at the subhepatic IVC compared to the Fontan tunnel, indicating that most of the respiratory-derived pulsatility in the Fontan tunnel must be explained by the HV flow contribution.

Respiration indeed strongly influenced HV flow in Fontan patients ( $Q_{\text{insp}}/Q_{\text{exp}}$  2.9-4.4), significantly higher compared to healthy controls ( $Q_{\text{insp}}/Q_{\text{exp}}$  1.7).(11, 28) The important increase in HV flow during inspiration is explained by the liver acting as a reservoir of blood with high venous capacitance, from which both the increased extra- to intra-thoracic venous pressure gradient, as well as the direct pressure of the diaphragmatic descent on the liver, can draw blood towards the Fontan tunnel during inspiration.(44) Presence of a fenestration was associated with a significantly higher inspiratory-to-expiratory fraction; 4.4 versus 3.0.(25) Since central venous pressure is lowered by the presence of a fenestration between the Fontan tunnel and the atrium, the decreased afterload for HV flow likely causes the increased flow rates during inspiration. Importantly,

plication of the diaphragm in Fontan patients with a diaphragm paresis does not fully restore normal respiratory mechanics, evidenced by a significantly smaller inspiratory-to-expiratory ratio of HV flow; 2.3 versus 3.2.(26) However, respiration likely also does not affect net forward HV flow, in line with observations in the Fontan tunnel. This might explain why Fontan patients with a diaphragm paresis have similar cardiac index and exercise capacity compared to patients with a normal functioning diaphragm.(45)

Studies on the influence of respiration on SVC flow, contributing approximately 35% of total systemic venous return, have been conflicting. ( $Q_{\text{insp}}/Q_{\text{exp}}$  1.0-1.9) (5, 12, 16, 28). Wei et al. reported an inspiratory-to-expiratory ratio of 1.9 in the SVC, higher compared to the fraction of 1.6 they observed in the Fontan tunnel.(16) This is in strong contrast to a previous study using 2D real-time flow MRI, which did not find an effect of breathing on SVC flow rates, in line with observations in healthy controls.(5, 12) It remains the question from which vascular region with high venous capacitance (analogue to the HVs providing most of the pulsatility observed in the Fontan tunnel) blood would be drawn towards the SVC during inspiration.

In normal subjects, aortic flow rate or ventricular stroke volume only slightly increase during expiration and decreases during inspiration, opposite to systemic venous return. Compared to mean aortic flow rates, flow rates are 0-6% higher at (end)-expiration and 1-6% lower at (end)-inspiration.(5) A similar, modest effect of respiration on aortic flow has been observed in Fontan patients, ranging from a 7% increase during expiration, to a 4% decrease during inspiration.(5, 12) Therefore, since systemic venous flow (predominantly HV and Fontan tunnel flow) rates are markedly raised during inspiration while aortic flow rates are not, the pulmonary circulation and lungs act as a reservoir with a large inspiratory capacity, releasing blood towards the single ventricle during expiration.(12) In contrast to the systemic venous part of the Fontan circulation, respiration thus has a minimal influence on pulsatility in the aorta, which is primarily caused by the cardiac contraction. An example of flow rates during free breathing and under breath-hold conditions in the subhepatic IVC, HVs, Fontan tunnel and aorta are shown in Figure 3. An overview of the influence of respiration on flow rates and a schematic representation are presented in Table 1 and Figure 4.

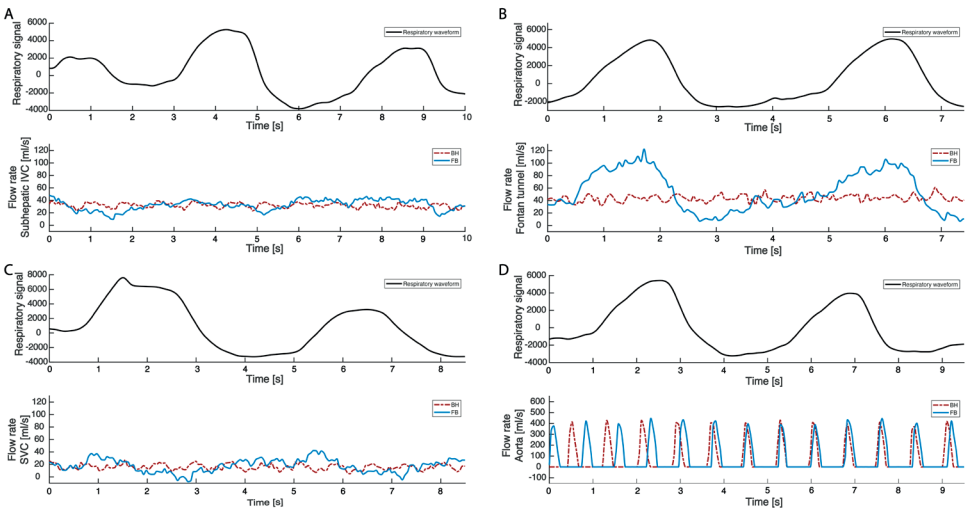


**Figure 3.** 2D real-time flow MRI measurements in the IVC, Fontan tunnel, SVC and aorta

2D real-time flow MRI measurements are shown under both free breathing (FB, blue line) and breath-hold (BH, red line) conditions for the subhepatic IVC (A), Fontan tunnel (B), SVC (C) and ascending aorta (D). Under breath-hold conditions, negligible cardiac-cycle related pulsatility is present in all venous vessels due to the absence of a subpulmonary ventricle in Fontan patients. During free breathing conditions, predominantly the Fontan tunnel flow is influenced by respiration, with a significant augmentation of flow rates during inspiration compared to expiration. Since the effect of respiration on subhepatic IVC flow is only minimal, most respiratory pulsatility in the Fontan tunnel originates from the hepatic veins. The influence of respiration on flow rates in the SVC and aorta is also minimal, although studies have reported conflicting results regarding respiratory pulsatility in the SVC.

**Table 1.** influence of respiration on blood flow at multiple locations within the Fontan circulation

Parameter	Fontan					Healthy				
	Fontan Tunnel	Subhepatic IVC	HV	SVC	Aorta	Suprahepatic IVC	Subhepatic IVC	HV	SVC	Aorta
Inspiratory-to-expiratory flow ratio: $Q_{insp}/Q_{exp}$	1.6-3.0	1.3-1.6	2.9-4.4	1.0-1.9			1.2	1.7	1.2	
Inspiratory flow fraction: $Q_{insp}/Q_{avg}$	1.7-1.9	-	-	-	0.96	1.2	-	-	-	0.94-0.99
Respiratory-dependent flow fraction: $(Q_{insp}-Q_{exp})/(Q_{insp}+Q_{exp})$	30%	14%	55%	-	-	15%	11%	25%	-	-

IVC/SVC; inferior/superior vena cava, HV; hepatic veins,  $Q_{insp}$ ; inspiratory flow rate,  $Q_{exp}$ ; expiratory flow rate,  $Q_{avg}$ ; flow rate during the entire respiratory cycle

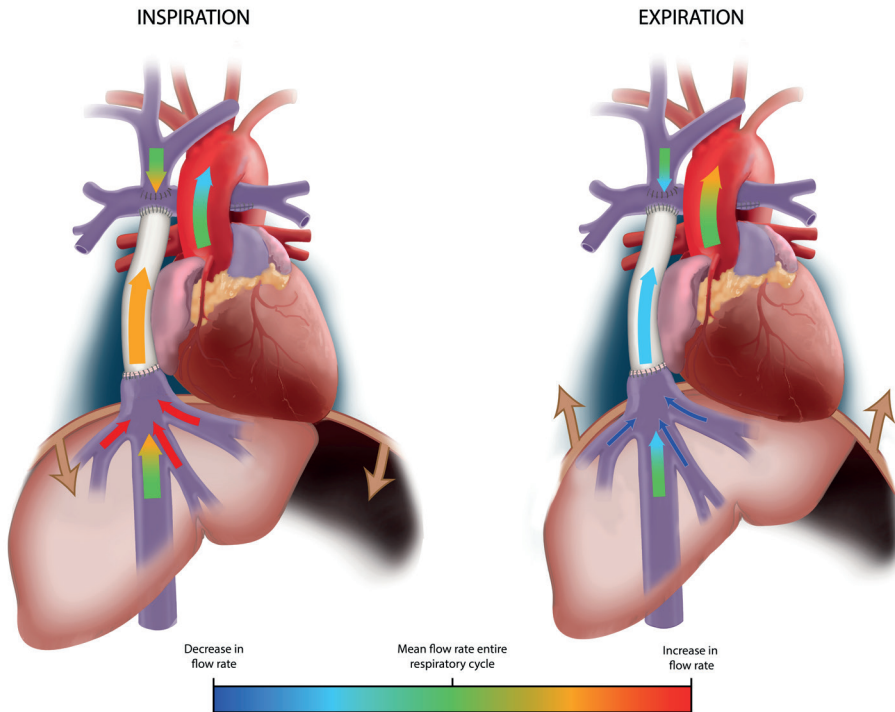


**Figure 4.** schematic representation of the influence of respiration on flow rates in the TCPC and aorta

A schematic representation of flow rates in the TCPC and aorta is shown during inspiration (left image) and expiration (right image). Arrows are color-coded by the change in flow rate in each vessel during inspiration and expiration using a linear gradient towards red (strong increase) or dark blue (strong decrease), compared to the average flow rate during the entire respiratory cycle (light green). Change in width of the arrows for each vessel schematically represent the change in flow rates between inspiration and expiration. Flow rates in the subhepatic IVC, SVC\* and aorta are only minimally influenced by respiration. Predominantly HV flow is strongly influenced by respiration, with a significant increase in flow rate during inspiration and decrease during expiration. Therefore, Fontan tunnel flow rates also show a considerable increase in flow rate during inspiration and decrease during expiration, primarily caused by the contribution from the HVs. \*Of note, studies report conflicting results regarding respiratory pulsatility in the SVC, ranging from only minimal to considerable pulsatility.

SVC/IVC; superior/inferior vena cava, HV; hepatic veins.

### Clinical relevance of pulsatility

It is currently not known if respiratory derived pulsatility plays an important role in maintaining low pulmonary vascular resistance. The negligible blood flow pulsatility along the cardiac cycle has been thought to negatively influence pulmonary vascular resistance and endothelial function in Fontan patients, by altering the passive recruitment of capillaries and shear stress-mediated nitric oxide release.(46) In turn, the respiratory derived pulsatility in the Fontan tunnel is profoundly different in amplitude

and frequency compared to the cardiac pulsatility (Figure 3B). Recently, no significant difference was found in pulmonary vascular resistance between Fontan patients with or without diaphragm paresis, indicating that respiration derived pulsatility might not be important for healthy pulmonary vasculature.(45)

### **Retrograde flow**

While flow rates increase during inspiration, flow rates in the Fontan tunnel strongly decrease during expiration with potential back flow during the early expiratory phase. On average, backflow represents approximately 5-11% (range 0-30%) of mean forward flow volume in the Fontan tunnel (7, 12, 15), reducing to only 2.9% under exercise conditions.(12) Similar percentages are observed in the suprahepatic IVC in healthy controls with a mean backflow of 6% (range 0-20%). Other studies used the retrograde-to-forward flow rate ratio to express back flow, but this parameter does not represent retrograde-to-antegrade flow *volume*, as the duration of antegrade and retrograde flow are not taken into account. In the subhepatic IVC and HVs, a retrograde-to-forward flow rate ratio of 0.06-0.07 and 0.27, respectively, were observed.(11, 24, 25) Importantly, backflow is also observed in healthy persons as a result of the atrial contraction and is not related to respiration, while backflow in Fontan patients is related to the expiratory phase.(7, 29) Retrograde flow is usually negligible in the SVC, accounting for only 0-1% of mean forward flow volume.(12)

### **The influence of respiration on blood flow during exercise**

Currently, the influence of respiration on flow rates under exercise conditions in Fontan patients has only been investigated in the Fontan tunnel, SVC and aorta. During lower-leg exercise conditions, the predominance of inspiratory flow augmentation in the Fontan tunnel seems to become less pronounced. Hjortdal et al. found a mean inspiratory fraction ( $Q_{\text{insp}}/Q_{\text{average respiratory cycle}}$ ) decrease from 1.9 in rest, to 1.4 under 1W/kg lower-leg exercise conditions. Peripheral muscle contractions were responsible for an almost three-fold increase in expiratory flow rates, while inspiratory flow rates only increased by 1.6-fold.(15) Of interest, Cordina *et al.* also showed predominantly increased expiratory flow rates in rest in patients after 20 weeks of peripheral muscle resistance training. The increased flow rates are explained by the presence of increased peripheral muscle mass leading to reduced venous compliance, thereby presumably increasing systemic filling pressures leading to increased preload and cardiac output.(10) The reason why the muscle pump predominantly increases expiratory flow rates compared to inspiratory flow rates, thereby leading to reduced “respiratory dependence”, remain incompletely understood. Although speculative, there may be a limit in the venous capacity in the inspiratory phase, leading to a diminished response to increased filling pressures caused by the muscle pump.

## Effect of respiration on clinically used flow parameters

### *PC-MRI derived clinical flow parameters*

Previous paragraphs have shown the variable influence of respiration on flow rates observed at multiple locations in the TCP. Most conventional PC-MRI sequences are focused to capture flow changes during the cardiac contraction (ECG-gating) only and do not take respiration into account. Therefore, knowledge about the effect of (not) incorporating respiration on flow and flow-related clinical measurements are important for the correct interpretation of MRI examinations in Fontan patients.

### *Net forward flow vs pulsatility*

Since respiration predominantly affects pulsatility but not net forward flow(7, 16), conventional ECG-gated 2D flow MRI sequences did not show significantly different net forward flow rates between patients scanned under free-breathing versus breath-hold conditions.(52) However, dynamic flow characteristics specific to part of the respiratory cycle, such as retrograde flow during expiration, or peak velocities during inspiration will not be captured.(7, 53) The same likely applies for ECG-gated sequences using a respiratory navigator (as the acceptance window contains the last part of expiration, the end-expiratory phase and the first part of inspiration), although no studies exist in Fontan patients comparing free-breathing navigator-gated PC-MRI with PC-MRI acquisitions during breath-hold conditions.

### *Net forward flow-derived flow parameters*

Clinical parameters derived from net forward flow rates can thus most likely be accurately determined using ECG-gated sequences, since respiration minimally affects net forward flow rates. Only limited data exist of studies that have evaluated the effect of respiration on these parameters. Using a 4D flow MRI sequence able to provide cardiac-cycle resolved flow data based on inspiratory or expiratory data only, Rutkowski et al. showed a non-significant difference in pulmonary flow distribution (52% vs 64% based on expiratory and inspiratory data, respectively).(30) Modeling studies using computational fluid dynamics (CFD) found similar results, with differences <5% in right-to-left pulmonary flow distribution along the respiratory cycle.(54, 55)

### *Hepatic flow distribution*

Fontan patients require a certain amount of hepatic venous flow towards both lungs in order to prevent the formation of pulmonary arteriovenous malformations.(56) The hepatic flow distribution (HFD) can be determined by tracking particles from the Fontan tunnel towards the PAs based on time-resolved, three-dimensional velocity fields acquired with 4D-(48, 57) or 5D flow MRI(32), or derived from computational fluid dynamic (CFD) models.(44, 58, 59) Bastkowski et al. used a novel 5D flow MRI sequence to reconstruct four ECG-gated flow fields using data from 4 respiratory phases:

inspiration, end-inspiration, expiration and end-expiration. On average, the maximum differences in HFD between the four respiratory-phases was 20% (range 9-30%). Hence, the contribution of hepatic flow towards the PA changes during the respiratory cycle because of the flow pulsatility in the Fontan tunnel associated with respiration. However, the necessity of including respiration for accurate average HFD quantification was not investigated.(32) A recent study using patient-specific CFD models with both 2D real-time MRI acquired under free-breathing and breath-hold as boundary conditions, showed that respiration has negligible influence on average HFD with mean differences of 1% (range -3 to 7%).(53)

### **CFD-derived hemodynamic metrics of the TCPC**

CFD models are increasingly used to study flow dynamics in the TCPC in Fontan patients, and can now be performed using patient-specific 3D TCPC reconstructions and patient-specific physiological data. It allows not only for the visualization of time-resolved 3D flow patterns within the TCPC, but also for quantification of advanced velocity and pressure-related hemodynamic parameters, including power loss, viscous energy loss rate, wall shear stress and stagnation volume.(61-63)

#### ***Importance of including respiration-derived pulsatility in CFD simulations***

##### *Flow patterns*

Previous studies using CFD, in vitro models or 4D flow MRI have shown the presence of adverse secondary flow patterns, including helical, swirling flow patterns at the IVC-to-conduit junction(50) and in the PAs(69, 70) or caval flow collision leading to chaotic flow disturbances at the central Fontan confluence.(71, 72) The appearance of adverse, energy-consuming flow patterns increase blood flow resistance that may lead to an increased risk of complications.(9) Importantly, these dynamic, 3D flow patterns change when respiration is included.(53, 64) Furthermore, potential deleterious effects of backflow on the splanchnic circulation and its association with liver fibrosis can only be studied by incorporating respiration into the models, as backflow is exclusively observed during (early) expiration. In addition, incorporation of respiration may also be important to study whether the pulsatile HV hemodynamics effect the presence and magnitude of local secondary flow patterns observed in the IVC-to-conduit junction using 4D flow MRI.(50)

##### *Energy loss*

Power loss and viscous energy loss describe the flow efficiency in the TCPC in Fontan patients which is related to the presence of adverse flow patterns and geometries (e.g. PA stenosis or undersized extracardiac conduit).(73, 74) Increased power loss and TCPC resistance have been associated with reduced exercise capacity(80) and increased levels of liver fibrosis.(81) Inclusion of respiration is important for accurate power loss

measurements, as incorporation of respiration resulted in a 1.4-3.1 fold increase in power loss, consistently higher compared to simulations incorporating the cardiac cycle only.(53, 54, 64, 66)

Importantly, although not incorporating respiration in CFD models leads to an underestimation of power loss, it did not affect the ranking of multiple surgical TCPC options created using “virtual surgery” CFD platforms.(68) Virtual surgery platforms allow for the pre-operative determination of the optimal TCPC geometry by evaluating the flow efficiency and HFD within the proposed TCPC using patient-specific CFD simulations.(82)

#### *Thrombosis markers*

Thrombosis can occur in some Fontan patients within the TCPC. Although no clear markers can currently predict thrombosis risk, regions with low wall shear stress and/or high stagnation volumes have been reported as potential markers. Stagnation volume (blood volume with a velocity  $<0.01$  m/s) can be specifically high during expiration in large conduits with significantly reduced flow stagnation during inspiration.(62) Thus, it is emphasized that incorporation of respiration is important when local hemodynamic metrics are of interest, including wall shear stress and stagnation volume, due to the high temporal variation of such metrics during the respiratory cycle.(54, 62, 66) As a result, inclusion of pulsatile boundary conditions acquired under free-breathing in patient-specific CFD models is recommended.(16, 64, 83)

## **Conclusion**

In conclusion, in contrast to the healthy circulation, respiration is the main source of blood flow pulsatility in the TCPC, whereas cardiac contraction mostly drives the net forward flow rate. Consequently, conventional ECG-gated PC-MRI acquisitions (i.e. 2D flow MRI and 4D flow MRI) can be used for measurements of clinical parameters based on net forward flow. Inclusion of respiratory pulsatility in state-of-the-art patient-specific CFD models are recommended for evaluation of detailed, time-resolved hemodynamic metrics (e.g. wall shear stress and viscous energy loss rate), continuing to provide important insights for clinicians in the functioning of the TCPC.

## **Acknowledgements**

The authors gratefully thank Ron Slagter for the illustrations in Figure 1 and 4.



## References

1. Mozaffarian D, Benjamin EJ, Go AS, Arnett DK, Blaha MJ, Cushman M, et al. Heart disease and stroke statistics--2015 update: a report from the American Heart Association. *Circulation*. 2015;131(4):e29-322.
2. de Leval MR, Kilner P, Gewillig M, Bull C. Total cavopulmonary connection: a logical alternative to atriopulmonary connection for complex Fontan operations. Experimental studies and early clinical experience. *J Thorac Cardiovasc Surg*. 1988;96(5):682-95.
3. Gewillig M, Brown SC. The Fontan circulation after 45 years: update in physiology. *Heart*. 2016;102(14):1081-6.
4. Rychik J, Atz AM, Celermajer DS, Deal BJ, Gatzoulis MA, Gewillig MH, et al. Evaluation and Management of the Child and Adult With Fontan Circulation: A Scientific Statement From the American Heart Association. *Circulation*. 2019.
5. Korperich H, Barth P, Gieseke J, Muller K, Burchert W, Esdorn H, et al. Impact of respiration on stroke volumes in paediatric controls and in patients after Fontan procedure assessed by MR real-time phase-velocity mapping. *Eur Heart J Cardiovasc Imaging*. 2015;16(2):198-209.
6. Hsia TY, Khambadkone S, Deanfield JE, Taylor JF, Migliavacca F, De Leval MR. Subdiaphragmatic venous hemodynamics in the Fontan circulation. *J Thorac Cardiovasc Surg*. 2001;121(3):436-47.
7. Gabbert DD, Hart C, Jerosch-Herold M, Wegner P, Salehi Ravesh M, Voges I, et al. Heart beat but not respiration is the main driving force of the systemic venous return in the Fontan circulation. *Sci Rep*. 2019;9(1):2034.
8. Shafer KM, Garcia JA, Babb TG, Fixler DE, Ayers CR, Levine BD. The importance of the muscle and ventilatory blood pumps during exercise in patients without a subpulmonary ventricle (Fontan operation). *J Am Coll Cardiol*. 2012;60(20):2115-21.
9. Rijnberg FM, Hazekamp MG, Wentzel JJ, de Koning PJH, Westenberg JJM, Jongbloed MRM, et al. Energetics of Blood Flow in Cardiovascular Disease: Concept and Clinical Implications of Adverse Energetics in Patients With a Fontan Circulation. *Circulation*. 2018;137(22):2393-407.
10. Cordina RL, O'Meagher S, Karmali A, Rae CL, Liess C, Kemp GJ, et al. Resistance training improves cardiac output, exercise capacity and tolerance to positive airway pressure in Fontan physiology. *Int J Cardiol*. 2013;168(2):780-8.
11. Hsia TY, Khambadkone S, Redington AN, Migliavacca F, Deanfield JE, de Leval MR. Effects of respiration and gravity on infradiaphragmatic venous flow in normal and Fontan patients. *Circulation*. 2000;102(19 Suppl 3):III148-53.
12. Hjortdal VE, Emmertsen K, Stenbog E, Frund T, Schmidt MR, Kromann O, et al. Effects of exercise and respiration on blood flow in total cavopulmonary connection: a real-time magnetic resonance flow study. *Circulation*. 2003;108(10):1227-31.
13. Fratz S, Chung T, Greil GF, Samyn MM, Taylor AM, Valsangiacomo Buechel ER, et al. Guidelines and protocols for cardiovascular magnetic resonance in children and adults with congenital heart disease: SCMR expert consensus group on congenital heart disease. *J Cardiovasc Magn Reson*. 2013;15:51.
14. Marcelletti C, Corno A, Giannico S, Marino B. Inferior vena cava-pulmonary artery extracardiac conduit. A new form of right heart bypass. *J Thorac Cardiovasc Surg*. 1990;100(2):228-32.
15. Hjortdal VE, Christensen TD, Larsen SH, Emmertsen K, Pedersen EM. Caval blood flow during supine exercise in normal and Fontan patients. *Ann Thorac Surg*. 2008;85(2):599-603.

16. Wei Z, Whitehead KK, Khiabani RH, Tree M, Tang E, Paridon SM, et al. Respiratory Effects on Fontan Circulation During Rest and Exercise Using Real-Time Cardiac Magnetic Resonance Imaging. *Ann Thorac Surg*. 2016;101(5):1818-25.
17. Young DB. Control of Cardiac Output. Colloquium Series on Integrated Systems Physiology: From Molecule to Function to Disease. San Rafael (CA)2010.
18. Jolley M, Colan SD, Rhodes J, DiNardo J. Fontan physiology revisited. *Anesth Analg*. 2015;121(1):172-82.
19. Schafer M, Frank BS, Humphries SM, Hunter KS, Carmody KL, Jacobsen R, et al. Flow profile characteristics in Fontan circulation are associated with the single ventricle dilation and function: principal component analysis study. *Am J Physiol Heart Circ Physiol*. 2020;318(5):H1032-H40.
20. Shachar GB, Fuhrman BP, Wang Y, Lucas RV, Jr., Lock JE. Rest and exercise hemodynamics after the Fontan procedure. *Circulation*. 1982;65(6):1043-8.
21. Shekerdeman LS, Bush A, Shore DF, Lincoln C, Redington AN. Cardiopulmonary interactions after Fontan operations: augmentation of cardiac output using negative pressure ventilation. *Circulation*. 1997;96(11):3934-42.
22. Charla P, Karur GR, Yamamura K, Yoo SJ, Granton JT, Oechslin EN, et al. Augmentation of pulmonary blood flow and cardiac output by non-invasive external ventilation late after Fontan palliation. *Heart*. 2021;107(2):142-9.
23. Widrich J, Shetty M. Physiology, Pulmonary Vascular Resistance. StatPearls. Treasure Island (FL)2021.
24. Kaulitz R, Luhmer I, Kallfelz HC. Pulsed Doppler echocardiographic assessment of patterns of venous flow after the modified Fontan operation: potential clinical implications. *Cardiol Young*. 1998;8(1):54-62.
25. Hsia TY, Khambadkone S, Redington AN, de Leval MR. Effect of fenestration on the sub-diaphragmatic venous hemodynamics in the total-cavopulmonary connection. *Eur J Cardiothorac Surg*. 2001;19(6):785-92.
26. HsiaTY,KhambadkoneS,BradleySM,deLevalMR.Subdiaphragmaticvenoushemodynamics in patients with biventricular and Fontan circulation after diaphragm plication. *J Thorac Cardiovasc Surg*. 2007;134(6):1397-405; discussion 405.
27. Kaulitz R, Bergman P, Luhmer I, Paul T, Hausdorf G. Instantaneous pressure-flow velocity relations of systemic venous return in patients with univentricular circulation. *Heart*. 1999;82(3):294-9.
28. Ha KS, Choi JY, Jung SY, Park HK. Characterization of Flow Efficiency, Pulsatility, and Respiratory Variability in Different Types of Fontan Circuits Using Quantitative Parameters. *Yonsei Med J*. 2019;60(1):56-64.
29. Ha KS, Choi JY, Jung JW, Kim NK. Impact of Flow Differentials According to Cardiac and Respiratory Cycles on Three Types of Fontan Operation. *Pediatr Cardiol*. 2018;39(6):1144-55.
30. Rutkowski DR, Barton G, Francois CJ, Bartlett HL, Anagnostopoulos PV, Roldan-Alzate A. Analysis of cavopulmonary and cardiac flow characteristics in fontan Patients: Comparison with healthy volunteers. *J Magn Reson Imaging*. 2019;49(6):1786-99.
31. Korperich H, Muller K, Barth P, Gieseke J, Haas N, Schulze-Neick I, et al. Differentiation of Impaired From Preserved Hemodynamics in Patients With Fontan Circulation Using Real-time Phase-velocity Cardiovascular Magnetic Resonance. *J Thorac Imaging*. 2017;32(3):159-68.
32. Bastkowski R, Bindermann R, Brockmeier K, Weiss K, Maintz D, Giese D. Respiration Dependency of Caval Blood Flow in Patients with Fontan Circulation: Quantification Using 5D Flow MRI. *Radiology: Cardiothoracic Imaging*. 2019;1(4):e190005.

33. Ota H, Takase K, Rikimaru H, Tsuboi M, Yamada T, Sato A, et al. Quantitative vascular measurements in arterial occlusive disease. *Radiographics*. 2005;25(5):1141-58.
34. Harris PK, L. Quantitative Doppler echocardiography. *BJA Education*. 2015;16(2):46-52.
35. Markl M, Frydrychowicz A, Kozerke S, Hope M, Wieben O. 4D flow MRI. *J Magn Reson Imaging*. 2012;36(5):1015-36.
36. Andersson C, Kihlberg J, Ebbers T, Lindstrom L, Carlhall CJ, Engvall JE. Phase-contrast MRI volume flow--a comparison of breath held and navigator based acquisitions. *BMC Med Imaging*. 2016;16:26.
37. Markl M, Schnell S, Wu C, Bollache E, Jarvis K, Barker AJ, et al. Advanced flow MRI: emerging techniques and applications. *Clin Radiol*. 2016;71(8):779-95.
38. Rijnberg FMA, H.C. van; Juffermans, J.F.; Kroft, L.J.M.; Boogaard, P.J. van den; Koning, P.J.H. de; Hazekamp, M.G.; Woude, S.F.S. van der; Warmerdam, E.G.; Leiner, T; Grotenhuis, H.B.; Goeman, J.J.; Lamb, H.J.; Roest, A.A.W.; Westenberg, J.J.M. Reduced scan time and superior image quality with 3D flow MRI compared to 4D flow MRI for hemodynamic evaluation of the Fontan pathway. *Sci Rep*. 2021;In press.
39. Dyverfeldt P, Bissell M, Barker AJ, Bolger AF, Carlhall CJ, Ebbers T, et al. 4D flow cardiovascular magnetic resonance consensus statement. *J Cardiovasc Magn Reson*. 2015;17:72.
40. Fogel MA, Weinberg PM, Hoydu A, Hubbard A, Rychik J, Jacobs M, et al. The nature of flow in the systemic venous pathway measured by magnetic resonance blood tagging in patients having the Fontan operation. *J Thorac Cardiovasc Surg*. 1997;114(6):1032-41.
41. Laohachai K, Winlaw D, Selvadurai H, Gnanappa GK, d'Udekem Y, Celermajer D, et al. Inspiratory Muscle Training Is Associated With Improved Inspiratory Muscle Strength, Resting Cardiac Output, and the Ventilatory Efficiency of Exercise in Patients With a Fontan Circulation. *J Am Heart Assoc*. 2017;6(8).
42. Becker H, Wattenberg M, Barth P, Laser KT, Burchert W, Korperich H. Impact of different respiratory monitoring techniques on respiration-dependent stroke-volume measurements assessed by real-time magnetic resonance imaging. *Z Med Phys*. 2019;29(4):349-58.
43. Salim MA, DiSessa TG, Arheart KL, Alpert BS. Contribution of superior vena caval flow to total cardiac output in children. A Doppler echocardiographic study. *Circulation*. 1995;92(7):1860-5.
44. Redington A. The physiology of the Fontan circulation. *Progress in Pediatric Cardiology*. 2006;22:179-86.
45. Komori M, Hoashi T, Shimada M, Kitano M, Ohuchi H, Kurosaki K, et al. Impact of Phrenic Nerve Palsy on Late Fontan Circulation. *Ann Thorac Surg*. 2020;109(6):1897-902.
46. Khambadkone S, Li J, de Leval MR, Cullen S, Deanfield JE, Redington AN. Basal pulmonary vascular resistance and nitric oxide responsiveness late after Fontan-type operation. *Circulation*. 2003;107(25):3204-8.
47. Alsaied T, Sleeper LA, Masci M, Ghelani SJ, Azcue N, Geva T, et al. Maldistribution of pulmonary blood flow in patients after the Fontan operation is associated with worse exercise capacity. *J Cardiovasc Magn Reson*. 2018;20(1):85.
48. Bachler P, Valverde I, Pinochet N, Nordmeyer S, Kuehne T, Crelier G, et al. Caval blood flow distribution in patients with Fontan circulation: quantification by using particle traces from 4D flow MR imaging. *Radiology*. 2013;267(1):67-75.
49. Grosse-Wortmann L, Al-Otay A, Yoo SJ. Aortopulmonary collaterals after bidirectional cavopulmonary connection or Fontan completion: quantification with MRI. *Circ Cardiovasc Imaging*. 2009;2(3):219-25.

50. Rijnberg FM, Elbaz MSM, Westenberg JJM, Kamphuis VP, Helbing WA, Kroft LJ, et al. Four-dimensional flow magnetic resonance imaging-derived blood flow energetics of the inferior vena cava-to-extracardiac conduit junction in Fontan patients. *Eur J Cardiothorac Surg*. 2019;55(6):1202-10.
51. Valverde I, Nordmeyer S, Uribe S, Greil G, Berger F, Kuehne T, et al. Systemic-to-pulmonary collateral flow in patients with palliated univentricular heart physiology: measurement using cardiovascular magnetic resonance 4D velocity acquisition. *J Cardiovasc Magn Reson*. 2012;14:25.
52. Whitehead KK, Sundareshwaran KS, Parks WJ, Harris MA, Yoganathan AP, Fogel MA. Blood flow distribution in a large series of patients having the Fontan operation: a cardiac magnetic resonance velocity mapping study. *J Thorac Cardiovasc Surg*. 2009;138(1):96-102.
53. Tang E, Wei ZA, Trusty PM, Whitehead KK, Mirabella L, Veneziani A, et al. The effect of respiration-driven flow waveforms on hemodynamic metrics used in Fontan surgical planning. *J Biomech*. 2019;82:87-95.
54. Liu J, Qian Y, Sun Q, Liu J, Umezu M. Use of computational fluid dynamics to estimate hemodynamic effects of respiration on hypoplastic left heart syndrome surgery: total cavopulmonary connection treatments. *ScientificWorldJournal*. 2013;2013:131597.
55. Baretta A CC, Marsden AL, Vignon-Clementel IE, Hsia TY, Dubini G, Migliavacca F, Pennati G. Respiratory effects on hemodynamics in patient-specific CFD models of the Fontan circulation under exercise conditions. *European Journal of Mechanics - B/Fluids*. 2012;35:61-9.
56. Kavarana MN, Jones JA, Stroud RE, Bradley SM, Ikonomidis JS, Mukherjee R. Pulmonary arteriovenous malformations after the superior cavopulmonary shunt: mechanisms and clinical implications. *Expert Rev Cardiovasc Ther*. 2014;12(6):703-13.
57. Jarvis K, Schnell S, Barker AJ, Garcia J, Lorenz R, Rose M, et al. Evaluation of blood flow distribution asymmetry and vascular geometry in patients with Fontan circulation using 4-D flow MRI. *Pediatr Radiol*. 2016;46(11):1507-19.
58. Yang W, Vignon-Clementel IE, Troianowski G, Reddy VM, Feinstein JA, Marsden AL. Hepatic blood flow distribution and performance in conventional and novel Y-graft Fontan geometries: a case series computational fluid dynamics study. *J Thorac Cardiovasc Surg*. 2012;143(5):1086-97.
59. Rijnberg FMW, S.F.S. van der; Assen, H.C. van; Juffermans, J.F.; Hazekamp, M.G.; Jongbloed, M.R.M.; Kenjeres, S.; Lamb, H.J.; Westenberg, J.J.M.; Wentzel, J.J.; Roest, A.A.W. Non-uniform mixing of hepatic venous flow and inferior vena cava flow in the Fontan conduit. *Journal of the Royal Society interface*. 2021;in press.
60. Elger D LB, Crowe C, Robertson J. *Engineering Fluid Mechanics*. 11th ed: WILEY; 2015.
61. Cibis M, Jarvis K, Markl M, Rose M, Rigsby C, Barker AJ, et al. The effect of resolution on viscous dissipation measured with 4D flow MRI in patients with Fontan circulation: Evaluation using computational fluid dynamics. *J Biomech*. 2015;48(12):2984-9.
62. Itatani K, Miyaji K, Tomoyasu T, Nakahata Y, Ohara K, Takamoto S, et al. Optimal conduit size of the extracardiac Fontan operation based on energy loss and flow stagnation. *Ann Thorac Surg*. 2009;88(2):565-72; discussion 72-3.
63. Wei ZA, Tree M, Trusty PM, Wu W, Singh-Gryzbon S, Yoganathan A. The Advantages of Viscous Dissipation Rate over Simplified Power Loss as a Fontan Hemodynamic Metric. *Ann Biomed Eng*. 2018;46(3):404-16.
64. Marsden AL, Vignon-Clementel IE, Chan FP, Feinstein JA, Taylor CA. Effects of exercise and respiration on hemodynamic efficiency in CFD simulations of the total cavopulmonary connection. *Ann Biomed Eng*. 2007;35(2):250-63.

65. Hong H, Dur O, Zhang H, Zhu Z, Pekkan K, Liu J. Fontan conversion templates: patient-specific hemodynamic performance of the lateral tunnel versus the intraatrial conduit with fenestration. *Pediatr Cardiol.* 2013;34(6):1447-54.
66. Qian Y, Liu JL, Liu JF. Hemodynamic simulation for surgical treatment of congenital heart disease. *Annu Int Conf IEEE Eng Med Biol Soc.* 2012;2012:661-4.
67. Watrous RL, Chin AJ. Model-Based Comparison of the Normal and Fontan Circulatory Systems-Part III. *World J Pediatr Congenit Heart Surg.* 2017;8(2):148-60.
68. Wei ZA, Trusty PM, Zhang Y, Tang E, Whitehead KK, Fogel MA, et al. Impact of Free-Breathing Phase-Contrast MRI on Decision-Making in Fontan Surgical Planning. *J Cardiovasc Transl Res.* 2020;13(4):640-7.
69. Houtzager JH, Westenberg JJ, de Koning PJ, Hazekamp MG, Roest AA. Helical flow pattern in the right pulmonary artery after Fontan palliation. *Eur Heart J Cardiovasc Imaging.* 2014;15(10):1183.
70. Rijnberg FM, van Assen HC, Hazekamp MG, Roest AAW. Tornado-like flow in the Fontan circulation: insights from quantification and visualization of viscous energy loss rate using 4D flow MRI. *Eur Heart J.* 2019;40(26):2170.
71. Sharma S, Ensley AE, Hopkins K, Chatzimavroudis GP, Healy TM, Tam VK, et al. In vivo flow dynamics of the total cavopulmonary connection from three-dimensional multislice magnetic resonance imaging. *Ann Thorac Surg.* 2001;71(3):889-98.
72. Sharma S, Goudy S, Walker P, Panchal S, Ensley A, Kanter K, et al. In vitro flow experiments for determination of optimal geometry of total cavopulmonary connection for surgical repair of children with functional single ventricle. *J Am Coll Cardiol.* 1996;27(5):1264-9.
73. Dasi LP, Krishnankuttyrema R, Kitajima HD, Pekkan K, Sundareswaran KS, Fogel M, et al. Fontan hemodynamics: importance of pulmonary artery diameter. *J Thorac Cardiovasc Surg.* 2009;137(3):560-4.
74. Tang E, Wei ZA, Whitehead KK, Khiabani RH, Restrepo M, Mirabella L, et al. Effect of Fontan geometry on exercise haemodynamics and its potential implications. *Heart.* 2017;103(22):1806-12.
75. Sundareswaran KS, Pekkan K, Dasi LP, Whitehead K, Sharma S, Kanter KR, et al. The total cavopulmonary connection resistance: a significant impact on single ventricle hemodynamics at rest and exercise. *Am J Physiol Heart Circ Physiol.* 2008;295(6):H2427-35.
76. Ohuchi H, Yasuda K, Miyazaki A, Kitano M, Sakaguchi H, Yazaki S, et al. Haemodynamic characteristics before and after the onset of protein losing enteropathy in patients after the Fontan operation. *Eur J Cardiothorac Surg.* 2013;43(3):e49-57.
77. Goldberg DJ, Surrey LF, Glatz AC, Dodds K, O'Byrne ML, Lin HC, et al. Hepatic Fibrosis Is Universal Following Fontan Operation, and Severity is Associated With Time From Surgery: A Liver Biopsy and Hemodynamic Study. *J Am Heart Assoc.* 2017;6(5).
78. Mertens L, Hagler DJ, Sauer U, Somerville J, Gewillig M. Protein-losing enteropathy after the Fontan operation: an international multicenter study. PLE study group. *J Thorac Cardiovasc Surg.* 1998;115(5):1063-73.
79. Rijnberg FM, Blom NA, Sojak V, Bruggemans EF, Kuipers IM, Rammeloo LAJ, et al. A 45-year experience with the Fontan procedure: tachyarrhythmia, an important sign for adverse outcome. *Interact Cardiovasc Thorac Surg.* 2019;29(3):461-8.
80. Khiabani RH, Whitehead KK, Han D, Restrepo M, Tang E, Bethel J, et al. Exercise capacity in single-ventricle patients after Fontan correlates with haemodynamic energy loss in TCPC. *Heart.* 2015;101(2):139-43.

81. Trusty PM, Wei ZA, Rychik J, Graham A, Russo PA, Surrey LF, et al. Cardiac Magnetic Resonance-Derived Metrics Are Predictive of Liver Fibrosis in Fontan Patients. *Ann Thorac Surg.* 2020;109(6):1904-11.
82. Trusty PM, Slesnick TC, Wei ZA, Rossignac J, Kanter KR, Fogel MA, et al. Fontan Surgical Planning: Previous Accomplishments, Current Challenges, and Future Directions. *J Cardiovasc Transl Res.* 2018;11(2):133-44.
83. Tree M, Wei ZA, Trusty PM, Raghav V, Fogel M, Maher K, et al. Using a Novel In Vitro Fontan Model and Condition-Specific Real-Time MRI Data to Examine Hemodynamic Effects of Respiration and Exercise. *Ann Biomed Eng.* 2018;46(1):135-47.

## CHAPTER 5

# 5

# Reduced scan time and superior image quality with 3D flow MRI compared to 4D flow MRI for hemodynamic evaluation of the Fontan pathway

Rijnberg FM, van Assen HC, Juffermans JF, Kroft LJM, van den Boogaard PJ, de Koning PJH, Hazekamp MG, van der Woude SFS, Warmerdam EG, Leiner T, Grotenhuis HB, Goeman JJ, Lamb HJ, Roest AAW, Westenberg JJM



# **Abstract**

## **Aims**

Long scan times prohibit a widespread clinical applicability of 4D flow MRI in Fontan patients. As pulsatility in the Fontan pathway is minimal during the cardiac cycle, acquiring non-ECG gated 3D flow MRI may result in a reduction of scan time while accurately obtaining time-averaged clinical parameters in comparison with 2D and 4D flow MRI.

## **Methods**

Thirty-two Fontan patients prospectively underwent 2D (reference), 3D and 4D flow MRI of the Fontan pathway. Multiple clinical parameters were assessed from time-averaged flow rates, including the right-to-left pulmonary flow distribution (main endpoint) and systemic-to-pulmonary collateral flow (SPCF).

## **Results**

A ten-fold reduction in scan time was achieved (4D flow 15.9min (SD 2.7min) and 3D flow 1.6min (SD 7.8sec),  $p<0.001$ ) with a superior signal-to-noise ratio (mean ratio of SNRs 1.7 (0.8),  $p<0.001$ ) and vessel sharpness (mean ratio 1.2 (0.4),  $p=0.01$ ) with 3D flow. Compared to 2D flow, good-excellent agreement was shown for mean flow rates (ICC 0.82-0.96) and right-to-left pulmonary flow distribution (ICC 0.97). SPCF derived from 3D flow showed good agreement with that from 4D flow (ICC 0.86).

## **Conclusions**

3D flow MRI allows for obtaining time-averaged flowrates and derived clinical parameters in the Fontan pathway with good-excellent agreement with 2D and 4D flow, but with a tenfold reduction in scan time and significantly improved image quality compared to 4D flow.

## Introduction

The Fontan circulation provides a palliative solution for patients with an univentricular heart defect, by directly connecting the caval veins with the pulmonary arteries (PAs), also called the total cavopulmonary connection (TCPC). Today, around 70.000 Fontan patients are alive and this population is expected to double in the next 20 years. Due to the vulnerability of the Fontan physiology to adverse hemodynamics, regular MRI evaluation of the Fontan pathway every 2-3 years is recommended for the early detection of (subclinical) complications(1). With MRI, important prognostic parameters of both the single ventricle as well as the venous Fontan pathway can be acquired. Parameters of clinical interest of the venous Fontan pathway include the quantification of 1) the pulmonary right-to-left flow distribution(2-4), associated with exercise capacity(5), 2) caval flow contribution(6-8), including the distribution of conduit flow towards the left PA known as hepatic flow distribution (HFD)(9), and 3) systemic-to-pulmonary collateral flow (SPCF)(2, 4, 10-12). Additionally, the inferior vena cava (IVC)-to-extracardiac conduit mismatch (IVC-conduit mismatch) can be quantified to evaluate the adequacy of implanted conduit size(13).

Although two-dimensional phase-contrast MRI (2D flow MRI) is the current clinical standard for flow quantification(4, 12), measurements at all vessels of interest require extensive, time-consuming planning by a specialized technician(2, 10). ECG-gated 4D flow MRI can measure above mentioned parameters within a single acquisition(2), by acquiring time-resolved (i.e. usually for 20-30 phases in the cardiac cycle), three-directional velocities within a volume of interest. 4D flow also uniquely allows for visualization of flow patterns within the TCPC(13-15) and altered, energy-consuming TCPC flow patterns have been associated with adverse outcome(16). However, clinical applicability of 4D flow remains limited due to long scan times, a significant burden especially for children.

Time-resolved flow acquisition is often required, as flow can be highly pulsatile with significant periodic movement of the region of interest or to obtain flow information at specific phases in the cardiac cycle. In the Fontan pathway, due to the absence of a subpulmonary ventricle, only minimal pulsatility along the cardiac cycle is present(17, 18). Thus, clinical parameters of interest are mostly based on cardiac-cycle averaged flow information.

Consequently, non ECG-gated 3D flow MRI may be sufficient for quantification of cardiac-cycle-averaged parameters. With 3D flow, a single, cardiac-cycle averaged 3D velocity field within a volume of interest is obtained by acquiring data irrespective of the phase in the cardiac cycle, requiring much shorter scan time compared to 4D

flow. The feasibility of 3D flow has been theoretically shown for non-pulsatile portal venous flow using time-averaged 4D flow reconstructions(19). The aim of this study was to compare flowrates in the Fontan pathway and important flow-derived clinical parameters in Fontan patients between 2D, 3D and 4D flow. We hypothesized that 3D flow can provide accurate, equivalent cardiac-cycle averaged parameters compared to 2D and 4D flow, within a significantly shorter scan time which can contribute to a more widespread clinical use.

## **Materials and Methods**

### **Study population**

The study was approved by the institutional review board of the Leiden University Medical Center. All experiments were performed in accordance with relevant guidelines and regulations. Informed consent was obtained from all subjects and/or their guardians. Thirty-two consecutive Fontan patients were prospectively recruited between November 2018 and October 2019 (Table 1). All patients >8 years without contraindications for MRI were considered eligible for inclusion.

### **MRI protocol**

Details of MRI acquisitions are listed in Table 2 (3T, Ingenia, Philips Healthcare, Best, the Netherlands). Three-directional velocity encoded 2D flow acquisition was acquired at five positions (Figure 1A): the IVC (below the hepatic veins), Fontan conduit, superior vena cava (SVC) and the left (LPA) and right pulmonary arteries (RPA). For this study, flow was quantified using the through-plane velocity component only as through-plane 2D flow is the current clinical standard. The three-directional velocity encoding sequence in our protocol was chosen to study different research questions not part of this study.

All patients underwent retrospective ECG- and respiratory navigator-gated 4D flow of the Fontan pathway. The acquired volume of interest also covered the right (n=28) and left (n=19) pulmonary veins (PVs). Since the 4D flow acquisition was primarily focused on the TCPC, the pulmonary veins were not always present in the field of view. Selecting a larger field of view was not possible in those cases as it would lead to clinically unacceptable 4D flow scan times. Within the same MRI examination, 3D flow was acquired in all patients using an identical acquisition as 4D flow except for the absence of ECG-gating. The 3D flow acquisition was repeated in consecutive order to assess scan-rescan reproducibility (n=10).

**Table 1.** Patient characteristics

Male, n (%)	17 (53%)
Height, cm	164.5 (13.4)
Weight, kg	55.5 (14.9)
BSA, m <sup>2</sup>	1.6 (0.3)
Age at MRI, years	17.0 (5.4)
Fontan type (ECC/LT)	29/3
Conduit size (16/18/20mm)	15/13/1

Values are reported as mean (standard deviation) unless otherwise specified. BSA; body surface area (Haycock), ECC; extracardiac conduit, LT; lateral tunnel, mm; millimeter

**Table 2.** MRI acquisition details

	2D flow MRI	3D flow MRI	4D flow MRI
No. of slices (orientation)	1 (per vessel)	27 (coronal)	27 (coronal)
Field of view, mm	350x271x5	350x271x56	350x271x56
ECG-gating	Retrospective	-	Retrospective
No. of reconstructed cardiac phases	24-30	-	24
No. of signal averages	1	1	1
Respiratory compensation	none	navigator	navigator
Typical navigator efficiency	-	40-60%	40-60%
Acquired spatial resolution (mm)	1.5x1.5x5.0	2.4x2.4x2.4	2.4x2.4x2.4
Reconstructed spatial resolution (mm)	0.6x0.6x0.6	2.1x2.1x2.1	2.1x2.1x2.1
Acquired temporal resolution, ms (SD)	35.7 (12.0)	-	32.0
Flip angle (°)	10	10	10
TE (ms)	3.5-4.5	4.5	4.5
TR (ms)	5.8-8.0	8.0	8.0
VENC (cm/s)	40-80	80	80
Scan time (minutes)	1.4 (18.6 sec)	1.6 (7.8 sec)	15.9 (2.7)
Acceleration methods	Segmentation factor 1-2, SENSE factor 1.4, AP direction	SENSE factor 1.5, RL direction, EPI factor 5 Segmentation factor 1	SENSE factor 1.5, RL direction, EPI factor 5, Segmentation factor 1

SD; standard deviation, ms; milliseconds, mm; millimeter, TE; echo time, TR; repetition time, VENC; velocity encoding, SENSE; sensitivity encoding, AP; anterior-posterior, EPI; echo planar imaging readout, ECG; electrocardiogram

## Image quality and 4D flow pulsatility index

To assess 3D and 4D flow acquisition quality, vessel sharpness and signal-to-noise ratio (SNR) were determined (Supplemental Figure 1). Relative SNR and vessel sharpness between 3D and 4D flow acquisitions are reported as a ratio. The pulsatility index ( $(Q_{\max} - Q_{\min})/Q_{\text{mean}}$ , where Q is flowrate in ml/s) was calculated in the PAs from 4D flow to verify the low-pulsatile character of flow in the Fontan pathway(17, 18).

## Flow Quantification and Comparisons

Data was pre-processed using automatic background and velocity aliasing correction (CAAS MR Solutions, v5.1, Pie Medical Imaging, Maastricht, the Netherlands). Flow was quantified from 3D and 4D flow using retrospectively placed 2D planes, positioned at corresponding positions of the 2D flow acquisitions (Figure 1A). Time-averaged flow rates (at the conduit, SVC, RPA and LPA), mean velocity (at the IVC and conduit) and derived parameters were compared between 2D (reference method), 3D and 4D flow acquisitions. PV flow, SPCF and caval flow contribution were compared between 3D and 4D flow only.

## Clinical parameters

Multiple parameters were calculated from the time-averaged flowrate (Q) or mean velocity (v, at IVC and conduit only) measurements: 1) the systemic venous lower-to-upper body flow distribution ( $Q_{\text{conduit}}/(Q_{\text{conduit}} + Q_{\text{SVC}})$ ), 2) the right-to-left pulmonary flow distribution ( $Q_{\text{RPA}}/(Q_{\text{RPA}} + Q_{\text{LPA}})$ ), 3) right, left and total (when both available) SPCF, using the pulmonary estimator ( $Q_{\text{RPV}} - Q_{\text{RPA}}$  (n=28) and  $Q_{\text{LPV}} - Q_{\text{LPA}}$  (n=19))(2, 11). Furthermore, the percentage of 4) IVC-conduit mismatch (excluding lateral tunnel Fontan patients) was quantified by assessing the relative increase in mean velocity from the IVC (below entry of the hepatic veins) towards the extracardiac conduit ( $(v_{\text{conduit}} - v_{\text{IVC}})/v_{\text{IVC}} * 100\%$ )(13).

## Caval flow contribution

The contribution of SVC and conduit flow towards each PA was quantified from 4D flow using a previously described particle tracing method (n=28) using open-source Paraview(6, 7). Particles were released from the SVC and conduit and particles arriving at the PAs were recorded (6). Caval flow contribution was quantified as follows(6, 20):

$$\text{Conduit-LPA contribution} = \frac{P_{\text{conduit\_LPA}}}{P_{\text{conduit\_RPA}} + P_{\text{conduit\_LPA}}} \text{ and SVC-RPA contribution} = \frac{P_{\text{SVC\_RPA}}}{P_{\text{SVC\_RPA}} + P_{\text{SVC\_LPA}}}, \text{ where P is the number of particles reaching each PA.}$$

The number of missing particles (i.e. the percentage of total emitted particles not reaching one of the PAs) was calculated as a measure of analysis quality(20). For 3D flow, caval flow contribution was quantified using streamline tracing instead of particle

tracing. Under the assumption of (relatively) steady flow, central in this study, streamlines are equal to pathlines.

## Statistical analysis

Fifteen Fontan patients who underwent 2D and 4D flow as part of a previous prospective study(21) were used for the power calculation, using the right-to-left pulmonary flow distribution as the main endpoint. These patients were not included in this study. The difference between 2D and 3D flow was assumed to be in the same order of magnitude. Based on the mean absolute difference (2.5%) and the standard deviation of this difference (SD, 1.6%) in flow distribution, it was found that a sample size of only 4 patients would provide 90% power (assuming a normal distribution) for detecting equivalence (at equivalence margin 5%) between 2D and 3D flow.

The mean absolute difference ( $\pm 1.96$  standard error of the mean (SEM)) between methods was the primary endpoint of interest, indicating how much on average *individual* measurements differ (under- or overestimation). In contrast, the mean difference (as assessed by Bland-Altman analysis) reflects how much on average measurements differ on a cohort-level. Since clinicians care for individual patients, the mean absolute difference is considered the more important, informative parameter.

Measurements were considered to be equivalent for the main endpoint right-to-left pulmonary flow distribution when the upper limit (mean absolute difference + 1.96 SEM) was  $\leq 5\%$  between methods. Since only evident asymmetric pulmonary flow distribution may require intervention, differences  $\leq 5\%$  were considered clinically irrelevant.

Bland-Altman plots and intraclass correlation (ICC) analysis were used to assess agreement between methods and intra- and interobserver variability (moderate  $< 0.7$ , good  $\geq 0.7$ - $0.9$  and excellent  $> 0.9$ ). Measurements between different acquisition methods were compared using a paired t-test. A p-value  $< 0.05$  was considered statistically significant. Continuous data were presented as mean (standard deviation, SD). Data were analyzed with SPSS 25.0 (IBM-SPSS, Chicago, IL) and Prism 8.0 (Graphpad Software, La Jolla, CA).

## Results

2D flow was incomplete in two patients. 4D flow was unsuccessful in one 10 year old patient due to excessive movement. 3D flow was successful in all patients. Total scan time of 4D and 3D flow were 15.9 (SD 2.7 minutes) and 1.6 (SD 7.8 seconds) minutes, respectively (including a typical navigator efficiency of 50%). Compared with 4D flow, 3D flow showed superior image quality: an improved SNR (mean ratio of SNRs 1.7 (0.8),

$p<0.001$ ) and vessel sharpness (mean ratio 1.2 (0.4),  $p=0.01$ ). The 4D flow pulsatility index in the RPA and LPA were 0.70 (SD 0.23) and 0.81 (SD 0.34), respectively, corresponding to 14% and 18% of values in healthy persons (Figure 1B) (22). Streamline visualization of flow patterns acquired from 4D and 3D flow showed nearly identical flow patterns including the presence of a vortex in the proximal LPA, further illustrating the lack of significant pulsatility in the TCPC (Figure 1C-D, Supplemental video 1).

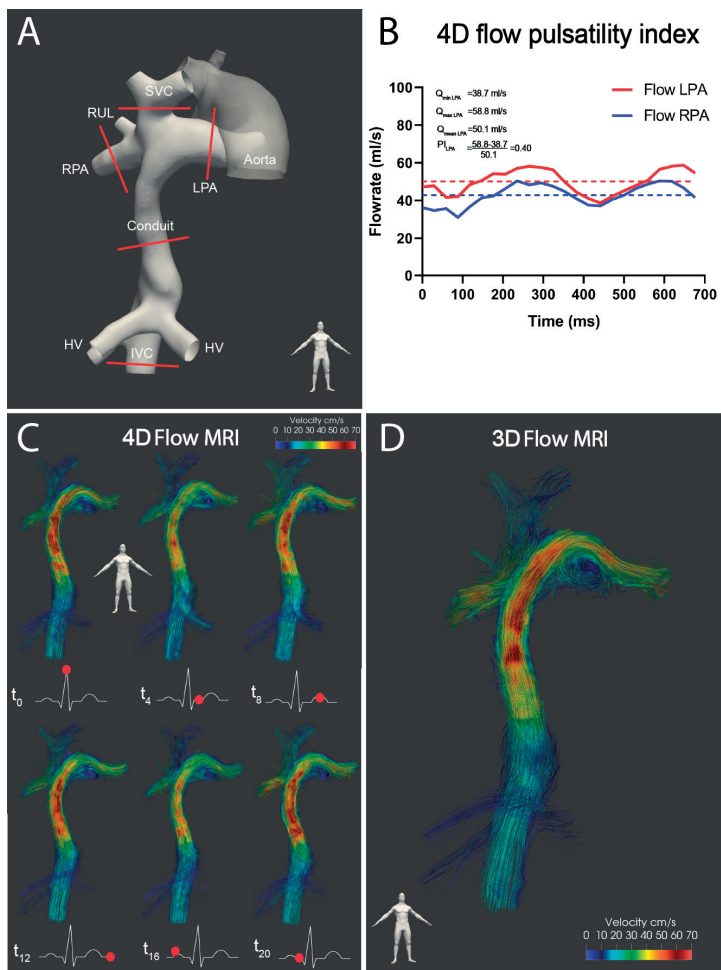


**Figure 1.** Figure 1 shows a typical extracardiac conduit Fontan patient (female, 21 years old). **(A)** The positions of the 2D flow MRI planes are indicated in red. The aorta is shown for orientation purposes only. **(B)** Calculation of the 4D flow pulsatility index for the LPA is shown. **(C)** Streamline visualization is shown for every 4th phase in the cardiac cycle (4D flow) and for the **(D)** single, time-averaged phase acquired with 3D flow. Note how nearly identical flow patterns are captured with 4D and 3D flow, including the appearance of an vortex in the proximal LPA **(C-D)**.

RPA/LPA; right/left pulmonary artery, RUL; right upper lobe, IVC/SVC; inferior/superior vena cava, HV; hepatic veins, ms; millisecond, ml; milliliter, MRI; magnetic resonance imaging.

## Flow

Results of the comparison of methods are shown in Table 3. Agreement between flow measurements between 2D and 3D flow were good-to-excellent (mean absolute difference 2.3-5.6 ml/s, ICC 0.82-0.96). Mean absolute differences were all similar or smaller compared to mean absolute differences between 2D and 4D flow (mean absolute difference 2.6-6.1 ml/s, ICC 0.78-0.91). 3D flow measured significantly lower conduit and LPA flow in comparison with 2D flow (Table 3). However, mean absolute differences were lower (conduit flow 5.6 vs 6.1 ml/s) or similar (LPA flow 3.3 ml/s) compared to mean absolute differences between 2D and 4D flow, reflecting the larger variation in both under- and overestimation of 4D flow compared with 2D flow.

When comparing 4D with 3D flow, good-to-excellent agreement was achieved for flow measurements at all vessels (mean absolute differences 3.1-7.0 ml/s, ICC 0.74-0.93, Table 3). 3D flow measured significantly lower flow in the conduit, LPA and PVs, however, mean absolute differences were relatively small and in the same order of magnitude as mean absolute differences between 2D and 3D or 2D and 4D.

## Mean velocity IVC and conduit

Compared with 2D flow, mean velocities were significantly lower in the IVC (3D and 4D flow) and conduit (3D flow, Table 3). Compared with 4D flow, 3D flow measured significantly lower mean velocities in the conduit and IVC.

## Clinical parameters

Bland-Altman plots for the comparison between acquisition methods for all clinical parameters are shown in Figure 2 and 3.

## Pulmonary right-to-left flow distribution and lower-to-upper body flow distribution

Pulmonary right-to-left and lower-to-upper body flow distributions derived from 2D and 3D flow showed significant, but small mean absolute differences (2.6-2.9%) with excellent agreement (ICC 0.92-0.97). Again, mean absolute differences were similar/smaller compared with differences observed between 2D and 4D flow (Table 3).

## Systemic-to-pulmonary collateral flow

SPCF derived from 3D flow and 4D flow showed good agreement (mean absolute differences 3.3-5.0 ml/s, ICC 0.75-0.87), although 3D flow measured significantly lower SPCF in the right lung and total SPCF compared with 4D flow.



**Table 3.** Comparison of 2D, 3D and 4D flow MRI measurements in the Fontan pathway

	2D flow MRI(n=30)	4D flow MRI(n=31)	3D flow MRI(n=32)	2Dvs4D			2Dvs3D			4Dvs3D		
				Mean absolute difference	ICC	P value	Mean absolute difference	ICC	P value	Mean absolute difference	ICC	P value
<b>Flow+Velocity</b>												
Conduit, ml/s	47.5(14.3)	48.5 (13.1)	43.2(11.7)	6.1(4.3-7.9)	0.81	0.88	5.6(3.3-7.9)	0.82	<b>0.01</b>	6.1(3.8-8.4)	0.81	<b>0.002</b>
SVC, ml/s	22.0(5.0)	22.2 (5.1)	22.3(5.3)	2.6(1.9-3.4)	0.78	0.56	2.3(1.8-2.8)	0.88	0.39	3.1(2.3-3.8)	0.74	0.86
RPA, ml/s	34.3(10.8)	34.3 (10.2)	33.3(10.1)	3.1(2.1-4.0)	0.91	0.70	2.6(1.8-3.3)	0.96	0.55	3.2(2.3-4.2)	0.91	0.51
LPA, ml/s	27.8(10.1)	29.0 (11.0)	25.9(9.8)	3.3(2.2-4.4)	0.88	0.23	3.3(2.2-4.4)	0.92	<b>0.01</b>	4.2(2.9-5.5)	0.90	<b>0.002</b>
PV right, ml/s (n=28)	-	45.8 (11.0)	42.8(11.0)	-	-	-	-	-	-	4.0(3.0-5.2)	0.93	<b>&lt;0.001</b>
PV left, ml/s (n=19)	-	35.7 (9.0)	32.4(8.6)	-	-	-	-	-	-	4.1(3.0-5.2)	0.87	<b>0.006</b>
PV total, ml/s (n=19)	-	80.9 (17.0)	75.8(15.1)	-	-	-	-	-	-	7.0(4.1-9.8)	0.88	<b>0.02</b>
IVC, cm/s (n=28)	15.1(3.0)	12.9 (2.5)	12.2(2.6)	2.4(1.8-3.1)	0.72	<b>&lt;0.001</b>	2.8(2.2-3.5)	0.80	<b>&lt;0.001</b>	1.5(1.2-1.8)	0.82	<b>0.03</b>
Conduit, cm/s (n=28)	25.3(5.7)	23.8 (7.0)	20.9(6.4)	4.5(3.6-5.5)	0.78	0.13	4.8(3.6-6.1)	0.85	<b>&lt;0.001</b>	3.5(2.4-4.6)	0.83	<b>0.001</b>
<b>Derived parameters</b>												
SPCF right, ml/s	-	10.5 (7.0)	8.2(6.8)	-	-	-	-	-	-	3.7(2.8-4.5)	0.87	<b>0.002</b>
SPCF left, ml/s	-	7.2 (5.8)	5.7(4.1)	-	-	-	-	-	-	3.3(2.5-4.2)	0.75	0.07
SPCF total, ml/s	-	17.6(10.7)	14.2(8.8)	-	-	-	-	-	-	5.0(3.4-6.7)	0.86	<b>0.01</b>
Lower-to-upper body flow distribution, %	67.3(7.8)	67.9(7.7)	65.2(7.4)	3.5(2.6-4.3)	0.82	0.77	2.9(2.0-3.8)	0.92	<b>0.002</b>	4.1(3.2-5.0)	0.82	<b>0.01</b>
Right-to-left pulmonary flow distribution, %	55.5(11.4)	54.6(12.6)	56.5(11.7)	2.7(2.1-3.4)	0.96	0.61	2.6(1.8-3.3)	0.97	<b>&lt;0.001</b>	3.1(2.2-3.9)	0.97	<b>0.001</b>
Conduit-LPA, %	-	51.4(20.6)	52.9(26.4)	-	-	-	-	-	-	10.0(7.0-12.9)	0.85	0.52
SVC-RPA, %	-	59.3(32.3)	65.2(28.9)	-	-	-	-	-	-	13.6(8.8-18.4)	0.83	0.09
IVC-conduit mismatch, %	75.2(61.6)	88.1(60.6)	79.7(58.5)	28.1(15.9-40.3)	0.77	0.05	21.6(15.4-27.8)	0.91	0.18	26.0(15.9-36.1)	0.81	0.25

Values are reported as mean (±1.96 standard error of the mean). P-values of the paired t-tests between acquisitions are given. ml/s; milliliter per second, IVC/SVC; inferior/superior vena cava, RPA/LPA; right/left pulmonary artery. PV; pulmonary veins, SPCF; systemic-to-pulmonary collateral flow.

## IVC-conduit mismatch

Overall, good-to-excellent agreement was observed between 2D, 3D and 4D flow for IVC-conduit mismatch (ICC 0.77-0.93), with a range of the mean absolute differences of 21.6-28.1%. Of note, when comparing 2D with 3D flow or 2D with 4D flow, differences in IVC-conduit mismatch were particularly highest at low values (IVC-conduit mismatch <100%), with better agreement at values >100% (Figure 2).

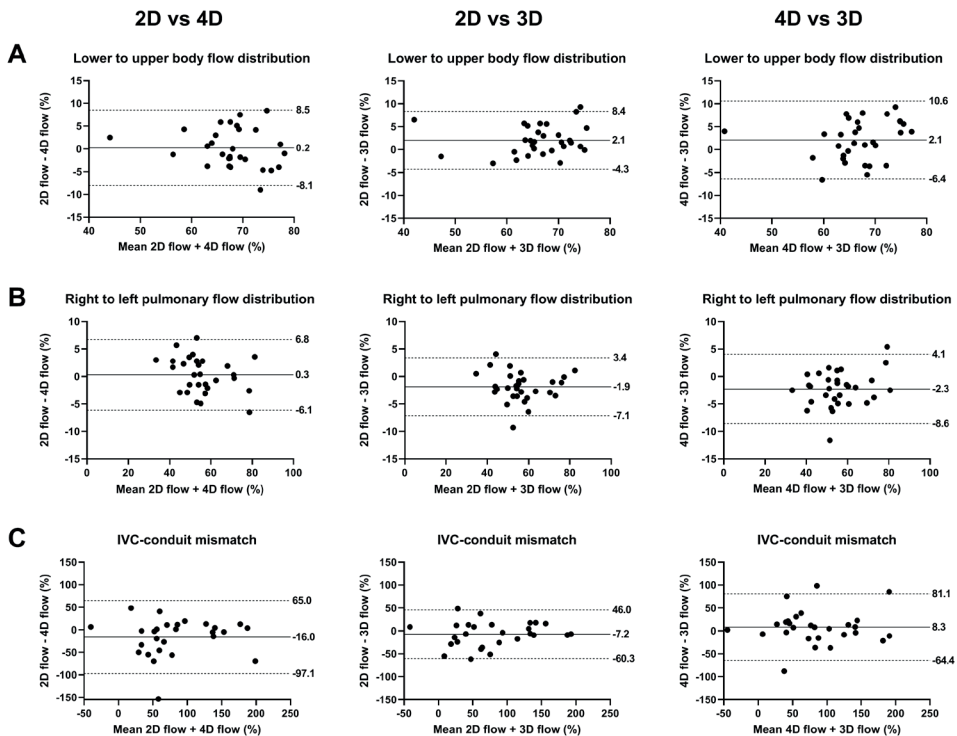


**Figure 2.** Bland-Altman plots comparing lower-to-upper body flow distribution (A), right-to-left pulmonary flow distribution (B) and IVC-conduit mismatch (C) between 2D, 3D and 4D flow. Mean bias and limits of agreement are shown. IVC; inferior vena cava

## Caval flow contribution

Caval flow contribution derived from 3D flow and 4D flow showed important variability, with mean absolute differences above the equivalence range (upper limit of mean absolute difference 12.9-18.1%). The mean percentage of missing streamlines was significantly higher in 3D flow (conduit 29.8%, SVC 32.2%) compared with missing particles in 4D flow (conduit 18.0%, SVC 24.0%,  $p < 0.001$  and  $p = 0.01$ , respectively).

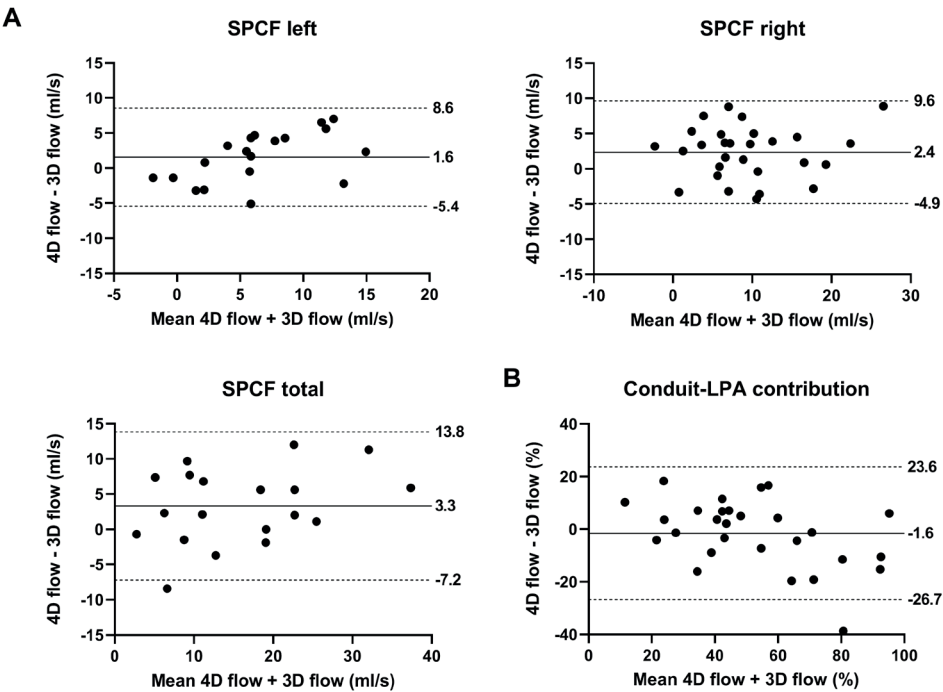


**Figure 3.** Bland-Altman plots comparing left, right and total SPCF (A) and conduit-LPA contribution (B) between 4D and 3D flow. Mean bias and limits of agreement are shown.

LPA; left pulmonary artery, SPCF; systemic-to-pulmonary collateral flow

### Intra- and interobserver and scan-rescan analysis

Overall, good-to-excellent intra- and interobserver agreement was shown for all parameters for both 4D (ICC 0.73-0.99) and 3D flow MRI (ICC 0.81-0.99), with mean differences for all flow measurements <1ml/s (Supplemental Table 1). Good-to-excellent reproducibility (scan-rescan) of the 3D flow acquisition was achieved for all flow measurements (mean difference 0.0-0.8 ml/s) and derived clinical parameters (mean difference in right-to-left pulmonary flow distribution 0.3%), except for caval flow contribution (ICC 0.73-0.99, Supplemental Table 2).

### Discussion

This study is the first to evaluate the Fontan pathway using non ECG-gated 3D flow MRI and compares measurements with ECG-gated 2D and 4D flow MRI. The main findings are that important cardiac-cycle averaged parameters of clinical interest in

Fontan patients can be acquired with 3D flow when compared to gold standard 2D flow MRI, with similar/smaller mean absolute differences for all parameters compared with differences between 2D and 4D flow. A ten-fold reduction in scan time and superior SNR and vessel sharpness was achieved with 3D flow compared to 4D flow. Since clinical important parameters from the venous Fontan pathway are mostly based on cardiac-cycle-averaged flow information, 3D flow acquisition may therefore replace 2D and 4D flow acquisitions to allow for fast, non-invasive hemodynamic flow assessment in the Fontan pathway.

### **Clinical relevance of 3D flow for evaluation of the Fontan pathway**

Due to the vulnerable state of the Fontan circulation and its dependence on favorable flow hemodynamics, serial surveillance with MRI every 2-3 years is recommended(1). Phase-contrast MRI flow measurements are an important part of current MRI protocols, and 4D flow MRI is emerging as an alternative to multiple 2D flow measurements in the single ventricle and venous Fontan pathway(2). However, since the Fontan pathway is characterized by flow with low velocities (usually <60cm/s), a dedicated 4D flow for the heart (VENC 150-200cm/s) and for the Fontan pathway (VENC 60-80cm/s) is necessary. However, the need for 2 long 4D flow scans prohibit its routine use in standard clinical MRI slots. Furthermore, it provides a significant burden for young children and in general long scan times reduce image quality (e.g. due to patient movement). Importantly, repeating a long 4D flow acquisition in case of problems (e.g. poor quality, patient movement etc) is often not possible due to time constraints in already long scan protocols. This study shows that 3D flow can be used as an alternative for 4D flow of the Fontan pathway for quantification of multiple, clinically relevant parameters: scan time is reduced from 16 minutes to only a 1.5 minute scan (including a 50% navigator efficiency) with a 100% success rate, thereby easily implementable in current MRI scan protocols. Besides offering an important reduction in scan time, also less post-processing time is required (one delineation per vessel in 3D flow compared to 20-30 (one per cardiac phase) delineations per vessel with subsequent manual adjustments in 4D flow).

### **Flow derived parameters**

Right-to-left pulmonary flow distribution derived from 3D flow measurements showed excellent agreement with 2D and 4D flow, thereby able to accurately identify patients with (severe) asymmetric flow distributions. This parameter is important in the evaluation of the Fontan pathway, as the combination of flow and morphological information (e.g. PA hypoplasia or stenosis) is essential for clinical decision making regarding possible interventional treatment. An unbalanced right-to-left pulmonary flow distribution has been associated with reduced exercise capacity(23).

Quantification of systemic-to-pulmonary collateral flow is important in Fontan patients (24) and can be treated by collateral coiling, making non-invasive assessment of SPCF relevant to identify patients that may require coiling. While 2D and 4D flow MRI can non-invasively quantify SPCF(2, 10, 11), both have specific disadvantages. Planning of multiple 2D flow planes is labor intensive and time-consuming to acquire. Furthermore, RPA flow is often acquired distal to the (early branching) right upper lobe PA, leading to errors in calculated pulmonary flow distribution and right SPCF. 4D flow has the advantage of minimal user input (single acquisition), but scan time is long(2). This study demonstrates that 3D flow overcomes the 2D and 4D flow MRI limitations by allowing for SPCF quantification within a 1.5 minute acquisition and, importantly, showed a high reproducibility (scan-rescan). 3D flow measured systematically lower SPCF compared with 4D, but no comparison with gold standard 2D flow derived SPCF could be made in this study. However, a previous study comparing 2D and 4D flow derived SPCF also measured lower SPCF with 2D compared to 4D flow (mean 0.41 vs 0.62 L/min/m<sup>2</sup>, respectively)(2).

Regular evaluation of extracardiac conduit size adequacy, implanted at 3-5 years of age, is important to ensure an efficient TCPC(25, 26). An early cohort of Fontan patients with 16mm conduits are reaching adulthood and it is unknown whether these conduits are suitable for adult patients or need replacement for larger conduits(1). The MRI derived IVC-conduit mismatch percentage (relative increase in mean velocity from IVC towards the conduit) can be useful for identification of patients developing evident IVC-conduit mismatch during somatic growth(13). Good agreement between 2D and 3D flow was observed, especially for values >100%. 3D flow therefore allows for the accurate identification of patients with evident mismatch, which can be in the order of >200%(13), and may guide when replacement is indicated. Since this parameter is based on mean velocities, some observed variability may be explained by user-variability in correct alignment of the 2D plane perpendicular to the vessel.

Unbalanced caval flow contribution, especially the contribution of conduit flow towards the left PA known as the hepatic flow distribution (HFD)(9), is associated with pulmonary arteriovenous malformations. While 4D flow MRI has been used for the quantification of caval flow contribution, in our study on average 18-24% of emitted particles did not reach the pulmonary arteries. The percentage of missing particles, related to factors such as velocity noise or low spatial resolution, is often not reported(6, 7), but will influence the accuracy of results(20). 3D flow showed important variability in measured caval flow contribution (using streamline tracing) compared with 4D flow and thus is unsuitable for this parameter.

Of important note, although some measurements were significantly different between 2D and 3D flow while not between 2D and 4D flow, mean absolute differences were similar/lower for all parameters between 2D and 3D compared to 2D and 4D. This reflects an important observation: there is larger variability in measurements with 4D flow (both under- and overestimation, resulting on average in a non-significant difference) compared to 2D flow, while differences with 3D flow were more systematic (similar/smaller absolute differences, but in general underestimation resulting in a significant difference). Systemic errors can be corrected for which is not possible for random errors, making 3D flow the preferable approach from the perspective of the individual patient.

Of note, 3D and 4D flow acquisitions (end-expiratory navigated acquisitions) are expected to measure lower flowrates in comparison with 2D flow (free-breathing) since flow is lowest during expiration with augmentation during inspiration (27-29), most pronounced from the lower body. The significant lower mean velocities and/or flow in the IVC and conduit measured with 3D flow compared to 2D flow is therefore in line with this difference in physiology

## Limitations

The different protocols (free breathing versus respiratory navigator) may have affected flow conditions and subsequent comparisons. Furthermore, 2D-three-directional flow was acquired instead of through-plane 2D flow, which may have introduced differences with clinical standard through-plane 2D flow due to longer acquisition times. Additionally, although respiratory motion suppression improves data quality in 3D and 4D flow, the influence of respiration on flow characteristics in the TCPC are not captured with 2D, 3D or 4D flow measurements.

## Future perspectives

Optimization of 3D flow (e.g. increased spatial resolution, multiple signal averages) can allow for scanning of younger children with smaller vessels. As smaller voxel sizes increase scan time, this optimization is not possible with current 4D flow acquisitions without exceeding clinical acceptable scan times. Importantly, the achieved reduction in scan time from 4D to 3D flow did not require different acceleration techniques (e.g. compressed SENSE), and application of such techniques to the 3D flow sequence can further decrease scan time.

Comparison of 3D- and 4D-flow-derived hemodynamic parameters (e.g. viscous energy loss) are of interest (13, 25), as flow patterns captured with both methods were almost identical.

## Conclusions

3D flow MRI can be used to acquire multiple important cardiac-cycle averaged parameters of interest in the evaluation of the Fontan pathway: right-to-left pulmonary flow distribution, lower-to-upper body flow distribution, SPCF and IVC-conduit mismatch. A ten-fold reduction in scan time with improved image quality was achieved compared to 4D flow MRI. Since primarily cardiac-cycle averaged parameters are of clinical interest, 3D flow may replace time-resolved 2D and 4D flow MRI acquisitions to allow for a fast, accurate hemodynamic evaluation of the Fontan pathway. This could lead to shorter MRI protocols, allow for evaluation of younger Fontan patients, and improve the applicability of state-of-the-art three-dimensional flow imaging in clinical practice.

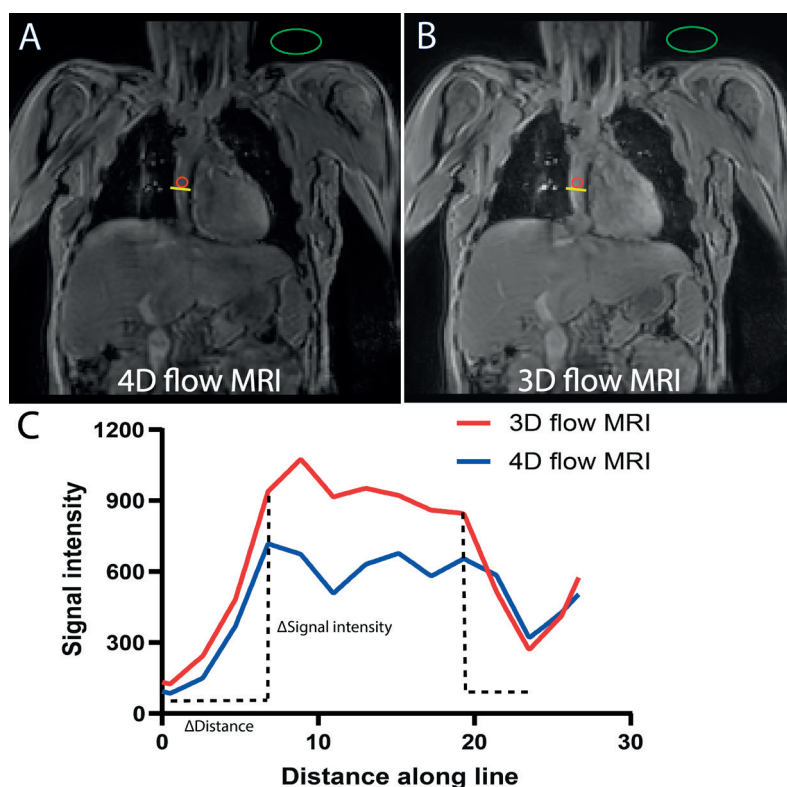
## References

1. Rychik J, Atz AM, Celermajer DS, Deal BJ, Gatzoulis MA, Gewillig MH, et al. Evaluation and Management of the Child and Adult With Fontan Circulation: A Scientific Statement From the American Heart Association. *Circulation*. 2019.
2. Valverde I, Nordmeyer S, Uribe S, Greil G, Berger F, Kuehne T, et al. Systemic-to-pulmonary collateral flow in patients with palliated univentricular heart physiology: measurement using cardiovascular magnetic resonance 4D velocity acquisition. *J Cardiovasc Magn Reson*. 2012;14:25.
3. Whitehead KK, Sundareswaran KS, Parks WJ, Harris MA, Yoganathan AP, Fogel MA. Blood flow distribution in a large series of patients having the Fontan operation: a cardiac magnetic resonance velocity mapping study. *J Thorac Cardiovasc Surg*. 2009;138(1):96-102.
4. Valsangiacomo Buechel ER, Grosse-Wortmann L, Fratz S, Eichhorn J, Sarikouch S, Greil GF, et al. Indications for cardiovascular magnetic resonance in children with congenital and acquired heart disease: an expert consensus paper of the Imaging Working Group of the AEPC and the Cardiovascular Magnetic Resonance Section of the EACVI. *Eur Heart J Cardiovasc Imaging*. 2015;16(3):281-97.
5. Akins CW, Travis B, Yoganathan AP. Energy loss for evaluating heart valve performance. *J Thorac Cardiovasc Surg*. 2008;136(4):820-33.
6. Bachler P, Valverde I, Pinochet N, Nordmeyer S, Kuehne T, Crelieu G, et al. Caval blood flow distribution in patients with Fontan circulation: quantification by using particle traces from 4D flow MR imaging. *Radiology*. 2013;267(1):67-75.
7. Jarvis K, Schnell S, Barker AJ, Garcia J, Lorenz R, Rose M, et al. Evaluation of blood flow distribution asymmetry and vascular geometry in patients with Fontan circulation using 4-D flow MRI. *Pediatr Radiol*. 2016;46(11):1507-19.
8. Jarvis K, Schnell S, Barker AJ, Rose M, Robinson JD, Rigsby CK, et al. Caval to pulmonary 3D flow distribution in patients with Fontan circulation and impact of potential 4D flow MRI error sources. *Magn Reson Med*. 2019;81(2):1205-18.
9. Dasi LP, Whitehead K, Pekkan K, de Zelicourt D, Sundareswaran K, Kanter K, et al. Pulmonary hepatic flow distribution in total cavopulmonary connections: extracardiac versus intracardiac. *J Thorac Cardiovasc Surg*. 2011;141(1):207-14.10. Grosse-Wortmann L, Al-Otay A, Yoo SJ. Aortopulmonary collaterals after bidirectional cavopulmonary connection or Fontan completion: quantification with MRI. *Circ Cardiovasc Imaging*. 2009;2(3):219-25.
11. Whitehead KK, Gillespie MJ, Harris MA, Fogel MA, Rome JJ. Noninvasive quantification of systemic-to-pulmonary collateral flow: a major source of inefficiency in patients with superior cavopulmonary connections. *Circ Cardiovasc Imaging*. 2009;2(5):405-11.
12. Fratz S, Chung T, Greil GF, Samyn MM, Taylor AM, Valsangiacomo Buechel ER, et al. Guidelines and protocols for cardiovascular magnetic resonance in children and adults with congenital heart disease: SCMR expert consensus group on congenital heart disease. *J Cardiovasc Magn Reson*. 2013;15:51.
13. Rijnberg FM, Elbaz MSM, Westenberg JJM, Kamphuis VP, Helbing WA, Kroft LJ, et al. Four-dimensional flow magnetic resonance imaging-derived blood flow energetics of the inferior vena cava-to-extracardiac conduit junction in Fontan patients. *Eur J Cardiothorac Surg*. 2019;55(6):1202-10.



14. Markl M, Geiger J, Kilner PJ, Foll D, Stiller B, Beyersdorf F, et al. Time-resolved three-dimensional magnetic resonance velocity mapping of cardiovascular flow paths in volunteers and patients with Fontan circulation. *Eur J Cardiothorac Surg*. 2011;39(2):206-12.
15. Sundareswaran KS, Haggerty CM, de Zelicourt D, Dasi LP, Pekkan K, Frakes DH, et al. Visualization of flow structures in Fontan patients using 3-dimensional phase contrast magnetic resonance imaging. *J Thorac Cardiovasc Surg*. 2012;143(5):1108-16.
16. Khiabani RH, Whitehead KK, Han D, Restrepo M, Tang E, Bethel J, et al. Exercise capacity in single-ventricle patients after Fontan correlates with haemodynamic energy loss in TCPC. *Heart*. 2015;101(2):139-43.
17. Houliind K, Stenbog EV, Sorensen KE, Emmertsen K, Hansen OK, Rybro L, et al. Pulmonary and caval flow dynamics after total cavopulmonary connection. *Heart*. 1999;81(1):67-72.
18. Klimes K, Abdul-Khaliq H, Ovroutski S, Hui W, Alexi-Meskishvili V, Spors B, et al. Pulmonary and caval blood flow patterns in patients with intracardiac and extracardiac Fontan: a magnetic resonance study. *Clin Res Cardiol*. 2007;96(3):160-7.
19. Landgraf BR, Johnson KM, Roldan-Alzate A, Francois CJ, Wieben O, Reeder SB. Effect of temporal resolution on 4D flow MRI in the portal circulation. *J Magn Reson Imaging*. 2014;39(4):819-26.
20. Ha H, Kang H, Huh H, Choi W, Koo HJ, Kwon J, et al. Accuracy evaluation of blood flow distribution in the Fontan circulation: effects of resolution and velocity noise. *Journal of Visualization*. 2019;22(2):245-57.
21. Kamphuis VP, Elbaz MSM, van den Boogaard PJ, Kroft LJM, van der Geest RJ, de Roos A, et al. Disproportionate intraventricular viscous energy loss in Fontan patients: analysis by 4D flow MRI. *Eur Heart J Cardiovasc Imaging*. 2019;20(3):323-33.
22. Paz R, Mohiaddin RH, Longmore DB. Magnetic resonance assessment of the pulmonary arterial trunk anatomy, flow, pulsatility and distensibility. *Eur Heart J*. 1993;14(11):1524-30.
23. Alsaied T, Sleeper LA, Masci M, Ghelani SJ, Azcue N, Geva T, et al. Maldistribution of pulmonary blood flow in patients after the Fontan operation is associated with worse exercise capacity. *J Cardiovasc Magn Reson*. 2018;20(1):85.
24. Prakash A, Rathod RH, Powell AJ, McElhinney DB, Banka P, Geva T. Relation of systemic-to-pulmonary artery collateral flow in single ventricle physiology to palliative stage and clinical status. *Am J Cardiol*. 2012;109(7):1038-45.
25. Rijnberg FM, Hazekamp MG, Wentzel JJ, de Koning PJH, Westenberg JJM, Jongbloed MRM, et al. Energetics of Blood Flow in Cardiovascular Disease: Concept and Clinical Implications of Adverse Energetics in Patients With a Fontan Circulation. *Circulation*. 2018;137(22):2393-407.
26. Tang E, Restrepo M, Haggerty CM, Mirabella L, Bethel J, Whitehead KK, et al. Geometric characterization of patient-specific total cavopulmonary connections and its relationship to hemodynamics. *JACC Cardiovasc Imaging*. 2014;7(3):215-24.
27. Hjortdal VE, Emmertsen K, Stenbog E, Frund T, Schmidt MR, Kromann O, et al. Effects of exercise and respiration on blood flow in total cavopulmonary connection: a real-time magnetic resonance flow study. *Circulation*. 2003;108(10):1227-31.
28. Korperich H, Barth P, Gieseke J, Muller K, Burchert W, Esdorn H, et al. Impact of respiration on stroke volumes in paediatric controls and in patients after Fontan procedure assessed by MR real-time phase-velocity mapping. *Eur Heart J Cardiovasc Imaging*. 2015;16(2):198-209.
29. Wei Z, Whitehead KK, Khiabani RH, Tree M, Tang E, Paridon SM, et al. Respiratory Effects on Fontan Circulation During Rest and Exercise Using Real-Time Cardiac Magnetic Resonance Imaging. *Ann Thorac Surg*. 2016;101(5):1818-25.

## Supplementary materials



**Supplemental Figure 1. vessel sharpness and SNR.**

Magnitude images of **(A)** 4D (phase 0) and **(B)** 3D flow MRI acquisitions are shown for a Fontan patient with an extracardiac conduit.

**(B)** The vessel sharpness was quantified by placing a measurement line perpendicular to the Fontan conduit. **(C)** A line intensity profile was determined and the slope of this profile was calculated at either side of the vessel and then averaged, resulting in an overall vessel sharpness measurement. The slopes were calculated by dividing the difference in minimal and maximal signal intensity by the difference in distance. **(A-B)** SNR was determined by placement of standardized region of interests (ROIs) in the Fontan conduit (red,  $\pm 0.5\text{cm}^2$ ) and in the air (green,  $\pm 5\text{cm}^2$ ). The SNR was calculated by dividing the mean signal intensity in the ROI in the Fontan conduit by the standard deviation of the signal intensity in the ROI in the air. The same positions of lines and ROIs were used in both datasets per patient

**Supplemental Table 1.** Inter- and intraobserver analysis of 3D and 4D flow MRI measurements (n=10)

	4D flow MRI	4D flow MRI intra	4D flow MRI inter	3D flow MRI	3D flow MRI intra	3D flow MRI inter	4D vs 4D <sub>inter</sub>	3D vs 3D <sub>inter</sub>	Paired t-test P-value
<b>Flow + Velocity</b>									
Conduit, ml/s	47.5 (10.8)	47.8 (10.6)	45.8 (9.6)	46.0 (10.7)	46.8 (11.1)	45.4 (9.8)	0.72	0.06	0.36
SVC, ml/s	23.9 (6.9)	24.1 (6.2)	24.0 (6.4)	23.9 (7.3)	23.4 (6.5)	23.6 (7.9)	0.80	0.98	0.72
RPA, ml/s	35.9 (11.0)	36.4 (11.6)	35.0 (10.9)	34.5 (10.4)	34.8 (10.6)	34.9 (10.9)	0.56	<b>0.02</b>	0.23
LPA, ml/s	28.2 (13.2)	27.9 (12.8)	29.1 (14.9)	26.6 (12.5)	26.9 (12.1)	27.6 (13.7)	0.74	0.22	0.36
PV right, ml/s	47.9 (9.7)	47.9 (8.7)	47.0 (11.1)	44.4 (10.8)	44.5 (11.5)	44.2 (11.0)	0.94	0.40	0.56
PV left, ml/s	36.8 (10.9)	36.1 (8.9)	37.1 (12.1)	33.1 (10.8)	33.3 (9.8)	32.6 (10.7)	0.50	0.75	0.42
PV total, ml/s	83.5 (19.0)	84.0 (14.4)	84.0 (19.6)	77.8 (18.3)	77.7 (18.1)	76.8 (18.5)	0.67	0.66	0.36
IVC, cm/s	13.1 (2.4)	13.3 (2.4)	13.7 (2.3)	12.5 (2.5)	12.6 (2.5)	13.3 (2.5)	0.32	<b>0.03</b>	0.07
Conduit, cm/s	23.1 (7.4)	25.0 (7.1)	26.0 (7.2)	22.6 (6.6)	23.5 (8.0)	23.3 (7.4)	0.15	<b>0.02</b>	0.42
<b>Derived parameters</b>									
SPCF right, ml/s	12.0 (10.1)	11.5 (11.6)	11.9 (10.9)	9.9 (8.1)	9.6 (8.2)	9.2 (8.5)	0.61	0.97	<b>0.03</b>
SPCF left, ml/s	8.7 (6.3)	8.2 (7.8)	8.0 (7.0)	6.5 (4.0)	6.4 (3.8)	5.1 (5.4)	0.61	0.21	0.15
SPCF total, ml/s	20.7 (13.1)	19.7 (13.8)	20.0 (14.7)	16.4 (9.5)	16.0 (8.9)	14.5 (9.7)	0.47	0.67	0.07
Lower-to-upper body flow distribution, %	66.5 (6.9)	66.3 (6.5)	65.7 (6.3)	65.9 (4.9)	66.6 (4.9)	65.9 (6.7)	0.80	0.07	0.97
Right-to-left pulmonary flow distribution, %	56.9 (15.3)	57.2 (16.3)	56.0 (16.3)	57.1 (13.8)	57.0 (13.3)	56.6 (14.2)	0.71	0.11	0.67
IVC-Conduit mismatch, %	76.5 (52.5)	88.6 (44.3)	89.7 (42.6)	84.2 (53.5)	87.8 (52.3)	75.9 (49.8)	0.31	0.22	0.42

Values are reported as mean (SD). ml/s; milliliter per second. MRI; magnetic resonance imaging, IVC/SVC; inferior/superior vena cava, RPA/LPA; right/left pulmonary artery. Right-to-left pulmonary flow distribution: RPA flow/ LPA flow \*100%  
PV; pulmonary veins, SPCF; systemic-to-pulmonary collateral flow (pulmonary vein – pulmonary artery flow).

**Supplemental Table 1.** Continued intraobserver analysis

	<b>4D vs 4D<sub>intra</sub></b>			<b>3D vs 3D<sub>intra</sub></b>		
	Bland-Altman		Intraclass correlation	Bland-Altman		Intraclass correlation
	Mean difference	LoA	ICC	Mean difference	LoA	ICC
<b>Flow + Velocity</b>						
Conduit, ml/s	- 0.3	-4.6 – 4.0	0.98	-0.7	-3.3 – 1.8	0.99
SVC, ml/s	- 0.2	-3.7 – 3.4	0.97	0.6	-2.2 – 3.3	0.98
RPA, ml/s	-0.4	-4.6 – 3.8	0.98	-0.4	-1.6 – 0.9	0.99
LPA, ml/s	0.2	-4.0 – 4.4	0.99	-0.2	-3.3 – 2.8	0.99
PV right, ml/s	0.1	-4.5 – 4.6	0.97	-0.1	-2.1 – 2.0	0.99
PV left, ml/s	0.7	-5.6 – 7.0	0.95	-0.2	-3.3 – 3.0	0.99
PV total, ml/s	0.8	-9.1 – 10.7	0.96	-0.2	-3.7 – 3.3	0.99
IVC, cm/s	-0.2	-1.6 – 1.1	0.96	-0.1	-1.9 – 1.7	0.94
Conduit, cm/s	-1.9	-9.3 – 5.5	0.85	-0.8	-6.4 – 4.7	0.93
<b>Derived parameters</b>						
SPCF right, ml/s	0.5	-5.0 – 6.0	0.97	0.3	-2.0 – 2.6	0.99
SPCF left, ml/s	0.5	-5.2 – 6.2	0.92	0.1	-3.1 – 3.2	0.92
SPCF total, ml/s	1.0	-6.9 – 8.8	0.96	0.4	-3.2 – 4.0	0.98
Lower-to-upper body flow distribution, %	0.1	-4.1 – 4.4	0.95	-0.8	-4.1 – 2.6	0.93
Right-to-left pulmonary flow distribution, %	-0.3	-4.5 – 3.9	0.99	0.1	-1.9 – 2.0	0.99
IVC-conduit mismatch, %	-12.1	-81.9 – 57.7	0.73	-3.9	-63.4 – 55.6	0.85

**Supplemental Table 1.** Continued observer analysis

	4D vs 4D <sub>inter</sub>			3D vs 3D <sub>inter</sub>		
	Bland-Altman		Intraclass correlation	Bland-Altman		Intraclass correlation
	Mean difference	LoA	ICC	Mean difference	LoA	ICC
<b>Flow + Velocity</b>						
Conduit, ml/s	1.8	-3.2 – 6.7	0.96	0.7	-3.6 – 5.0	0.97
SVC, ml/s	0.0	-2.7 – 2.6	0.98	0.3	-4.5 – 5.0	0.95
RPA, ml/s	0.9	-1.1 – 2.9	0.99	-0.5	-2.7 – 1.7	0.99
LPA, ml/s	0.9	-5.1 – 3.3	0.99	-0.9	-6.8 – 5.0	0.97
PV right, ml/s	1.0	-5.7 – 7.6	0.95	0.2	-2.0 – 2.4	0.99
PV left, ml/s	0.2	-4.7 – 4.2	0.98	0.5	-2.9 – 3.9	0.99
PV total, ml/s	0.7	-9.0 – 10.4	0.97	1.0	-3.5 – 5.5	0.99
IVC, cm/s	-0.6	-2.0 – 0.8	0.93	-0.8	-3.3 – 1.7	0.84
Conduit, cm/s	-2.8	-9.0 – 3.4	0.85	-0.6	-5.2 – 4.0	0.95
<b>Derived parameters</b>						
SPCF right, ml/s	0.1	-7.3 – 7.4	0.94	0.7	-0.9 – 2.3	0.99
SPCF left, ml/s	0.7	-2.3 – 3.7	0.97	1.4	-4.1 – 6.8	0.81
SPCF total, ml/s	0.7	-9.4 – 10.8	0.94	2.1	-3.5 – 7.6	0.94
Lower-to-upper body flow distribution, %	0.8	-1.7 – 3.4	0.98	0.0	-6.0 – 5.9	0.82
Right-to-left pulmonary flow distribution, %	0.9	-2.2 – 4.0	0.99	0.5	-6.6 – 7.6	0.97
IVC-conduit mismatch, %	-13.2	-75.1 – 48.8	0.77	8.3	-52.8 – 69.4	0.82

Values are reported as mean (SD). ml/s; milliliter per second, MRI; magnetic resonance imaging, LoA; limits of agreement, IVC/SVC; inferior/superior vena cava, RPA/LPA; right/left pulmonary artery. Right-to-left pulmonary flow distribution: RPA flow/ LPA flow \*100%, PV; pulmonary veins, SPCF; systemic-to-pulmonary collateral flow (pulmonary vein – pulmonary artery flow).

**Supplemental table 2.** Scan-rescan analysis of 3D flow MRI.

	Measurements		3D vs 3Drescan flow				Mean absolute difference
	3D flow MRI	3D flow MRI rescan	T-test	Bland-Altman	Intraclass correlation		
	(N=10)	(n=10)					
Flow + Velocity			P-value	Mean difference	LoA	ICC	(± 1.96 SEM)
Conduit, ml/s	46.9 (9.6)	46.2 (10.2)	0.50	0.6	-4.7 – 6.0	0.96	2.2 (1.2-3.2)
SVC, ml/s	23.5 (4.8)	23.5 (4.3)	0.97	0.0	-4.7 – 4.7	0.86	1.7 (0.6-2.7)
RPA, ml/s	36.5 (8.4)	36.4 (8.6)	0.86	0.1	-3.7 – 3.9	0.97	1.6 (1.1-2.2)
LPA, ml/s	29.5 (9.9)	29.4 (8.5)	0.92	0.1	-4.5 – 4.6	0.97	1.9 (1.2-2.6)
PV right, ml/s	44.9 (11.8)	44.7 (11.3)	0.88	0.1	-4.9 – 5.1	0.98	1.6 (0.4-2.8)
PV left, ml/s (n=6)	35.3 (10.3)	35.1 (9.8)	0.85	0.2	-4.3 – 4.6	0.98	1.6 (0.5-2.8)
PV total, ml/s (n=6)	84.4 (16.4)	83.6 (17.6)	0.22	0.8	-2.0 – 3.6	0.99	1.3 (0.5-2.0)
IVC, cm/s	13.2 (2.4)	13.4 (2.2)	0.39	-0.3	-2.6 – 1.9	0.89	0.9 (0.4-1.4)
Conduit, cm/s	20.9 (5.3)	21.2 (5.5)	0.66	-0.3	-3.7 – 3.2	0.95	1.4 (0.7-2.0)
Derived parameters							
SPCF right, ml/s	8.3 (7.5)	8.3 (8.5)	0.99	0.0	-5.1 – 5.2	0.95	2.0 (1.0-3.0)
SPCF left, ml/s (n=6)	5.6 (2.7)	5.9 (2.9)	0.71	-0.3	-4.4 – 3.7	0.73	1.5 (0.5-2.5)
SPCF total, ml/s (n=6)	16.6 (6.3)	17.6 (8.0)	0.37	-1.0	-5.8 – 3.8	0.94	1.9 (0.6-3.2)
Lower-to-upper body flow distribution, %	66.4 (3.8)	66.1 (4.1)	0.72	0.3	-4.9 – 5.6	0.77	2.1 (1.0-3.1)
Right-to-left pulmonary flow distribution, %	55.8 (8.1)	55.5 (8.2)	0.62	0.3	-3.7 – 4.4	0.97	1.6 (0.8-2.4)
Conduit-LPA, %	57.4 (28.5)	48.6 (18.4)	<b>0.04</b>	8.8	-14.3 – 31.9	0.83	11.7 (6.3-17.0)
SVC-RPA, %	69.3 (20.2)	73.5 (29.3)	0.53	-4.2	-44.0 – 35.7	0.67	15.6 (7.7-23.5)
IVC-conduit mismatch, % (n=9)	66.5 (63.2)	60.10 (45.9)	0.42	6.4	-38.5 – 51.3	0.91	17.3 (7.3-27.3)

\* Values are in ml/s unless otherwise specified. Values are reported as mean (SD). LoA; limits of agreement, IVC/ SVC; inferior/superior vena cava, RPA/LPA; right/left pulmonary artery. PV; pulmonary veins, SPCF; systemic-to-pulmonary collateral flow (pulmonary venous – pulmonary artery flow). SEM; standard error of the mean



# CHAPTER 6

# Segmental analysis of blood flow dynamics in the TCPC



# CHAPTER 6A

# Segmental assessment of blood flow efficiency in the total cavopulmonary connection using 4D flow MRI: vortical flow is associated with increased viscous energy loss

Friso M. Rijnberg, Joe F. Juffermans, Mark G. Hazekamp, Willem A. Helbing, Hildo J. Lamb, Arno A.W. Roest, Jos J.M. Westenberg, Hans C. van Assen.

# Abstract

## Objectives

To study flow-related energetics in multiple anatomical segments of the total cavopulmonary connection (TCPC) in Fontan patients from 4D flow MRI, and to study the relationship between adverse flow patterns and segment-specific energetics.

## Methods

Twenty-six extracardiac Fontan patients underwent 4D flow MRI of the TCPC. A segmentation of the TCPC was automatically divided into 5 anatomical segments (conduit, superior vena cava, right/left pulmonary artery (PA) and the Fontan confluence). The presence of vortical flow in the PAs or Fontan confluence was qualitatively scored. Kinetic energy, viscous energy loss and vorticity were calculated from the 4D flow MRI velocity field and normalized for segment length and/or inflow. Energetics were compared between segments and the relationship between vortical flow and segment cross-sectional area (CSA) with segment-specific energetics was determined.

## Results

Vortical flow in the LPA (n=6) and Fontan confluence (n=12) were associated with significantly higher vorticity ( $p=0.001$  and  $p=0.015$ , respectively) and viscous energy loss rate ( $p=0.046$  and  $p=0.04$ , respectively) compared to patients without vortical flow. The LPA and conduit segments showed the highest kinetic energy and viscous energy loss rate, while most favorable energetics were observed in the superior vena cava. Conduit CSA inversely correlated with kinetic energy ( $r=-0.614$ ,  $p=0.019$ ) and viscous energy loss rate ( $r=-0.652$ ,  $p=0.011$ ).

## Conclusions

Vortical flow in the Fontan confluence and LPA associated with significantly increased viscous energy loss rate. 4D flow MRI derived energetics may be used as a screening tool for direct, MRI-based assessment of flow efficiency in the TCPC.

## Introduction

The Fontan circulation redirects systemic venous blood flow directly towards the pulmonary arteries (PAs), the so called total cavopulmonary connection (TCPC). Consequently, a relatively non-pulsatile, passive pulmonary circulation is present leading to increased central venous pressure and reduced cardiac output(1, 2), both associated with important morbidity. Computational fluid dynamic (CFD) studies have found correlations between adverse, energy-consuming flow patterns and TCPC geometries and adverse outcome, including an elevated central venous pressure(3), reduced cardiac output(4) and reduced exercise performance(5). Therefore, ideally the geometry of the TCPC needs to maximally conserve the limited available energy in the blood flow to achieve optimal hemodynamics, and inefficient areas may be improved by targeted interventions.

Altered flow patterns have been identified in various TCPC segments(6-9). However, 4D flow MRI is able not only to visualize flow patterns in the TCPC *in vivo*(6, 8-10), but also allows novel, voxel-wise quantitative measurements of energy in the flow, e.g. viscous energy loss(6, 8, 11, 12). Thus, 4D flow can provide insights in the energetic consequences of these adverse flow patterns.

However, the comparison of 4D flow derived TCPC energetics in the heterogeneous Fontan population is subject to unique challenges that requires a standardized analysis approach which is currently not available. For example, part of the TCPC can often not be evaluated due to device-related (e.g. fenestration closure device) artefacts making direct comparison between patients without these devices unfeasible. To study 4D flow MRI derived energetics in the TCPC, a standardized analysis approach is needed that divides the TCPC into multiple anatomical segments: extracardiac conduit, Fontan confluence, the left (LPA) and right PAs (RPA) and the superior vena cava (SVC). This approach allows for the direct comparison of segment-specific energetics between patients and between different segments within a patient, but also allows to compare energetics from serial 4D flow scans within one patient.

The aim of this study was to use an automated, segmental analysis approach to 1) evaluate 4D flow derived energetics within five anatomical segments of the TCPC and 2) correlate adverse flow patterns to blood flow energetics within these segments.

## Material and Methods

Twenty-six patients with a previous Fontan operation using an extracardiac conduit were retrospectively selected from a local database containing both clinical (routine follow-up, n=7) and research 4D flow MRI scans (n=19) acquired between 2013-2017 (3T, Ingenia, Philips Healthcare, Best, the Netherlands). 4D flow acquisition details are presented in Supplemental Table 1. All 4D flow MRI acquisitions were performed under free-breathing conditions without the use of a respiratory navigator. All patients in this study had either 1) no fenestration performed during surgery or 2) a closed fenestration, either spontaneously or with the use of a fenestration closure device. Long-term outcome was assessed by reviewing the latest medical records for deterioration in NYHA class, newly-onset tachyarrhythmia or failure of the Fontan circulation (cardiac transplant, protein losing enteropathy, death, Fontan take-down) in April 2021. The study was approved by the Medical Ethical Committee and written informed-consent was obtained from all patients and/or guardians.

### Division of the TCPC into standardized segments

A 3D reconstruction of the TCPC, covering the extracardiac conduit, SVC (below the brachiocephalic vein), Fontan confluence and the right- and left PAs, was semi-automatically segmented on magnitude-weighted velocity images at the cardiac phase with highest flow (CAAS, MR Solutions, Pie Medical Imaging, Figure 1A-B). In patients with a fenestration closure device or PA stent in situ, only part of the conduit (distal to the device) or PA (proximal to the stent) was included in the segmentation because of device-related flow artifacts. TCPC segments (RPA, LPA, conduit and SVC) with a centerline length <1.5cm were excluded to ensure a sufficient number of voxels in each segment.

To divide the 3D TCPC segmentation into five standardized anatomical segments, the following steps were required; firstly, vessel centerlines were automatically generated between all vessels (Figure 1A, using in-house developed software(13)). Subsequently, the TCPC was automatically divided into five anatomical segments, by clipping the geometry perpendicular to the centerline at the centerline bifurcation points (Figure 1B). The functional caval offset (in millimeter, mm), representing how much conduit and SVC flows are set apart to avoid flow collision, was quantified as the distance between the projection of the bifurcation vectors of the conduit and SVC on a plane between the bifurcation vectors of the RPA and LPA (Figure 1C). The cross-sectional area of the conduit, SVC, LPA and RPA were determined perpendicularly to the centerline at a 1mm interval. The mean CSA of the segment was used and normalized for body surface area (BSA).

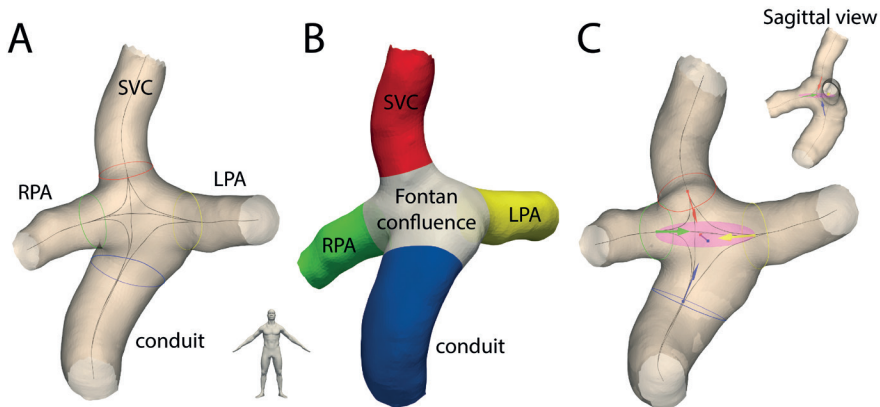


**Figure 1.** The 3D geometry of the TCPC was automatically divided into 5 anatomical segments by dividing the geometry perpendicular to the centerline (black lines) bifurcation points (colored circles, Figure 1A). The resulting division in 5 anatomical segments is shown in Figure 1B. The functional caval offset (in millimeter, mm) was quantified as the distance between the projection of the bifurcation vectors of the conduit and SVC on a plane (pink) between the bifurcation vectors of the RPA and LPA (Figure 1C).

*SVC; superior vena cava, RPA/LPA; right/left pulmonary artery*

## Qualification of flow patterns

The presence of vortical flow was qualitatively rated within the standardized segments of the Fontan confluence, RPA and LPA. Vortical flow was defined as the presence of a swirling flow  $>360$  degrees in the majority ( $>50\%$ ) of streamlines and/or pathlines. Flow collision between conduit and SVC flow within the Fontan confluence was qualitatively determined, defined as collision of  $>50\%$  of streamlines/pathlines.

Segments were dichotomized based on the presence/absence of vortical flow (LPA, RPA, Fontan confluence) or caval flow collision (Fontan confluence) and normalized flow energetics (see below) within these segments were compared between the groups. To determine the reproducibility of the qualitative rating of flow patterns, inter-observer analysis was performed on blinded datasets for all cases.

## Blood flow energetics

Multiple flow-related energetics were quantified from 4D flow MRI for each voxel within the segments(11, 14). The total amount of each energetic in the different segments was computed for each cardiac phase (25-30 phases per cardiac cycle) by summing voxel-wise energetics within the segment. The cardiac-cycle averaged energetic values were reported. Quantitative energetics included kinetic energy (KE, in millijoules [mJ]), viscous energy loss rate ( $\dot{E}_L$ , in milliwatts [mW]) and vorticity (Vort, in 1/s). KE is the amount of energy present in the blood flow due to motion.  $\dot{E}_L$  represents the amount

of KE within the blood flow lost per second due to viscosity-induced frictional forces(11, 14). Vorticity represents the amount of spinning motion of the blood flow around a common axis(15). In addition, the proportionality of viscous energy loss to the total amount of KE present during the cardiac cycle was calculated using the dimensionless  $EL_{index}$  ( $EL/KE$ ) as a marker of flow efficiency (16).

### Normalization of blood flow energetics

Segmental energetics of the LPA, RPA, SVC and conduit were normalized for inflow rate (in L/min) through each segment and for centerline length of the segment to correct for differences in the extent of the TCPC segmentation (e.g. part of the TCPC can often not be evaluated due to device-related artefacts);  $EL_{norm\_flow+length}$  and  $KE_{norm\_flow+length}$  in mW and mJ, both per L/min per cm segment, respectively, and  $Vort_{norm\_flow+length}$  in 1/s per L/min per cm segment. The rationale of the chosen normalization is given in the discussion. The Fontan confluence segment was normalized for flow only ( $KE_{norm\_flow}$ ,  $EL_{norm\_flow}$  and  $Vort_{norm\_flow}$ ) as this segment is always completely included in the segmentation in all patients.

### Statistical analysis

Continuous data were presented as median + interquartile range (IQR). Energetics comparisons between segments were performed using the Kruskal Wallis test or Mann-Whitney U test, with post-hoc Dunn's test for multiple comparisons. Inter-observer variability was tested using Cohen's Kappa test (0-0.2 poor, 0.2-0.4 fair, 0.4-0.6 moderate, 0.6-0.8 good, 0.8-1.0 very good agreement. A p-value <0.05 was considered statistically significant. Data were analyzed with SPSS 25.0 (SPSS, IBM Corp., Armonk, NY, USA) and Prism 8.0 (Graphpad Software, La Jolla, CA, USA).

## Results

Characteristics of the study population are presented in Table 1. The following number of segments were excluded from analysis: conduit n=12, SVC n=8, LPA n=2, RPA n=4. Main reasons for the exclusion of the segments (centerline length <1.5cm) were the presence of a fenestration closure device (conduit segments, n=13), PA stent (LPA segment, n=1), or because of only a small contribution to the TCPC (RPA and SVC segments). Since the SVC and conduit are often anastomosed close to the hilum of the right lung, the length of the RPA before subdivision into the segmental branches or the length of the SVC below the brachiocephalic vein can be short.

## Qualitative flow patterns vs quantitative blood flow energetics

Results of qualitative flow patterns versus quantitative energetics are shown in Table 2-3. Vortical flow was present within the Fontan confluence in 12 patients (46%, Figure 2A, Supplemental video 1), with a significantly higher  $Vort_{norm\_flow}$  (7746 (IQR 4084) vs 5825 (IQR 2592) per second per L/min inflow,  $p=0.015$ ) and  $\dot{E}L_{norm\_flow}$  (0.018 (IQR 0.0073) vs 0.013 (IQR 0.0072) mW per L/min,  $p=0.046$ ) compared to patients without vortical flow (Table 2).

**Table 1.** Characteristics of the study population

Male/Female	12/14
Primary diagnosis, n (%):	
HLHS	9 (35)
DILV + TGA	2 (8)
DORV +/- TGA	3 (11)
TA +/- TGA	5 (19)
ccTGA	2 (8)
PA+IVS	2 (8)
Other	3 (11)
Characteristics at 4D flow MRI	
Age (years)	14.4 (4.6, range 10.2-29.2)
Height (cm)	161 (17)
Weight (kg)	47 (21)
BSA (m <sup>2</sup> )	1.4 (0.4)
Conduit size (16mm/18mm/20mm)	18/5/3
NYHA class I-II, n (%)	26 (100)
Ejection fraction (%)	51 (8)

Values are presented as median (IQR). MRI; magnetic resonance imaging, BSA; body surface area (Haycock), HLHS; hypoplastic left heart syndrome, DILV; double inlet left ventricle, DORV; double outlet right ventricle, (cc) TGA; (congenitally corrected) transposition of great arteries, TA; tricuspid atresia

Caval flow collision was present in 8 (33%) patients. Patients with caval flow collision had significantly decreased caval offset (2.3mm (IQR 1.2) vs 5.2mm (IQR 3.4),  $p<0.001$ ). Only 3/8 patients with caval flow collision also showed vortical flow in the Fontan confluence with extension into the LPA in 2 patients. Patients with caval flow collision showed significantly lower  $KE_{norm\_flow}$ ,  $\dot{E}L_{norm\_flow}$  and  $Vort_{norm\_flow}$  compared to patients without caval flow collision (Table 2).



**Table 2.** Comparison of qualitative flow patterns vs quantitative energetics in the Fontan confluence

<b>Energetic</b>	<b>Vortical flow FC (n=12)</b>	<b>No Vortical flow FC (n=14)</b>	<b>P value</b>	<b>Caval flow collision (n=8)</b>	<b>No caval flow collision (n=18)</b>	<b>P value</b>
Vort <sub>norm_flow</sub>	7746 (4084)	5825 (2592)	<b>0.015</b>	5224 (2632)	7450 (2608)	<b>0.011</b>
KE <sub>norm_flow</sub>	0.069 (0.036)	0.050 (0.034)	0.053	0.041 (0.019)	0.069 (0.032)	<b>0.002</b>
ĖL <sub>norm_flow</sub>	0.022 (0.011)	0.016 (0.013)	<b>0.046</b>	0.011 (0.0058)	0.020 (0.0066)	<b>0.001</b>
EL <sub>index</sub>	0.20 (0.09)	0.18 (0.08)	0.35	0.19 (0.04)	0.19 (0.09)	0.94

Values are represented as median (interquartile range). Vort<sub>norm\_flow</sub>; vorticity in 1/s per L/min, KE<sub>norm\_flow</sub>; kinetic energy in millijoule per L/min, ĖL<sub>norm\_flow</sub>; viscous energy loss rate in milliwatt per L/min. L/min; liter per minute inflow (conduit + superior vena cava flow)

**Table 3.** Vortical flow patterns versus energetics in the left pulmonary artery

<b>Energetic</b>	<b>Vortical flow LPA (n=6)</b>	<b>No vortical flow LPA (n=18)</b>	<b>P value</b>
Vort <sub>norm_flow+length</sub>	3748 (1380)	2449 (684)	<b>0.001</b>
KE <sub>norm_flow+length</sub>	0.032 (0.019)	0.023 (0.015)	0.09
ĖL <sub>norm_flow+length</sub>	0.0085 (0.0058)	0.0060 (0.0035)	<b>0.04</b>
EL <sub>index</sub>	0.19 (0.05)	0.16 (0.06)	0.22

Values are represented as median (interquartile range). Vort<sub>norm\_flow+length</sub>; vorticity in 1/s per L/min per cm segment, KE<sub>norm\_flow+length</sub>; kinetic energy in millijoule per L/min per cm segment, ĖL<sub>norm\_flow+length</sub>; viscous energy loss rate in milliwatt per L/min per cm segment. L/min; liter per minute inflow, LPA; left pulmonary artery

Vortical flow was present in 6/24 LPA segments (Figure 2B, Supplemental Video 2) and 3/22 RPA segments. Patients with vortical flow inside the LPA showed significantly increased Vort<sub>norm\_flow+length</sub>, ĖL<sub>norm\_flow+length</sub> and KE<sub>norm\_flow+length</sub> compared to patients without vortical flow (Table 3). No significant differences in energetics could be identified between patients with/without vortical flow in the RPA.

Interobserver agreement was very good for the qualitative rating of caval flow collision and vortical flow in the Fontan confluence ( $\kappa=0.91$  and  $1.0$ , respectively) and good for the rating of vortical flow in the LPA ( $\kappa=0.78$ ) and RPA ( $\kappa=0.78$ ).

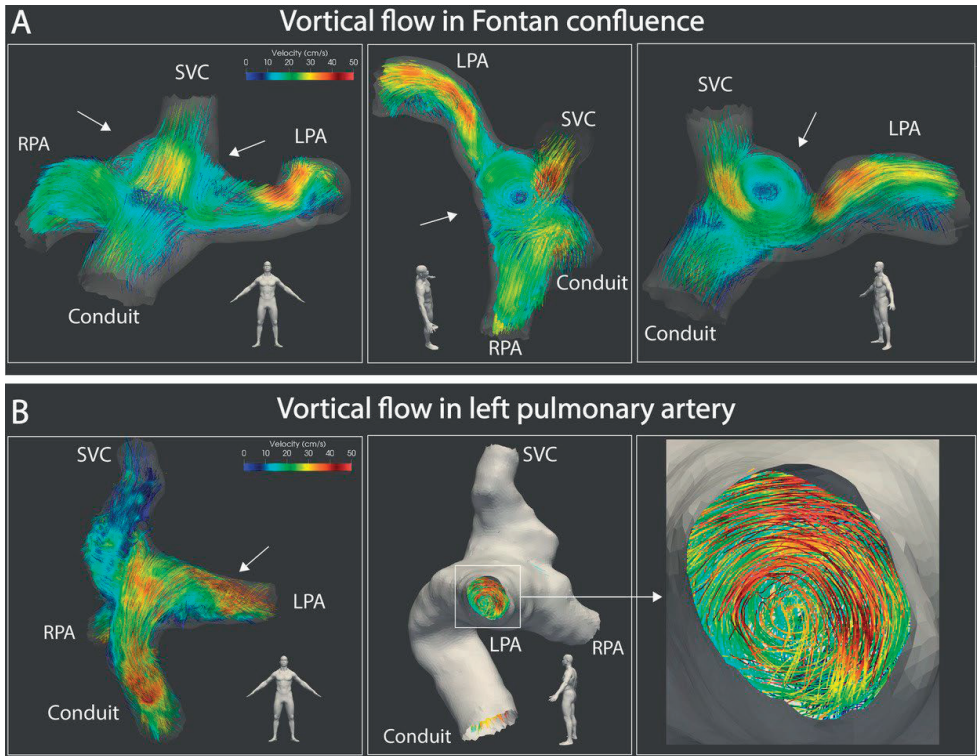


**Figure 2.** Streamline representation of blood flow in the TCPC is shown from multiple views for 2 patients with a previous Fontan operation using an extracardiac conduit (A-B). (A) A central vortex is shown at the Fontan confluence due to interaction between SVC and conduit flows. (B) Vortical flow is shown in the LPA.

### Energetics between TCPC segments

Results of energetics within the different segments are shown in Table 4.  $KE_{\text{norm\_flow+length}}$  was significantly higher in the conduit (0.029 (IQR 0.016)) and LPA (0.025 (IQR 0.013)) compared with the SVC (0.016 (IQR 0.0058) mJ per L/min inflow per cm segment,  $p=0.004$  and  $p<0.001$ , respectively).  $\dot{E}L_{\text{norm\_flow+length}}$  was significantly higher in the LPA (0.0060 (IQR 0.0040) compared with the SVC (0.0030 (IQR 0.0023),  $p<0.001$ ) and RPA (0.0038 (IQR 0.0028) mW per L/min inflow per cm segment,  $p=0.027$ ).  $\dot{E}L_{\text{norm\_flow+length}}$  in the conduit compared to the SVC did not reach significance ( $p=0.053$ ).  $EL_{\text{index}}$  was significantly higher in the FC (0.19 (IQR 0.075)) compared with the RPA (0.14 (IQR 0.050),  $p<0.001$ ) and conduit (0.15 (IQR 0.083),  $p=0.041$ ).  $Vort_{\text{norm\_flow+length}}$  was significantly higher in the LPA (2651 (IQR 1273)) compared with the RPA (1714 (IQR 758),  $p<0.001$ ).

### TCPC geometry

The mean CSA/BSA of the conduit, SVC, LPA and RPA are indicated in Table 5. A good inverse correlation was shown between normalized conduit CSA and  $KE_{\text{norm\_flow+length}}$  and

$\dot{E}L_{\text{norm\_flow+length}}$  and a moderate inverse correlation between normalized RPA CSA and  $\dot{E}L_{\text{norm\_flow+length}}$ . Furthermore, a positive correlation was present between normalized LPA CSA and  $\text{Vort}_{\text{norm\_flow+length}}$ .

Patients with vortical flow in the LPA (n=6) had significantly higher normalized LPA CSA compared to patients without vortical flow (138 (53) vs 94 (50) mm<sup>2</sup>/m<sup>2</sup>, p=0.014, respectively). Also patients with vortical flow in the RPA (n=3) had significantly higher normalized RPA CSA compared to patients without vortical flow (127 (range 102-172) vs 85 (28) mm<sup>2</sup>/m<sup>2</sup>, p=0.009, respectively).

## Follow-up

Mean follow-up after 4D flow MRI scan was 4.2 (SD 1.1) years. No patients experienced deterioration in NYHA class, newly-onset tachyarrhythmia or failure of the Fontan circulation (cardiac transplant, protein losing enteropathy, death, Fontan take-down).

**Table 4.** Blood flow energetics in the five anatomical segments of the TCPC

Anatomical segments	$KE_{\text{norm\_flow+length}}$	$\dot{E}L_{\text{norm\_flow+length}}$	$\text{Vort}_{\text{norm\_flow+length}}$	$EL_{\text{index}}$
Conduit (n=14)	0.029 (0.016)	0.0059 (0.0040)	2337 (412)	0.15 (0.083)
SVC (n=18)	0.016 (0.0058)	0.0030 (0.0023)	2335 (1204)	0.18 (0.040)
RPA (n=22)	0.023 (0.010)	0.0038 (0.0028)	1834 (658)	0.14 (0.050)
LPA (n=24)	0.025 (0.013)	0.0060 (0.0040)	2651 (1273)	0.17 (0.049)
Fontan confluence (n=26)	-	-	-	0.19 (0.075)

Values are represented as median (interquartile range).  $\text{Vort}_{\text{norm\_flow+length}}$ : vorticity in 1/s per L/min per cm segment,  $KE_{\text{norm\_flow+length}}$ : kinetic energy in millijoule per L/min per cm segment,  $\dot{E}L_{\text{norm\_flow+length}}$ : viscous energy loss rate in milliwatt per L/min per cm segment. L/min; liter per minute inflow.  $\dot{E}L$ , KE and Vort in the Fontan confluence were normalized for flow only and therefore not presented in this table. SVC; superior vena cava, RPA/LPA; right/left pulmonary artery, TCPC; total cavopulmonary connection

**Table 5.** Correlation between segment cross-sectional area and energetics

Anatomical segment	CSA/BSA (mm <sup>2</sup> /m <sup>2</sup> )	KE <sub>norm, flow+length</sub>			E <sub>L</sub> <sub>norm, flow+length</sub>			Vort <sub>norm, flow+length</sub>			E <sub>L</sub> <sub>index</sub>	
		Correlation coefficient	p-value		Correlation coefficient	p-value		Correlation coefficient	p-value		Correlation coefficient	p-value
Conduit (n=14)	130 (46)	-0.614	<b>0.019</b>		-0.652	<b>0.011</b>		-0.245	0.399		-0.499	0.069
SVC (n=18)	99 (26)	0.234	0.349		-0.044	0.862		0.335	0.174		-0.117	0.643
RPA (n=22)	89 (31)	-0.338	0.124		-0.440	<b>0.041</b>		-0.292	0.188		0.103	0.647
LPA (n=24)	103 (48)	-0.082	0.703		-0.068	0.753		<b>0.445</b>	<b>0.029</b>		0.252	0.234

Values are indicated as median (interquartile range). Correlation coefficients represent Pearson or Spearman rank analysis. Vort<sub>norm, flow+length</sub>; vorticity in 1/s per L/min per cm segment, KE<sub>norm, flow+length</sub>; kinetic energy in millijoule per L/min per cm segment, E<sub>L</sub><sub>norm, flow+length</sub>; viscous energy loss rate in milliwatt per L/min per cm segment. L/min; liter per minute inflow. SVC; superior vena cava, RPA/LPA; right/left pulmonary artery, CSA; cross-sectional area, BSA; body surface area (Haycock)

## Discussion

This study quantified in vivo 4D flow energetics in a cohort of patients with a previous Fontan operation using an automated analysis approach that divides the TCPC into standardized anatomical segments. Correlations between adverse vortical flow patterns in the LPA and Fontan confluence with quantitative flow-related energetics could be determined. The LPA and conduit segments were the segments with the most inefficient energetics. Furthermore,  $EL_{index}$  was highest in the Fontan confluence, indicative that a higher proportion of KE is dissipated at the area where both caval flows meet. Patients with vortical flow in the PA had significantly elevated viscous energy loss, but also significantly larger PA CSA, indicating that PA CSA alone may insufficiently characterize the hemodynamic resistance for pulmonary blood flow. Eventually, this approach may be of interest as a screening tool for direct, MRI-based assessment of flow efficiency in specific segments of the TCPC.

### Segmental analysis

In this study, an automated analysis approach was used by subdividing the TCPC into five standardized anatomical segments. This is of importance, as certain parts of the TCPC cannot be evaluated with 4D flow due to device-related artefacts (e.g. stents or fenestration closure devices). Without the applied segmental approach, almost 50% of patients in our study could not have been evaluated with 4D flow energetics due to these device-related artefacts, as these make direct comparison with patients without these devices impossible since inclusion of a larger part of the TCPC will result in higher energetic values. With the segmental approach, the other TCPC segments without artefacts could still be evaluated and compared leading to important insights in segment-specific adverse flow patterns and energetics.

### Qualitative flow patterns versus quantitative blood flow energetics

#### *Vortical flow*

4D flow MRI has revealed abnormal flow patterns within the TCPC, including helical and vortical flow in the PAs and Fontan confluence(7, 9, 10), at the junction between the IVC and extracardiac conduit(6) or in an attached, blind-ending pulmonary trunk(8). However, how these flow patterns relate to quantitative energetics within these segments with altered flow is not known. In our study cohort, vortical flow was present in the LPA (25%) and Fontan confluence (46%), with significantly higher vorticity compared to patients without vortical flow. The presence of vortical flow was also associated with a significantly higher viscous energy loss rate in these segments. Therefore, as expected, observed vortical flow patterns are related to quantitative 4D flow MRI derived vorticity, and are associated with reduced flow efficiency. The increased  $EL$  can be explained as

the swirling blood flow leads to increased dissipative velocity gradients (i.e. difference in velocities between adjacent blood elements resulting in energy-dissipating frictional forces) within the blood flow and between the flow and the vessel wall(17).

Vortical flow occurred most often in the LPA which could partially be explained by the presence of a blind-ending pulmonary trunk that was still attached to the LPA in 2 patients, as previously reported(8). Other speculative factors such as interaction of conduit and SVC flow, anastomosis angles and potential influence of the aorta on LPA flow may all play a role but could not be studied in this cohort.

### ***Caval flow collision***

Previous in-vitro studies have shown that collision of caval flows result in chaotic, intensely disorganized flow patterns, with helical flow extending into the PAs(18). Incorporating a degree of caval offset resulted in significantly reduced energy loss by avoiding these head collisions of both caval flows(18). In our cohort, caval offset was as expected significantly lower in patients with caval flow collision. Of interest, we surprisingly observed significantly lower  $\dot{E}L_{\text{norm\_flow+length}}$ ,  $KE_{\text{norm\_flow+length}}$  and  $Vort_{\text{norm\_flow+length}}$  in the Fontan confluence in patients with caval flow collision, at first sight suggesting it to be a favorable flow pattern. However, this is likely not true based on previous obtained results(18, 19) and multiple reasons can contribute to this conflicting result. Most importantly, the relatively low spatial resolution of 4D flow data (see limitations) allows only for assessment of flow patterns on a relatively large scale, and energy-consuming chaotic flow disturbances on a smaller scale, that have been described in the area of flow collision using in vitro models(19), are therefore likely not accounted for. As a result, on a larger scale caval flow collision can cause a decrease in velocity of both caval flows within the Fontan confluence leading to the observed lower energetics. Furthermore, caval flow collision may result in more chaotic flow characteristics in the Fontan confluence with associated turbulent energy losses that are not accounted for by the viscous energy loss metric that assumes laminar flow(14), thereby underestimating total energy loss.

### ***Segment-specific flow energetics***

In general,  $KE_{\text{norm\_flow+length}}$  (conduit+LPA) and  $\dot{E}L_{\text{norm\_flow+length}}$  (LPA) were highest in the conduit and LPA, while the SVC had the most favorable energetics. This observation could be due to relatively small diameters of the PA and conduit segments in some patients. CFD studies have demonstrated that the PA and Fontan conduit diameters are the most important factor associated with adverse flow efficiency(20, 21). The velocities in these vessels are often higher, e.g. due to relatively small LPA, often caused by compression by a dilated aortic root, or by the presence of undersized conduits in a proportion of patients leading to increased KE. Significant IVC-conduit mismatch has

previous been shown with 4D flow MRI, especially in adolescent patients with 16mm conduits(6). The increased velocities will lead to stronger velocity gradients between the vessel wall and the peak of the flow profile leading to higher  $\dot{E}L$ . Interestingly, also patients with higher LPA CSA showed increased  $\dot{E}L_{\text{norm\_flow+length}}$  when vortical flow was present in the LPA, indicating that PA CSA alone may be insufficient to characterize the hemodynamic resistance towards the lung.

The SVC, however, is not restricted as no synthetic material is used and vessel size can adapt to rising flow rates with somatic growth, keeping blood flow velocities and related energetics in the SVC low and favorable. Importantly, clinical decision making regarding the need for intervention is difficult for patients without an evident focal stenosis of the PA or Fontan conduit, but in whom an undersized conduit or overall hypoplastic LPA is present as pressure gradients from catheterization can be absent or minimal. The quantification of segment specific energetics may be helpful to evaluate the significance of these adverse geometries non-invasively.

Overall, the segmental analysis of 4D flow energetics performed in this study illustrates that the LPA and conduit are two important areas in the TCPC that may benefit from optimization by intervention.

### ***Normalization of 4D flow MRI energetics***

In order to compare energetics between patients or segments, we chose to normalize energetics in the SVC, conduit, RPA and LPA for inflow and segment length for multiple reasons. Since total energetics are computed using the sum of voxel-wise energetics, total energetics will be influenced by the size of the TCPC. This will be related to the body size of patients, but also by the presence of device-related artefacts that exclude part of the TCPC from 4D flow analysis. Furthermore, under laminar flow conditions, energetics such as  $\dot{E}L$  are proportional to flow rate(11, 23), which will differ between patients, but also between different segments within a patient (e.g. the conduit carries 65% of venous return with variable flow splits to both PAs). Therefore, energetics in the SVC, conduit, RPA and LPA were normalized for inflow and segment-length to correct for differences in extent of the segmentation. The Fontan confluence was normalized for flow only, as this segment of the TCPC is always completely available for the analysis. By normalizing energetics in the Fontan confluence for inflow rate, differences in Fontan confluence sizes due to different body sizes will also be corrected for, as flow is considered proportional to BSA(24).

### **Limitations**

The quantification of energetic markers from 4D flow MRI in this study is subject to multiple limitations. Firstly, the spatial resolution of 4D flow is relatively low (2.5mm

isotropic). The absolute amount of viscous energy loss is dependent on the spatial resolution and 4D flow derived viscous EL have shown to be orders of magnitude lower compared to “true” CFD-derived values(12). Due to the relatively low spatial resolution, flow phenomena and associated energy losses on a smaller scale are not captured using 4D flow MRI. However, despite measurements of lower energy losses with 4D flow, the relative performance of the TCPC between patients remains intact, thereby still allowing for a relative comparison between patients and most likely also between TCPC segments within patients(12). Furthermore, MRI-related errors such as partial volume artifacts at the vessel borders and the presence of velocity noise will all affect the accuracy of measured velocities and derived energetics. 4D flow protocols have to be optimized for this application, in which optimal compromises between spatial resolution, signal-to-noise-ratio and total scan durations have to be made. Recently, we introduced a non ECG-gated 3D flow MRI sequence (as opposed to ECG-gated 4D flow MRI), allowing for acquisition of cardiac-cycle averaged flow rates and flow rate derived clinical parameters in a <1.5min scan with superior image quality compared to conventional 4D flow MRI.(25)

Importantly, the effect of respiration is not taken into account with the use of 4D flow MRI, thereby not allowing to study the effect of in- and expiration on flow patterns and related energetics. In patients that underwent an Fontan operation, especially conduit flow rate is affected by respiration due to an increase in hepatic venous flow during inspiration(26). However, although respiration influences pulsatility observed in the TCPC, the heart beat is the main driving force for systemic venous return in the Fontan circulation, not affected by respiration(27), which can be adequately captured with the free breathing ECG-gated 4D flow MRI approach used in our study.

### **Future directions and role on clinical outcome**

This cohort represented relatively healthy teenage/adolescent patients after previous Fontan operation that underwent MRI examination as part of routine follow-up, with no events occurring during follow-up. However, the adverse flow patterns present in a subset of patients may provide a chronic burden that may only become apparent later in life. Larger studies with longer follow-up are required to determine its effect on long term outcome, including exercise capacity and degree of liver cirrhosis. Future studies using serial 4D flow scans may provide insights in how segment-specific energetics develop over time, as TCPC blood flow may become increasingly inefficient with time(22), and the proposed standardized segmental approach in this study is important for this serial follow-up.



## Conclusions

In conclusion, this study uses a segmental analysis approach to quantify segment-specific 4D flow MRI energetic measurements in the TCPC, allowing for the direct comparison of segment-specific energetics between patients. Furthermore, the segmental approach allows for comparison of energetics between heterogeneous patients with a previous Fontan operation and allow for serial follow-up of hemodynamics using 4D flow MRI. Vortical flow in the Fontan confluence and LPA, observed in 25-46% of patients, was associated with significantly increased viscous energy loss rate. Segmental analysis indicated that the LPA and conduit segments were associated with highest normalized viscous energy loss rate which may be optimized by targeted intervention in these segments. Importantly, patients with vortical flow in the PAs had a significantly larger PA cross-sectional area, indicating that PA CSA alone does not fully characterize the hemodynamic resistance for pulmonary blood flow. 4D flow MRI energetics has the potential to be used as a screening tool for direct, MRI-based assessment of flow efficiency in the TCPC.

## References

1. Rijnberg FM, Hazekamp MG, Wentzel JJ, de Koning PJH, Westenberg JJM, Jongbloed MRM, et al. Energetics of Blood Flow in Cardiovascular Disease: Concept and Clinical Implications of Adverse Energetics in Patients With a Fontan Circulation. *Circulation*. 2018 May 29;137(22):2393-407.
2. Gewillig M, Brown SC. The Fontan circulation after 45 years: update in physiology. *Heart*. 2016 Jul 15;102(14):1081-6. PubMed PMID: 27220691. Pubmed Central PMCID: PMC4941188.
3. Sundareswaran KS, Pekkan K, Dasi LP, Whitehead K, Sharma S, Kanter KR, et al. The total cavopulmonary connection resistance: a significant impact on single ventricle hemodynamics at rest and exercise. *Am J Physiol Heart Circ Physiol*. 2008 Dec;295(6).
4. Haggerty CM, Whitehead KK, Bethel J, Fogel MA, Yoganathan AP. Relationship of single ventricle filling and preload to total cavopulmonary connection hemodynamics. *Ann Thorac Surg*. 2015 Mar;99(3):911-7.
5. Khiabani RH, Whitehead KK, Han D, Restrepo M, Tang E, Bethel J, et al. Exercise capacity in single-ventricle patients after Fontan correlates with haemodynamic energy loss in TCPC. *Heart*. 2015 Jan;101(2):139-43.
6. Rijnberg FM, Elbaz MSM, Westenberg JJM, Kamphuis VP, Helbing WA, Kroft LJ, et al. Four-dimensional flow magnetic resonance imaging-derived blood flow energetics of the inferior vena cava-to-extracardiac conduit junction in Fontan patients. *Eur J Cardiothorac Surg*. 2019 Jun 1;55(6):1202-10.
7. Houtzager JH, Westenberg JJ, de Koning PJ, Hazekamp MG, Roest AA. Helical flow pattern in the right pulmonary artery after Fontan palliation. *Eur Heart J Cardiovasc Imaging*. 2014 Oct;15(10):1183.
8. Rijnberg FM, van Assen HC, Hazekamp MG, Roest AAW. Tornado-like flow in the Fontan circulation: insights from quantification and visualization of viscous energy loss rate using 4D flow MRI. *Eur Heart J*. 2019 Jul 1;40(26):2170.
9. Sundareswaran KS, Haggerty CM, de Zelicourt D, Dasi LP, Pekkan K, Frakes DH, et al. Visualization of flow structures in Fontan patients using 3-dimensional phase contrast magnetic resonance imaging. *J Thorac Cardiovasc Surg*. 2012 May;143(5):1108-16.
10. Markl M, Geiger J, Kilner PJ, Foll D, Stiller B, Beyersdorf F, et al. Time-resolved three-dimensional magnetic resonance velocity mapping of cardiovascular flow paths in volunteers and patients with Fontan circulation. *Eur J Cardiothorac Surg*. 2011 Feb;39(2):206-12.
11. Elbaz MS, van der Geest RJ, Calkoen EE, de Roos A, Lelieveldt BP, Roest AA, et al. Assessment of viscous energy loss and the association with three-dimensional vortex ring formation in left ventricular inflow: In vivo evaluation using four-dimensional flow MRI. *Magn Reson Med*. 2017 Feb;77(2):794-805.
12. Cibis M, Jarvis K, Markl M, Rose M, Rigsby C, Barker AJ, et al. The effect of resolution on viscous dissipation measured with 4D flow MRI in patients with Fontan circulation: Evaluation using computational fluid dynamics. *J Biomech*. 2015 Sep 18;48(12):2984-9. PubMed PMID: 26298492.
13. Antiga L, Piccinelli M, Botti L, Ene-Iordache B, Remuzzi A, Steinman DA. An image-based modeling framework for patient-specific computational hemodynamics. *Med Biol Eng Comput*. 2008 Nov;46(11):1097-112.

14. Venkatachari AK, Halliburton SS, Setser RM, White RD, Chatzimavroudis GP. Noninvasive quantification of fluid mechanical energy losses in the total cavopulmonary connection with magnetic resonance phase velocity mapping. *Magn Reson Imaging*. 2007 Jan;25(1):101-9.
15. Fenster BE, Browning J, Schroeder JD, Schafer M, Podgorski CA, Smyser J, et al. Vorticity is a marker of right ventricular diastolic dysfunction. *Am J Physiol Heart Circ Physiol*. 2015 Sep 15;309(6):H1087-93.
16. Kamphuis VP, Westenberg JJM, van der Palen RLF, van den Boogaard PJ, van der Geest RJ, de Roos A, et al. Scan-rescan reproducibility of diastolic left ventricular kinetic energy, viscous energy loss and vorticity assessment using 4D flow MRI: analysis in healthy subjects. *Int J Cardiovasc Imaging*. 2018 Jun;34(6):905-20.
17. Wang C, Pekkan K, de Zelicourt D, Horner M, Parihar A, Kulkarni A, et al. Progress in the CFD modeling of flow instabilities in anatomical total cavopulmonary connections. *Ann Biomed Eng*. 2007 Nov;35(11):1840-56.
18. Sharma S, Goudy S, Walker P, Panchal S, Ensley A, Kanter K, et al. In vitro flow experiments for determination of optimal geometry of total cavopulmonary connection for surgical repair of children with functional single ventricle. *J Am Coll Cardiol*. 1996 Apr;27(5):1264-9. .
19. Amodeo A, Grigioni M, Oppido G, Daniele C, D'Avenio G, Pedrizzetti G, et al. The beneficial vortex and best spatial arrangement in total extracardiac cavopulmonary connection. *J Thorac Cardiovasc Surg*. 2002 Sep;124(3):471-8.
20. Tang E, Wei ZA, Whitehead KK, Khiabani RH, Restrepo M, Mirabella L, et al. Effect of Fontan geometry on exercise haemodynamics and its potential implications. *Heart*. 2017 Nov;103(22):1806-12.
21. Dasi LP, Krishnankuttyrema R, Kitajima HD, Pekkan K, Sundareswaran KS, Fogel M, et al. Fontan hemodynamics: importance of pulmonary artery diameter. *J Thorac Cardiovasc Surg*. 2009 Mar;137(3):560-4. PubMed PMID: 19258065.
22. Restrepo M, Tang E, Haggerty CM, Khiabani RH, Mirabella L, Bethel J, et al. Energetic implications of vessel growth and flow changes over time in Fontan patients. *Ann Thorac Surg*. 2015 Jan;99(1):163-70.
23. Akins CW, Travis B, Yoganathan AP. Energy loss for evaluating heart valve performance. *J Thorac Cardiovasc Surg*. 2008 Oct;136(4):820-33. PubMed PMID: 18954618.
24. Lange PE, Onnasch DG, Schaupp GH, Zill C, Heintzen PH. Size and function of the human left and right ventricles during growth. Normative angiographic data. *Pediatr Cardiol*. 1982;3(3):205-11.
25. Rijnberg FM, van Assen HC, Juffermans JF, Kroft LJM, van den Boogaard PJ, de Koning PJH, et al. Reduced scan time and superior image quality with 3D flow MRI compared to 4D flow MRI for hemodynamic evaluation of the Fontan pathway. *Sci Rep*. 2021 Mar 22;11(1):6507.
26. Hsia TY, Khambadkone S, Redington AN, Migliavacca F, Deanfield JE, de Leval MR. Effects of respiration and gravity on infradiaphragmatic venous flow in normal and Fontan patients. *Circulation*. 2000 Nov 7;102(19 Suppl 3):III148-53.
27. Gabbert DD, Hart C, Jerosch-Herold M, Wegner P, Ravesh MS, Voges I, et al. Heart beat but not respiration is the main driving force of the systemic venous return in the Fontan circulation. *Sci Rep*. 2019 Feb 14;9(1):2034.

Supplementary materials

Supplemental Table 1. 4D flow MRI acquisition details

Respiratory compensation	None (free-breathing)
Cardiac gating	retrospective, 25-30 phases
Spatial resolution (mm)	2.5x2.5x2.5
Temporal resolution (ms)	31.4
Flip angle (°)	10
TE (ms)	3.9
TR (ms)	7.9
VENC (cm/s)	80
Scan duration (minutes)	8-10
Acceleration methods	SENSE factor 2, AP direction EPI factor 5

Typical scan parameters and scan duration are presented.

T; Tesla, ms; milliseconds, TE; echo time, TR; repetition time, VENC; velocity encoding, SENSE; sensitivity encoding, AP; anterior-posterior, EPI; echo planar imaging readout.

# CHAPTER 6B

# Four-dimensional flow magnetic resonance imaging-derived blood flow energetics of the inferior vena cava-to-extracardiac conduit junction in Fontan patients

Rijnberg FM, Elbaz MSM, Blom NA, Westenberg JW, Kroft LJ, Kamphuis V, Helbing WA, Hazekamp MG, Roest AAW

# **Abstract**

## **Objectives**

In patients with a Fontan circulation, systemic venous return flows passively towards the lungs. Due to an absent subpulmonary ventricle, favorable blood flow patterns with minimal energy loss are clinically relevant. The region where the inferior vena cava, hepatic veins and extracardiac conduit join (IVC-conduit junction) is a potential source of increased energy loss. The aim of this study was to evaluate the relationship between geometry and blood flow patterns in the IVC-conduit junction with associated kinetic energy and energy loss using four-dimensional flow MRI.

## **Methods**

Fourteen extracardiac conduit-Fontan patients underwent four-dimensional flow MRI. IVC-conduit junctions were ranked into 3 groups for 3 categories: geometry, flow complexity and conduit mean velocity. The relative increase in mean velocity from the IVC to conduit (representing IVC-conduit mismatch) was determined. Peak and mean kinetic energy and energy loss were determined and normalized for volume.

## **Results**

In 4/14 patients, adverse geometries led to helical flow patterns and/or acute changes in flow direction. For each category, the most adverse IVC-conduit junctions were associated with an approximate 2.3-3.2 and 2.0-2.9 fold increase in kinetic energy and energy loss, respectively. IVC-conduit mismatch strongly correlated with mean kinetic energy and energy loss ( $r=0.80$ ,  $p=0.001$  and  $r=0.83$ ,  $p<0.001$ , respectively) and with body surface area in patients with 16mm conduits ( $r=0.88$ ,  $p=0.010$ ).

## **Conclusions**

The IVC-conduit junction is a potential source of increased energy loss. Junctions with increased energy loss showed 1) distorted geometry leading to adverse blood flow patterns and/or 2) IVC-conduit mismatch. 16mm conduits appear to be inadequate for older patients.

## Introduction

The Fontan procedure is the current palliative approach for children with a univentricular heart defect. After completion of the Fontan circulation (total cavopulmonary connection, TCPC), the systemic venous return flows passively towards the lungs. Due to the absence of a subpulmonary ventricle, favorable blood flow patterns within the Fontan circulation with minimal energy loss are clinically relevant.(1) Previous computational fluid dynamic studies have identified relationships between increased energy loss in the TCPC and decreased exercise capacity(2, 3), altered cardiac function parameters (e.g. cardiac output, diastolic function) (4, 5) and an increased central venous pressure.(6) These studies, however, only modeled blood flow in the TCPC from the level of the Fontan tunnel to the pulmonary arteries. Until now, no studies have reported on energy loss levels in the blood flow in the region below the conduit, where the inferior vena cava (IVC), hepatic veins and conduit join (IVC-conduit junction). Subsequently, little is currently known about the geometry, blood flow patterns and associated energy loss in this region. We hypothesize that within the Fontan circulation, the IVC-conduit junction is another potential source of increased energy loss due to variable geometries.

More knowledge about this region could possibly have implications for diagnostic work-up in Fontan patients, as currently there is little focus on the IVC-conduit junction as a potential region of adverse hemodynamics.

Four-dimensional (4D) flow MRI has emerged as a novel technique capable of assessing in vivo 3D, time-resolved (i.e. over a cardiac cycle) blood flow.(7) 4D flow MRI enables in vivo acquisition of the 3D velocity field needed to visualize the dynamic 3D blood flow patterns and to quantify novel energetic markers.(8) Therefore, the aim of this study was to evaluate the relationship between altered geometry and blood flow patterns in the IVC-conduit junction with associated kinetic energy and energy loss using 4D flow MRI.

## Material and methods

### Study population

Fourteen extracardiac conduit-Fontan patients were retrospectively selected from a local database comprising both clinical 4D flow MRI examinations (as part of routine follow-up) and 4D flow scans that are part of an ongoing prospective multi-center study. All patients were randomly selected and did not have a clinical indication for the MRI. Patients with sufficient quality 4D flow data (free of motion/clips artifacts) in the IVC-conduit junction region were included. The study was approved by the Medical



Ethical Committee of the Erasmus Medical Center with the local approval of the Leiden University Medical Center. Informed consent was obtained from all participants and/or their legal representatives.

### **MRI acquisition**

4D flow MRI (Ingenia, Philips Healthcare, Best, the Netherlands) of the Fontan circulation was performed at Leiden University Medical Center between May 2014-March 2017. The 4D flow MRI acquisition covered the entire Fontan circulation from the IVC and superior vena cava towards both pulmonary arteries. Acquisition details are summarized in Supplementary Table 1.

### **4D flow MRI analysis**

The area of interest for this study was the IVC-conduit junction, which consists of three parts: 1) the IVC below entry of the hepatic veins (IVC), 2) the area of the IVC where the hepatic veins enter (IVC-HV) and 3) the conduit (Figure 1, Video 1). The hepatic veins were excluded from the analysis due to inadequate spatial resolution of the 4D flow MRI data in these small vessels. The segmentation of the IVC-conduit junction was standardized to allow for comparison of blood flow energetics between cases and comprised 6cm in total, starting at the first 2 cm of the conduit downwards (Figure 1B). The vessel lumen was manually segmented on the phase with the highest contrast on magnitude-weighted speed images of the 4D flow data using in-house developed MASS software, and subsequently propagated towards the other phases.

### **Ranking of the IVC-conduit junction**

To evaluate the impact of differences in geometry, flow patterns and conduit velocities on energetics, the IVC-conduit junction was ranked using 3 categories: geometry, flow complexity and mean velocity in the conduit. For each category, the study group was subdivided into 3 groups as defined below. Segmentations, pathline movies and streamline images were obtained and could be freely rotated in 3D to allow for optimal qualitative assessment of maximum angles and flow patterns used for the ranking (CAAS MR solutions v5.0, Pie Medical Imaging, Maastricht, the Netherlands). The maximum angle between 1) the IVC and the IVC-HV connection (the part of the IVC where the hepatic veins enter the IVC) and 2) between the IVC-HV connection and the conduit, were qualitatively determined (Figure 1B).

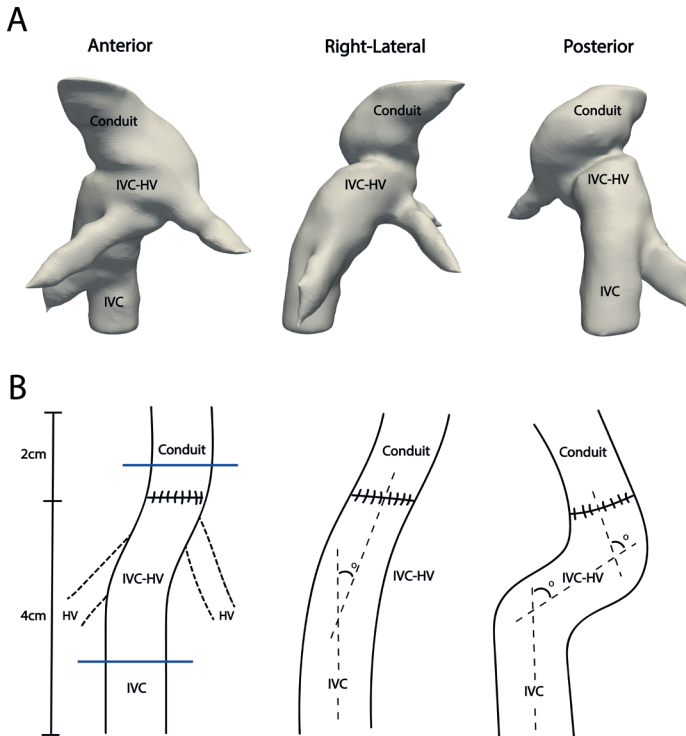


**Figure 1.** (A) Anterior, right-lateral and posterior view of a distorted IVC-conduit junction in a 12-year old female patient with an 18mm conduit. HVs are included for orientation. (B) Schematic representation of the IVC-conduit junction. HVs are shown for orientation (**left image**). Position of 2D flow planes is shown (**blue lines**). Angles between the IVC and IVC-HV and IVC-HV and conduit are shown for a relatively straight (**middle image**) and distorted IVC-conduit junction (**right image**). IVC; inferior vena cava, HV; hepatic veins.

Accordingly, the geometry was divided into three groups based on the sum of above-mentioned angles: 1) a cumulative angle  $<50^\circ$ , 2)  $50^\circ$ - $90^\circ$  or 3)  $>90^\circ$ . Flow complexity was divided into three groups: 1) well developed flow without helical flow patterns (defined by the curvature of the path- and streamlines representing a corkscrew flow pattern), 2) minor helical flow  $\leq 180^\circ$  in the majority of pathlines/streamlines or flow distortion (defined as helicity  $\geq 180^\circ$  or acute (single angle  $>90^\circ$ ) change in flow direction) in only a small part of the pathlines/streamlines, and 3) helicity  $\geq 180^\circ$  and/or acute change in flow direction of the majority of pathlines/streamlines in the IVC-conduit junction.

To determine the reproducibility of the geometry and flow complexity rankings, the inter- and intraobserver analysis was performed on blinded datasets for all cases. The intraobserver analysis was performed  $>8$  weeks after the first ranking.

IVC-conduit mismatch was defined by an increase in mean velocity from the IVC towards the conduit. Mean velocity in the conduit was arbitrarily grouped into 1) <25cm/s, 2) 25-35cm/s and 3) >35cm/s, with the rationale that higher velocity suggests higher IVC-conduit mismatch when mean velocities in the IVC are similar between groups. In addition, the percentage of IVC-conduit mismatch was also quantified, by assessing the relative increase of mean velocity in the conduit versus IVC for each phase with forward flow ( $V_{\text{conduit}} - V_{\text{IVC}} / V_{\text{IVC}} \times 100\%$ , where  $V$  is the mean velocity), using 2D planes positioned perpendicular on the 4D flow data of the IVC and conduit (Figure 1B).

### **Blood flow energetics: viscous energy loss and kinetic energy**

The amount of kinetic energy and viscous energy loss in the IVC-conduit junction was computed from 4D flow MRI velocity data using custom developed software.(8) Kinetic energy is the amount of energy the blood flow possesses due to its motion. In short, for each voxel in the IVC-conduit junction, the kinetic energy was computed as  $\frac{1}{2}mv^2$ , where ( $m$ ) is the mass of a voxel and ( $v$ ) is the velocity acquired with 4D flow MRI. The total amount of kinetic energy (in milliJoule, [mJ]) is computed for each phase in the cardiac cycle (i.e. one cardiac cycle is reconstructed into 25-30 phases) by summing the kinetic energy of all voxels within the IVC-conduit junction. The peak kinetic energy ( $KE_{\text{peak}}$ ) represents the phase in the cardiac cycle in which the blood flow contains the most kinetic energy volume and the mean kinetic energy ( $KE_{\text{mean}}$ ) is the kinetic energy volume present in the blood flow averaged over all the phases of the cardiac cycle.

Viscous energy loss is the kinetic energy that is lost due to viscosity-induced frictional forces in the flow and can be computed using the viscous dissipation function, assuming blood flow to be laminar.(1, 8) Of note, helical flow patterns in the Fontan circulation still represent laminar flow from a fluid dynamic perspective (based on Reynolds numbers <2300), as blood flow in the TCPC has been reported to be well within this laminar flow regime.(1, 9, 10)

Similar to kinetic energy, for each phase in the cardiac cycle, the total viscous energy loss rate (in milliWatt, mW) of the blood flow in the IVC-conduit junction was computed. The peak energy loss rate ( $EL_{\text{peak}}$ ) represents the phase in the cardiac cycle in which the most energy loss volume is present in the blood flow. The mean energy loss rate ( $EL_{\text{mean}}$ ) represents the energy loss rate volume in the blood flow averaged over all the phases of the cardiac cycle. As total kinetic energy and energy loss amount is proportional to the volume, these parameters were normalized by the segmented IVC-conduit junction volume ( $\text{norm\_KE (J/m}^3\text{)}$  and  $\text{norm\_EL (W/m}^3\text{)}$ ), in line with previous studies.(8, 11, 12)

## Statistical analysis

Continuous data are presented as median + interquartile range (IQR). Comparisons between energetics between groups were performed using the Kruskal Wallis test with post-hoc Dunn's test for multiple comparisons. Correlation between IVC-conduit mean velocity increase and energetics was assessed using the Pearson correlation coefficient ( $r$ ) (normal distributed data), or the Spearman correlation coefficient ( $r$ ) (non-normal distributed data). Inter- and intraobserver variability was tested using the linear weighted Cohen's Kappa test. A P value  $<0.05$  (two-tailed) was considered statistically significant. Data were analyzed with SPSS 24.0 (IBM-SPSS, Chicago, IL) and Prism 7.0 (GraphPad Software, La Jolla, CA).

## Results

Baseline characteristics of the study population are presented in Table 1. The IVC-conduit junction was characterized by remarkable differences in geometry, associated flow patterns and/or conduit mean velocity.

### Geometry and Flow complexity

Small cumulative angles ( $<50^\circ$ , group 1) were present in 6 patients, which was mostly directed in the posterior-anterior direction as the IVC is directed from parallel to the vertebral column towards the more anteriorly situated conduit (Figure 2A). These patients (group 1) showed well developed flow without any associated helical flow patterns or acute changes in flow direction. On the other end of the spectrum (group 3), 4 patients showed a highly distorted geometry, characterized by (cumulative) angles  $>90^\circ$  resulting in a distorted and/or spiraling IVC-conduit junction (Figure 1A). These adverse junctions resulted in flow distortion with acute (single angle  $>90^\circ$ ) changes in flow directions and/or the occurrence of a helical flow pattern (Figure 2C-D). Note how a distorted junction caused a severe helical flow pattern extending into the conduit (Figure 2D). Of note, ranking of the geometry of the IVC-conduit junction showed strong similarities with flow complexity, as these two factors are obviously highly correlated.

The results of kinetic energy and energy loss analysis are presented in Table 2. Kinetic energy and energy loss showed a strong positive correlation ( $\rho=0.92$ ,  $p<0.001$ , figure 3A). Significant differences were present between group 3 and group 1 when categorized by geometry, with a 2.3-2.9 and 2.6-2.9 fold increase in peak and mean kinetic energy and energy loss, respectively, in group 3. When categorized by flow complexity, only peak and mean energy loss was significantly different with a 2.0-2.7 fold increase in group 3 versus group 1. Post-hoc analysis did not show significant differences between group 1-2 and group 2-3 for both categories.

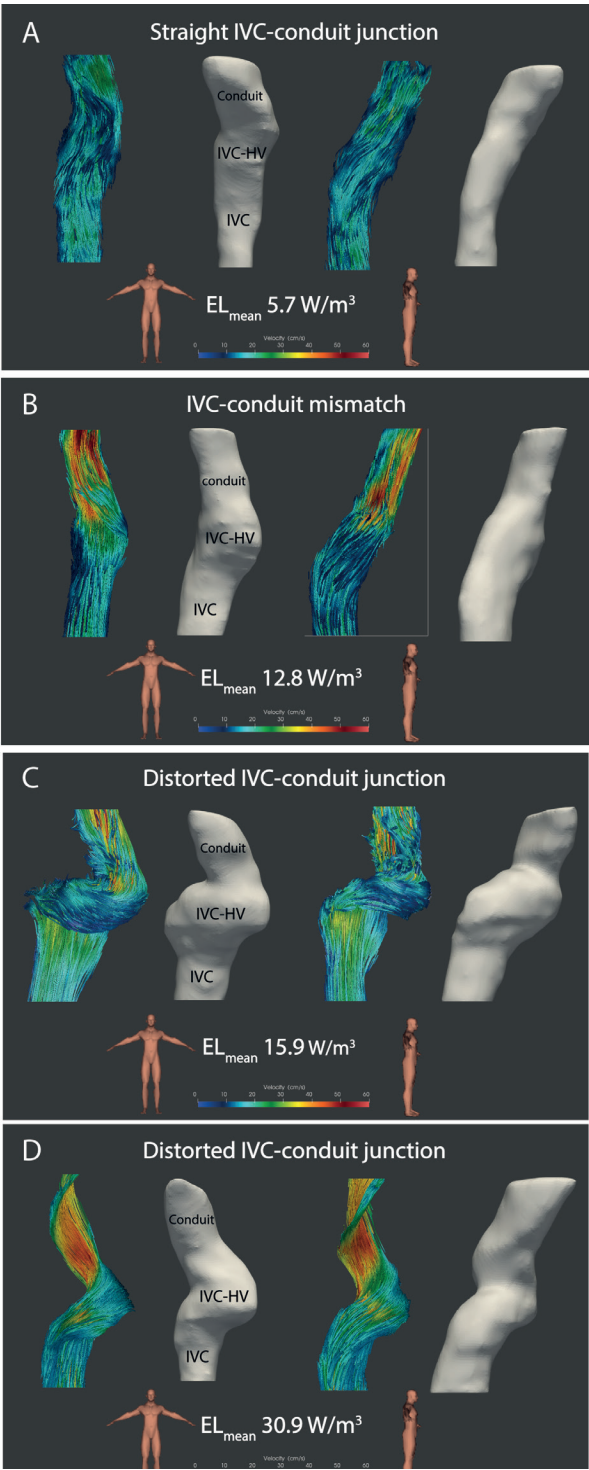


**Figure 2. (opposite)** Pathline images of 4D flow MRI derived blood flow in the IVC-conduit junction, excluding the HVs, is shown for 4 representative cases. Normalized mean energy loss values ( $W/m^3$ ) are reported.

**(A)** IVC-conduit junction of an 11-year old male patient with 18mm conduit. A relatively straight junction is shown with a small angle in the posterior-anterior direction. **(B)** IVC-conduit junction of an 18-year old female patient with 16mm conduit. A sudden increase in velocity in the conduit is observed, indicating IVC-conduit mismatch. **(C-D)** A distorted IVC-conduit junction is shown in a **(C)** 18-year old female patient with 16mm conduit and a **(D)** 12-year old patient with 18mm conduit. Note how large angles are present in multiple directions creating helical flow patterns with acute changes in flow direction.

Of note, a larger part of the conduit is shown in some figures for visualization purpose only. In the energetic analysis, only a standardized part of the conduit was included (Figure 1B). IVC; inferior vena cava, HV; hepatic veins. W; Watt.

**Table 1.** Baseline characteristics of the study population

Male, n (%)	5 (36)
Primary diagnosis, n (%):	
HLHS	5 (36)
DILV	2 (14)
DORV +/- TGA +/- cAVSD	3 (21)
TA	2 (14)
Other	1 (7)
Pre-Fontan characteristics	
Age at ECC-Fontan (years)	3.4 (1.3)
Height (cm)	97 (8)
Weight (kg)	14.6 (2.7)
BSA ( $m^2$ )	0.64 (0.08)
Pre-MRI characteristics	
Age at 4D flow MRI (years)	14.2 (7.6)
Height (cm)	154 (21)
Weight (kg)	42.0 (19.2)
BSA ( $m^2$ )	1.3 (0.4)
Conduit size (16mm/18mm/20mm)	7/5/2
Mean velocity IVC (cm/s)	15.2 (4.0)
Mean velocity ECC (cm/s)	24.5 (16.1)

Values are presented as median (IQR). MRI; magnetic resonance imaging, BSA; body surface area (Haycock), HLHS; hypoplastic left heart syndrome, DILV; double inlet left ventricle, DORV; double outlet right ventricle, TGA; transposition of great arteries, cAVSD; complete atrioventricular septum defect, TA; tricuspid atresia, IVC; inferior vena cava, 4D; four-dimensional

A strong reproducibility of the ranking of the IVC-conduit junction was shown and was equal for both inter- and intraobserver variability ( $\kappa=0.921$ ,  $p<0.001$  and  $\kappa=0.915$ ,  $p<0.001$  for geometry and flow complexity, respectively). Only 2 patients were ranked differently (1 patient per observer with differences between group 1 and 2 only) compared with the initial ranking.

## Mean velocity conduit

Mean velocity in the IVC and conduit are presented in Table 1. Mean velocity in the IVC between the 3 groups of conduit mean velocity was not significantly different (median 13.9 cm/s (6.2), median 15.1 cm/s (1.6) and median 16.2 cm/s (6.7) for groups 1-3, respectively,  $p=0.243$ ). A 2.7-3.2 and a 2.6 fold increase in peak and mean kinetic energy and energy loss, respectively, was found in group 3 compared with group 1 (Table 2). Post-hoc analysis did not show significant differences between group 1-2 and group 2-3.

**Table 2.** Impact of geometry, flow complexity and mean conduit velocity on energetics in the IVC-conduit junction

<b>Geometry</b>	<b>Group 1 (n=6)</b>	<b>Group 2 (n=4)</b>	<b>Group 3 (n=4)</b>	<b>P value</b>
norm_KE <sub>mean</sub> (J/m <sup>3</sup> )	10.0(4.8)	16.3(9.6)	29.2(10.9)	0.009
norm_KE <sub>peak</sub> (J/m <sup>3</sup> )	14.2(12.3)	24.6(13.6)	33.3(13.4)	0.014
norm_EL <sub>mean</sub> (W/m <sup>3</sup> )	6.0(2.6)	8.5(3.8)	17.2(13.0)	0.007
norm_EL <sub>peak</sub> (W/m <sup>3</sup> )	8.0(6.5)	14.7(7.2)	20.7(17.8)	0.014
<b>Flow Complexity</b>	<b>Group 1 (n=6)</b>	<b>Group 2 (n=5)</b>	<b>Group 3 (n=3)a</b>	<b>P value</b>
norm_KE <sub>mean</sub> (J/m <sup>3</sup> )	10.8(12.0)	15.8(12.9)	28.8(21.5-35.9)	0.096
norm_KE <sub>peak</sub> (J/m <sup>3</sup> )	18.6(13.2)	20.3(18.8)	32.8(24.5-42.1)	0.135
norm_EL <sub>mean</sub> (W/m <sup>3</sup> )	6.9(4.7)	8.1(5.2)	18.5(16.0-30.9)	0.034
norm_EL <sub>peak</sub> (W/m <sup>3</sup> )	11.0(7.7)	11.9(9.1)	22.0(19.3-40.4)	0.031
<b>Conduit mean velocity</b>	<b>Group 1 (n=5)</b>	<b>Group 2 (n=4)</b>	<b>Group 3 (n=5)</b>	<b>P value</b>
norm_KE <sub>mean</sub> (J/m <sup>3</sup> )	9.1(5.8)	18.1(8.6)	28.8(12.2)	0.016
norm_KE <sub>peak</sub> (J/m <sup>3</sup> )	13.2(6.6)	24.1(5.5)	32.8(11.7)	0.007
norm_EL <sub>mean</sub> (W/m <sup>3</sup> )	5.7(1.9)	8.7(8.6)	14.5(12.6)	0.015
norm_EL <sub>peak</sub> (W/m <sup>3</sup> )	7.0(3.2)	13.2(7.6)	18.6(12.3)	0.007

Values are reported as median (interquartile range). <sup>a</sup>total range. P values represent overall Kruskal Wallis test. KE; kinetic energy, EL; viscous energy loss, mW; milliWatt, W; Watt, mJ; milliJoule, J; joule, IVC; inferior vena cava

The mean IVC-conduit mismatch in the study cohort was 55.8% (SD: 48%, range -20% to 167%). One outlier was excluded from the analysis as this case showed helical flow extending into the conduit (Figure 2D). Therefore, 2D through-plane velocity analysis in the conduit significantly underestimated true antegrade velocity in this case, thereby compromising the assessment of the IVC-conduit velocity increase. Results of correlation analysis between IVC-conduit velocity increase and kinetic energy and energy loss are mentioned in Supplementary Table 2, including results with the outlier included for completeness. A strong positive correlation was found between IVC-conduit velocity increase and norm\_KE<sub>mean</sub> ( $r=0.80$ ,  $p=0.001$ , Figure 3B) and norm\_EL<sub>mean</sub> ( $r=0.83$ ,  $p<0.001$ , Figure 3C). To determine the effect of body size on IVC-conduit mismatch, correlation analysis was performed between BSA and IVC-conduit velocity increase according to conduit size. A strong correlation was found between BSA and

IVC-conduit velocity increase in the 16mm group ( $r=0.88$ ,  $p=0.010$ , Figure 3D). The groups with 18mm and 20mm conduit size were too small for further evaluation.

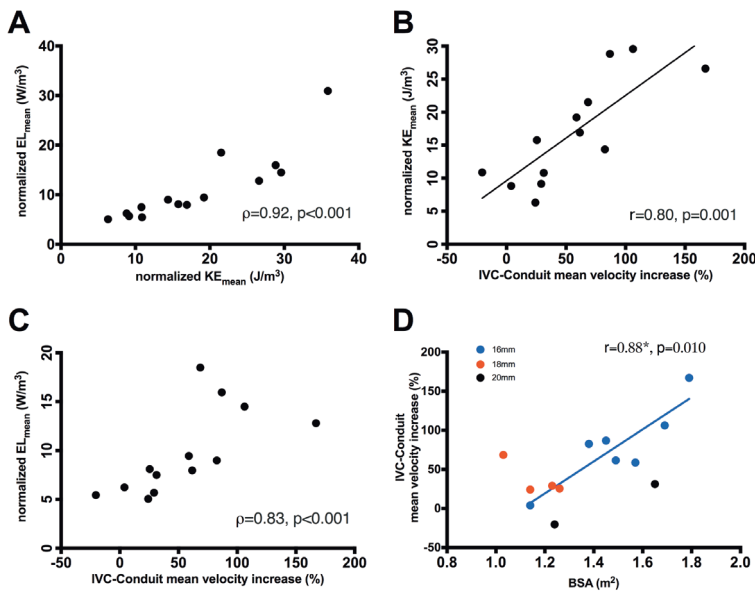


**Figure 3.** A strong positive correlation is shown between IVC-conduit mean velocity increase (representing IVC-conduit mismatch) and normalized  $KE_{mean}$  (A) and  $EL_{mean}$  (B). A strong positive correlation between normalized  $KE_{mean}$  and  $EL_{mean}$  is shown (C). A strong positive correlation is shown between IVC-conduit mean velocity increase and BSA in patients with 16mm conduits\* (D).

IVC; inferior vena cava, KE; kinetic energy, EL; viscous energy loss, BSA; body surface area, W; Watt, J; Joule

## Discussion

The aim of this study was to evaluate the relationship between altered geometry and blood flow patterns in the IVC-conduit junction with associated energetics (kinetic energy and energy loss) using in vivo 4D flow MRI. The main findings show that the IVC-conduit junction is characterized by heterogeneous geometry leading to variable flow patterns. Important characteristics of the junctions associated with adverse energetics were 1) a distorted geometry, characterized by (cumulative) angles  $>90^\circ$  resulting in adverse flow patterns with acute changes in flow direction and/or helical flow patterns, and 2) IVC-conduit mismatch. The most adverse junctions showed 2.3-3.2 and 2.0-2.9 fold increase in peak and mean kinetic energy and energy loss, respectively, and these adverse connections are therefore of potential clinical significance in Fontan patients. Furthermore, IVC-conduit mismatch was strongly associated with BSA in patients with



16mm conduits, indicating that these conduits may be inadequate for older Fontan patients.

The geometrical distortion of the IVC-conduit junction we observed in a subset of patients was surprising and it is unclear whether this is caused by natural variability in anatomy of the IVC and IVC-HV region in healthy humans, or is related to the Fontan procedure. Subsequently, longitudinal information of changes in geometry of this region with growth after completion of the Fontan circulation is essential as major changes occur in body composition from Fontan completion to adulthood. Finally, if reintervention is considered after Fontan completion, detailed evaluation of this region is important as this also may be an adverse factor in the complications occurring in these patients which can potentially be optimized.

Our data showed a strong positive correlation between IVC-conduit mismatch and normalized mean kinetic energy and energy loss. Furthermore, a strong positive correlation was present between BSA and IVC-conduit mismatch in patients with 16mm conduits. While the use of 16mm conduits has been reported to provide good short to mid-term results in small-sized patients(13, 14), results in full grown adults remain mostly unknown and, according to our data, may only be sufficient for small adults. In our center, 16mm conduits have been used in the early periods but have been abandoned since many years due to concerns of inadequate size in the long term. Our data seem to justify this approach from an energetic point of view. Basically, optimal conduit size varies with age and is a trade-off situation: in young patients with large conduits, flow expansions at the IVC-conduit junction leads to flow separation which is also associated with increased energy loss. Furthermore, these oversized conduits increase areas of flow stagnation or flow reversal, which potentially increases risk of thrombosis and therefore limits the amount of conduit oversizing by the surgeon.(15) In older, larger patients, energy loss increases if the used conduit becomes too small.(16) As Fontan tunnel diameter has been described as the most important geometric factor of the TCPC associated with increased energy loss, large patients with 16mm conduits may therefore be at increased risk of complications.(1, 17) Importantly, whether 18mm and 20mm conduits will be large enough for the adult Fontan patient could not be investigated in this study due to small sample sizes. The 18mm patients in this study were relatively young with a low BSA and observed IVC-conduit mismatch would increase when these patients grow.

Comparing absolute values of energy loss derived from 4D flow MRI with previous reported in vitro or computational fluid dynamic studies is challenging. On the one hand, 4D flow MRI has been shown to systematically underestimate “true” energy loss compared with computational fluid dynamics due to the limited spatial resolution

of 4D flow MRI.(10) On the other hand, simulated blood flow and energetics using computational fluid dynamic modelling can be influenced by simplified assumptions and boundary conditions.(1) In a study by Cibis et al.(10), the only study to date that calculated viscous energy loss in the Fontan circulation using 4D flow MRI, mean peak energy loss rate was 0.56mW (SD: 0.28) in the TCPC (covering the area from the Fontan tunnel, superior vena cava and both pulmonary arteries). In our study, absolute peak energy loss rate in the IVC-conduit junction was a median of 0.26 mW with a total range of 0.11-0.94mW, and may therefore be a relevant, previously unidentified source of energy loss in the Fontan circulation.

In the past decades, extensive knowledge has been acquired with in vitro and computer models about the effect of TCPC geometry on energy loss.(1, 3, 4, 6, 9) Energy loss in the TCPC has been linked to several clinically important complications seen in Fontan patients, including a reduced exercise capacity and altered cardiac function parameters. (1, 2, 4, 6) Increased energy loss (resistance) results in elevated central venous pressure(6), which is an important factor in the pathogenesis of the well-known upstream Fontan complications, including liver fibrosis/cirrhosis, protein losing enteropathy or venovenous collateral formation.(18, 19) To date, various energy-consuming geometric factors of the TCPC have been identified (e.g. small pulmonary artery size(20)) and our data suggest that the IVC-conduit junction is an additional geometric factor with potential increased energy loss. Future studies with larger sample sizes are necessary to better clarify the role of adverse geometry and blood flow patterns in the IVC-conduit junction and TCPC on adverse outcome in Fontan patients. Evaluation of the Fontan circulation using 4D flow MRI is promising, by directly measuring *in vivo* energy loss from 4D blood flow data, and may be of particular interest in failing Fontan patients(21), as these patients in particular may have adverse geometries and/or blood flow patterns which can be optimized by surgical or catheter-based intervention.

## Limitations

This study is limited by a small sample size, but represents randomly selected Fontan patients. Furthermore, different mechanisms of energy loss (IVC-conduit mismatch and distorted geometry with abnormal flow patterns) could occur simultaneously, making the relative contribution of each mechanism on calculated energetics difficult. Two patients underwent 4D flow MRI on a 1.5T scanner and lower signal-to-noise ratio in these patients may have affected calculated energetics. Analysis was performed on a static segmentation of the IVC-conduit junction and minor movement between phases may have introduced small errors. However, this may have been present in the same order of magnitude in all patients. The 4D flow MRI protocol used free-breathing with no respiratory gating, and therefore no distinction between inspiration and expiration

flow data can be made. As such, the influence of respiration on observed flow patterns and energetics could not be assessed in this study.

## Conclusions

In conclusion, the IVC-conduit junction is a currently undervalued source of increased energy loss. The most adverse junctions show a probable clinically relevant 2.3-3.8 and 2.0-3.5 fold increase in kinetic energy and energy loss, respectively. Identified mechanisms of energy loss are 1) distorted geometry leading to adverse blood flow patterns, and 2) IVC-conduit mismatch. IVC-conduit mismatch was strongly correlated with kinetic energy and energy loss. Furthermore, IVC-conduit mismatch strongly correlated with BSA in patients with 16mm conduits, indicating that these conduits may be inadequate for adult Fontan patients. Therefore, these patients are potentially at increased risk for experiencing complications. Whether 18mm and 20mm conduits will be large enough could not be determined due to small sample size and is subject to future studies. Larger sample sizes are warranted to further clarify the importance of adverse IVC-conduit junctions on long-term clinical outcome.

## References

1. Rijnberg FM, Hazekamp MG, Wentzel JJ, de Koning PJH, Westenberg JJM, Jongbloed MRM, et al. Energetics of Blood Flow in Cardiovascular Disease: Concept and Clinical Implications of Adverse Energetics in Patients With a Fontan Circulation. *Circulation*. 2018;137(22):2393-407.
2. Khiabani RH, Whitehead KK, Han D, Restrepo M, Tang E, Bethel J, et al. Exercise capacity in single-ventricle patients after Fontan correlates with haemodynamic energy loss in TCPC. *Heart*. 2015;101(2):139-43.
3. Tang E, Wei ZA, Whitehead KK, Khiabani RH, Restrepo M, Mirabella L, et al. Effect of Fontan geometry on exercise haemodynamics and its potential implications. *Heart*. 2017;103(22):1806-12.
4. Haggerty CM, Whitehead KK, Bethel J, Fogel MA, Yoganathan AP. Relationship of single ventricle filling and preload to total cavopulmonary connection hemodynamics. *Ann Thorac Surg*. 2015;99(3):911-7.
5. Honda T, Itatani K, Takanashi M, Mineo E, Kitagawa A, Ando H, et al. Quantitative evaluation of hemodynamics in the Fontan circulation: a cross-sectional study measuring energy loss in vivo. *Pediatr Cardiol*. 2014;35(2):361-7.
6. Sundareswaran KS, Pekkan K, Dasi LP, Whitehead K, Sharma S, Kanter KR, et al. The total cavopulmonary connection resistance: a significant impact on single ventricle hemodynamics at rest and exercise. *Am J Physiol Heart Circ Physiol*. 2008;295(6):H2427-35.
7. Kamphuis VP, Westenberg JJM, van der Palen RLF, Blom NA, de Roos A, van der Geest R, et al. Unravelling cardiovascular disease using four dimensional flow cardiovascular magnetic resonance. *Int J Cardiovasc Imaging*. 2017;33(7):1069-81.
8. Elbaz MS, van der Geest RJ, Calkoen EE, de Roos A, Lelieveldt BP, Roest AA, et al. Assessment of viscous energy loss and the association with three-dimensional vortex ring formation in left ventricular inflow: In vivo evaluation using four-dimensional flow MRI. *Magn Reson Med*. 2017;77(2):794-805.
9. Bossers SS, Cibis M, Gijzen FJ, Schokking M, Strengers JL, Verhaart RF, et al. Computational fluid dynamics in Fontan patients to evaluate power loss during simulated exercise. *Heart*. 2014;100(9):696-701.
10. Cibis M, Jarvis K, Markl M, Rose M, Rigsby C, Barker AJ, et al. The effect of resolution on viscous dissipation measured with 4D flow MRI in patients with Fontan circulation: Evaluation using computational fluid dynamics. *J Biomech*. 2015;48(12):2984-9.
11. Kamphuis VP, Elbaz MSM, van den Boogaard PJ, Kroft LJM, van der Geest RJ, de Roos A, et al. Disproportionate intraventricular viscous energy loss in Fontan patients: analysis by 4D flow MRI. *Eur Heart J Cardiovasc Imaging*. 2018.
12. Kamphuis VP, Westenberg JJM, van der Palen RLF, van den Boogaard PJ, van der Geest RJ, de Roos A, et al. Scan-rescan reproducibility of diastolic left ventricular kinetic energy, viscous energy loss and vorticity assessment using 4D flow MRI: analysis in healthy subjects. *Int J Cardiovasc Imaging*. 2018;34(6):905-20.
13. Cho S, Kim WH, Choi ES, Kwak JG, Chang HW, Hyun K, et al. Outcomes after extracardiac Fontan procedure with a 16-mm polytetrafluoroethylene conduit. *Eur J Cardio-Thorac*. 2018;53(1):269-75.
14. Ikai A, Fujimoto Y, Hirose K, Ota N, Tosaka Y, Nakata T, et al. Feasibility of the extracardiac conduit Fontan procedure in patients weighing less than 10 kilograms. *J Thorac Cardiovasc Surg*. 2008;135(5):1145-52.

15. Lardo AC, Webber SA, Friehs I, del Nido PJ, Cape EG. Fluid dynamic comparison of intra-atrial and extracardiac total cavopulmonary connections. *J Thorac Cardiovasc Surg.* 1999;117(4):697-704.
16. Itatani K, Miyaji K, Tomoyasu T, Nakahata Y, Ohara K, Takamoto S, et al. Optimal conduit size of the extracardiac Fontan operation based on energy loss and flow stagnation. *Ann Thorac Surg.* 2009;88(2):565-72; discussion 72-3.
17. Tang E, Restrepo M, Haggerty CM, Mirabella L, Bethel J, Whitehead KK, et al. Geometric characterization of patient-specific total cavopulmonary connections and its relationship to hemodynamics. *JACC Cardiovasc Imaging.* 2014;7(3):215-24.
18. Ohuchi H, Yasuda K, Miyazaki A, Kitano M, Sakaguchi H, Yazaki S, et al. Haemodynamic characteristics before and after the onset of protein losing enteropathy in patients after the Fontan operation. *Eur J Cardiothorac Surg.* 2013;43(3):e49-57.
19. Rychik J, Veldtman G, Rand E, Russo P, Rome JJ, Krok K, et al. The precarious state of the liver after a Fontan operation: summary of a multidisciplinary symposium. *Pediatr Cardiol.* 2012;33(7):1001-12.
20. Dasi LP, Krishnankuttyrema R, Kitajima HD, Pekkan K, Sundareswaran KS, Fogel M, et al. Fontan hemodynamics: importance of pulmonary artery diameter. *J Thorac Cardiovasc Surg.* 2009;137(3):560-4.
21. Deal BJ, Jacobs ML. Management of the failing Fontan circulation. *Heart.* 2012;98(14):1098-104.

## Supplementary materials

**Supplementary Table 1.** 4D flow MRI acquisition details

Field strength (n)	1.5T (2), 3T (12)
Respiratory compensation	none
Cardiac gating	retrospective, 25-30 phases
Spatial resolution (mm)	2.5x2.5x2.5
Temporal resolution (ms)	31.4 (1.6)
Flip angle (°)	10
TE (ms)	3.9±0.2)
TR (ms)	7.9±0.4)
VENC (cm/s)	80
Scan duration (minutes)	8-10
Acceleration methods	SENSE factor 2, AP direction EPI factor 5

Values are represented as mean (SD).

*T*; Tesla, *ms*; milliseconds, *TE*; echo time, *TR*; repetition time, *VENC*; velocity encoding, *SENSE*; sensitivity encoding, *AP*; anterior-posterior, *EPI*; echo planar imaging readout.

**Supplementary Table 2.** Correlation between IVC-conduit velocity increase and energetics

Blood flow energetics	Correlation coefficient	p value	Correlation coefficient (outlier included)	p value
norm_KE_mean (J/m <sup>3</sup> )	0.80 <sup>a</sup>	0.001	0.69 <sup>a</sup>	0.007
norm_KE_peak (J/m <sup>3</sup> )	0.78 <sup>a</sup>	0.002	0.52 <sup>a</sup>	0.057
norm_EL_mean (W/m <sup>3</sup> )	0.83 <sup>b</sup>	<0.001	0.70 <sup>b</sup>	0.006
norm_EL_peak (W/m <sup>3</sup> )	0.73 <sup>b</sup>	0.005	0.53 <sup>b</sup>	0.054

<sup>a</sup>Pearson correlation coefficient, <sup>b</sup>Spearman's rank coefficient

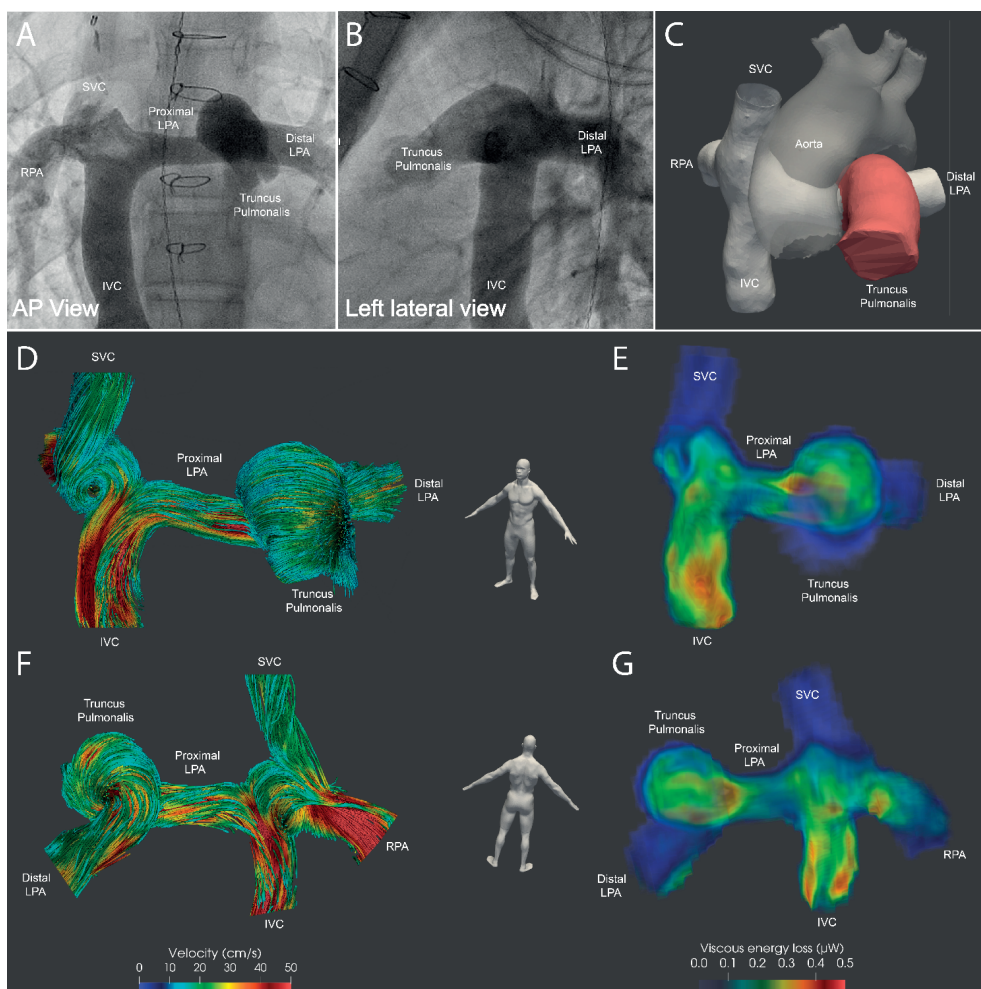
*KE*; kinetic energy, *EL*, viscous energy loss, *mW*; milliWatt, *W*; Watt, *mJ*; milliJoule, *J*; joule, *IVC*; inferior vena cava

# CHAPTER 6C

# Tornado-like flow in the Fontan circulation: insights from quantification and visualization of viscous energy loss rate using 4D flow MRI

Friso M Rijnberg, Hans C van Assen, Mark G Hazekamp, Arno A W Roest





IVC, inferior vena cava; LPA, left pulmonary artery; RPA, right pulmonary artery; SVC, superior vena cava.

A female patient with tricuspid and pulmonary atresia underwent total cavopulmonary connection (TCPC) completion with a 16mm extracardiac conduit, without detachment of the pulmonary trunk at 4 years. At 17 years, the patient underwent a catheterization procedure to close veno-venous collaterals. Angiographic TCPC assessment showed the presence of a blind-ending, dilated pulmonary trunk (Panels A–C, segmented with CAAS MR Solutions v5.1, Pie Medical Imaging. red: pulmonary trunk, Supplementary material online, Videos S1 and S2). The significance of this observation, however, was unclear at that time. The following year, a magnetic resonance imaging (MRI) examination, including 4D flow MRI, was performed as part of routine follow-up. Visualization of flow patterns within the TCPC revealed a Tornado-like helical flow pattern inside the dilated pulmonary trunk (Panels D and F, Supplementary material online, Video S3). To evaluate the haemodynamic impact of this flow pattern, peak viscous energy loss rate (EL), a novel energetic marker representing kinetic energy loss due to friction, was calculated. Thirty-four percent of total viscous EL in the TCPC occurred in the pulmonary trunk (0.35 mW and 0.12 mW, respectively). Colour-coded visualization of the spatial distribution of viscous EL revealed the primary locations of increased EL (Panels E and G, Supplementary material online, Video S4). This case illustrates the complementary role of 4D flow MRI by allowing visualization of flow patterns and flow-related energetic parameters, thereby revealing locations of increased EL within the TCPC. In these patients, minimal EL in the TCPC is important to maximally conserve the reduced energy present in the Fontan circulation. Furthermore, to ensure a smooth pulmonary artery, detachment of the pulmonary trunk should be considered in univentricular patients with pulmonary atresia to avoid distorted, energy-consuming blood flow.

# 7

## CHAPTER 7

# Assessment of extracardiac conduit adequacy

# CHAPTER 7A

# Hemodynamic consequences of an undersized extracardiac conduit in an adult Fontan patient revealed by 4D flow MRI

Friso Rijnberg, Hans van Assen, Mark Hazekamp, Arno Roest, Jos Westenberg



## Hemodynamic consequences of an undersized extracardiac conduit in an adult Fontan patient revealed by 4D flow MRI.

A 20 year old female patient born with a double inlet left ventricle with transposition of the great arteries previously underwent a bidirectional Glenn shunt at the age of 7 months. Final completion of the Fontan circulation (total cavopulmonary connection, TCPC) was performed at the age of 3 years and a body surface area of  $0.6\text{m}^2$ , by connecting the subhepatic IVC and hepatic veins (HVs) with the pulmonary arteries (PAs) using a rigid 16mm extracardiac Goretex conduit. Seventeen years after Fontan completion (body surface area  $1.8\text{m}^2$ ), an MRI examination was performed as part of routine follow-up including 4D flow MRI. A 3D reconstruction of the TCPC revealed a small, flattened extracardiac conduit (**Figure 1A**, CAAS v5.2, MR Solutions, Pie Medical Imaging). Furthermore, an important dilatation of the distal SVC was observed. The cross-sectional area of the subhepatic IVC and conduit were  $259\text{mm}^2$  and  $186\text{mm}^2$ , respectively. The flow rate at the subhepatic IVC and conduit were 1.7 and 2.5 L/min, respectively, indicating a contribution of 0.8 L/min (32% of total conduit flow) from the splanchnic circulation through the HVs. A 2.1-fold increase in mean velocity from the subhepatic IVC (11cm/s) towards the extracardiac conduit (23cm/s, **Figure 1B**) was present, indicative of an undersized extracardiac conduit (IVC-conduit velocity mismatch). While most of the conduit flow is directed towards the left PA, part of the accelerated conduit flow formed a swirling, vortical flow pattern intruding into the distal part of the SVC before reaching the right PA (**Figure 1B, Supplemental Video 1**). The entry of conduit flow into the SVC was associated with the area where the SVC was strongly dilated; the cross-sectional area of the dilated part of the SVC was a 2.4-fold higher compared to the level of the SVC just proximal to the dilatation ( $204\text{mm}^2$  vs  $481\text{mm}^2$ ). Quantification of wall shear stress and viscous energy loss rate derived from 4D flow MRI revealed insights into the hemodynamic consequences of these altered flow patterns. Firstly, the increase in blood flow velocity from the subhepatic IVC and HVs towards the conduit extended into the LPA, leading to areas of elevated wall shear stress (WSS) in the conduit and LPA (**Figure 1C**). These areas with elevated WSS strongly correlated with areas of inefficient blood flow with an increased viscous energy loss rate (**Figure 1D, Supplemental Video 2**). The entry of accelerated conduit flow into the SVC did not result in an important increase in WSS, but rather resulted in the dilatation of the distal SVC. The venous tissue of the SVC is likely more susceptible to increased mechanical stresses caused by the accelerated conduit flow entering the SVC, resulting in adaptive vessel dilatation to keep WSS within a narrow, physiological range. The arterial wall of the LPA may be less susceptible to increased mechanical stresses caused by the accelerated conduit flow, and therefore increased levels of WSS and viscous energy loss are observed without adaptive dilatation of the pulmonary artery.



Single ventricle heart defects represent the most severe end of the spectrum of congenital heart disease, with the Fontan-circulation as a palliative approach. Currently most centers complete the Fontan circulation at the age of 3 to 5 years with the use of an extracardiac conduit<sup>1</sup>, as was performed in this case. The main drawback of the extracardiac conduit Fontan technique is the lack of growth potential of the Goretex conduit. Therefore, ideally an oversized conduit is implanted to avoid future somatic overgrowth requiring conduit replacement. Currently, however, it is not known which conduit size is ideal for adult Fontan patients, despite the fact that optimal conduit sizing is of utmost importance to ensure efficient blood flow with minimal energy loss<sup>2</sup>. Regular echocardiographic qualitative assessment of the conduit during follow-up is often only able to identify patients with a distinct focal stenosis or thrombus. Blood flow obstruction due to an undersized conduit is often not recognized with echocardiography and may only become apparent during invasive angiography.<sup>3</sup> This case shows how 4D flow MRI reveals that the 16mm extracardiac conduit has become relatively undersized 17 years after Fontan completion, a timeframe in which body size tripled. The undersized conduit led to accelerated flow in the conduit, associated with increased viscous energy losses affecting the efficiency of blood flow towards the PAs. Because of the absence of a subpulmonary ventricle in Fontan patients and thus a relatively passive pulmonary blood flow, areas with increased energy loss are undesirable.<sup>4</sup> Furthermore, important downstream effects of the accelerated conduit flow were observed, with conduit flow entering the SVC leading to dilatation of the vessel. The competitive flow from the conduit into the SVC may pose increased afterload for SVC flow.

This case raises important concern on the hemodynamic adequacy of the 16mm conduit used in the Fontan circulation and highlights how 4D flow MRI derived blood flow and hemodynamic parameters provide intuitive information about the hemodynamic performance of the TCPC during follow-up. We recommend regular evaluation of the TCPC with 4D flow MRI during somatic growth to allow for early identification of patients with inadequately sized conduits leading to adverse TCPC hemodynamics. As such, this case illustrates the additional role of 4D flow MRI as an *in vivo*, non-invasive screening tool that can identify patients that may require further invasive hemodynamic evaluation and possible intervention.

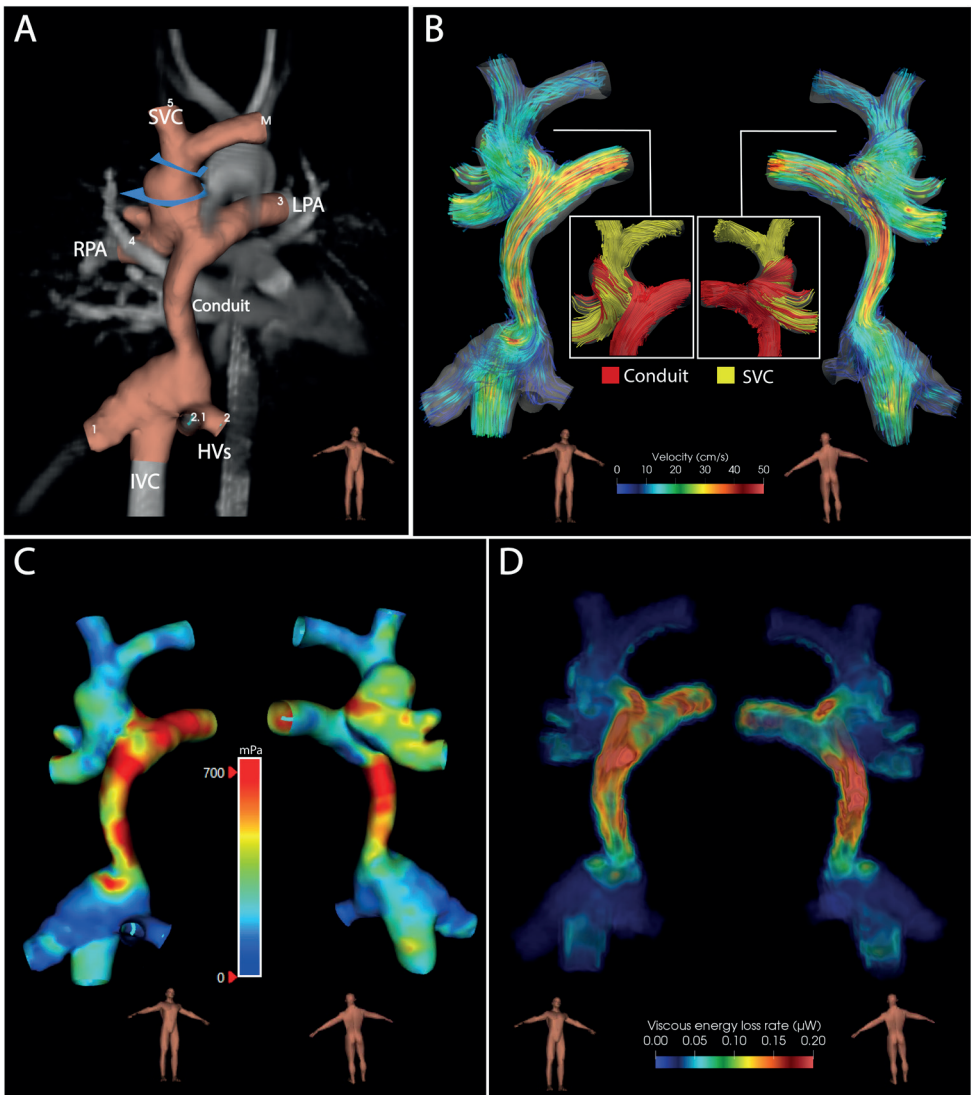


**Figure legend.** The 3D reconstruction of the TCPC is presented, including the subhepatic IVC and HVs (A). The blue planes indicate the two levels where the cross-sectional area of the SVC is measured; at the dilatation and just proximal to the dilatation. Velocity color-coded streamlines illustrate acceleration of blood flow from the level of the subhepatic IVC towards the conduit extending into the LPA. This accelerated conduit flow partially enters the distal SVC into a swirling flow pattern, correlating with the area of SVC dilatation (B). The accelerated blood flow resulted in areas of elevated WSS in the extracardiac conduit and anterior LPA (C), illustrating the relative undersized extracardiac conduit in this patient. No elevated WSS was observed in the dilated SVC. The areas of increased WSS strongly associated with areas of increased viscous energy loss rate indicative of decreased flow efficiency (D).

HVs; hepatic veins, IVC/SVC; inferior/superior vena cava, RPA/LPA; right/left pulmonary artery. mPa; millipascal,  $\mu$ W; microwatt

## References

1. Rychik J, Atz AM, Celermajer DS, Deal BJ, Gatzoulis MA, Gewillig MH, Hsia TY, Hsu DT, Kovacs AH, McCrindle BW et al. American Heart Association Council on Cardiovascular Disease in the Y, Council on C and Stroke N. Evaluation and Management of the Child and Adult With Fontan Circulation: A Scientific Statement From the American Heart Association. *Circulation*. 2019.
2. Tang E, Restrepo M, Haggerty CM, Mirabella L, Bethel J, Whitehead KK, Fogel MA and Yoganathan AP. Geometric characterization of patient-specific total cavopulmonary connections and its relationship to hemodynamics. *JACC Cardiovasc Imaging*. 2014;7:215-224.
3. Hagler DJ, Miranda WR, Haggerty BJ, Anderson JH, Johnson JN, Cetta F, Said SM and Taggart NW. Fate of the Fontan connection: Mechanisms of stenosis and management. *Congenit Heart Dis*. 2019;14:571-581.
4. Rijnberg FM, Hazekamp MG, Wentzel JJ, de Koning PJH, Westenbergh JJM, Jongbloed MRM, Blom NA and Roest AAW. Energetics of Blood Flow in Cardiovascular Disease: Concept and Clinical Implications of Adverse Energetics in Patients With a Fontan Circulation. *Circulation*. 2018;137:2393-2407.



# CHAPTER 7B

# Extracardiac conduit adequacy along the respiratory cycle in adolescent Fontan patients

Friso Rijnberg, Séline van der Woude, Mark Hazekamp, Pieter van den Boogaard, Hildo Lamb, Covadonga Terol Espinosa de Los Monteros, Lucia Kroft, Sasa Kenjeres, Tawab Karim, Monique Jongbloed, Jos Westenberg, Jolanda Wentzel, Arno Roest

# Abstract

## Background

Adequacy of 16-20mm extracardiac conduits for adolescent Fontan patients remains unknown. This study aims to evaluate conduit adequacy using the inferior vena cava (IVC)-conduit velocity mismatch factor along the respiratory cycle.

## Methods

Real-time 2D flow MRI was prospectively acquired in 50 extracardiac (16-20mm conduits) Fontan patients (mean age  $16.9 \pm 4.5$  years) at the subhepatic IVC, conduit and superior vena cava. Hepatic venous (HV) flow was determined by subtracting IVC flow from conduit flow. The cross-sectional area (CSA) was reported for each vessel. Mean flow and velocity was calculated during the average respiratory cycle, inspiration and expiration. The IVC-conduit velocity mismatch factor was determined as follows:  $V_{\text{conduit}}/V_{\text{IVC}}$ , where V is the mean velocity.

## Results

Median conduit CSA and IVC CSA were  $221\text{mm}^2$  (Q1-Q3 201-255) and  $244\text{mm}^2$  (Q1-Q3 203-265), respectively. From the IVC towards the conduit, flow rates increased significantly due to entry of HV flow (IVC 1.9, Q1-Q3 1.5-2.2) vs conduit (3.3, Q1-Q3 2.5-4.0 L/min,  $p < 0.001$ ). Consequently, mean velocity significantly increased (IVC 12 (Q1-Q3 11-14 cm/s) vs conduit 25 (Q1-Q3 17-31cm/s),  $p < 0.001$ ), resulting in a median IVC-conduit velocity mismatch of 1.8 (Q1-Q3 1.5-2.4), further augmenting during inspiration (median 2.3, Q1-Q3 1.8-3.0). IVC-conduit mismatch was inversely related to measured conduit size and positively correlated with conduit flow. A weak inverse correlation was present between the expiratory normalized mismatch factor and peak  $\text{VO}_2$  ( $r=0.37$ ,  $p=0.014$ ).

## Conclusion

Important blood flow accelerations are observed from the IVC towards the conduit in adolescent Fontan patients which is related to peak  $\text{VO}_2$ . This study therefore raises concerns that implanted 16-20mm conduits have become undersized for older Fontan patients and future studies should clarify its effect on long-term outcome.

## Introduction

The Fontan procedure provides a palliative solution for single ventricle patients, by connecting both the superior (SVC) and inferior vena cava (IVC) directly to the pulmonary arteries (i.e. Total CavoPulmonary Connection, TCPC). Nowadays, most centers complete the TCPC by connecting the IVC to the right PA using a Goretex extracardiac conduit at an age of 2-4 years[1]. However, the lack of growth potential remains concerning for older Fontan patients. To date, optimal conduit size for adult Fontan patients is unknown as no clear definition is available to describe the hemodynamic adequacy of extracardiac conduits during follow-up, beyond identifying a distinct stenosis within the Fontan conduit.

The extracardiac conduit directs 65-70% of total systemic venous return towards the PAs[2]. Since blood flow resistance is inversely related to the fourth power of the vessel radius (law of Hagen-Poiseuille), an undersized conduit leads to reduced TCPC flow efficiency[3-5]. Exercise performance has been associated with conduit size[6, 7], which is related to TCPC flow efficiency[3, 8]. On top of that, TCPC flow efficiency has been associated with the degree of liver fibrosis, a common complication in Fontan palliated patients[9].

Recently, the *IVC-conduit velocity mismatch factor* has been proposed as a marker of conduit adequacy, describing the change in mean velocity from the subhepatic IVC towards the conduit[10]. In that study, 4D flow MRI revealed important blood flow acceleration at the level of the conduit that were associated with increased viscous energy losses resulting in less efficient TCPC blood flow.[10] Since conduit flow changes along the respiratory cycle due to intrathoracic pressure changes, evaluation of the IVC-conduit velocity mismatch along the respiratory cycle may reveal important insights in the adequacy of the conduit size during both inspiration (highest flow) and expiration (lowest flow).

The hypothesis is that adolescent Fontan patients may outgrow implanted conduit size, leading to an increased blood flow velocity from the subhepatic IVC towards the conduit. Therefore, the aim is to assess conduit adequacy along the respiratory cycle by evaluating the IVC-conduit velocity mismatch factor using real-time 2D flow MRI and determine its relationship with exercise performance.



## Material and Methods

### Study population

Fontan patients with an extracardiac Goretex conduit prospectively underwent MRI between 2018-2020 at the Leiden University Medical Center, Leiden, the Netherlands. All patients >8 years old without contraindications for MRI were eligible for inclusion. The study was approved by the medical ethical review board of the hospital. Written informed consent was obtained from all patients and/or their parents.

### Magnetic resonance imaging

MRI acquisition details are presented in Supplemental Table 1. Real-time 2D phase contrast MRI measurements were obtained at the level of the subhepatic IVC (below entry of the HVs), the extracardiac conduit and the SVC (Figure 1A). HV flow was indirectly determined by subtracting IVC flow from conduit flow. Measurements consisted of 250 real-time (non ECG-gated) flow acquisitions with a sample rate of approximately 15 frames per second. The respiratory signal was continuously monitored using an air-filled abdominal belt. Flow rate (Q), mean velocity (V) and cross-sectional area (CSA) of each vessel was acquired by manual segmentation of the vessel lumen on all phase-contrast images (Figure 1B, Mass software, Leiden, the Netherlands). The mean CSA during the entire flow acquisition is reported.

The workflow of the real-time 2D flow MRI analysis is shown in Figure 1 and Supplemental material 1. Typically, 2-4 consecutive respiratory cycles and associated flow and velocity curves were automatically cut into inspiration and expiration phases using in-house developed software (Figure 1C). A single flow curve was derived (Figure 1D-F) from the average inspiratory and expiratory flow curves, which was used for the analysis of the flow parameters. To determine real-time HV flow, inspiratory and expiratory flow curves from the IVC and conduit were aligned and subsequently subtracted.

Mean flowrates and velocities (V) were determined during the entire respiratory cycle, inspiration and expiration. The ratio between mean inspiratory and mean expiratory flowrates was calculated as a marker of respiration-driven pulsatility ( $Q_{\text{insp}}/Q_{\text{exp}}$ ). Retrograde flow fraction was calculated by dividing retrograde flow volume (retrograde flow rate \* duration of retrograde flow) by antegrade flow volume.

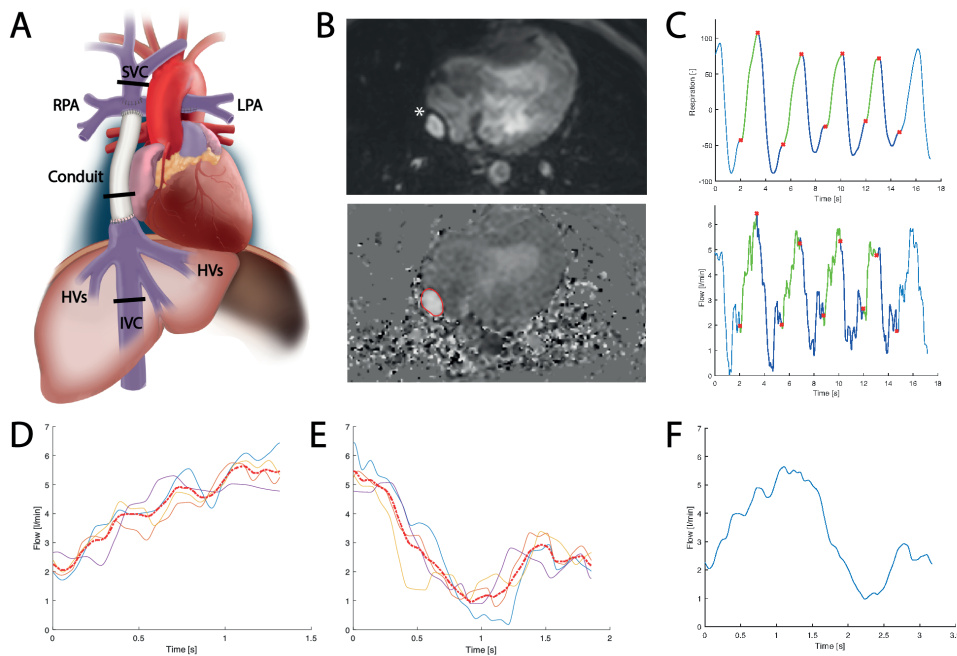


**Figure 1.** Figure 1 shows the workflow of the real-time 2D flow MRI analysis of a conduit flow measurement. The same analysis is applied to the subhepatic IVC and SVC. The position of the 2D flow planes are shown (A). The lumen of the conduit (\*) was manually delineated on the phase contrast images. Multiple consecutive respiratory curves and corresponding flow curves (C) were automatically divided into multiple inspiration (green) and expiration (blue) parts. After interpolation, a single average curve was generated from the individual inspiratory (D) and expiratory (E) curves and subsequently combined to acquire the average respiratory cycle (F).

## IVC-conduit velocity mismatch factor

The IVC-conduit velocity mismatch factor was determined for the average respiratory cycle, inspiration and expiration phases as follows:  $V_{\text{conduit}}/V_{\text{IVC}}$ , where  $V$  is the mean velocity in the conduit and subhepatic IVC, respectively. A mismatch factor of 1 represents equal mean velocity (ideal), <1 represent a decrease in mean velocity (oversized conduit) and >1 represents an increase in mean velocity (undersized conduit).

The relation between the IVC-conduit velocity mismatch factor and mean conduit flow rates was analyzed by grouping patients in tertiles of measured conduit CSA: <209mm<sup>2</sup> (n=16), 209-241mm<sup>2</sup> (n=17) and >241mm<sup>2</sup> (n=17). Grouping patients on measured conduit size rather than on implanted conduit size is based on observations that conduit CSA can variably decrease after implantation due to neointima formation and conduit stretching[7, 11, 12]. To put CSA values in perspective to implanted conduit diameters, the theoretical CSA corresponding to 16-20mm circular conduits is 201mm<sup>2</sup>

(16mm), 254mm<sup>2</sup> (18mm) and 314mm<sup>2</sup> (20mm). Furthermore, vessel CSA normalized for the average flow rate during the respiratory cycle in each vessel is presented. To compare IVC-conduit velocity mismatch between measured conduit size groups, values were normalized for indexed conduit flow rate (L/min/m<sup>2</sup>).

### **Cardiopulmonary exercise testing**

Cardiopulmonary exercise testing was performed on an upright bicycle ergometer (GE Healthcare, Wisconsin, USA). A continuous incremental bicycle protocol was executed according to the Godfrey protocol. Patients had to maintain a pedaling rate of 60 revolutions/min and were encouraged to cycle to exhaustion. Peak VO<sub>2</sub> (ml/kg/min) was determined in all patients with a respiratory exchange ratio >1.0.

### **Statistical analysis**

Data were presented as median (Q1-Q3) or mean (standard deviation). Normal distributions of continuous data were tested using the Shapiro-Wilk test. Correlation analysis was performed using Pearson or Spearman correlation (weak 0.3-0.5, moderate 0.5-0.7, strong ≥0.7-0.9 and very strong >0.9). Measurements between the different vessels were compared using a paired t-test or Wilcoxon signed-rank test. Comparison of normalized mismatch factor between measured conduit size tertiles were performed using the Kruskal-Wallis test (adjusted for multiple comparisons using Bonferroni). A p-value <0.05 was considered statistically significant. Data were analyzed with SPSS 25.0 (IBM Corp., Armonk, NY, USA) and Graphpad Prism 8.0 (GraphPad Software, La Jolla, California, USA ).

## **Results**

Fifty-seven extracardiac conduit Fontan patients underwent MRI examination. Seven patients with incomplete 2D real-time MRI examinations were excluded from analysis. Patient characteristics are provided in Table 1. CPET was performed in 47/50 patients, with 44 patients reaching maximal effort (median time between CPET and MRI 0 days (Q1-Q3 0-15 days).

**Table 1.** Patient characteristics

Male/Female, n	24/26
Primary diagnosis, n(%)	
- TA	12(24)
- HLHS	10(20)
- DILV + TGA	10(20)
- DORV	6(12)
- uAVSD	4(8)
- ccTGA	4(8)
- PA + IVS	2(4)
- Other	2(4)
Dominant ventricle	
Left, n(%)	29(58)
Right, n(%)	16(32)
Biventricular/indeterminate, n(%)	5(10)
<b>Characteristics at Fontan procedure</b>	
Age at Fontan, years	3.7(1.9)
Implanted conduit size (16/18/20mm), n	26/18/6
Height, cm	99(11)
Weight, kg	15.0(2.9)
BSA, m <sup>2</sup>	0.64(0.09)
<b>Characteristics at time of MRI</b>	
Age at MRI, years	16.9(4.5)
Height, cm	167(11)
Weight, kg	57(14)
BSA, m <sup>2</sup>	1.62(0.24)
Time between Fontan and MRI, years	13.2(4.1)
NYHA-class I-II, n (%)	50(100)
<b>CPET</b>	
Peak VO <sub>2</sub> (n=44), ml/kg/min	26.4(5.6)

Values are reported as mean (SD) unless otherwise specified. TA; tricuspid atresia, HLHS; hypoplastic left heart syndrome, DILV; double inlet left ventricle, (cc)TGA; (congenital corrected) transposition of the great arteries, DORV; double outlet right ventricle, uAVSD; unbalanced atrioventricular septal defect, PA+IVS; pulmonary atresia with intact ventricular septum, CPET; cardiopulmonary exercise testing

## Cross-sectional area

IVC and conduit CSA were a median of 244mm<sup>2</sup> (Q1-Q3 203-265) and 221mm<sup>2</sup> (Q1-Q3 201-255), respectively. CSA decreased from the subhepatic IVC towards the conduit with a median of 9% (Q1-Q3 -18-15), with IVC CSA exceeding conduit CSA in 30 patients (60%). Median normalized conduit CSA (66mm<sup>2</sup> per L/min, Q1-Q3 54-97) was smaller compared to normalized IVC CSA (129mm<sup>2</sup> per L/min, Q1-Q3 118-148, p<0.001), decreasing a median of 44% (Q1-Q3 33-58% decrease).

Measured conduit CSA of implanted 16-20mm conduits were 101% (Q1-Q3 93-109%), 97% (Q1-Q3 88-108%) and 94% (Q1-Q3 70-96%) of theoretical expected conduit CSA, respectively. Of note, measured conduit CSA exceeded the theoretically expected conduit CSA in some patients which can be explained by methodological reasons (see limitation section). In 2/6 patients with a 20mm conduit, measured conduit CSA was 232mm<sup>2</sup> and 192mm<sup>2</sup>, 27% and 39% decreased compared to expected theoretical conduit CSA. The median measured conduit CSA after subdividing the patients in tertiles were per group 191mm<sup>2</sup> (Q1-Q3 172-201), 220mm<sup>2</sup> (Q1-Q3 214-228) and 277mm<sup>2</sup> (Q1-Q3 251-302), respectively.

## Flow

Along the entire respiratory cycle, flow rates increased from the IVC (median 1.9, Q1-Q3 1.5-2.2 L/min) towards the conduit (median 3.3, Q1-Q3 2.5-4.0 L/min,  $p < 0.001$ , Table 2) because of entry of HV flow (median increase 77% (Q1-Q3 59-104%)). HV flow was strongly dependent on respiration, with a median  $Q_{\text{insp}}/Q_{\text{exp}}$  ratio of 3.0 (Q1-Q3 2.2-4.1). During inspiration, expiration and the entire respiratory cycle, respectively, 57% (Q1-Q3 50-60), 30% (Q1-Q3 21-39) and 43% (Q1-Q3 37-51) of total conduit flow originated from the HVs.

The median  $Q_{\text{insp}}/Q_{\text{exp}}$  ratio was 1.2 (Q1-Q3 1.1-1.4) in the SVC, 1.1 (Q1-Q3 1.0-1.3) in the IVC and 1.7 (Q1-Q3 1.5-2.1) in the conduit. Therefore, most pulsatility observed in the conduit originates from the pulsatile HV flow. Retrograde flow was negligible at the level of the conduit, SVC and IVC in all patients, but occurred in the HVs in 43 (86%) patients, exclusively in (early) expiration.

## IVC-conduit velocity mismatch

Mean velocities in the IVC and SVC were generally low (range 10-14cm/s) during all respiratory phases (Table 2). The combination of a decrease in CSA and an increase in flow rate resulted in higher mean velocity in the conduit compared to the IVC ( $p < 0.001$  for all respiratory phases). The median IVC-conduit velocity mismatch factor during the entire respiratory cycle was 1.8 (Q1-Q3 1.5-2.4), indicating a 1.8 fold increase of the mean velocity from the subhepatic IVC towards the conduit.

**Table 2.** Subhepatic IVC, HV, conduit and SVC characteristics

Cross-sectional area (mm <sup>2</sup> )	Absolute CSA (mm <sup>2</sup> )		Normalized CSA (mm <sup>2</sup> per L/min)	
IVC	244(203-265)		129(118-148)	
Conduit	221(201-255)		66(54-97)	
SVC	218(161-256)		150(129-197)	
Change in CSA from IVC to conduit,%	-9(-18-15)		-44(-58- -33)	
Flow(L/min)	Entire respiratory cycle	Inspiration	Expiration	Q <sub>insp</sub> /Q <sub>exp</sub> ratio
IVC	1.9(1.5-2.2) <sup>†,‡</sup>	2.1(1.6-2.5) <sup>‡,§</sup>	1.7(1.3-2.1) <sup>†,§</sup>	1.1(1.0-1.3)
HV	1.5(1.0-1.8) <sup>†,‡</sup>	2.6(2.1-3.1) <sup>‡,§</sup>	0.7(0.5-1.2) <sup>†,§</sup>	3.0*(2.2-4.1)
Conduit	3.3(2.5-4.0) <sup>†,‡</sup>	4.5(3.9-5.3) <sup>‡,§</sup>	2.6(1.9-3.3) <sup>†,§</sup>	1.7(1.5-2.1)
SVC	1.3(1.1-1.6) <sup>†,‡</sup>	1.5(1.3-1.8) <sup>‡,§</sup>	1.2(1.0-1.5) <sup>†,§</sup>	1.2(1.1-1.4)
Change in flow from IVC to conduit,%	77(59-104) <sup>†,‡</sup>	131(99-152) <sup>‡,§</sup>	44(27-65) <sup>†,§</sup>	
Contribution of HV flow to conduit flow,%	43(37-51) <sup>†,‡</sup>	57(50-60) <sup>‡,§</sup>	30(21-39) <sup>†,§</sup>	
Retrograde-to-antegrade flow ratio IVC,%	0(0-0)	0(0-0)	0(0-0)	
Retrograde-to-antegrade flow ratio HV,%	5(1-9) <sup>†,‡</sup>	0(0-0) <sup>‡,§</sup>	13(3-31) <sup>†,§</sup>	
Retrograde-to-antegrade flow ratio Conduit,%	0(0-0)	0(0-0)	0(0-0)	
Retrograde-to-antegrade flow ratio SVC,%	0(0-0)	0(0-0)	0(0-0)	
Mean velocity(cm/s)	Entire respiratory cycle	Inspiration	Expiration	
IVC	12(11-14) <sup>†,‡</sup>	13(12-16) <sup>‡,§</sup>	12(10-14) <sup>†,§</sup>	
Conduit	25(17-31) <sup>†,‡</sup>	35(25-40) <sup>‡,§</sup>	19(12-25) <sup>†,§</sup>	
SVC	11(9-13) <sup>†,‡</sup>	13(10-15) <sup>‡,§</sup>	10(8-12) <sup>†,§</sup>	
IVC-conduit velocity mismatch factor	1.8(1.5-2.4) <sup>†,‡</sup>	2.3(1.8-3.0) <sup>‡,§</sup>	1.5(1.2-2.1) <sup>†,§</sup>	

Values are reported as median (Q1-Q3). IVC/SVC; inferior/superior vena cava, HV; hepatic venous, CSA; cross-sectional area, L/min, liter per minute, cm/s, centimeter per second. \*3 cases with negative ratios were excluded. P-value <0.001 compared to inspiration<sup>†</sup>, expiration<sup>‡</sup> or the entire respiratory cycle<sup>§</sup>.

Because of the important respiratory dependency of HV flow, IVC-conduit velocity mismatch was higher during inspiration (median 2.3, Q1-Q3 1.8-3.0),  $P < 0.001$ ) and lower during expiration (median 1.6, Q1-Q3 1.2-2.1,  $P < 0.001$ , Figure 2, Supplemental Video 1) compared to the entire respiratory cycle. A moderate positive correlation was found between mean conduit flow rate and the IVC-conduit velocity mismatch factor during the entire respiratory cycle ( $r = 0.58$ ), inspiration ( $r = 0.42$ ) and expiration ( $r = 0.69$ , Figure 3). Highest mismatch was present in the group with smallest conduits (Group 1  $< 209 \text{ mm}^2$ , Figure 3&4). Up to a 4.4-fold increase in mean velocity was observed during inspiration in Group 1 patients with high flow rates (Figure 3B). Importantly, only 5 patients (10%) had a mismatch factor  $< 1$  during expiration indicating flow expansion due to an relatively oversized conduit (all in Group 2-3, age 10-14 years, Figure 3B).

The normalized IVC-conduit velocity mismatch factor during expiration and the entire respiratory cycle correlated with peak VO<sub>2</sub> ( $r = -0.37$ ,  $p = 0.014$  and  $r = -0.31$ ,  $p = 0.04$ , respectively).

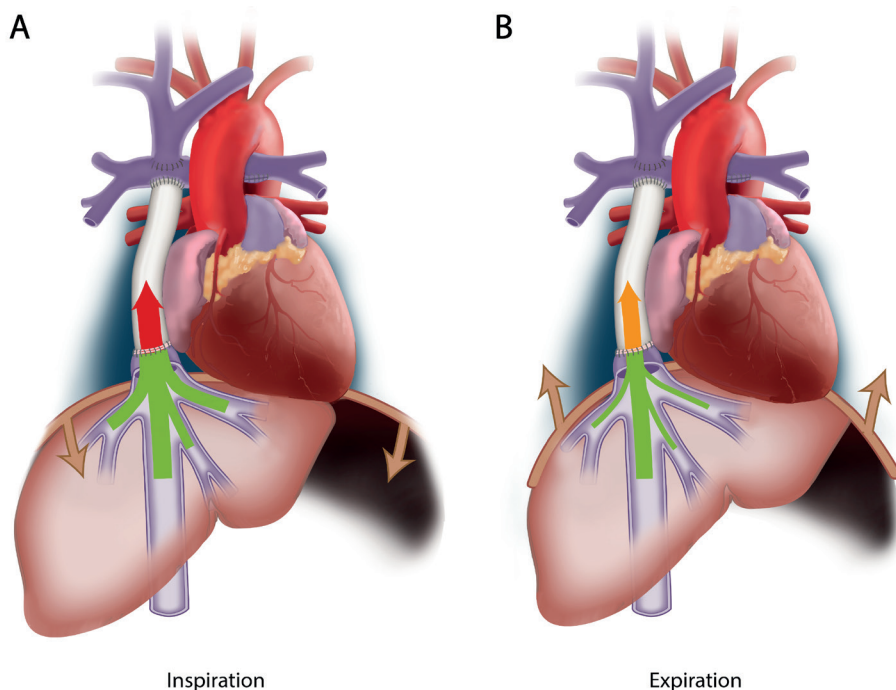


**Figure 2.** The presence of IVC-conduit velocity mismatch is schematically shown during inspiration (**A**) and expiration (**B**). The thickness of the arrow indicates the amount of flow and the color indicates the blood flow velocity. An important increase in mean velocity is observed from the subhepatic IVC towards the conduit in both inspiration (highest mismatch) and expiration.

A moderate positive correlation was found between BSA and mean conduit flow during all respiratory phases ( $r = 0.62$ - $0.70$ ), with considerable variation in flow rates between patients with similar body sizes (Supplemental Figure 1). No correlation was found between IVC mean velocity and BSA ( $r = 0.26$ ,  $p = 0.06$ ).

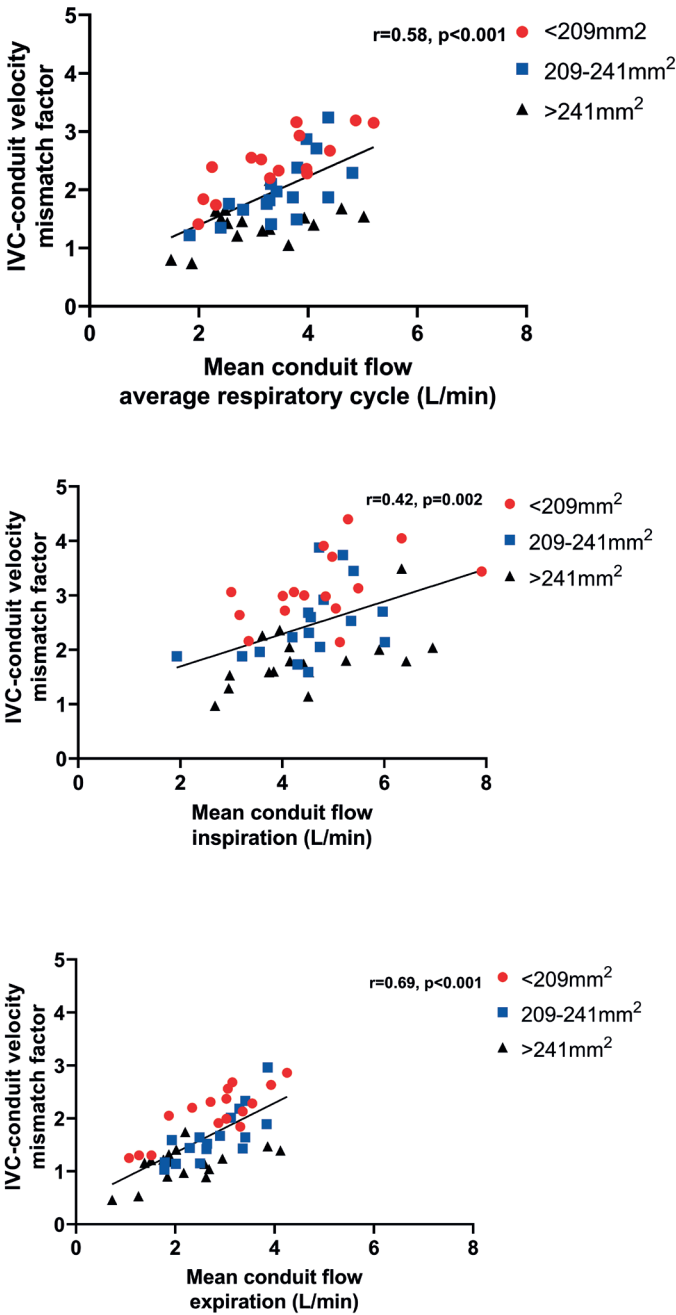


**Figure 3.** The correlation between conduit flow rate and IVC-conduit velocity mismatch factor is shown for the entire respiratory cycle (A), inspiration (B) and expiration (C). Patients are color-coded into three groups based on the measured conduit size for visualization purposes only.



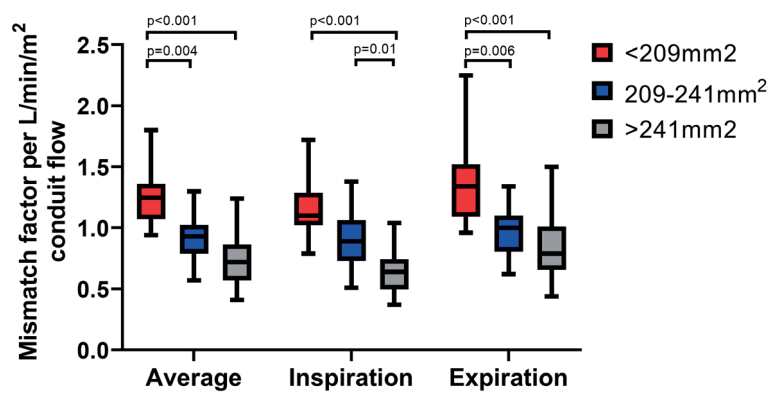


**Figure 4.** The IVC-conduit velocity mismatch factor normalized for conduit flow rate per BSA is shown for the average respiratory cycle, inspiration and expiration for the 3 groups of measured conduit size. E.g., a normalized IVC-conduit mismatch factor of 0.5 means an increase in velocity from the IVC towards the conduit when conduit flow rate is >2 L/min/m<sup>2</sup>.

## Discussion

This study evaluated the hemodynamic adequacy of implanted 16-20mm extracardiac conduit sizes along the respiratory cycle at a mean interval of 13 years after Fontan completion. The main findings show that at a mean age of 17 years, absolute conduit CSA is 9% smaller as compared to the CSA of the subhepatic IVC, even though all HV flow still needs to enter the IVC. Consequently, important blood flow accelerations (IVC-conduit velocity mismatch) are present from the subhepatic IVC towards the conduit which are further augmented during inspiration. The normalized IVC-conduit mismatch factor during expiration and the entire respiratory cycle inversely correlated with peak VO<sub>2</sub>. This study raises concerns that implanted 16-20mm conduits have become undersized for adolescent Fontan patients.

Currently, typically 16-20mm conduits are implanted in a ‘one size fits all approach’, with all children receiving approximately the same conduit size despite different projected adult body size and related flow conditions. Itatani et al. recommended 16-18mm conduits for 2-3 year old patients based on evaluation of energy loss and flow stagnation using computational fluid dynamics in young Fontan patients (mean BSA 0.5, 3.0 years old, mean conduit flow 0.85 L/min). Conduit size recommendations for older Fontan patients could therefore not be determined. In comparison, in our study BSA and conduit flow rates were approximately 3-4 times higher. In a recent expert review, implantation of 16-18mm conduits are recommended, with larger conduit sizes being associated with worse exercise capacity.[6, 13] However, late studies evaluating

hemodynamics of these conduit sizes in older Fontan patients are currently lacking. The proposed adequacy of 16-20mm conduit sizes for adult Fontan patients has also been based on IVC diameters in healthy adults[12, 14]. Interestingly, the subhepatic IVC diameter is already in the order of 18mm in healthy adults.[15] The mean suprahepatic IVC diameter, distal to entry of the HVs, is significantly larger to account for the increase in flow rate caused by the HVs; a mean of 24mm (CSA 452mm<sup>2</sup>) in healthy adults[16], 27mm (CSA 572mm<sup>2</sup>) in adults with congenital heart disease[16] up to even 770mm<sup>2</sup> in adult Fontan patients[17]. In our study, median conduit CSA was only 221mm<sup>2</sup> and a median 9% smaller compared to the **sub**hepatic IVC CSA, indicating that implanted conduits have become undersized. This is a result of both somatic growth leading to increased flow rates and CSA of surrounding vessels, but also by a decrease in actual conduit CSA during follow-up due to stretching/neo-intima formation in some patients. [7, 11, 12] Congestion most likely did not play a role in the size of the IVC, as no negative correlation was found between BSA and IVC mean velocity.

Previously, our group published the concept of IVC-conduit velocity mismatch based on observations using 4D flow MRI[10]. This parameter is based on the concept that both flow expansion (decrease in velocity) and flow contraction (increase in velocity) should ideally be absent to avoid increased energy loss and/or thrombosis risk.[18] Indeed, mean velocities remained in a relatively narrow range in the native subhepatic IVC and SVC, indicating that these vessels adapt to change in flow rates over time. The rigid extracardiac conduits lacks this physiologic adaptation, explaining the increase in mean conduit velocity with higher conduit flow rates. This becomes evident when looking at the vessels CSA normalized for flow, which was a median 44% smaller for the conduit compared to the IVC. Importantly, IVC-conduit velocity mismatch >1 was already present during expiration in 90% of patients, furthermore indicating that these conduits have become relatively undersized even during the respiratory phase with lowest flow rates.

In light of the reported normal suprahepatic IVC diameters in healthy adults, it is not surprising that we observed a median mismatch factor of 1.8, as median conduit size was only 221mm<sup>2</sup>. Since  $Q=V \cdot A$  (where Q is the flow rate, V is the mean velocity and A is the cross-sectional area), conduit CSA must theoretically be a 1.8-fold higher in our cohort to avoid an increase in mean velocity, effectively indicating a long-segmental stenosis of approximately 50%. These projected values would be in line with suprahepatic CSA observed in healthy persons[16]. Interestingly, the CSA of an intra-atrial lateral Fontan tunnel, in which part of the tunnel wall consists of atrial tissue with growth potential, is already 420-580mm<sup>2</sup> (23-27mm) at an age of 10-15 years.[19, 20] Thus, the physiologic response to increased flow rates during somatic growth seems to lead to importantly larger intra-atrial Fontan tunnels compared to the rigid extracardiac conduit.

***Clinical relevance: TCPC efficiency and long-term outcome***

The observed IVC-conduit velocity mismatch may be of clinical relevance, as the conduit plays an important role in TCPC hemodynamics. Efficient and unobstructed TCPC blood flow with minimal energy loss is desired to minimize the elevation in CVP while ensuring optimal preload in Fontan patients.[5, 21] On average, 65-70% of total systemic venous return enters the TCPC via the conduit, further increasing to 79% during lower-leg exercise[2]. Since blood flow resistance is inversely proportional to the fourth power of the vessel radius (law of Hagen-Poiseuille), undersized conduits are among the most important factors of TCPC resistance.[3] In a large study of CFD simulations during resting conditions, patients with small Fontan conduits showed a 3-fold higher TCPC resistance compared to the mean resistance of the entire study cohort, potentially reaching values up to 35-50% of normal pulmonary vascular resistance.[5] TCPC resistance further increases exponentially during exercise[22] while pulmonary vascular resistance decreases during exercise[23], making TCPCs with a relatively undersized conduit a potential bottleneck in the Fontan circulation.[4, 24]

Decreased TCPC flow efficiency is associated with reduced preload and thereby cardiac output, associated with a decreased exercise capacity.[5, 21, 25] Our study showed a weak inverse correlation between the normalized IVC-conduit velocity mismatch factor and peak VO<sub>2</sub>, which might be explained by the increased TCPC resistance in patients with smaller conduits with higher mismatch. This is in line with recent findings by Patel et al, who found a correlation between minimum conduit size and predicted peak VO<sub>2</sub>. [7]

The increased resistance caused by undersized conduits will lead to an elevated central venous pressure (CVP) to maintain cardiac output, which plays an important role in the pathophysiology of protein losing enteropathy and liver cirrhosis. Fontan patients with an extracardiac conduit show a faster progression of liver fibrosis compared to intra-atrial tunnel Fontan patients.[26] We speculate that the presence of undersized conduits showing important IVC-conduit velocity mismatch might be one of the reasons by increasing afterload for HV flow, especially during inspiration. The acceleration of blood flow in the conduit may also have adverse effects on downstream energy-consuming flow patterns (e.g. vortices, helices) or caval flow collision within the Fontan confluence, further decreasing TCPC flow efficiency.[24]

**Potential implications for surgical strategy**

Our current practice is to implant 18mm fenestrated conduits in our patients and since long we have abandoned implanting 16mm conduits. However, this study shows that a strategy of implanting rigid conduits in children aged 2-4 years results in suboptimal hemodynamics at older age and is therefore not ideal. As implantation of larger conduit sizes in young children is unfeasible by anatomical constraints as well as undesirable

as they will cause sluggish flow increasing thrombosis risk[14, 18], we believe that conduits of other materials should be considered rather than implanting larger conduits. Currently, stretchable ePTFE grafts (PECALabs) are available which could potentially minimize the decrease in conduit CSA caused by stretching during somatic growth and can be dilated to some extent when the child becomes older. Furthermore, tissue-engineered conduits are being developed and may be promising by allowing for growth.[27]

Based on the current study, it is impossible to speculate which levels of IVC-conduit velocity mismatch warrants replacement of the conduit. It will be important to know how observed IVC-conduit velocity mismatch relates to hemodynamic markers such as pressure drop and resistance and how the mismatch develops over time, which will be essential information for clinical decision making about possible intervention. Essentially any pressure drop from the caval veins towards the PAs is undesirable and pressure gradients as low as  $\pm 1$ mmHg already may form an indication to intervene, although exact cut-off points are not available at this moment. Furthermore, although our cohort represented relatively asymptomatic patients without signs of Fontan failure, the chronic negative effects of IVC-conduit velocity mismatch may only become apparent later in life. Serial studies with comprehensive MRI flow evaluation and longer follow-up are needed to determine the effect of undersized conduits on long-term outcome.

## Limitations

Flow rates were analyzed along the respiratory cycle only, irrespective of the phase of the cardiac cycle. Since flow pulsatility along the cardiac cycle is only minimal[28] and predominantly is determined by the respiratory cycle[29], inaccuracies are likely small. Furthermore, CSA was measured from 2D real-time PC-MRI which has a limited spatial resolution and can overestimate CSA when the flow acquisition is not planned precisely perpendicular to the vessel lumen. However, these errors are likely systematic as CSA of all vessels were measured using the same method. HV flow was only measured indirectly by subtracting IVC flow from conduit flow, but results are in strong agreement with a previous study that directly measured HV flow using echocardiography.[30]

## Conclusion

This study evaluated the hemodynamic adequacy of extracardiac Goretex conduits sized 16-20mms along the respiratory cycle in Fontan patients. Important IVC-conduit velocity mismatch, i.e. an increase in velocity from the subhepatic IVC towards the conduit, is observed at a mean interval of 13 years after Fontan completion. This raises

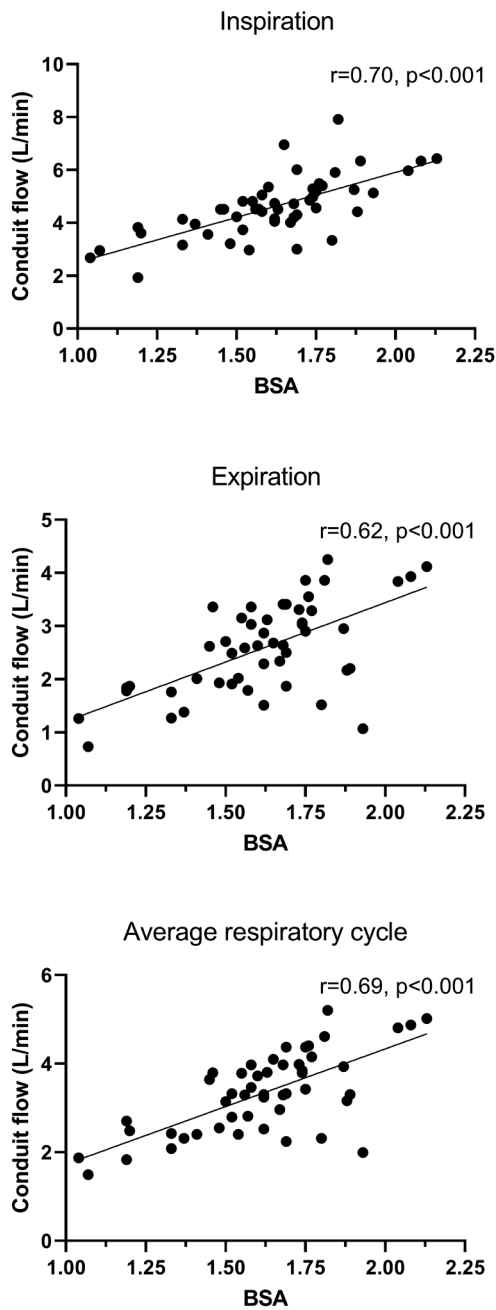
concerns that implanted 16-20mm conduits have become undersized for older Fontan patients. The normalized IVC-conduit velocity mismatch factor showed an inverse weak correlation with peak  $\dot{V}O_2$ . Future studies are warranted to clarify the long-term effect of IVC-conduit velocity mismatch on clinical outcome.

## References

- [1] Rychik J, Atz AM, Celermajer DS, Deal BJ, Gatzoulis MA, Gewillig MH et al. Evaluation and Management of the Child and Adult With Fontan Circulation: A Scientific Statement From the American Heart Association. *Circulation* 2019.
- [2] Hjortdal VE, Emmertsen K, Stenbog E, Frund T, Schmidt MR, Kromann O et al. Effects of exercise and respiration on blood flow in total cavopulmonary connection: a real-time magnetic resonance flow study. *Circulation* 2003;108:1227-31.
- [3] Tang E, Restrepo M, Haggerty CM, Mirabella L, Bethel J, Whitehead KK et al. Geometric characterization of patient-specific total cavopulmonary connections and its relationship to hemodynamics. *JACC Cardiovasc Imaging* 2014;7:215-24.
- [4] Rijnberg FM, Hazekamp MG, Wentzel JJ, de Koning PJH, Westenberg JJM, Jongbloed MRM et al. Energetics of Blood Flow in Cardiovascular Disease: Concept and Clinical Implications of Adverse Energetics in Patients With a Fontan Circulation. *Circulation* 2018;137:2393-407.
- [5] Haggerty CM, Restrepo M, Tang E, de Zelicourt DA, Sundareswaran KS, Mirabella L et al. Fontan hemodynamics from 100 patient-specific cardiac magnetic resonance studies: a computational fluid dynamics analysis. *J Thorac Cardiovasc Surg* 2014;148:1481-9.
- [6] Lee SY, Song MK, Kim GB, Bae EJ, Kim SH, Jang SI et al. Relation Between Exercise Capacity and Extracardiac Conduit Size in Patients with Fontan Circulation. *Pediatr Cardiol* 2019;40:1584-90.
- [7] Patel ND, Friedman C, Herrington C, Wood JC, Cheng AL. Progression in Fontan conduit stenosis and hemodynamic impact during childhood and adolescence. *J Thorac Cardiovasc Surg* 2020.
- [8] Khiabani RH, Whitehead KK, Han D, Restrepo M, Tang E, Bethel J et al. Exercise capacity in single-ventricle patients after Fontan correlates with haemodynamic energy loss in TCPC. *Heart* 2015;101:139-43.
- [9] Trusty PM, Wei ZA, Rychik J, Graham A, Russo PA, Surrey LF et al. Cardiac Magnetic Resonance-Derived Metrics Are Predictive of Liver Fibrosis in Fontan Patients. *Ann Thorac Surg* 2020;109:1904-11.
- [10] Rijnberg FM, Elbaz MSM, Westenberg JJM, Kamphuis VP, Helbing WA, Kroft LJ et al. Four-dimensional flow magnetic resonance imaging-derived blood flow energetics of the inferior vena cava-to-extracardiac conduit junction in Fontan patients. *Eur J Cardiothorac Surg* 2019;55:1202-10.
- [11] Amodeo A, Galletti L, Marianeschi S, Picardo S, Giannico S, Di Renzi P et al. Extracardiac Fontan operation for complex cardiac anomalies: seven years' experience. *J Thorac Cardiovasc Surg* 1997;114:1020-30; discussion 30-1.
- [12] Cho S, Kim WH, Choi ES, Kwak JG, Chang HW, Hyun K et al. Outcomes after extracardiac Fontan procedure with a 16-mm polytetrafluoroethylene conduit. *Eur J Cardiothorac Surg* 2018;53:269-75.
- [13] Daley M, d'Udekem Y. The optimal Fontan operation: Lateral tunnel or extracardiac conduit? *J Thorac Cardiovasc Surg* 2020.
- [14] Alexi-Meskishvili V, Ovroutski S, Ewert P, Dahnert I, Berger F, Lange PE et al. Optimal conduit size for extracardiac Fontan operation. *Eur J Cardiothorac Surg* 2000;18:690-5.
- [15] Moreno FL, Hagan AD, Holmen JR, Pryor TA, Strickland RD, Castle CH. Evaluation of size and dynamics of the inferior vena cava as an index of right-sided cardiac function. *Am J Cardiol* 1984;53:579-85.

- [16] E. Ettinger IS. Angiocardiographic measurement of the cardiac segment of the inferior vena cava in health and in cardiovascular disease. *Circulation* 1962;26:508-15.
- [17] P. Zielinski IM, E. Kowalik, A. Mierzynska, A. Klisiewicz, M. Kowalczyk, P. Kwiatek, M. Kusmierczyk, J. Rozanski, M. Kowalski, P. Hoffman. Is there any role for computed tomography imaging in anticipating the functional status in adults late after total cavopulmonary connection? A retrospective evaluation. *Kardiologia Polska* 2019.
- [18] Itatani K, Miyaji K, Tomoyasu T, Nakahata Y, Ohara K, Takamoto S et al. Optimal conduit size of the extracardiac Fontan operation based on energy loss and flow stagnation. *Ann Thorac Surg* 2009;88:565-72; discussion 72-3.
- [19] Bossers SS, Cibis M, Gijzen FJ, Schokking M, Strengers JL, Verhaart RF et al. Computational fluid dynamics in Fontan patients to evaluate power loss during simulated exercise. *Heart* 2014;100:696-701.
- [20] Restrepo M, Mirabella L, Tang E, Haggerty CM, Khiabani RH, Fynn-Thompson F et al. Fontan pathway growth: a quantitative evaluation of lateral tunnel and extracardiac cavopulmonary connections using serial cardiac magnetic resonance. *Ann Thorac Surg* 2014;97:916-22.
- [21] Sundareswaran KS, Pekkan K, Dasi LP, Whitehead K, Sharma S, Kanter KR et al. The total cavopulmonary connection resistance: a significant impact on single ventricle hemodynamics at rest and exercise. *Am J Physiol Heart Circ Physiol* 2008;295:H2427-35.
- [22] Whitehead KK, Pekkan K, Kitajima HD, Paridon SM, Yoganathan AP, Fogel MA. Nonlinear power loss during exercise in single-ventricle patients after the Fontan: insights from computational fluid dynamics. *Circulation* 2007;116:1165-71.
- [23] Schmitt B, Steendijk P, Ovroutski S, Lunze K, Rahmzadeh P, Maarouf N et al. Pulmonary vascular resistance, collateral flow, and ventricular function in patients with a Fontan circulation at rest and during dobutamine stress. *Circ Cardiovasc Imaging* 2010;3:623-31.
- [24] Rijnberg FM, van Assen HC, Hazekamp MG, Roest AAW, Westenberg JJM. Hemodynamic Consequences of an Undersized Extracardiac Conduit in an Adult Fontan Patient Revealed by 4-Dimensional Flow Magnetic Resonance Imaging. *Circ Cardiovasc Imaging* 2021;14:e012612.
- [25] Goldberg DJ, Avitabile CM, McBride MG, Paridon SM. Exercise capacity in the Fontan circulation. *Cardiol Young* 2013;23:824-30.
- [26] Evans WN, Acherman RJ, Mayman GA, Galindo A, Rothman A, Winn BJ et al. The Rate of Hepatic Fibrosis Progression in Patients Post-Fontan. *Pediatr Cardiol* 2020;41:905-09.
- [27] Schwarz EL, Kelly JM, Blum KM, Hor KN, Yates AR, Zbinden JC et al. Hemodynamic performance of tissue-engineered vascular grafts in Fontan patients. *NPJ Regen Med* 2021;6:38.
- [28] Rijnberg FM, van Assen HC, Juffermans JF, Kroft LJM, van den Boogaard PJ, de Koning PJH et al. Reduced scan time and superior image quality with 3D flow MRI compared to 4D flow MRI for hemodynamic evaluation of the Fontan pathway. *Sci Rep* 2021;11:6507.
- [29] van der Woude SFS, Rijnberg FM, Hazekamp MG, Jongbloed MRM, Kenjeres S, Lamb HJ et al. The Influence of Respiration on Blood Flow in the Fontan Circulation: Insights for Imaging-Based Clinical Evaluation of the Total Cavopulmonary Connection. *Front Cardiovasc Med* 2021;8:683849.
- [30] Hsia TY, Khambadkone S, Deanfield JE, Taylor JF, Migliaavacca F, De Leval MR. Subdiaphragmatic venous hemodynamics in the Fontan circulation. *J Thorac Cardiovasc Surg* 2001;121:436-47.

Supplementary materials



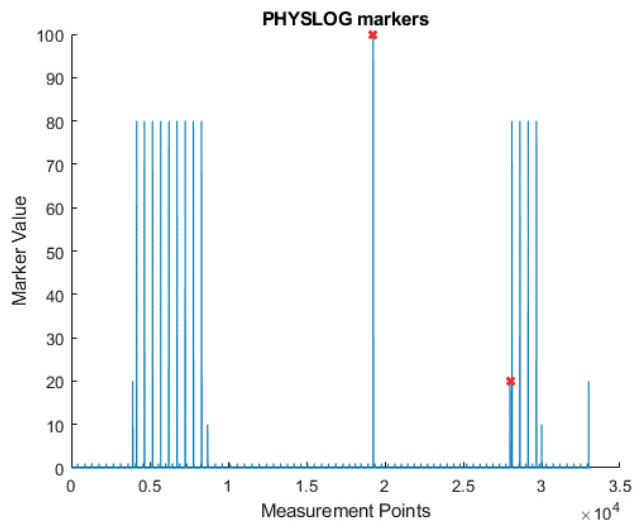
**Supplemental Figure 1.** A moderate to strong relationship is shown between BSA (Haycock) and conduit flow. However, important variability is observed in flow rates for patients with similar BSA



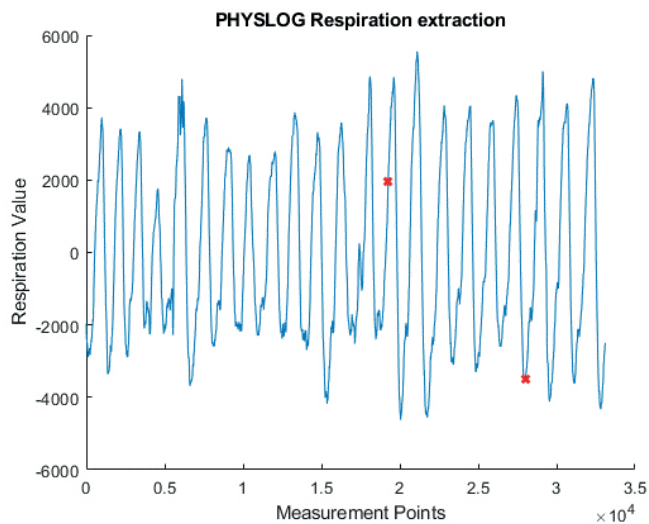
## Supplemental material 1: 2D real-time flow MRI methodology

Multiple steps were performed to determine flow rates along the average respiratory cycle, inspiration and expiration from 2D real-time flow MRI acquisitions.

Philips physiology log files (PHYSLOG) were exported from the scanner for offline analysis of the respiratory signal at time of each 2D real-time flow acquisition. From these PHYSLOG files, the part of the respiratory signal corresponding to the 2D real-time flow acquisition was determined based on the manual start marker (marker value 100) and the stop marker (marker value 20) of each 2D flow acquisition (Supplemental Figure 1A-B).

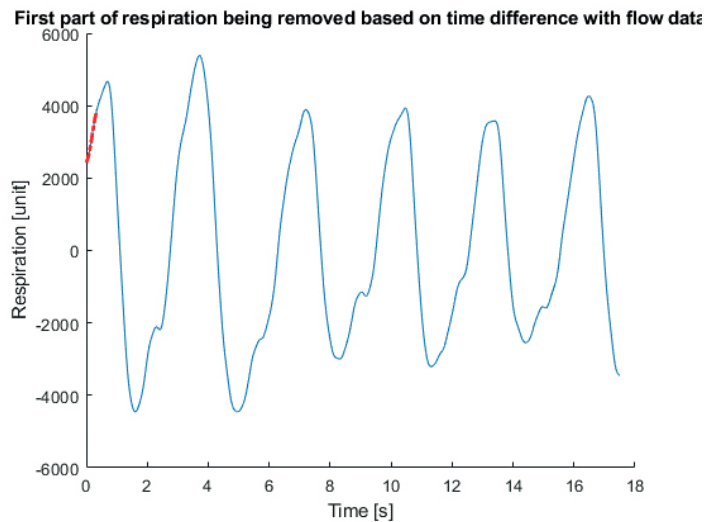


Supplemental Figure 1A



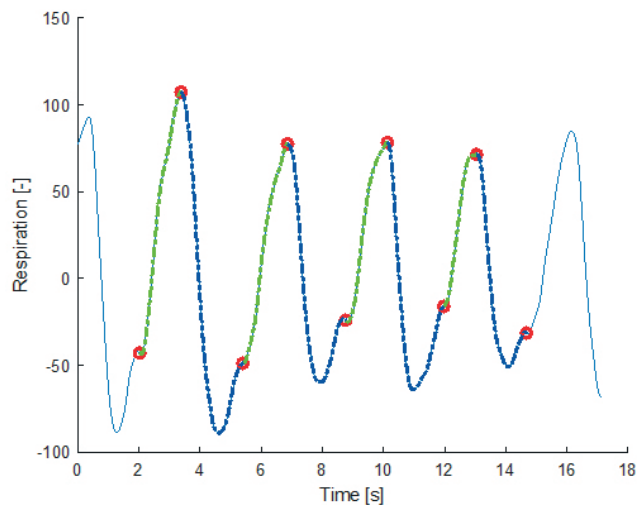
Supplemental Figure 1B

Since the start marker is known to not properly synchronize with the onset of the first flow volume<sup>1</sup>, the duration of the respiratory signal from the PHYSLOG file slightly exceeded the duration of the corresponding flow acquisition. Therefore, the difference in duration between the respiratory signal and flow acquisition was removed from the first part of the respiratory signal (Supplemental Figure 1C, red part).



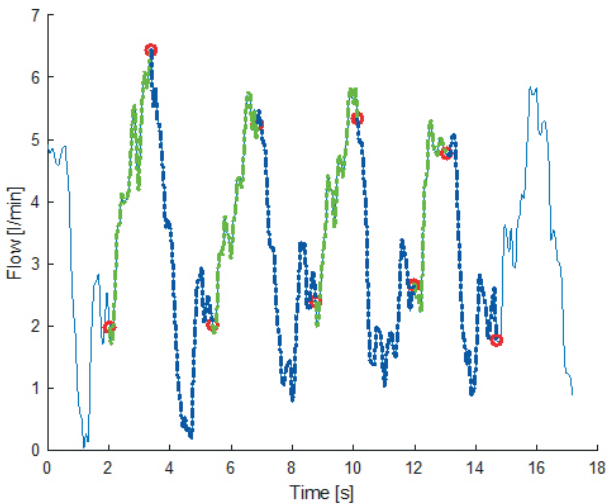
Supplemental Figure 1C

In general 2-4 consecutive respiratory cycles were extracted from the respiratory curve and subsequently divided into inspiration and expiration. Expiration was defined as the start of the downward deflection from the maximum value (Supplemental Figure 1D, blue). Inspiration started at the (last) bendpoint in the upward signal (Supplemental Figure 1D, green). The presence of an end-expiratory, upward drift of the respiratory signal towards the baseline was the reason why the start of the upward signal can not be used to mark the start of the inspiration.



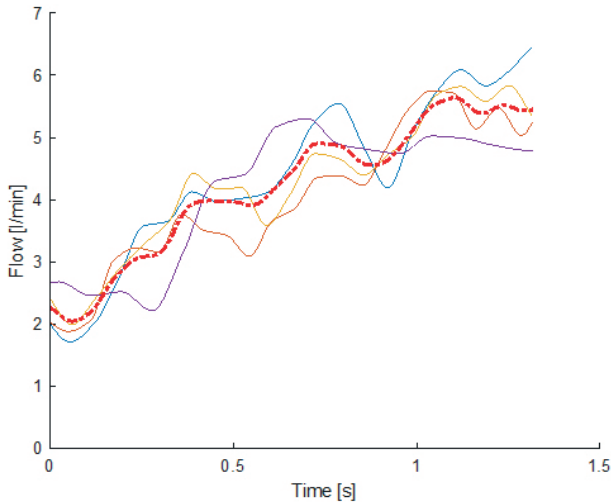
**Supplemental Figure 1D**

Subsequently, the flow and velocity curve were divided into the corresponding inspiratory and expiratory parts (Supplemental Figure 1E, showing the flow curve only).

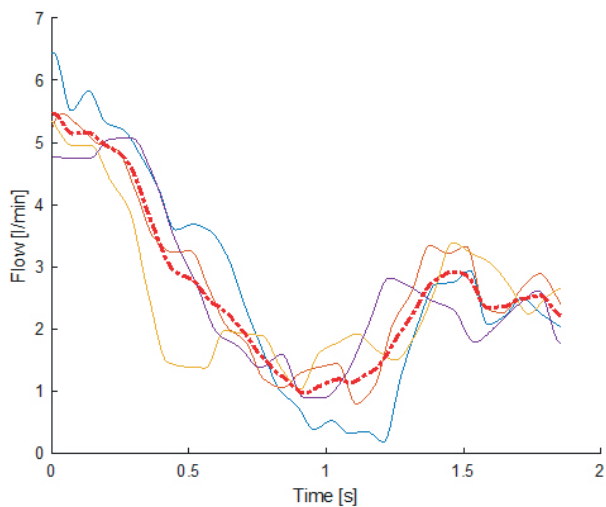


**Supplemental Figure 1E**

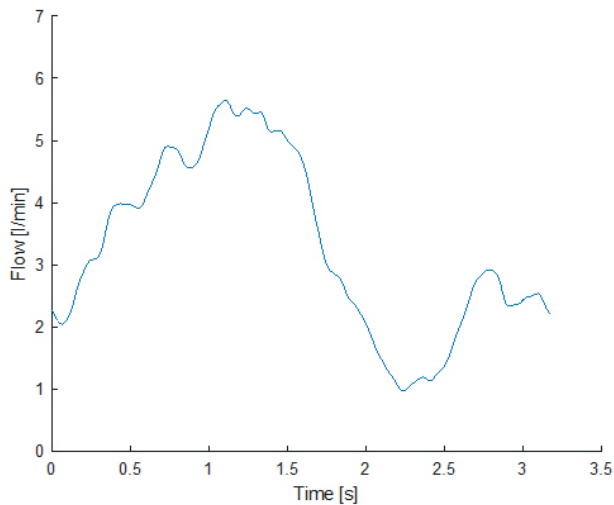
A single, average curve (Supplemental Figure 1H) was derived from the 2-4 individual inspiratory (Supplemental Figure 1F) and expiratory (Supplemental Figure 1G) curves using interpolation. Flow and velocity parameters were determined based on the average curves.



**Supplemental Figure 1F**

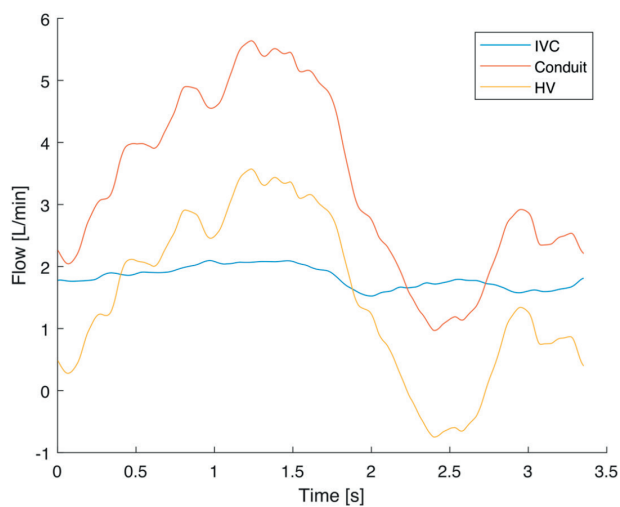


Supplemental Figure 1G



Supplemental Figure 1H

To acquire the real-time HV flow curve, the average inspiratory and expiratory flow curves from the IVC and conduit were aligned using interpolation. Subsequently, based on conservation of mass, HV flow was determined by subtracting IVC flow from conduit flow (Supplemental Figure 1i).



Supplemental Figure 1i

References

1. <https://nl.mathworks.com/matlabcentral/fileexchange/42100-readphilipsscanphyslog-filename-channels-skipprep>

Supplemental Table 1. 2D realtime flow MRI details

MRI details	2D realtime PC-MRI
Slice thickness (mm)	6
Acquired in-plane spatial resolution	2.5 x 2.5
Reconstructed in-plane spatial resolution (mm)	1.12 x 1.12
Temporal resolution	63-67ms
Nr of samples	250
ECG-gating	-
Respiratory compensation	-
Flip angle	20
TR (ms)	16
TE (ms)	8.7
Acceleration methods	SENSE factor 3, EPI 11

mm; millimetre, ECG; electrocardiogram, PC-MRI; phase contrast, MRI; magnetic resonance imaging

## CHAPTER 8



# 4D flow MRI derived energetics in the Fontan circulation correlate with exercise capacity and cT1 liver mapping

Friso M. Rijnberg, Jos J.M. Westenberg, Hans C. van Assen, Joe F. Juffermans, Lucia J.M. Kroft, Pieter J. van den Boogaard, Covadonga Terol Espinosa de Los Monteros, Evangeline G. Warmerdam, Tim Leiner, Heynric B. Grotenhuis, Monique R.M. Jongbloed, Mark G. Hazekamp, Arno A.W. Roest, Hildo J. Lamb



# Abstract

## Aim

This study explores the relationship between in vivo 4D flow MRI derived blood flow energetics in the TCPC, exercise capacity and MRI-derived liver fibrosis/congestion.

## Background

The Fontan circulation, in which both caval veins are directly connected with the pulmonary arteries (i.e. the total cavopulmonary connection ,TCPC) is the palliative approach for single ventricle patients. Blood flow efficiency in the TCPC has been associated with exercise capacity and liver fibrosis using in silico computational fluid dynamic modelling. Nowadays, 4D flow MRI allows for assessment of in vivo blood flow energetics, including kinetic energy (KE) and viscous energy loss rate (EL).

## Methods

Fontan patients were prospectively evaluated using a comprehensive cardiovascular and liver MRI protocol, including 4D flow imaging of the TCPC, between 2018-2021. Peak VO<sub>2</sub> was determined using cardiopulmonary exercise testing (CPET). Iron-corrected whole liver T1 mapping was performed as a marker of liver fibrosis/congestion (cT1). KE and EL in the TCPC were computed from 4D flow MRI and normalized for inflow. Furthermore, blood flow energetics were compared between standardized segments of the TCPC.

## Results

Sixty-two Fontan patients were included (53% male, mean age 17.3±5.1 years). Maximal effort CPET was obtained in 50 patients (mean peak VO<sub>2</sub> 27.1±6.2 ml/kg/min, 56±12% of predicted). Both KE and EL in the entire TCPC (n=28) were significantly correlated with cT1 (r=0.50, p=0.006 and r=0.39, p=0.04, respectively), peak V02 (r=-0.61, p=0.003 and r=-0.54, p=0.009, respectively) and predicted peak V02 (r=-0.44, p=0.04 and r=-0.46, p=0.03, respectively). Segmental analysis indicated that the most adverse flow energetics were found in the Fontan tunnel and left pulmonary artery.

## Conclusions

Adverse 4D flow MRI derived kinetic energy and viscous energy loss rate in the TCPC correlate with decreased exercise capacity and increased levels of liver fibrosis/congestion. 4D flow MRI is promising as a non-invasive screening tool for identification of patients with adverse TCPC flow efficiency that may guide treatment strategies during follow-up.

## Introduction

The Fontan procedure provides a unique surgical solution for congenital heart disease patients with a functionally univentricular heart defect, by connecting the systemic venous return directly with the pulmonary arteries (i.e. the total cavopulmonary connection: TCPC). Consequently, the Fontan circulation requires increased central venous pressure (CVP) to overcome the serial resistance in the TCPC and pulmonary vascular bed to maintain an adequate cardiac output. The chronic exposure to elevated venous pressures provides a significant burden for upstream organs, including an almost universal occurrence of liver fibrosis.<sup>1</sup> Furthermore, the ability to increase preload and thereby cardiac output during exercise is limited leading to a diminished exercise capacity.<sup>2</sup>

Being one of the few modifiable factors in the Fontan circulation, blood flow efficiency in the TCPC has been widely studied using predominantly in silico computational fluid dynamic (CFD) models.<sup>3-5</sup> Highly variable blood flow efficiency in the TCPC has been reported, related to the presence of energy-consuming geometric factors that can become apparent during follow-up.<sup>3,5</sup> Recently, correlations were found between CFD-derived TCPC blood flow efficiency and clinical outcome, including liver fibrosis<sup>6</sup> and exercise capacity.<sup>7</sup>

Drawbacks of CFD modelling are that it is time-consuming and requires expert knowledge and infrastructure, limiting widespread use in clinical care. 4D flow magnetic resonance imaging (MRI) is emerging as a non-invasive screening tool for visualization of energy-consuming flow patterns in the TCPC and quantification of flow-related hemodynamic parameters including kinetic energy (KE) and viscous energy loss rate (EL).<sup>8-10</sup> The hypothesis in this study is that these in vivo 4D flow MRI-derived energetics in the TCPC are associated with exercise capacity and liver fibrosis/congestion. Subsequently, the aim of this study is to determine KE and EL in the TCPC using 4D flow MRI and assess the relationship with exercise capacity and MR-based assessment of liver fibrosis/congestion.

## Materials and methods

### Study population

Sixty-two Fontan patients were prospectively evaluated using a comprehensive cardiovascular and liver MRI protocol, including 4D flow imaging of the TCPC, between

2018-2021 at the Leiden University Medical Center. All patients >8 years old without contraindications for MRI were eligible for inclusion.

### **Cardiopulmonary exercise testing**

Cardiopulmonary exercise testing (CPET) was performed on an upright bicycle ergometer (GE Healthcare, Wisconsin, USA) including peak oxygen uptake assessment (VO<sub>2</sub>). CPET was performed on the same day or within 6 months of MRI. A continuous incremental bicycle protocol was executed according to the Godfrey protocol.<sup>11</sup> Peak VO<sub>2</sub> (ml/kg/min) and percentage of predicted peak VO<sub>2</sub> (%) were determined in all patients that achieved maximal effort (respiratory exchange ratio >1.0) using previously reported reference values.<sup>12</sup>

### **Laboratory data**

Standard laboratory assessment was performed on the same day or within 6 months of MRI, including liver enzymes, total protein, albumin, total bilirubin, and international normalized ratio (INR). Additionally, a feces sample was tested on alfa-1-antitrypsin excretion as a marker of (early) protein losing enteropathy. Results were interpreted using the hospital's standard age- and gender-specific reference values.

### **Magnetic resonance imaging**

All MRI examinations were performed on a 3T Philips scanner (Ingenia, Philips Healthcare, Best, the Netherlands).

#### ***Multiparametric Liver imaging***

Patients underwent multiparametric liver imaging using proton density fat-fraction (PDFF), T2\*, and iron-corrected T1 mapping (cT1) for the assessment of liver fat, iron, and fibrosis/inflammation/congestion, respectively (Liver MultiScan™, Perspectum Diagnostics Ltd., Oxford, UK).<sup>13</sup> Patients underwent liver imaging after fasting for at least 4 hours. No intravenous contrast agent was used. Values were calculated from segmentation of whole liver regions (cT1 and PDFF) or one or more regions of interest (T2\*) on one or more transversal slices. cT1 mapping allows for quantification of extracellular fluid in the liver, which is increased in both liver fibrosis, inflammation and venous congestion. Since inflammation is usually absent in liver fibrosis in Fontan patients<sup>14</sup> and liver enzymes are usually normal or only mildly elevated, elevated cT1 values in Fontan patients will predominantly reflect fibrosis and/or venous congestion. Reference values of PDFF, T2\* and cT1 are <5.6%, >12.5ms and 633-794ms, respectively.<sup>15-17</sup> All liver scans were anonymized and subsequently analyzed by Perspectum Diagnostics (Oxford, UK) using an online portal.

### ***Ventricular function***

Ventricular ejection fraction and cardiac output were calculated by ventricular volume analysis (MASS software, Leiden, the Netherlands) of multislice two-dimensional cine transversal images using a steady-state-free-precession sequence. The cardiac index was derived by normalizing cardiac output for body surface area (Haycock).

### ***4D flow MRI***

Patients underwent retrospective ECG- and respiratory navigator-gated 4D flow MRI examination dedicated for imaging of the TCPC. Acquisition details for 4D flow MRI are covered in Supplemental Table 1.

A 3D reconstruction of the TCPC was semi-automatically segmented on magnitude-weighted speed images of a time-averaged reconstruction of the 4D flow velocity field (CAAS v5.1, MR Solutions, Pie Medical Imaging). The region of interest covered the area between the Fontan tunnel (above entry of the hepatic veins), SVC (below the brachiocephalic vein) and the right- and left pulmonary arteries (PAs) up to the levels of the segmental branches. The right upper lobe branch was excluded from the segmentation since the resolution of the 4D flow MRI for this small vessel is insufficient.

Both the KE and EL of blood flow in the TCPC were computed from the 4D flow MRI velocity field using in-house developed software, as previously described.<sup>18</sup> KE represents the amount of energy in the blood flow due to its motion. EL represents the rate of kinetic energy lost in the blood flow due to friction and can be computed from three-dimensional velocity gradients derived from 4D flow MRI. EL was computed using the viscous dissipation function from the Navier-Stokes equation, assuming laminar blood flow.<sup>18</sup> The total amount of KE (in millijoule, [mJ]) and EL (in milliwatts, mW) within the TCPC is computed by summing voxel-wise energetics for each time-phase (24 phases per cardiac cycle). The cardiac-cycle averaged values are reported. In patients in whom the entire TCPC was available for analysis, energetics were normalized for inflow (SVC + Fontan tunnel flow, in L/min);  $KE_{\text{norm\_flow}}$  in mJ per L/min and  $EL_{\text{norm\_flow}}$  in mW per L/min.<sup>19</sup>

### ***Segmental analysis***

To further explore and compare the energetics in the specific components of the TCPC, a sub analysis was performed to determine segment-specific energetics (Fontan tunnel, central Fontan confluence, SVC, LPA and RPA), using in-house developed software as previously described.<sup>19</sup> Additional benefit of this approach is that in patients with a fenestration closure device or PA stent in situ, in whom the entire TCPC cannot be segmented because of device-related flow artefacts, energetics in the TCPC segments without device-related artefacts can still be studied. In these patients, only part of the Fontan tunnel (distal to the device) or PA (proximal to the stent) can be included in

the segmentation. Segments with a length <1.5cm were excluded from the analysis to ensure sufficient voxels for energetic analysis.<sup>19</sup>

In summary, the TCPC was automatically divided into 5 segments. Energetics within each segment were normalized for segment-specific inflow (Fontan confluence) or inflow + length (Fontan tunnel, SVC, LPA, RPA;  $KE_{\text{norm\_flow+length}}$  and  $EL_{\text{norm\_flow+length}}$ ).<sup>19</sup> Cross-sectional areas (CSA) normalized for BSA of the included conduit, SVC, LPA and RPA segments were determined perpendicularly to their centerlines at a 1mm interval.<sup>20</sup> The mean CSA of each segment is reported.

## Statistical analysis

Continuous data were presented as mean (standard deviation) or median (interquartile range, IQR), as appropriate. Normal distributions of continuous data were tested using the Shapiro-Wilk test. Pearson and/or Spearman correlation analysis (weak 0.3-0.5, moderate 0.5-0.7, strong  $\geq 0.7$ -0.9 and excellent  $>0.9$ ) was performed between the main endpoints (cT1 liver mapping and maximal exercise capacity) and MRI parameters; ventricular function and 4D flow energetics in the entire TCPC. Segment-specific energetics (Fontan tunnel, SVC, LPA and RPA) were compared with each other using the Kruskal Wallis test (adjusted by the Bonferroni method for multiple tests). Correlation analysis was performed between segment-specific energetics and normalized CSA. A p-value <0.05 was considered statistically significant. Data were analyzed with SPSS 25.0 (IBM Corp., Armonk, NY, USA) and GraphPad Prism 8.0 (GraphPad Software, La Jolla, California, USA ).

## Results

### Study population

Patient characteristics are shown in Table 1. Fifty-three percent of patients was male. Mean age at MRI of  $17.3 \pm 5.1$  years and mean time between Fontan completion and MRI was  $13.6 \pm 4.8$  years. The majority of patients (94%) underwent Fontan completion using a (fenestrated) 16-20mm extracardiac Goretex conduit. Fenestrations closed spontaneously or were routinely closed after Fontan completion using a fenestration closure device. One patient still had a patent fenestration at time of MRI. All but two patients were in good clinical condition (New York Heart Association class I-II).

**Table 1.** Patient characteristics

Male/Female, n	33/29
Primary diagnosis, n (%)	
- TA	14(23)
- HLHS	12(19)
- DILV + TGA	10(16)
- DORV	6(10)
- uAVSD	5(8)
- ccTGA	5(8)
- PA + IVS	5(8)
- Other	5(8)
Dominant ventricle	
Left, n (%)	35(56)
Right, n (%)	21(34)
Biventricular/indeterminate, n (%)	6(10)
<b>Characteristics at Fontan procedure</b>	
Previous bidirectional Glenn shunt, n(%)	62 (100)
Age at Fontan, years	3.7(1.8)
Fontan technique LT/ECC	4/58
Implanted conduit size (16/18/20mm), n	30/22/6
Fenestration, n(%)	38(61)
<b>Characteristics at time of MRI</b>	
Age at MRI, years	17.3(5.1)
Height, cm	167(12)
BSA, m <sup>2</sup>	1.6(0.3)
Time between Fontan and MRI, years	13.6(4.8)
NYHA-class I-II, n (%)	60(97)

Values are reported as mean (standard deviation) unless otherwise specified. TA; tricuspid atresia, HLHS; hypoplastic left heart syndrome, DILV; double inlet left ventricle, (cc)TGA; (congenital corrected) transposition of the great arteries, DORV; double outlet right ventricle, uAVSD; unbalanced atrioventricular septal defect, PA+IVS; pulmonary atresia with intact ventricular septum, LT; lateral tunnel, ECC; extracardiac conduit

### **CPET and laboratory**

CPET results are presented in Table 2. CPET was performed in 57 patients (92%), with 50 patients achieving maximal effort. Mean peak VO<sub>2</sub> was 27.1±6.2 ml/kg/min, 57%±12% of predicted peak VO<sub>2</sub>.

Laboratory results are provided in Table 3. Total protein and albumin were normal in all but one patient with refractory protein losing enteropathy. Alanine aminotransferase, Aspartate aminotransferase and gamma glutamyltransferase levels were normal or only mildly elevated in the majority of patients. Alfa-1-antitrypsin excretion in the feces was normal (n=48) or only mildly elevated (n=3) in all patients.

## Comprehensive MRI analysis

### *Multiparametric Liver imaging*

Multiparametric liver imaging was performed in all patients. cT1 analysis could not be performed in one patient due to insufficient data quality. cT1 (reference 633-794ms) was elevated in all patients (mean cT1  $964 \pm 63$ ms, range 824-1073ms). T2\* was within normal ranges (reference value  $>12.5$ ms) in all patients (mean T2\*  $22.6 \pm 3.4$ ms). Mean PDFF (reference value  $<5.6\%$ ) was  $1.7 \pm 3.3\%$ . Only one patient had an elevated PDFF of 27.1% indicating liver steatosis.

### *Ventricular function and 4D flow MRI energetics*

Mean cardiac index and ejection fraction were  $3.4 \pm 0.09$  L/min/m<sup>2</sup> and  $48 \pm 7\%$ , respectively. 4D flow MRI of the TCPC was acquired in 61 patients. One patient wanted to stop with the MRI examination before acquisition of 4D flow MRI was completed. Five patients were excluded from 4D flow analysis due to insufficient image quality (excessive patient movement related,  $n=4$ ) or because of the presence of multiple central device-related artefacts affecting the majority of the TCPC. The total TCPC without device-related MR artefacts was available for 4D flow energetic analysis in 28/56 patients (50%).

In the patients in whom the entire TCPC was available for analysis,  $KE_{\text{norm\_flow}}$  and  $EL_{\text{norm\_flow}}$  in the total TCPC were  $0.26 \pm 0.068$  mJ per L/min and  $0.075 \pm 0.022$  mW per L/min inflow. Energetics were not significantly different between genders ( $p=0.27-0.37$ ). A significant positive correlation was observed for  $KE_{\text{norm\_flow}}$  and  $EL_{\text{norm\_flow}}$  with cT1 ( $r=0.50$ ,  $p=0.006$  and  $r=0.39$ ,  $p=0.04$ , respectively, Figure 1). An example of TCPC blood flow patterns, related energetics and cT1 liver mapping is shown for two extracardiac Fontan patients in Figure 2. Furthermore,  $KE_{\text{norm\_flow}}$  and  $EL_{\text{norm\_flow}}$  showed a significant negative correlation with peak VO2 ( $r=-0.61$ ,  $p=0.003$  and  $r=-0.54$ ,  $p=0.009$ , respectively) and predicted % peak VO2 ( $r=-0.44$ ,  $p=0.04$  and  $r=-0.46$ ,  $p=0.03$ , respectively, Figure 1). No significant correlations were found between cardiac index or ejection fraction with cT1 or (predicted) peak VO2.

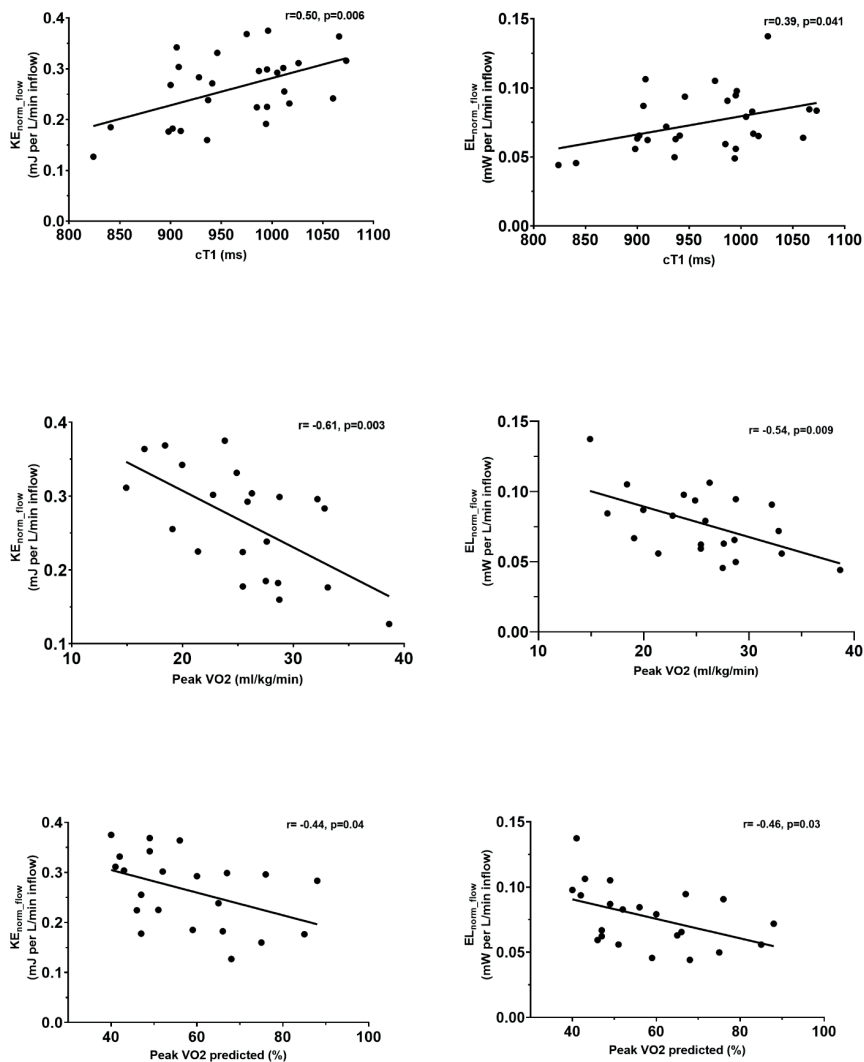


**Figure 1.** Correlation analysis between KE (left) and EL (right) in the total TCPC with cT1 (upper panel), peak VO2 (middle panel) and predicted peak VO2 (lower panel) are shown.

KE; kinetic energy, EL; viscous energy loss rate



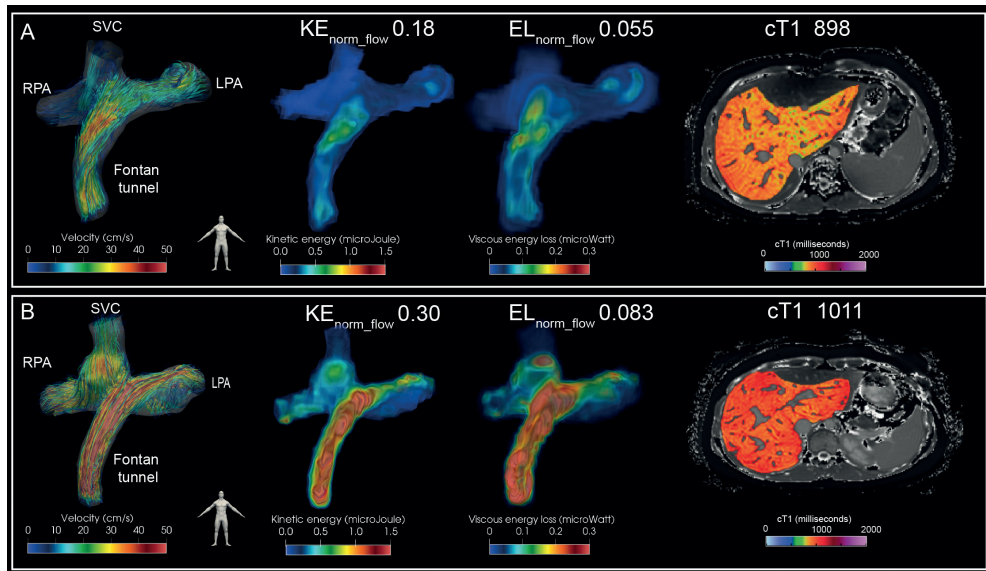


**Figure 2.** Streamline representation of blood flow in the TCPC is shown for two representative female extracardiac Fontan patients with a 16mm Goretex conduit (left panel) for the first phase of the cardiac cycle. Corresponding spatial distribution of KE and EL is shown (middle panels). The time-averaged normalized energetics values are indicated above. Whole liver cT1 mapping is shown for a transversal slice (right panel). Note how a strong difference in blood flow velocity is present at the level of the extracardiac conduit which is strongly correlated to the areas of increased KE and EL. Patient A: 17 years old, double inlet left ventricle + transposition of the great arteries, BSA 1.5. Patient B: 18 years old, tricuspid atresia, BSA 1.8).

BSA; body surface area, KE; kinetic energy, EL; viscous energy loss rate, cT1; iron-corrected T1 mapping, RPA/LPA; right/left pulmonary artery, SVC; superior vena cava.

### Segmental 4D flow MRI energetics

Results of segmental TCPC energetics are reported in Table 4.  $KE_{\text{norm\_flow+length}}$  was lowest in the SVC and lower compared to the Fontan tunnel ( $p<0.001$ ), RPA ( $p=0.002$ ) and LPA ( $p<0.001$ ).  $KE_{\text{norm\_flow+length}}$  was higher in the LPA compared to the RPA ( $p=0.027$ ).  $EL_{\text{norm\_flow+length}}$  was higher in the conduit ( $p=0.024$ ) and LPA ( $p<0.001$ ) compared to the SVC and higher in the LPA compared to the RPA ( $p<0.001$ ). In the Fontan tunnel, mean CSA showed a strong negative correlation with  $KE_{\text{norm\_flow+length}}$  ( $\rho = -0.80$ ,  $p<0.001$ ) and  $EL_{\text{norm\_flow+length}}$  ( $\rho = -0.78$ ,  $p<0.001$ , Supplemental Table 2). A weak correlation was found between mean LPA CSA and  $EL_{\text{norm\_flow+length}}$  ( $\rho = -0.31$ ,  $p=0.034$ ). Energetics in the RPA and SVC were not related to segment-specific CSA.

**Table 2.** CPET results

SBP <sub>basal</sub> , mmHg	124(15)
SBP <sub>peak</sub> , mmHg	172(26)
RER <sub>peak</sub>	1.1(0.09)
Power, watt	131(37)
% predicted	68(15)
HR <sub>rest</sub> , bpm	82(15)
HR <sub>peak</sub> , bpm	172(17)
% predicted	93(10)
HR <sub>reserve</sub> , bpm	91(25)
<b>Maximal exercise (n=50)</b>	
VO <sub>2</sub> peak, ml/kg/min	27.1(6.2)
% predicted	57(12)

Values are reported as mean (standard deviation). HR<sub>peak</sub>: maximal heart rate at peak exercise; HR<sub>reserve</sub>: maximal heart rate-resting heart rate; HR<sub>rest</sub>: resting heart rate; RER<sub>peak</sub>: respiratory exchange ratio at peak exercise; SBP<sub>basal/peak</sub>: systolic blood pressure at rest/peak; VO<sub>2peak</sub>: oxygen uptake at peak exercise

**Table 3.** Laboratory results

	n	Mean (SD)	Range	Abnormal level, n (%)
Total protein, g/L	56	71(7)	35-83	1 (2)
Albumin, g/L	59	48(5)	18-54	1 (2)
Aspartate aminotransferase, U/L	57	32(10)	18-74	22 (39)
Alanine aminotransferase, U/L	58	36(16)	15-111	14 (24)
Gamma glutamyltransferase, U/L	56	58(40)	18-185	25 (45)
Total bilirubin, $\mu$ mol/L	55	15(10)	5-49	13 (24)
INR*, (reference $\leq 1.2$ )	42	1.1(0.1)	1.0-1.5	3 (7)
Fecal alfa-1-antitrypsine, mg/g (reference <0.4)	51	0.2(0.1)	0.1-0.7	3 (6)

\*Patients on oral anticoagulation were excluded. SD, standard deviation

**Table 4.** 4D flow MRI derived energetics in the TCPC

4D flow MRI	n	KE <sub>norm_flow</sub>	EL <sub>norm_flow</sub>
Total TCPC	28	0.260(0.068)	0.075(0.022)
Segmental analysis		KE <sub>norm_flow+length</sub>	EL <sub>norm_flow+length</sub>
Fontan tunnel	35	0.034(0.011)	0.0087(0.0029)
SVC	31	0.023(0.007)	0.0065(0.0024)
LPA	46	0.040(0.018)	0.012(0.005)
RPA	49	0.031(0.01)	0.0081(0.0032)
Fontan confluence	56	0.094*(0.041)	0.031*(0.013)

\* Values are reported as mean (standard deviation). KE<sub>norm\_flow</sub> and EL<sub>norm\_flow</sub>. KE<sub>norm\_flow</sub> in mJ per L/min and EL<sub>norm\_flow</sub> in mW per L/min. KE<sub>norm\_flow+length</sub> in mJ per L/min per cm segment, EL<sub>norm\_flow+length</sub> in mW per L/min per cm segment. LPA/RPA; left/right pulmonary artery, SVC; superior vena cava, TCPC; total cavopulmonary connection, KE; kinetic energy, EL; viscous energy loss rate

## Discussion

This study for the first time shows the relationship between in vivo 4D flow MRI-derived TCPC blood flow energetics, exercise capacity and MR-based assessment of liver fibrosis/congestion (cT1 mapping). Liver cT1 values were elevated in all patients at a mean age of 17 years, indicating universal liver fibrosis/congestion.  $KE_{\text{norm\_flow}}$  and  $EL_{\text{norm\_flow}}$  in the TCPC correlated with maximal exercise capacity and liver cT1, while conventional parameters as ventricular ejection fraction and cardiac index did not. The Fontan tunnel and LPA were the segments with most adverse energetics.  $EL_{\text{norm\_flow}}$  was highest in patients with smallest Fontan tunnels raising concern on the current approach of Fontan completion with 16 to 20mm rigid conduits.

Surgical construction of an energy efficient TCPC with low resistance is important to keep the increase in CVP and reduction of preload towards the single ventricle to a minimum.<sup>21</sup> An elevated CVP and reduced cardiac output play an important role in the occurrence of liver fibrosis and decreased exercise capacity, respectively. In silico CFD modelling studies have identified PA stenosis and undersized Fontan tunnels to be associated with reduced flow efficiency<sup>4, 5, 22</sup>, which correlates with liver fibrosis stage and exercise capacity.<sup>6, 7</sup> Therefore, routine screening of Fontan patients on the occurrence of (subclinical) adverse TCPC flow efficiency is clinically relevant for timely identification of patients with adverse TCPC hemodynamics, in whom intervention may be beneficial.

Recently, 4D flow MRI has emerged as a promising non-invasive technique for quantification of in vivo TCPC flow efficiency. KE and EL in the TCPC are novel 4D flow MRI markers reflecting TCPC flow efficiency, influenced by adverse TCPC geometry (e.g. PA stenosis or undersized conduit) and related flow patterns. 4D flow MRI previously revealed adverse vortical/helical flow patterns in the Fontan confluence, PAs, or in a blind-ending pulmonary trunk, all areas associated with increased KE and EL.<sup>9, 19</sup> In this study, adverse 4D flow derived KE and EL in the TCPC correlated with reduced maximal exercise capacity and increased levels of liver fibrosis/congestion (cT1), and may therefore be important novel markers that can indicate adverse outcome.

### Exercise capacity

Decreased exercise capacity in Fontan patients is predominantly caused by a limited capability to maintain preload and stroke volume of the single ventricle during exercise.<sup>2</sup> Importantly, resting cardiac index and ejection fraction did not correlate with exercise capacity, but adverse 4D flow energetics in the TCPC did show a significant correlation. This might be explained by the fact that increased EL in the TCPC may particularly affect preload and thus cardiac output during exercise conditions only, since energy loss

in the TCPC increases non-linearly with exercise<sup>23</sup>, and are therefore not captured by evaluation of resting cardiac function parameters.

### **Liver fibrosis**

Presence of Fontan associated liver disease, including liver fibrosis, is universal in Fontan patients and the chronic exposure of the liver to an elevated CVP plays an important role.<sup>1</sup> The association between energetics and liver cT1 mapping can therefore be explained by the fact that elevated EL in the TCPC will require an increased CVP to maintain cardiac output. Fibrosis progression rate varies between patients and factors that lead to accelerated liver fibrosis are unknown as serial liver fibrosis assessment is lacking.<sup>24</sup> Future longitudinal studies with liver cT1 mapping could verify if patients with adverse TCPC energetics show faster progression in liver fibrosis.

### **Liver cT1 mapping**

Gold standard liver biopsy is subject to sampling errors and its invasiveness prohibits routine serial assessment. In this study a novel non-invasive approach was used based on iron-corrected T1 mapping to quantify increased levels of extracellular liver fluid, which is elevated in liver fibrosis and/or venous congestion. Although cT1 values showed good correlation with histologic liver fibrosis in adult patients with liver disease<sup>15</sup>, validation in Fontan patients is currently lacking. Especially venous congestion will influence T1 values in Fontan patients since increased CVP has been correlated with increased levels of liver T1.<sup>25</sup> Therefore, distinction between liver fibrosis or congestion due to increased CVP on elevated cT1 cannot be determined. However, since an increased CVP is associated with important morbidity such as PLE and liver fibrosis, measurement of cT1 as a combined marker of fibrosis/CVP is a promising non-invasive marker for adverse outcome.

### **Segmental analysis**

Analysis of the TCPC segments that most severely affected the adverse energetics of the entire TCPC indicated that the Fontan tunnel and LPA are the areas to focus on for improved TCPC efficiency. Increased KE and EL in the conduit, carrying 70% of total systemic venous return, can be explained by the presence of undersized extracardiac conduits (IVC-conduit velocity mismatch) caused by somatic overgrowth<sup>8</sup>, since a strong inverse correlation between conduit CSA and energetics was shown. LPA hypoplasia/stenosis, often observed in hypoplastic left heart syndrome patients, but also the presence of vortical flow in larger LPAs or in patients in whom the pulmonary trunk has not been detached, can explain the adverse energetics in the LPA.<sup>9,19</sup>

## Limitations

Compared to CFD, 4D flow MRI underestimates “true” energy loss and only captures relatively large-scale flow structures due to a limited spatial resolution. However, the relative performance of the TCPC between patients remains intact making comparison of TCPC energetics between Fontan patients still possible.<sup>26</sup> 4D flow MRI also does not capture the influence of respiration on TCPC blood flow<sup>27</sup>, which could significantly affect energy losses.<sup>28</sup> Novel 5D flow MRI sequences can be of interest to study the effect of respiration on TCPC energetics.<sup>29</sup> TCPC energetics could only be linked to current cT1 values in this study. Since the occurrence of liver fibrosis is presumably time-related, correlation of TCPC energetics with longitudinal cT1 mapping will be of interest and is subject to future research. Liver cT1 mapping has been shown to predict mortality and liver-related events in patients with chronic liver disease<sup>30</sup>, but its prognostic value in Fontan patients is currently unknown. Finally, the Fontan confluence segment could not be directly compared with the other four segments since Fontan confluence energetics were normalized for inflow only.

## Conclusion

Adverse 4D flow MRI derived kinetic energy and viscous energy loss rate in the TCPC significantly correlate with reduced exercise capacity and increased levels of liver fibrosis/congestion (cT1), while ventricular ejection fraction and cardiac index did not. Liver cT1 values were elevated in all patients indicating universal presence of liver fibrosis/congestion. The Fontan tunnel and LPA were the segments with most adverse energetics indicating potential room for improvement. 4D flow MRI is therefore promising as a non-invasive screening tool for identification of patients with adverse TCPC flow efficiency that may guide treatment strategies during follow-up.

## References

1. Goldberg DJ, Surrey LF, Glatz AC, Dodds K, O'Byrne ML, Lin HC, Fogel M, Rome JJ, Rand EB, Russo P and Rychik J. Hepatic Fibrosis Is Universal Following Fontan Operation, and Severity is Associated With Time From Surgery: A Liver Biopsy and Hemodynamic Study. *J Am Heart Assoc.* 2017;6.
2. Paridon SM, Mitchell PD, Colan SD, Williams RV, Blaufox A, Li JS, Margossian R, Mital S, Russell J, Rhodes J and Pediatric Heart Network I. A cross-sectional study of exercise performance during the first 2 decades of life after the Fontan operation. *J Am Coll Cardiol.* 2008;52:99-107.
3. Haggerty CM, Restrepo M, Tang E, de Zelicourt DA, Sundareswaran KS, Mirabella L, Bethel J, Whitehead KK, Fogel MA and Yoganathan AP. Fontan hemodynamics from 100 patient-specific cardiac magnetic resonance studies: a computational fluid dynamics analysis. *J Thorac Cardiovasc Surg.* 2014;148:1481-9.
4. Rijnberg FM, Hazekamp MG, Wentzel JJ, de Koning PJH, Westenberg JJM, Jongbloed MRM, Blom NA and Roest AAW. Energetics of Blood Flow in Cardiovascular Disease: Concept and Clinical Implications of Adverse Energetics in Patients With a Fontan Circulation. *Circulation.* 2018;137:2393-2407.
5. Tang E, Restrepo M, Haggerty CM, Mirabella L, Bethel J, Whitehead KK, Fogel MA and Yoganathan AP. Geometric characterization of patient-specific total cavopulmonary connections and its relationship to hemodynamics. *JACC Cardiovasc Imaging.* 2014;7:215-24.
6. Trusty PM, Wei ZA, Rychik J, Graham A, Russo PA, Surrey LF, Goldberg DJ, Yoganathan AP and Fogel MA. Cardiac Magnetic Resonance-Derived Metrics Are Predictive of Liver Fibrosis in Fontan Patients. *Ann Thorac Surg.* 2020;109:1904-1911.
7. Khiabani RH, Whitehead KK, Han D, Restrepo M, Tang E, Bethel J, Paridon SM, Fogel MA and Yoganathan AP. Exercise capacity in single-ventricle patients after Fontan correlates with haemodynamic energy loss in TCPC. *Heart.* 2015;101:139-43.
8. Rijnberg FM, Elbaz MSM, Westenberg JJM, Kamphuis VP, Helbing WA, Kroft LJ, Blom NA, Hazekamp MG and Roest AAW. Four-dimensional flow magnetic resonance imaging-derived blood flow energetics of the inferior vena cava-to-extracardiac conduit junction in Fontan patients. *Eur J Cardiothorac Surg.* 2019;55:1202-1210.
9. Rijnberg FM, van Assen HC, Hazekamp MG and Roest AAW. Tornado-like flow in the Fontan circulation: insights from quantification and visualization of viscous energy loss rate using 4D flow MRI. *Eur Heart J.* 2019;40:2170.
10. Rijnberg FM, van Assen HC, Hazekamp MG, Roest AAW and Westenberg JJM. Hemodynamic Consequences of an Undersized Extracardiac Conduit in an Adult Fontan Patient Revealed by 4-Dimensional Flow Magnetic Resonance Imaging. *Circ Cardiovasc Imaging.* 2021;14:e012612.
11. Godfrey S. *Exercise testing in children: applications in health and disease*: Saunders Limited.; 1974.
12. Ten Harkel AD, Takken T, Van Osch-Gevers M and Helbing WA. Normal values for cardiopulmonary exercise testing in children. *Eur J Cardiovasc Prev Rehabil.* 2011;18:48-54.
13. Schaapman JJ, Tushuizen ME, Coenraad MJ and Lamb HJ. Multiparametric MRI in Patients With Nonalcoholic Fatty Liver Disease. *J Magn Reson Imaging.* 2021;53:1623-1631.
14. Kendall TJ, Stedman B, Hacking N, Haw M, Vettukattill JJ, Salmon AP, Cope R, Sheron N, Millward-Sadler H, Veldtman GR and Iredale JP. Hepatic fibrosis and cirrhosis in the Fontan circulation: a detailed morphological study. *J Clin Pathol.* 2008;61:504-8.

15. Banerjee R, Pavlides M, Tunnicliffe EM, Piechnik SK, Sarania N, Philips R, Collier JD, Booth JC, Schneider JE, Wang LM, Delaney DW, Fleming KA, Robson MD, Barnes E and Neubauer S. Multiparametric magnetic resonance for the non-invasive diagnosis of liver disease. *J Hepatol*. 2014;60:69-77.
16. Szczepaniak LS, Nurenberg P, Leonard D, Browning JD, Reingold JS, Grundy S, Hobbs HH and Dobbins RL. Magnetic resonance spectroscopy to measure hepatic triglyceride content: prevalence of hepatic steatosis in the general population. *Am J Physiol Endocrinol Metab*. 2005;288:E462-8.
17. Mojtahed A, Kelly CJ, Herlihy AH, Kin S, Wilman HR, McKay A, Kelly M, Milanesi M, Neubauer S, Thomas EL, Bell JD, Banerjee R and Harisinghani M. Reference range of liver corrected T1 values in a population at low risk for fatty liver disease-a UK Biobank sub-study, with an appendix of interesting cases. *Abdom Radiol (NY)*. 2019;44:72-84.
18. Elbaz MS, van der Geest RJ, Calkoen EE, de Roos A, Lelieveldt BP, Roest AA and Westenberg JJ. Assessment of viscous energy loss and the association with three-dimensional vortex ring formation in left ventricular inflow: In vivo evaluation using four-dimensional flow MRI. *Magn Reson Med*. 2017;77:794-805.
19. Rijnberg FM, Juffermans JF, Hazekamp MG, Helbing WA, Lamb HJ, Roest AAW, Westenberg JJM, van Assen HC and Nagy E. Segmental assessment of blood flow efficiency in the total cavopulmonary connection using four-dimensional flow magnetic resonance imaging: vortical flow is associated with increased viscous energy loss rate. *European Heart Journal Open*. 2021;1.
20. Juffermans JF, Westenberg JJM, van den Boogaard PJ, Roest AAW, van Assen HC, van der Palen RLF and Lamb HJ. Reproducibility of Aorta Segmentation on 4D Flow MRI in Healthy Volunteers. *J Magn Reson Imaging*. 2021;53:1268-1279.
21. Sundareswaran KS, Pekkan K, Dasi LP, Whitehead K, Sharma S, Kanter KR, Fogel MA and Yoganathan AP. The total cavopulmonary connection resistance: a significant impact on single ventricle hemodynamics at rest and exercise. *Am J Physiol Heart Circ Physiol*. 2008;295:H2427-35.
22. Dasi LP, Krishnankuttyrema R, Kitajima HD, Pekkan K, Sundareswaran KS, Fogel M, Sharma S, Whitehead K, Kanter K and Yoganathan AP. Fontan hemodynamics: importance of pulmonary artery diameter. *J Thorac Cardiovasc Surg*. 2009;137:560-4.
23. Whitehead KK, Pekkan K, Kitajima HD, Paridon SM, Yoganathan AP and Fogel MA. Nonlinear power loss during exercise in single-ventricle patients after the Fontan: insights from computational fluid dynamics. *Circulation*. 2007;116:1165-71.
24. Evans WN, Acherman RJ, Mayman GA, Galindo A, Rothman A, Winn BJ, Yumiaco NS and Restrepo H. The Rate of Hepatic Fibrosis Progression in Patients Post-Fontan. *Pediatr Cardiol*. 2020;41:905-909.
25. de Lange C, Thrane KJ, Thomassen KS, Geier O, Nguyen B, Tomterstad A, Ording Müller LS, Thaulow E, Almaas R, Døhlen G, Suther KR and Möller T. Hepatic magnetic resonance T1-mapping and extracellular volume fraction compared to shear-wave elastography in pediatric Fontan-associated liver disease. *Pediatr Radiol*. 2021;51:66-76.
26. Cibis M, Jarvis K, Markl M, Rose M, Rigsby C, Barker AJ and Wentzel JJ. The effect of resolution on viscous dissipation measured with 4D flow MRI in patients with Fontan circulation: Evaluation using computational fluid dynamics. *J Biomech*. 2015;48:2984-9.
27. van der Woude SFS, Rijnberg FM, Hazekamp MG, Jongbloed MRM, Kenjeres S, Lamb HJ, Westenberg JJM, Roest AAW and Wentzel JJ. The Influence of Respiration on Blood Flow

- in the Fontan Circulation: Insights for Imaging-Based Clinical Evaluation of the Total Cavopulmonary Connection. *Front Cardiovasc Med*. 2021;8:683849.
28. Tang E, Wei ZA, Trusty PM, Whitehead KK, Mirabella L, Veneziani A, Fogel MA and Yoganathan AP. The effect of respiration-driven flow waveforms on hemodynamic metrics used in Fontan surgical planning. *J Biomech*. 2019;82:87-95.
  29. Bastkowski R, Bindermann R, Brockmeier K, Weiss K, Maintz D and Giese D. Respiration Dependency of Caval Blood Flow in Patients with Fontan Circulation: Quantification Using 5D Flow MRI. *Radiol Cardiothorac Imaging*. 2019;1:e190005.
  30. Pavlides M, Banerjee R, Sellwood J, Kelly CJ, Robson MD, Booth JC, Collier J, Neubauer S and Barnes E. Multiparametric magnetic resonance imaging predicts clinical outcomes in patients with chronic liver disease. *J Hepatol*. 2016;64:308-315.



## Supplementary materials

**Supplemental Table 1.** 4D flow MRI acquisition details

No. of slices (orientation)	27 (coronal)
Field of view, mm	350x271x56
ECG-gating	Retrospective
No. of reconstructed cardiac phases	24
No. of signal averages	1
Respiratory compensation	navigator
Typical navigator efficiency	40-60%
Acquired spatial resolution (mm)	2.4x2.4x2.4
Reconstructed spatial resolution (mm)	2.1x2.1x2.1
Acquired temporal resolution, ms (SD)	32.0
Flip angle (°)	10
TE (ms)	4.5
TR (ms)	8.0
VENC (cm/s)	80
Typical scan time (minutes)	12-18
Acceleration methods	SENSE factor 1.5, RL direction, EPI factor 5, Segmentation factor 1

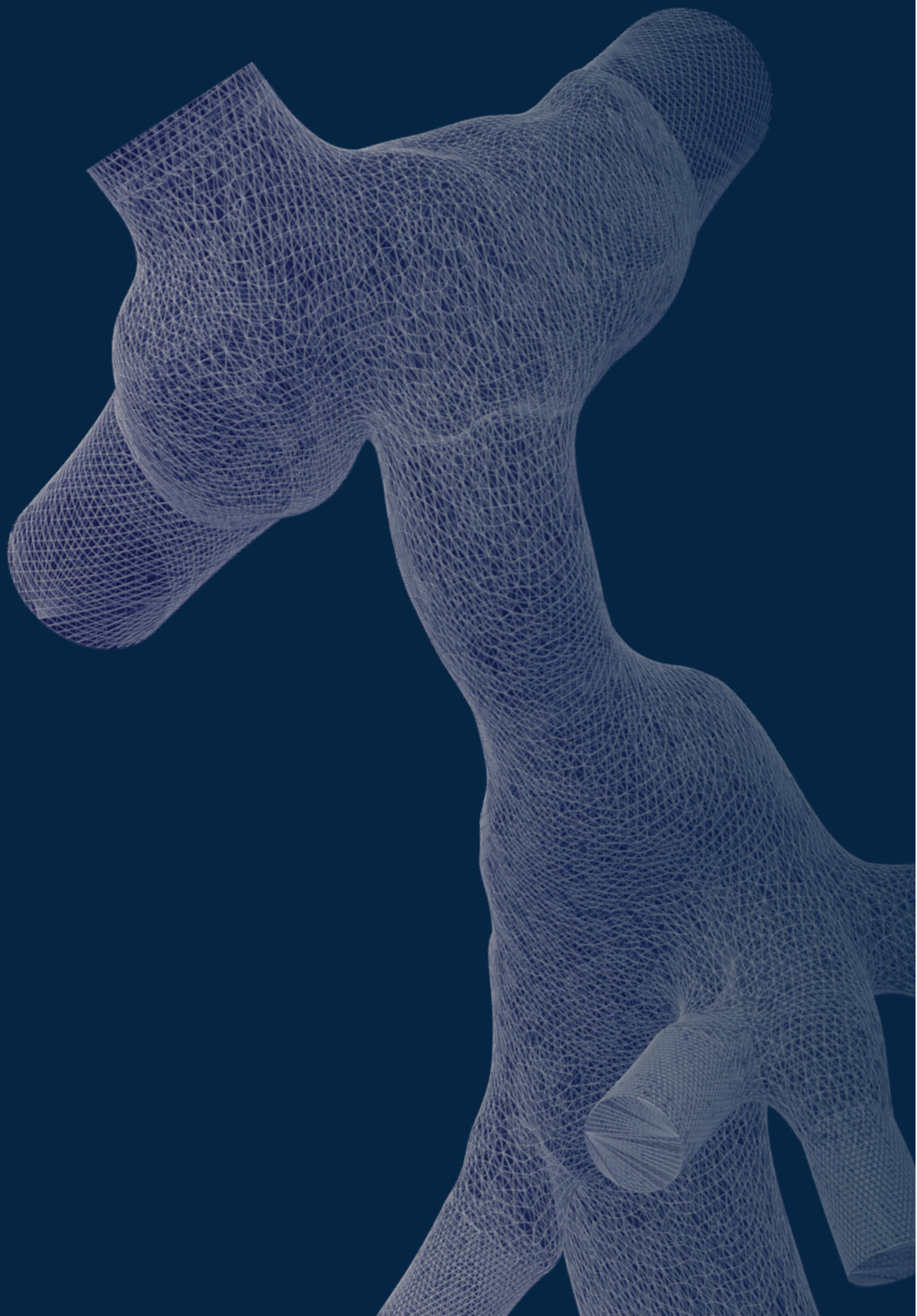
SD; standard deviation, ms; milliseconds, mm; millimeter, TE; echo time, TR; repetition time, VENC; velocity encoding, SENSE; sensitivity encoding, AP; anterior-posterior, EPI; echo planar imaging readout, ECG; electrocardiogram

**Supplemental Table 2.** Correlation analysis between cross-sectional area of the TCPC segments and 4D flow MRI energetics

	n	CSA (mm <sup>2</sup> /m <sup>2</sup> )	KE <sub>norm_flow+length</sub>		EL <sub>norm_flow+length</sub>	
			Correlation coefficient	p	Correlation coefficient	p
Fontan tunnel	35	106 (91-134)	-0.80	<b>&lt;0.001</b>	-0.78	<b>&lt;0.001</b>
SVC	31	96 (76-109)	0.23	0.21	-0.02	0.93
LPA	46	92 (70-113)	0.03	0.85	-0.31	<b>0.034</b>
RPA	49	88 (81-101)	-0.10	0.48	-0.10	0.50

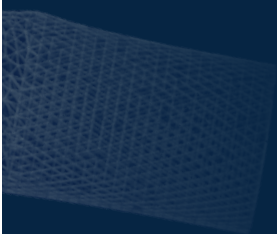
Correlation coefficients represent Pearson or Spearman rank analysis. SVC; superior vena cava, LPA/RPA; left/right pulmonary artery, CSA; cross-sectional area normalized for body surface area, TCPC; total cavopulmonary connection, KE; kinetic energy, EL; viscous energy loss rate





# PART III

Computational fluid dynamics of the  
Fontan circulation



**CHAPTER 9**



# Energetics of blood flow in cardiovascular disease: concept and clinical implications of adverse energetics in patients with a Fontan circulation

Rijnberg FM, Hazekamp MG, Wentzel JJ, de Koning PJH, Westenberg JJM, Jongbloed MRM, Blom NA, Roest AAW

## Abstract

Visualization and quantification of adverse effects of distorted blood flow is an important, emerging field in cardiology. Abnormal blood flow patterns can be seen in various cardiovascular diseases and are associated with increased energy loss. These adverse energetics can be measured and quantified using 3D blood flow data, derived from computational fluid dynamics and four-dimensional flow magnetic resonance imaging, and provide new, promising hemodynamic markers.

In patients with palliated single ventricular heart defects, the Fontan circulation passively directs systemic venous return to the pulmonary circulation in the absence of a functional subpulmonary ventricle. Therefore, the Fontan circulation is highly depending on favorable flow and energetics and minimal energy loss is of great importance. Focus on reducing energy loss led to the introduction of the total cavopulmonary connection (TCPC, as an alternative to the classical Fontan connection. Subsequently, many studies have investigated energy loss in the TCPC and energy-saving geometric factors have been implemented in clinical care. Great advances have been made in CFD modelling and can now be done in 3D, patient-specific models with increasingly accurate boundary conditions. Furthermore, the implementation of 4D flow MRI is promising and can be of complementary value to these models. Recently, correlations between energy loss in the TCPC and cardiac parameters and/or exercise intolerance have been reported. Furthermore, efficiency of blood flow through the TCPC is highly variable and inefficient blood flow is of clinical importance by reducing cardiac output and increasing central venous pressure, thereby increasing the risk of experiencing the well-known Fontan complications. Energy loss in the TCPC will be an important new hemodynamic parameter in addition to other well known risk factors such as pulmonary vascular resistance and can possibly be improved by patient-specific surgical design.

This review describes the theoretical background of mechanical energy of blood flow in the cardiovascular system, the methods of calculating energy loss and gives an overview of geometric factors associated with energy efficiency in the TCPC and its implications on clinical outcome. Furthermore, the role of 4D flow MRI and areas of future research are discussed.

## Introduction

Cardiology is flow.<sup>1</sup> The primary goal of the cardiovascular system is to drive, regulate and maintain adequate blood flow throughout the body.<sup>1</sup> Blood flows because potential pressure energy (systolic blood pressure), predominantly generated by the ventricles, is converted into kinetic energy (i.e. velocity) along its course through the body.<sup>2</sup> The ventricles must provide the flowing blood with enough energy to overcome the unavoidable frictional loss of energy throughout the circulation.<sup>2</sup> Energy consuming abnormal blood flow patterns<sup>3</sup> (e.g. flow separation, flow collision or helical flow) caused by abnormal geometry (e.g. vessel/valve stenosis or vessel aneurysms) provide an increased working load to the ventricles in order to maintain adequate flow throughout the cardiovascular system, which may ultimately result in heart failure.<sup>4</sup> Furthermore, blood flow induces mechanical forces on the vessel wall. Abnormal values of these forces, for example wall shear stress (WSS), have been identified in diseases such as atherosclerosis and aortic aneurysms.<sup>1,5</sup>

The degree of energy loss, and thereby its hemodynamic impact, is conventionally assessed with indirect, global parameters, such as vessel size, pressure gradients or effective orifice area, which may lead to inaccurate disease severity characterization.<sup>2,4-6</sup> While visualization and direct measurement of blood flow in all three dimensions (3D) has long been an elusive goal, emerging techniques such as four-dimensional flow magnetic resonance imaging (4D flow MRI) and patient-specific computational fluid dynamics (CFD) models are providing unprecedented, unique insights into physiological and pathophysiological flow in the human circulation. These techniques provide a time-resolved (i.e. during a cardiac cycle) 3D velocity vector field (from 4D flow MRI) or a combined velocity and pressure field (from CFD).<sup>5,7,8</sup> Using these techniques, complex intra-cardiac and vascular flow patterns including vortex formation and helical flow have been identified in various cardiovascular diseases, including ischemic and dilated cardiomyopathies, aortic disease, valvular disease and congenital heart disease.<sup>6,7,9,10</sup> Moreover, these techniques allow direct quantification of the energetics of the 3D, time-resolved blood flow data that lead to new hemodynamic parameters such as viscous energy loss, turbulent kinetic energy (TKE), WSS and kinetic energy.<sup>8</sup> Direct measurement of viscous energy loss (laminar flow) or TKE (turbulent flow) in patients with aortic valve disease or aortic dilatation also takes the hemodynamic impact of the abnormal, energy consuming flow patterns in the ascending aorta and aortic arch into account and may therefore better reflect disease severity complementary to conventional parameters.<sup>6,11</sup> The definitive role of these and other new energetic markers of blood flow in clinical decision making in various types of cardiovascular disease is promising and subject to future studies.



In patients with palliated single ventricular heart defects, the Fontan circulation passively directs systemic venous return to the pulmonary circulation in the absence of a functional subpulmonary ventricle. The Fontan circulation is especially depending on favorable flow and energetics and minimal energy loss is of great importance. Minimizing energy loss, via the rationale that an energy efficient total cavopulmonary connection (TCPC) leads to reduced central venous pressure and increased preload and therefore cardiac output, thereby aims to decrease the risk of well-known Fontan complications such as exercise intolerance, heart failure, protein losing enteropathy (PLE), venovenous collateral formation or liver fibrosis/cirrhosis.<sup>12, 13</sup> The concept and clinical implications of adverse energetics in patients with a Fontan circulation are the subject of this review, including the theoretical background and methods of calculating energy loss, factors associated with increased/reduced energy loss and the correlation with clinical parameters.

### **The Fontan procedure**

The Fontan procedure is the current standard palliative treatment of children with a functional univentricular heart. It creates a circulation in which systemic venous return enters the pulmonary circulation passively, without the support of a cardiac ventricle. Originally, the procedure incorporated the right atrium into the design in a so-called atriopulmonary connection (APC), with the rationale that contraction of the atrium can add forward energy to the otherwise passive flow entering the lungs. However, in a landmark in-vitro study by de Leval et al. in 1988<sup>14</sup>, it was shown that by incorporating a pulsatile atrium, turbulent flow inside this atrium led to increased rather than decreased energy loss, and the importance of energy efficiency was emphasized. It led to the recommendation of the TCPC, and subsequently its superiority over the APC in terms of efficiency was demonstrated.<sup>14-16</sup> Nowadays, the Fontan circulation is created in a staged approach. Most often a bidirectional cavopulmonary connection is performed by connecting the superior vena cava (SVC) end to side to the right pulmonary artery (RPA) at an age of 6-12 months (Glenn), with completion of the Fontan circulation (TCPC) using an intra-atrial lateral tunnel (LT) or extracardiac conduit (ECC) technique at an age of 3-5 years. Some centers use the so-called hemi-Fontan procedure instead of the Glenn procedure, in which the SVC is not disconnected from the right atrium, but instead a patch reconstruction is performed between the medial side of the SVC, the right atrium and the RPA. A second patch at the superior cavo-atrial junction prevents the blood flow from the inferior vena cava (IVC) from entering the PAs. With completion of the TCPC, this latter patch is removed and an intra-atrial lateral tunnel is constructed allowing IVC flow towards the PAs. Therefore, final geometry and flow characteristics between intra-atrial LT Fontan patients after Glenn or Hemi-Fontan are inherently different.

The TCPC has two important tasks<sup>17</sup>: it has 1) to be as energy efficient as possible, and 2) it has to distribute hepatic blood to both lungs. Adding IVC blood to the SVC flow from the bidirectional Glenn shunt makes for an almost complete separation of the pulmonary and systemic circulations. Only venous blood from the coronary circulation remains entering into the systemic circulation. Furthermore, IVC blood contains the important 'hepatic factor'. A lack of this 'hepatic factor' is associated with the formation of pulmonary arteriovenous malformations (PAVM), as a high prevalence has been reported after a Glenn shunt or Kawashima procedure, with reduction of these PAVMs after reincorporation of the hepatic veins into the Fontan circulation.<sup>18</sup>

Although short-term outcome after the Fontan procedure has improved considerably since its introduction in 1971<sup>12</sup>, long term morbidity and mortality remain significant, including a generally limited exercise tolerance.<sup>13, 19</sup>

Blood flow to the pulmonary vasculature in a Fontan patient is mainly driven by increased systemic venous pressure, which is formed by the remaining energy generated by the heart, by the peripheral muscle pump, and by intrathoracic pressure changes during respiration.<sup>20</sup> Because of the assumed importance of minimizing energy loss, the TCPC has been an area of extensive research. This has been done mainly via in-vitro models<sup>9, 14, 21-34</sup>, computational fluid dynamic (CFD) models<sup>3, 9, 16, 17, 26, 27, 30-67</sup> and in-vivo studies.<sup>10, 15, 34, 68-70</sup> In the past 10 years, growing evidence suggests a relationship between energy loss in the TCPC and Fontan hemodynamics<sup>47, 59-62, 69</sup> and exercise tolerance<sup>63, 66</sup>. To date, the influence of energy loss on other well-known complications such as protein losing enteropathy (PLE), plastic bronchitis or liver fibrosis/cirrhosis have not been studied.

## Energy loss within the TCPC

The theoretical background of mechanical energy in the human circulation and the methods of calculating and comparing energy loss are supplemented in Appendix A and B.

As the TCPC is basically a connection with two T-junctions with opposite flow directions, sudden changes in velocities and directions of flow around corners and over decreasing cross-sectional areas (e.g. PAs and branching) will inevitably lead to energy losses.<sup>35, 71</sup> These energy losses are predominantly through viscous dissipation (Appendix A) in laminar flow, although energy losses can be of greater magnitude when turbulent flow (Appendix C) occurs.<sup>2</sup>

The intrinsic instability of TCPC flow has been observed in multiple studies.<sup>3, 22, 26, 30, 31, 68, 72</sup> With CFD, when using steady inflow boundary conditions, still a highly disorganized

and unsteady flow appeared in the area of colliding blood flow from the SVC and IVC, extending into the PAs.<sup>31</sup> This includes areas of flow stagnation, formation of vortices and the occurrence of swirling, helical flow patterns (Supplemental videos 1 & 2) into the PAs (Figure 1, central image). Furthermore, these flow phenomena have been reported to change with varying cardiac outputs and RPA:LPA flow splits (percentage of total caval blood flow to each PA branch (RPA:LPA)) These flow patterns are characterized by high velocity gradients and are therefore highly dissipative, leading to increased energy loss in the TCPC.<sup>3</sup> Furthermore, wall shear stress (WSS) has also been identified as a major contributor of energy loss<sup>43</sup>, with most energy being dissipated near the PA walls<sup>26</sup> and the corners of the anastomosis.<sup>56</sup>

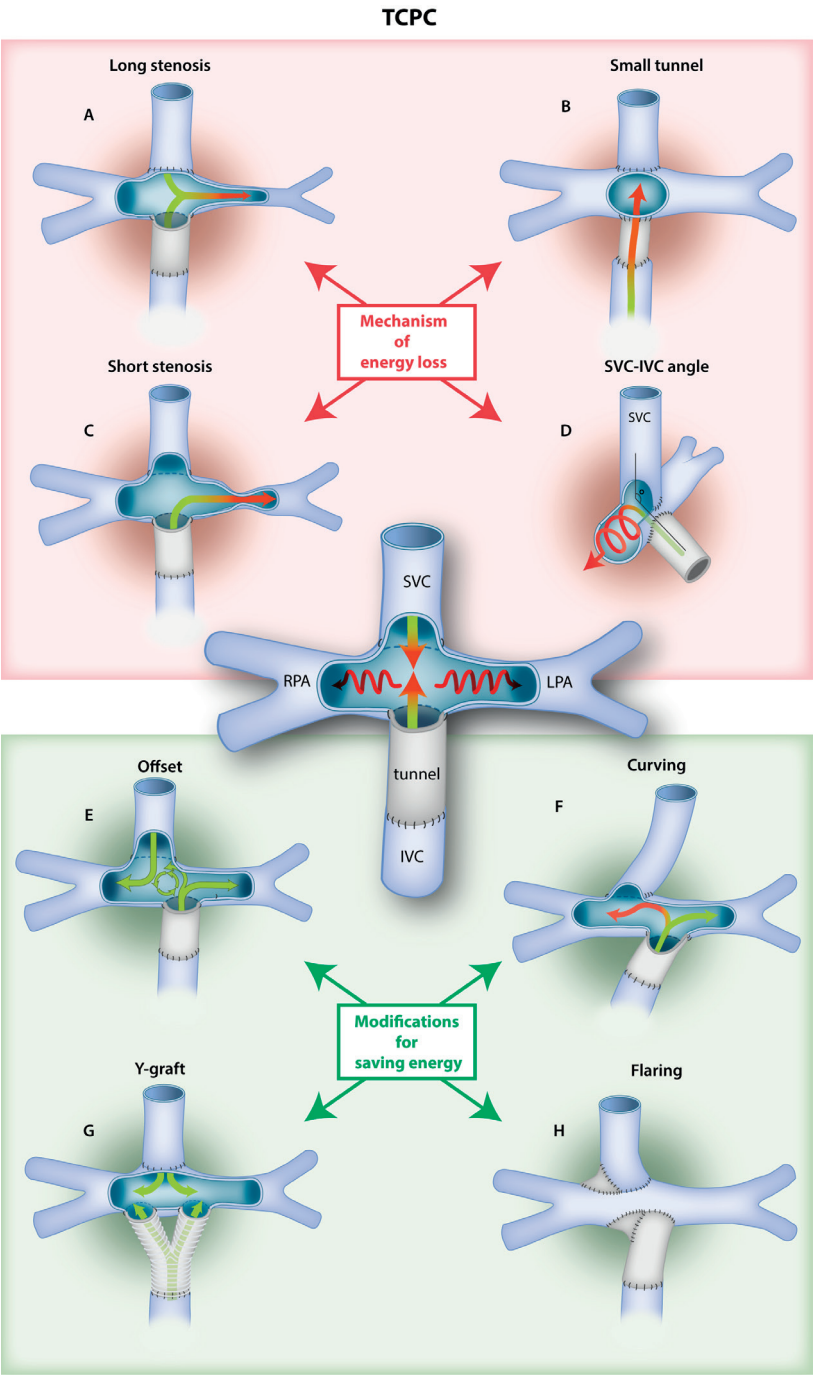
Some studies have questioned the relevance of the energy loss in the TCPC, as energy loss is generally low (Table 1) and may only contribute a small part to the whole energy loss in the pulmonary circulation. In one study, energy loss in the TCPC during rest represented only 13-20% of energy loss in the pulmonary circulation and only 2% of ventricular power.<sup>58, 60</sup> However, others have shown that TCPC resistance is highly variable and can be as high as 55% of pulmonary vascular resistance (PVR) in rest and increase up to 155% of PVR during simulated exercise.<sup>47</sup> In a recent study by Tang et al. reporting on TCPC energy loss in 47 patients during exercise, TCPC RI was on average 0.58 WU, but could be as high as 2.23 WU.

**Figure 1.** (opposite) Geometric factors associated with increased energy loss in the TCPC and modifications to reduce energy loss in the TCPC.

This figure illustrates the geometric factors associated with increased (**upper panel, central figure**) and decreased energy loss (**lower panel**) with depiction of a simplified, schematic extracardiac conduit TCPC, see text for further details. The same factors apply for lateral tunnel (LT) TCPCs. Coloured arrows represent blood flow and change from green to red represents increase in energy loss. When the inferior (IVC) and superior venae cavae (SVC) are connected to the pulmonary vasculature directly opposite to each other, collision of blood flow leads to a highly disorganized flow with areas of flow stagnation, flow separation and the occurrence of swirling, helical flow into the pulmonary arteries (PAs) (**central figure**).

**Upper panel:** Geometric factors associated with increased energy loss in the TCPC. The influence of a long or short PA stenosis (**A&C**) is illustrated, with a long, diffuse stenosis leading to more energy loss than a short, discrete stenosis. Together with a small Fontan tunnel (**B**), these are the most important factors associated with increased energy loss. The angle between the SVC and IVC is of influence on the formation of swirling, helical flow patterns when angles are small (towards 90 degrees), with improvement when angles are enlarged (**D**) to 150 degrees.

**Lower panel:** Modifications to reduce energy loss in the TCPC. Caval offset towards one of the PAs leads to less energy loss by avoiding flow collision and leads to the formation of a low-dissipative vortex (green circle), propelling blood flow into the PAs (**E**). Curving of the vena cavae towards a PA leads to lower energy loss compared with an offset model without curving. However, when IVC flow split does not match pulmonary flow towards that PA, some flow has to make a sharp bend increasing energy loss (red arrow) (**F**). Flaring of the anastomosis leads to reduced energy loss by avoiding dissipative sharp corners (**G**). The area-preserving Y-graft allows for balanced hepatic blood flow split and is associated with reduced energy loss (**H**).



### ***Magnitude of energy loss***

The range of calculated energy losses (in milliwatt, mW) and, when available, values of efficiency, resistance, resistance index (RI) or indexed power loss (iPL) in 3D, patient-specific TCPC models are reported in Table 1. Explanations of comparing TCPC efficiency using resistance, resistance index (RI) and iPL are covered in Appendix B. Efficiency of the TCPC, i.e. the energy of outflowing versus inflowing blood (Efficiency = Energy out/Energy in (%)), in which the difference is caused by viscous energy loss in the TCPC), is highly variable between patients and ranges between 63%-98% in rest and 63%-91% during exercise (Table 1). TCPC RI is also highly variable, and ranges between 0.05-1.6 Woods Unit (WU, Appendix B) in rest and 0.07-3.95 WU during exercise. To put this in perspective, in Fontan patients mean PVR has been reported to be 1.9 till 2.8 WU (range 1.0-4.3).<sup>47, 73</sup> IPL ranged from 0.007-0.122 in resting conditions, showing that iPL can be 12.2-16.7 times higher in the least efficient TCPCs compared with the most efficient TCPCs in rest.<sup>60, 62</sup>

### **Factors influencing energy loss in the TCPC: figure 1-upper panels**

#### ***Vessel sizes***

The effect of vessel sizes on energy loss has been reported in the TCPC<sup>26, 30, 61, 64, 66, 74</sup>, and is a logical result of the law of Hagen-Poiseuille, which states that with a laminar, steady flow, the resistance of flow through a blood vessel is inversely proportional to the fourth power of the radius.

The effect of small, hypoplastic or stenotic PAs (Figure 1A&C) are, together with the Fontan pathway diameter (Figure 1B)<sup>61</sup>, the most important geometry factors associated with increased energy loss.<sup>42, 46, 50, 53, 61, 75</sup> Pekkan et al. performed a virtual angioplasty of a short LPA stenosis of 85% which led to a 50% decrease of energy dissipation when the stenosis was virtually widened. It was also shown that diffuse (long segment) PA stenosis is more dissipative than a short stenosis.<sup>42</sup> This furthermore highlights the importance of well-developed PAs, as in small PAs blood flow velocity will increase, leading to high WSS and increased energy loss.<sup>30, 43, 61</sup>

Additionally, the effect of conduit sizes in ECC patients on energy loss has been studied. Hsia et al.<sup>40</sup> modelled 5 conduit sizes from 10-30 mm and showed decreased energy loss with increasing conduit size to 20 mm. However, an increased conduit size of 30 mm resulted in increased energy loss due to increased flow recirculation within the conduit. So although small vessels are detrimental in terms of energy loss, bigger is not always better. These areas of flow stagnation or recirculation not only increase energy loss, but may also increase the risk of thrombosis.<sup>76</sup>

**Table 1.** Energy loss in realistic, patient-specific 3D models

Study	Year	Method	TCPC Models (n)	Flow (L/min)	Energy loss (mW)	Efficiency % (Eout/Ein)	Resistance Index	Indexed PowerLoss
Bove <sup>39</sup>	2003	CFD	2LT,2ECC	2.29	4.1-56.6	-	-	-
Migliavacci <sup>98</sup>	2003	CFD	4LT,2ECC	2.28	15-55	-	-	-
Hsia <sup>40</sup>	2004	CFD	3LT,6ECC	1.65	-	89-91	-	-
Pekkan <sup>31</sup>	2005	CFD, IVT	1IA	1-3	10-270	-	-	-
de Zelicourt <sup>30</sup>	2005	CFD	1IA	1-3	15-210	-	-	-
Pekkan <sup>42</sup>	2005	CFD	1ECC	2.6	15-230	-	-	-
Marsden <sup>45</sup>	2006	CFD	2ECC	2.16-6.24	6.7-13.9 (19.5-169.4)	75-93 (69-91)	-	-
de Zelicourt <sup>9</sup>	2006	CFD, IVT	2ECC	2-4	5-28 (34-70)	-	-	-
Whitehead <sup>46</sup>	2007	CFD	9IA,1ECC	2.37-5.1 Cl, x2-3	5-20 (40-1200)*	-	0.25-0.75 (0.4-3.4)*	-
Sundareswaran <sup>47</sup>	2008	CFD	10ECC,6IA	2-10.5	-	-	0.10-1.08 (0.13-2.65)	-
Marsden <sup>49</sup>	2009	CFD	2ECC,2Y	1.9-5.6	-	87-90 (76-87)	-	-
Marsden <sup>50</sup>	2010	CFD	6ECC	1.6-3.8 Cl, x2-3	-	74-96 (63-93)	-	-
Baretta <sup>51</sup>	2011	CFD	2ECC,1Y	2.6 Cl	1.09-4.80	91-96	-	-
Haggerty <sup>54</sup>	2012	CFD	1ECC,3Y	2.6-3.3	1.3-5.1	-	0.18-0.35	-
Yang <sup>79</sup>	2012	CFD	8Y,11ECC	1.3-2.5, x2-3	1.8-8.2 (2.9-32.5)	-	-	-
Ding <sup>56</sup>	2013	CFD	6ECC	NS	5.5-16*	-	-	-
Haggerty <sup>57</sup>	2013	CFD	5Y,10ECC	3.0-3.8 Cl, x2-3	-	-	0.15-1.60 (0.32-3.95)	-
Hong <sup>99</sup>	2014	CFD	1ECC,1LT	NS	4.13-10.67	95-98	-	-
Sun <sup>100</sup>	2014	CFD	4ECC	2.48	4.5-13	81-95	-	-
Tang <sup>61</sup>	2013	CFD, IVT	1ECC	2.54	3.8-6.9	-	-	-
Honda <sup>69</sup>	2014	Cath	7ECC,1IA,1LT	NS	-	63-93	-	-
Haggerty <sup>60</sup>	2014	CFD	64IA,33ECC	2.89-3.10 Cl	-	-	0.05-0.66	0.007-0.117
Bossers <sup>59</sup>	2014	CFD	15LT,14ECC	3.2-5.3 Cl	mean 1.4-3.2/m2 (2.8-15.3/m2)	-	mean 0.06-0.16 (0.07-0.28)	-
Khiabani <sup>63</sup>	2014	CFD	21IA,9ECC	2.6-4.8 Cl	-	-	-	mean 0.04-0.05
Haggerty <sup>62</sup>	2015	CFD	25IA,5ECC	3.2 Cl	-	-	-	0.01-0.12

Table 1. Continued

Study	Year	Method	TCP Models (n)	Flow (L/min)	Energy loss (mW)	Efficiency % (Eout/Ein)	Resistance Index	Indexed PowerLoss
Restrepo <sup>64</sup>	2015	CFD	36LT,12ECC	3.0-3.3CI	-	-	-	mean 0.05-0.10
Cibis <sup>70</sup>	2015	4D MRI	2LT,4ECC	NS	mean 0.56	-	-	-
Trusty <sup>65</sup>	2016	CFD	30Y,30ECC/LT	1.57-2.07	-	-	mean 0.56-1.51†	-
Tang <sup>66</sup>	2017	CFD	33LT,14ECC	exercise, NS	-	-	mean 0.58	mean 0.05

LT; intra-atrial lateral tunnel (after Glenn), ECC; extra cardiac conduit, IA; intra-atrial LT (after Hemi-Fontan), CFD; computational fluid dynamics, IVT; in vitro, Cath; catheterization, 4D MRI; four-dimensional magnetic resonance imaging, CI; cardiac index, NS; not specified

\* estimation of values from published charts or graphics

† Resistance (not indexed)

Values are reported in ranges unless specified. Values in exercise conditions or simulated flow conditions >4L/min are in parentheses.

Itatani et al. recommended 16-18mm conduits for children of 2-3 years old, but whether this was also the ideal size for adult patients was not investigated.<sup>40, 48</sup> The ideal conduit size will probably be patient specific and efficiency will change while the patient grows. The size of the used conduit will likely be limited by the conduit-IVC ratio, as an increase in this ratio was associated with increased energy loss because of flow separation through expansion of flow from the sudden increase in diameter from IVC to Fontan tunnel.<sup>24</sup> Despite the fact that cardiac catheterization studies often show absent or minimal ( $\leq 2$ mmHg) pressure gradients in patients with Fontan tunnel stenosis<sup>77</sup>, energy loss from such an obstruction may nevertheless be significant and can exceed the total energy loss through the lungs. Restoring normal diameter with stenting has been shown to dramatically reduce this energy loss.<sup>78</sup> This example illustrates the importance of energy loss as a new, energetic marker as management based on pressure gradient can be misleading.

Finally, a recent study by Restrepo et al.<sup>64</sup> showed that a TCPC inherently becomes more dissipative with age, as it was reported that normalized vessel diameters (vessel diameters corrected for BSA) decrease with time. In other words, growth of IVC, SVC, RPA and LPA does not match somatic growth, making the TCPC less efficient with aging.

### ***Total blood flow and pulmonary flow split***

Energy loss in the TCPC will be larger with an increase of blood flow, as is demonstrated in multiple studies<sup>21, 23, 45, 46, 57, 59, 79</sup>, with energy loss increasing non-linearly with an average of 10.5 and 38.9 times baseline energy loss with doubled and tripled flow mimicking exercise.<sup>46</sup> In that study, resistance indices during rest (range 0.25-0.75 WU) increased non-linearly to resistance indices up to 3.4 WU during simulated exercise. In some patients, however, the simulated exercise conditions did not represent physiologic values.

Pulmonary flow splits are anywhere near 55%:45% in healthy humans, and are derived from the mass ratio of the right and left lung (i.e. more blood flows normally through the bigger right lung)<sup>17</sup>. Early in-vitro studies with different simplified models have shown that the least energy loss is observed with 45-55% blood flow to the RPA, with increasing energy loss when flow splits are highly skewed towards one lung.<sup>21, 23</sup> However, these values only apply for these specific models and conditions, as models with other geometric properties show other optimal flow splits, ranging from 30-70% RPA flow.<sup>26, 30, 32, 46</sup> For example, de Zelicourt et al.<sup>30</sup> showed the least energy loss for a 70% RPA flow split, as this patient specific model had a small LPA. Increased flow through this LPA resulted in increased energy loss. Additionally, Whitehead et al.<sup>46</sup> reported increased energy loss for most patients when flow towards the LPA increased, because in most patients the LPA is smaller than the RPA. However, in some patients the effect



of altering pulmonary flow split had only a minor effect on energy loss and in others increasing LPA flow split resulted in decreased energy loss. In these latter patients, relative RPA hypoplasia was present. The pulmonary flow split in patients is therefore, when assuming equal PVR in each lung, predominantly caused by PA size, with most blood flowing through the biggest PA.<sup>75</sup> In other words, blood flow follows the path of least resistance leading to skewed pulmonary flow splits when PA stenosis is present. Intuitively, in the ideal situation total caval blood flow needs to be proportionally distributed over both pulmonary vascular beds. Restoring of PA diameter will restore a more balanced pulmonary flow split.<sup>42</sup>

### ***Caval flow split***

Above mentioned studies stressed the importance of geometry (PA sizes) on optimal pulmonary flow split. In humans, IVC:SVC flow split changes from 51%:49% at birth, 45%:55% in children at the age of 2.5 years to the adult value of 65%:35% at an age of 6.6 years.<sup>80</sup> Furthermore, lower limb exercise will predominantly increase IVC flow up to 160%.<sup>81, 82</sup> The effect of respiration on caval blood flow has also been reported, with IVC flow increasing up to 60-87% during inspiration.<sup>20, 81</sup> The influence of inspiration on SVC flow is less clearly established, varying from no increase in SVC flow to increase of flow up to 90%.<sup>20, 81</sup> In a study by Hjortdal et al. it was shown that in resting conditions the caval flow split (IVC:SVC) was approximately 70:30 during inspiration and 40:60 during expiration.<sup>20</sup> During exercise, this ratio was 79:21 during inspiration and 64:36 during expiration.<sup>82</sup> Therefore overall, but especially during lower limb exercise and inspiration, most blood will enter the TCPC via the IVC. An optimal connection of the IVC to the PAs will therefore be of great importance. For example, Ensley et al modelled a connection in which the IVC was curved towards the RPA and the SVC towards the LPA. This resulted in low energy loss when pulmonary flow split to the RPA matched the caval flow split (i.e. 60% IVC flow and 60% RPA flow). With lower RPA splits, energy loss increased because blood had to make a sharp bend from the curved IVC towards the LPA. A connection as such may be clinically unreliable as pulmonary vascular resistance (PVR) can possibly change, influencing TCPC efficiency.<sup>22</sup> For this same reason, connecting the IVC to a smaller LPA, while carrying the majority of flow, will likely be not the most efficient connection, as blood flow has to be pushed through a smaller PA or has to make a sharp bend towards the RPA.

## **Factors influencing energy loss in the TCPC: figure 1-lower panels**

### ***Offset IVC vs SVC***

The influence of an offset (Figure 1E) between the IVC and SVC connection has been studied to avoid the head collision of SVC and IVC flows, which has been shown to lead to highly disorganized secondary flow patterns increasing energy dissipation.<sup>21, 22, 25, 29, 68</sup> Offsetting the venae cavae 1.0-1.5 diameters apart decreases energy loss up to 50%

and has been repeatedly tested as the most efficient connection,<sup>17, 21, 29, 35, 38</sup> with even further reduction when the anastomosis site on the RPA is enlarged.<sup>35, 39</sup> Such an offset leads to the formation of a beneficial, low dissipative vortex between the IVC and SVC anastomosis, propelling their flow towards the respective PAs.<sup>15, 21, 22, 25, 27</sup>

### **Anastomosis shape**

Furthermore, the addition of flaring (Figure 1F) or curving (Figure 1H) of the anastomosis was investigated, showing that flaring of the IVC and SVC anastomosis, thereby avoiding dissipative sharp corners<sup>14, 71</sup>, on all sides can reduce the energy loss with another 68% and was more efficient than a curvature of the SVC and IVC towards one PA<sup>22, 23</sup>. The angle between the IVC and SVC connection and the shape of the anastomosis, a slot-like incision versus an oval excision, have been tested and had a significant influence on measured energy loss in those models with up to 75% less energy loss when increasing the IVC-SVC angle from 90 to 150 degrees (Figure 1D), and up to 32% less energy loss over an oval shaped excision versus a slot-like incision.<sup>28, 56</sup> The avoidance of sharp corners as well as of large differences in cross-sectional areas has been emphasized in order to maximize energy efficiency.<sup>71</sup>

Besides above mentioned factors, multiple other modifications have been proposed for improving TCPC efficiency while keeping adequate hepatic flow distribution (HFD) to both lungs. Soerensen et al<sup>83</sup> proposed a so called 'OptiFlo' connection, in which both SVC and IVC were split towards both PAs, and this was shown to be 42% more efficient as compared to the offset model. However, clinical implementation was considered to be difficult because of anatomical constraints and the need for large areas of non-native tissue. To address those drawbacks, the Y-graft was introduced (Figure 1G).<sup>49</sup> Although the Y-graft showed decreased energy loss compared with the T-junction TCPC in that study, a recent study of 30 implanted Y-grafts showed that the TCPC resistance including the Y-graft was approximately 3 times higher than traditional ECC or LT TCPCs in rest and during exercise conditions, making this commercially available Y-graft inferior to the traditional TCPCs.<sup>65, 84</sup> The main reason for this adverse result was the use of commercially available Y-grafts, where the diameters of the 2 branches of the Y-graft were half the diameter of the base. This effectively reduces the cross-sectional-area with 50% and therefore acts as a 'long-segment obstruction'. The use of area preserving Y-grafts should give better results and is a promising area for future research.<sup>79</sup>

A flow divider has also been tested in a CFD model, in which a flow dividing device is placed inside the normal Fontan tunnel to mimic the effect of a Y-graft, and has been shown to reduce energy loss.<sup>85</sup>

## Hepatic flow distribution

Besides the importance of an energy efficient TCPC, balanced HFD is needed to prevent the formation of PAVMs in the “hepatic factor” deprived lung. Dasi et al.<sup>52</sup> identified caval offsetting to be the main factor associated with unbalanced HFD in ECC patients, as the SVC flow creates a “momentum barrier” for the IVC flow to cross towards the other PA, and this has subsequently been identified as one of the most important factors influencing HFD.<sup>60, 61</sup> Therefore, offsetting of the IVC is faced with a trade-off situation between reducing energy loss on the one hand and unbalanced HFD on the other hand. Secondly, pulmonary flow split has been found to be correlated with HFD.<sup>52, 60, 61</sup> Therefore, these data suggest that clinicians should consider a low threshold for intervention when factors associated with unbalanced pulmonary flow split, most importantly PA stenosis<sup>61, 75</sup>, are present due to its association with increased energy loss and unbalanced HFD. Pulmonary flow split has also been identified as the most important factor influencing HFD in intra-atrial LT (after Hemi-Fontan) patients. This is explained by increased mixing of hepatic and SVC blood flows in these patients, contrary to ECC patients, before flow enters the pulmonary circulation, leading to a strong correlation between HFD and pulmonary flow split (e.g. if more blood flows through the right lung, less hepatic blood flows through the left lung). Furthermore, Ding et al.<sup>56</sup> illustrated that increasing the angle between RPA and IVC from 45 till 75 degrees improved HFD towards the RPA. In other words, curving (Figure 1F) of the IVC towards the LPA reduced HFD towards the RPA in this model. Also, increase of the angle between the Fontan tunnel and the SVC has been shown to correlate with unbalanced HFD in patient-specific TCPC models.<sup>61</sup> However, Ding et al. investigated this Fontan tunnel-SVC angle experimentally in a TCPC CFD model and, although a decreased angle (Figure 1D) led to increased energy loss due to helical flow formation, change of angle did not affect HFD.<sup>56</sup> This illustrates that the influence of certain geometric factors on HFD is patient-specific, emphasizing the need for patient-specific “virtual” modelling.<sup>54, 76</sup>

To date it is not known, however, what the minimum amount of hepatic flow is to prevent the formation of PAVMs. Quantification of HFD in large, longitudinal follow-up series using 4D flow MRI<sup>10</sup> or CFD simulations<sup>52</sup> should provide more insight into this. This will help choosing the best surgical options created with “virtual surgery” with minimal energy loss while only providing the necessary, minimal amount of hepatic flow. While the use of novel Y-grafts also aimed to induce more balanced HFD<sup>79</sup>, first results show highly variable HFD, related to multiple geometric and hemodynamic factors, including pulmonary flow split and SVC position, emphasizing the need for patient-specific surgical planning when using these grafts.<sup>65</sup>

## Limitations of energy loss assessment

### *Computational Fluid Dynamics (CFD) studies*

CFD has been used extensively in the past three decades to model the hemodynamics and efficiency of the TCPC, first in highly simplified symmetrical cross-like models, and later, with advances in computer power and modeling possibilities, in 3D patient-specific image-based TCPC geometries (Table 1). The necessary steps for a CFD simulation and the drawbacks and challenges of these steps in CFD modelling have been written in detail in previous studies.<sup>86</sup> Boundary conditions have to be set accurately, and assumptions such as rigid vessel walls<sup>44, 87</sup>, steady versus pulsatile inflow conditions<sup>38, 55, 60, 67</sup> and the influence of respiration<sup>45</sup> have been studied and can change conclusions. For example, many studies have assumed steady flow of venous blood from the venae cavae to the PAs because of an absent right ventricle. However, flow in the IVC can increase up to 80% during inspiration in TCPC patients<sup>20, 81, 82</sup>, and the contribution of this unsteady inflow or 'pulsatility' on calculated energy loss differs between patients<sup>55</sup>. It has been demonstrated that IVC flow pulsatility changes significantly when changing from breath-held to free-breathing MRI flow acquisitions, emphasizing the influence of respiration on flow.<sup>81</sup> Therefore, by limiting the evaluation by using steady flow assumptions, the reported energy loss can be different between patients and this can affect the reported conclusions. In other words, although significant advances have been made, the capability of a CFD model to compute realistic pressure and velocity fields in the TCPC depends on the accuracy and precision of the generated geometry and mesh, applied boundary conditions and of the validity of the assumptions being made.

Besides that, large validation studies and larger series correlating CFD derived parameters to clinical outcomes are needed. The capability of predictive modelling to improve outcome, which is one of the main advantages of CFD modeling in which clinicians can 'virtually' test interventions or different surgical geometries in a patient-specific manner to determine the optimal treatment, needs to be confirmed in large series before clinical implementation can be considered.<sup>88</sup>

### *In-vitro studies*

While in-vitro modelling plays a very important role in the research of TCPC energy loss, it should be realized that the early models, which for example demonstrated the importance of geometric factors such as caval offsetting and flaring on energy loss, included highly simplified, symmetrical, cross-like rigid tubes with uniform diameters.<sup>14, 21-24, 26-28, 74</sup> Implementing more physiologic features in these models, such as unequal vessel diameters and non-planarity (i.e. PAs do not lie in a strictly left to right plane) of the PAs, significantly changed fluid hemodynamics.<sup>26</sup> Besides the limiting, simplified geometry, most models also used steady inflow conditions and rigid materials influencing reported conclusions.<sup>38, 44, 55, 67, 87</sup> Patient-specific MRI based

TCPC models have led to more accurate models, although these models still use rigid material and steady inflow conditions.<sup>9, 30, 34</sup> Recently, an promising in-vitro model has been introduced that uses a patient-specific MRI derived compliant TCPC model, based on the patient-specific compliance value, and uses condition-specific (breath-held, free breathing and exercise) real-time phase contrast MRI derived flow waveforms as inflow conditions.<sup>89</sup> First results have shown and quantified the effect of respiration and exercise on energy loss and demonstrated that the effect of these parameters was highly patient-specific. Therefore, it is emphasized that future CFD models should use patient-specific, condition-specific boundaries.

### ***In-vivo studies***

Only a limited amount of in-vivo studies has reported on calculated energy loss in the TCPC.<sup>69, 70, 90</sup> In-vivo energy loss studies can be subdivided into studies using catheterization or 4D MRI derived data to calculate energy loss. Advantage of these in-vivo methods is that the number of assumptions to obtain the energy losses are limited compared with CFD modelling.

### ***Catheterization studies***

The capability of the catheterization method to accurately capture the highly dynamic and 3D flow and pressure fields is limited. In a recent in-vivo study<sup>69</sup>, averaged pressures and velocities were used at the inlet and outlet sections, which have been shown to overestimate energy loss with 18%<sup>91</sup>, and are inherently associated with measurement errors, as the position and size of the catheter inside the vessel will influence measured pressure and velocity values. For example, when a swirling, helical flow pattern is present, central pressure measurement may not reflect true pressure. Also, when calculating cross-sectional area of the venae cavae and PAs, which is needed to calculate flow from velocity, vessels are assumed to be circular which is not necessarily true. Furthermore, the possibility to calculate these losses during exercise is limited, as catheterization with indwelling catheters<sup>73</sup> is not a routine practice.

### ***4D flow MRI studies***

One in-vivo study used 4D flow MRI to calculate energy loss in the TCPC using the viscous dissipation method (Appendix A), with an average energy loss of  $0.56 \pm 0.28$  mW.<sup>70</sup> To date, 2 studies calculated kinetic energy (KE) using 4D flow MRI in the TCPC, with an average loss of  $31 \pm 20\%$  in one study<sup>90</sup>, but an increase in KE of 142% in the other. In this latter study, increase of KE is explained by a 50% decrease of the combined cross sectional area of the SVC and IVC compared with the PAs.<sup>92</sup> It should be noted that KE is only part of the energy equation (Appendix A) and does not represent total energy loss. Although 4D flow MRI is a promising non-invasive technique which can be easily implemented in clinical care, spatial resolution (i.e. the size of the voxels in mm<sup>3</sup>) is a

major issue, as this has been shown to be the limiting factor in accurately calculating energy loss (Appendix A). However, although underestimating absolute “true” energy loss due to limited spatial resolution, the relative performance of the TCPC between subjects remains intact when compared to CFD values, indicating that comparison of subjects is still possible with 4D flow MRI.<sup>70</sup>

## **Clinical relevance of energy loss in the TCPC**

To date, increased energy loss in the TCPC has been linked to 1) reduced exercise capacity and 2) altered cardiac parameters and increased central venous pressure (CVP).

### ***Exercise capacity and energy loss in the TCPC***

Exercise capacity is generally limited in patients after a TCPC, with a peak oxygen consumption (VO<sub>2</sub> max) of only 65% of expected at an age of 12 years, which gradually worsens with increasing age.<sup>13, 93</sup> However, there is a considerable variability in exercise tolerance, varying from 19% of predicted VO<sub>2</sub> max to even supra-normal values, with only 28% of patients having a normal value.<sup>13</sup>

Although the lower exercise tolerance in Fontan patients is multifactorial, including chronotropic incompetence, arterial desaturation, diastolic dysfunction, peripheral factors (e.g. lean muscle mass) and SV stroke volume, the latter (stroke volume) has been marked as the most important factor, explaining up to 73% of variance in VO<sub>2</sub> max between patients.<sup>13, 19, 73</sup>

The resting cardiac output (CO) in a Fontan patient is generally 60-70% of predicted and the ability to increase CO during exercise is severely impaired because of preload deprivation. The role of pulmonary vascular resistance (PVR) as the main factor controlling CO by limiting preload has been well recognized.<sup>94</sup> The TCPC resistance can be seen as a separate resistance in series with the PVR. Because of the clear role of PVR on the disability to increase CO, the energy loss or resistance in the TCPC has been studied as a possible contributing factor of reduced CO and therefore reducing exercise tolerance via the same mechanism as PVR does.

In healthy adults, PVR has been shown to decrease up to 50% at exercise.<sup>95</sup> This means that the TCPC resistance (Appendix B), although possibly of minor influence in resting conditions, can be the predominant bottleneck during exercise. In other words, the focus of PVR as the most important factor of influence on preload can shift during exercise conditions towards the TCPC resistance in some patients, as the TCPC resistance has been shown to increase exponentially with exercise.<sup>46</sup>

The only study to date showing a correlation between energy loss and exercise capacity in TCPC patients is by Khiabani et al.<sup>63</sup> In this study, 30 patients performed metabolic exercise testing and flow rates were collected during rest and exercise using MRI. A significant negative linear correlation ( $r = -0.6$ ) was seen between iPL and VO<sub>2</sub> max and Work (per kg). These results were later confirmed in an extension of this study in 47 patients.<sup>66</sup> In that study, the TCPC diameter index - an index capturing the minimal diameters of all the 4 TCPC vessels (IVC,SVC,RPA,LPA) in one parameter - showed an significant moderate correlation ( $r=0.468$ ) with VO<sub>2</sub> max.

In a study by Bossers et al., MRI data were obtained in 29 patients during rest and during dobutamine infusion mimicking exercise. CFD models were constructed and, to simulate lower-body exercise, 2x IVC flow was simulated. In this study, using RI and energy loss normalized by BSA, no correlation was found between energy loss and exercise performance parameters. It has been suggested that normalizing energy loss with BSA is the reason this study found no difference in exercise capacity, as this parameter is highly flow dependent.<sup>96</sup>

### ***Cardiac parameters and energy loss in the TCPC***

The last decade, a number of studies have reported correlations between energy loss within the TCPC and cardiac parameters and central venous pressure (CVP).

In a lumped parameter model, Sundareswaran et al. showed a weak ( $r = -0.36$ ) negative linear correlation between TCPC resistance and CO<sup>47</sup>, with an expected CO decrease of 8.8% for each 10% increase in TCPC resistance. This has later been confirmed in the largest series to date using CFD modelling, in which iPL was inversely correlated with cardiac index ( $r = -0.21$ ) and systemic venous return ( $r = -0.31$ ).<sup>60</sup> Additionally, a significant, moderate inverse relationship between iPL and end diastolic ( $r = -0.48$ ), end systolic ( $r = -0.37$ ) and stroke volumes ( $r = -0.37$ ) was reported. Furthermore, a positive correlation was found between iPL and time to peak filling rate ( $r = 0.67$ ).<sup>62</sup>

Sundareswaran et al. reported both an increase in ventricular-vascular coupling mismatch ( $E_a/E_{es}$ ) and an increase of CVP with increasing TCPC resistance. CVP increased with 6.4% for each 10% increase in resistance. In a mathematical study using failing Fontan hemodynamics, 57% of the increase in CVP in failing Fontan patients, defined as NYHA class III-IV, supraventricular tachyarrhythmias, persistent effusions unresponsive to diuretic therapy and hypoalbuminemia, could be ascribed to TCPC resistance and the remaining increase to rise of atrial pressure.<sup>97</sup>

In the only in-vivo study to date correlating TCPC energetics with cardiac parameters, a positive correlation was found between energy loss measured during catheterization

and time constant  $\tau$  and systolic dPdt (contractility), reflecting diastolic and systolic function respectively. However, no correlation between energy loss and systemic venous flow was found.<sup>69</sup>

These data suggest the importance of energy loss in the TCPC on hemodynamics by reducing ventricular preload, preload-reserve and thereby cardiac output, and possibly by influencing diastolic function.

### Future directions and conclusions

In the past three decades, the factors associated with the energetics in the TCPC and the potential role of this energy loss on Fontan outcome has become more obvious. However, although an increasing amount of studies connect energy loss with cardiac parameters and exercise capacity, evidence is mainly based on small ( $n \leq 30$ ) series and some have conflicting results. Furthermore, to date, no studies exists connecting complications associated with failing Fontan physiology such as PLE, plastic bronchitis or liver cirrhosis with energy loss in the TCPC. Larger, multi-center series are needed and long-term follow-up should definitely clarify the role of energy loss in the TCPC on long term outcome and can thereby possibly predict adverse outcome early in time. Additionally, to date, energy loss is almost exclusively calculated via CFD modelling and the capability of this method to reflect reality depends on the accuracy of the boundary conditions and validity of underlying assumptions.

4D flow MRI can be of important complementary value by offering in-vivo, non-invasive acquisition of accurate time-resolved 3D velocity vector fields (Supplemental videos 1&2) after which energy loss, kinetic energy, turbulent kinetic energy and areas of increased wall shear stress in the TCPC can be calculated (Figure 2). However, main limitations include a long scan time, noisy velocity data and limited spatial and temporal resolution. Increasing resolution to better capture 3D flow and velocity gradients will decrease signal to noise ratio (SNR) and increase scanning time, and consequently its clinical use is therefore now limited. New sequences for accelerating acquisition of data are developed and can reduce scan time, however, at a possible cost of reduced accuracy. For implementation of 4D flow MRI techniques in the Fontan patient, optimal scan parameters and protocols have to be determined, in which compromises between resolution and clinical acceptable scanning times have to be made.<sup>8</sup>

Large 4D flow MRI series will be needed and should ideally put calculated TCPC resistance in context of patient specific PVR, both during rest and exercise conditions. Furthermore, large 4D flow MRI series should be obtained and used to validate CFD models in capturing the sometimes highly 3D, chaotic flows, which to date, has only been performed in a limited number of patients with a Fontan circulation.<sup>34, 60</sup> Furthermore,



confirmation of the impact of energy loss on clinical outcome based on in-vivo data with 4D flow MRI will likely increase confidence in computed results from CFD studies and may accelerate the clinical implementation of patient-specific CFD models in the future.

In conclusion, an extensive amount of studies has shown that the efficiency of the TCPC is highly variable, and therefore provides room for improvement. The TCPC resistance will likely be an important additional parameter, complementary to factors such as PVR, in determining outcome in patients with a Fontan circulation. Therefore, via the same rationale why efforts have been made trying to decrease PVR in Fontan patients, surgical modifications and patient-specific TCPC planning will aim to improve outcome by reducing TCPC resistance and thereby increasing TCPC efficiency.

When a more definitive correlation between energy loss in the TCPC and adverse outcomes such as PLE, plastic bronchitis, liver cirrhosis and exercise intolerance has been clarified, knowledge about the factors explaining the variability of the TCPC efficiency and the possibility of virtual surgery using CFD predictive modeling will likely guide future management in a patient-specific manner.

This review illustrates the important concept of adverse energetics in the TCPC in patients with a Fontan circulation. However, the same principles of visualization and quantification of 3D blood flow data and the adverse effects of distorted blood flow on energetics are promising in many cardiovascular diseases, including ischemic and dilated cardiomyopathies, valvular heart disease, aortic disease, heart failure and other congenital heart disease. Future studies should clarify the role of these new parameters in various cardiovascular diseases to determine its potential use in clinical care.

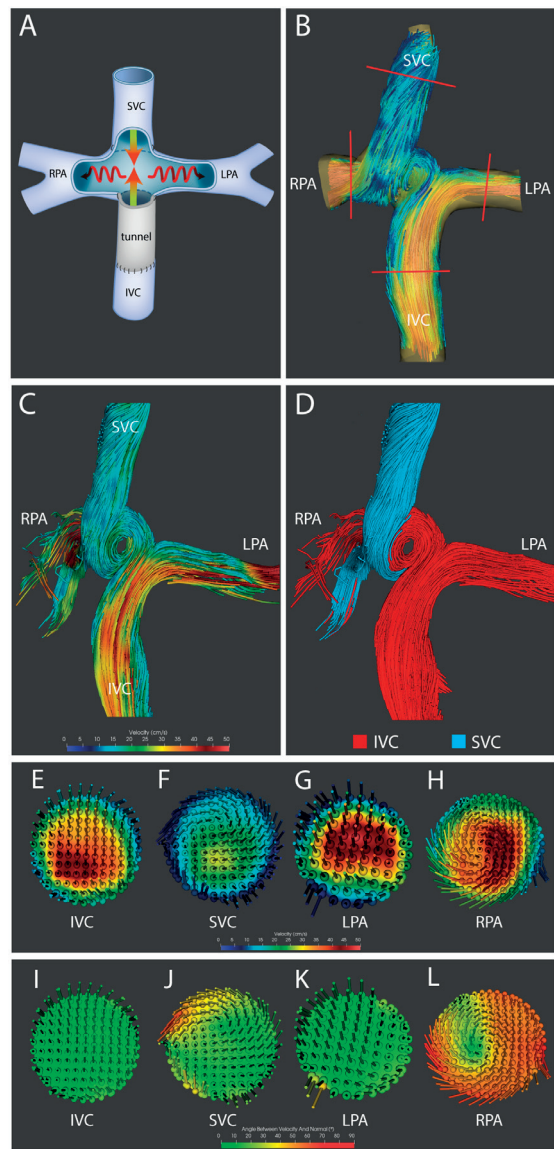


**Figure 2.** Visualisation of abnormal blood flow patterns in the TCPC with 4D MRI.

This figure shows some of the unprecedented possibilities of visualising blood flow patterns in-vivo in patients with a Fontan circulation by using 4D flow MRI.

The schematic TCPC with zero offset (Figure 1, central figure) is shown for orientation (**Panel A**). Images show the TCPC of an 18 year old patient with tricuspid atresia with a non-fenestrated 16 mm extracardiac conduit with offset, leading to predominant inferior vena cava (IVC) flow towards the left pulmonary artery (LPA) (**Panels B-L**). The orientation of the swirling blood flow within the crux of the TCPC and the location of the cross-sectional planes are shown (**Panel B**). Streamlines and particle tracings are shown from a left anterior oblique view (**Panel C&D**). Pathlines with velocity coding show areas of slow (blue) blood flow in the SVC and increased (red) velocities inside the tunnel and the distal PAs, with the formation of a swirling flow into the right pulmonary artery (RPA). Also, a swirling inflow from the vena anonyma (not included) into the proximal part of the SVC

is noted (**Panel C**). Particle tracing analysis shows the differential contribution and interaction between IVC and superior vena cava (SVC) blood flow. SVC flow is pushed anteriorly into the helical flow extending into the RPA. Additionally, SVC blood flows exclusively towards the RPA and predominant SVC flow to the lower right segmental pulmonary artery is shown (**Panel D**). The flow vectors are shown and visualized for velocity (**Panel E-H**) and for the angle to the normal (the normal is the vector perpendicular to the plane, **Panel I-L**). While most of the flow in the IVC, SVC and LPA shows laminar flow with no angle (i.e. blood flows parallel to the vessel wall), angles up to 70 degrees are shown in the RPA at site of the helical flow. These abnormal flow patterns are associated with increased energy loss.<sup>7</sup>

Please note, blood flow qualification (visualization) is only one of the many possibilities of 4D MRI. The acquired 4D flow data (velocity field) can also be used to calculate quantitative haemodynamic parameters based on these in-vivo velocity data (in contrast with CFD) amongst which are energy loss and wall shear stress (not shown here).

Of note, the figures were morphed for better display without editing the flow within the TCPC.

## References

1. Richter Y and Edelman ER. Cardiology is flow. *Circulation*. 2006;113:2679-82.
2. Akins CW, Travis B and Yoganathan AP. Energy loss for evaluating heart valve performance. *J Thorac Cardiovasc Surg*. 2008;136:820-33.
3. Wang C, Pekkan K, de Zelicourt D, Horner M, Parihar A, Kulkarni A and Yoganathan AP. Progress in the CFD modeling of flow instabilities in anatomical total cavopulmonary connections. *Ann Biomed Eng*. 2007;35:1840-56.
4. Dasi LP, Pekkan K, de Zelicourt D, Sundareswaran KS, Krishnankutty R, Delnido PJ and Yoganathan AP. Hemodynamic energy dissipation in the cardiovascular system: generalized theoretical analysis on disease states. *Ann Biomed Eng*. 2009;37:661-73.
5. Youssefi P, Sharma R, Figueroa CA and Jahangiri M. Functional assessment of thoracic aortic aneurysms - the future of risk prediction? *Br Med Bull*. 2017;121:61-71.
6. Barker AJ, van Ooij P, Bandi K, Garcia J, Albaghdadi M, McCarthy P, Bonow RO, Carr J, Collins J, Malaisrie SC and Markl M. Viscous energy loss in the presence of abnormal aortic flow. *Magn Reson Med*. 2014;72:620-8.
7. Calkoen EE, Roest AA, van der Geest RJ, de Roos A and Westenberg JJ. Cardiovascular function and flow by 4-dimensional magnetic resonance imaging techniques: new applications. *J Thorac Imaging*. 2014;29:185-96.
8. Dyverfeldt P, Bissell M, Barker AJ, Bolger AF, Carlhall CJ, Ebbers T, Francios CJ, Frydrychowicz A, Geiger J, Giese D, Hope MD, Kilner PJ, Kozerke S, Myerson S, Neubauer S, Wieben O and Markl M. 4D flow cardiovascular magnetic resonance consensus statement. *J Cardiovasc Magn Reson*. 2015;17:72.
9. de Zelicourt DA, Pekkan K, Parks J, Kanter K, Fogel M and Yoganathan AP. Flow study of an extracardiac connection with persistent left superior vena cava. *J Thorac Cardiovasc Surg*. 2006;131:785-91.
10. Jarvis K, Schnell S, Barker AJ, Garcia J, Lorenz R, Rose M, Chowdhary V, Carr J, Robinson JD, Rigsby CK and Markl M. Evaluation of blood flow distribution asymmetry and vascular geometry in patients with Fontan circulation using 4-D flow MRI. *Pediatr Radiol*. 2016;46:1507-19.
11. Binter C, Gotschy A, Sundermann SH, Frank M, Tanner FC, Luscher TF, Manka R and Kozerke S. Turbulent Kinetic Energy Assessed by Multipoint 4-Dimensional Flow Magnetic Resonance Imaging Provides Additional Information Relative to Echocardiography for the Determination of Aortic Stenosis Severity. *Circ Cardiovasc Imaging*. 2017;10.
12. d'Udekem Y, Iyengar AJ, Galati JC, Forsdick V, Weintraub RG, Wheaton GR, Bullock A, Justo RN, Grigg LE, Sholler GF, Hope S, Radford DJ, Gentles TL, Celermajer DS and Winlaw DS. Redefining expectations of long-term survival after the Fontan procedure: twenty-five years of follow-up from the entire population of Australia and New Zealand. *Circulation*. 2014;130:S32-8.
13. Paridon SM, Mitchell PD, Colan SD, Williams RV, Blaufox A, Li JS, Margossian R, Mital S, Russell J, Rhodes J and Pediatric Heart Network I. A cross-sectional study of exercise performance during the first 2 decades of life after the Fontan operation. *J Am Coll Cardiol*. 2008;52:99-107.
14. de Leval MR, Kilner P, Gewillig M and Bull C. Total cavopulmonary connection: a logical alternative to atriopulmonary connection for complex Fontan operations. Experimental studies and early clinical experience. *J Thorac Cardiovasc Surg*. 1988;96:682-95.

15. Be'eri E, Maier SE, Landzberg MJ, Chung T and Geva T. In vivo evaluation of Fontan pathway flow dynamics by multidimensional phase-velocity magnetic resonance imaging. *Circulation*. 1998;98:2873-82.
16. Van Haesdonck JM, Mertens L, Sizaïre R, Montas G, Purnode B, Daenen W, Crochet M and Gewillig M. Comparison by computerized numeric modeling of energy losses in different Fontan connections. *Circulation*. 1995;92:II322-6.
17. Dubini G, de Leval MR, Pietrabissa R, Montevecchi FM and Fumero R. A numerical fluid mechanical study of repaired congenital heart defects. Application to the total cavopulmonary connection. *J Biomech*. 1996;29:111-21.
18. McElhinney DB, Kreutzer J, Lang P, Mayer JE, Jr., del Nido PJ and Lock JE. Incorporation of the hepatic veins into the cavopulmonary circulation in patients with heterotaxy and pulmonary arteriovenous malformations after a Kawashima procedure. *Ann Thorac Surg*. 2005;80:1597-603.
19. Goldberg DJ, Avitabile CM, McBride MG and Paridon SM. Exercise capacity in the Fontan circulation. *Cardiol Young*. 2013;23:824-30.
20. Hjortdal VE, Emmertsen K, Stenbøg E, Frund T, Schmidt MR, Kromann O, Sørensen K and Pedersen EM. Effects of exercise and respiration on blood flow in total cavopulmonary connection: a real-time magnetic resonance flow study. *Circulation*. 2003;108:1227-31.
21. Sharma S, Goudy S, Walker P, Panchal S, Ensley A, Kanter K, Tam V, Fyfe D and Yoganathan A. In vitro flow experiments for determination of optimal geometry of total cavopulmonary connection for surgical repair of children with functional single ventricle. *J Am Coll Cardiol*. 1996;27:1264-9.
22. Ensley AE, Lynch P, Chatzimavroudis GP, Lucas C, Sharma S and Yoganathan AP. Toward designing the optimal total cavopulmonary connection: an in vitro study. *Ann Thorac Surg*. 1999;68:1384-90.
23. Gerdes A, Kunze J, Pfister G and Sievers HH. Addition of a small curvature reduces power losses across total cavopulmonary connections. *Ann Thorac Surg*. 1999;67:1760-4.
24. Lardo AC, Webber SA, Friehs I, del Nido PJ and Cape EG. Fluid dynamic comparison of intra-atrial and extracardiac total cavopulmonary connections. *J Thorac Cardiovasc Surg*. 1999;117:697-704.
25. Ensley AE, Ramuzat A, Healy TM, Chatzimavroudis GP, Lucas C, Sharma S, Pettigrew R and Yoganathan AP. Fluid mechanic assessment of the total cavopulmonary connection using magnetic resonance phase velocity mapping and digital particle image velocimetry. *Ann Biomed Eng*. 2000;28:1172-83.
26. Ryu K, Healy TM, Ensley AE, Sharma S, Lucas C and Yoganathan AP. Importance of accurate geometry in the study of the total cavopulmonary connection: computational simulations and in vitro experiments. *Ann Biomed Eng*. 2001;29:844-53.
27. Amodeo A, Grigioni M, Oppido G, Daniele C, D'Avenio G, Pedrizzetti G, Giannico S, Filippelli S and Di Donato RM. The beneficial vortex and best spatial arrangement in total extracardiac cavopulmonary connection. *J Thorac Cardiovasc Surg*. 2002;124:471-8.
28. Gerdes A, Benthin U and Sievers HH. Influence of arteriotomy shape on power losses across in vitro cavopulmonary connections. *J Cardiovasc Surg (Torino)*. 2002;43:787-91.
29. Amodeo A, Grigioni M, D'Avenio G, Daniele C and Di Donato RM. The patterns of flow in the total extracardiac cavopulmonary connection. *Cardiol Young*. 2004;14 Suppl 3:53-6.
30. de Zelicourt DA, Pekkan K, Wills L, Kanter K, Forbess J, Sharma S, Fogel M and Yoganathan AP. In vitro flow analysis of a patient-specific intraatrial total cavopulmonary connection. *Ann Thorac Surg*. 2005;79:2094-102.

31. Pekkan K, de Zelicourt D, Ge L, Sotiropoulos F, Frakes D, Fogel MA and Yoganathan AP. Physics-driven CFD modeling of complex anatomical cardiovascular flows-a TCPC case study. *Ann Biomed Eng.* 2005;33:284-300.
32. Soerensen DD, Pekkan K, de Zelicourt D, Sharma S, Kanter K, Fogel M and Yoganathan AP. Introduction of a new optimized total cavopulmonary connection. *Ann Thorac Surg.* 2007;83:2182-90.
33. Tang E, Haggerty CM, Khiabani RH, de Zelicourt D, Kanter J, Sotiropoulos F, Fogel MA and Yoganathan AP. Numerical and experimental investigation of pulsatile hemodynamics in the total cavopulmonary connection. *J Biomech.* 2013;46:373-82.
34. Roldan-Alzate A, Garcia-Rodriguez S, Anagnostopoulos PV, Srinivasan S, Wieben O and Francois CJ. Hemodynamic study of TCPC using in vivo and in vitro 4D Flow MRI and numerical simulation. *J Biomech.* 2015;48:1325-30.
35. de Leval MR, Dubini G, Migliavacca F, Jalali H, Camporini G, Redington A and Pietrabissa R. Use of computational fluid dynamics in the design of surgical procedures: application to the study of competitive flows in cavo-pulmonary connections. *J Thorac Cardiovasc Surg.* 1996;111:502-13.
36. Healy TM, Lucas C and Yoganathan AP. Noninvasive fluid dynamic power loss assessments for total cavopulmonary connections using the viscous dissipation function: a feasibility study. *J Biomech Eng.* 2001;123:317-24.
37. Bolzon G, Pedrizzetti G, Grigioni M, Zovatto L, Daniele C and D'Avenio G. Flow on the symmetry plane of a total cavo-pulmonary connection. *J Biomech.* 2002;35:595-608.
38. DeGroff CG and Shandas R. Designing the optimal Total Cavopulmonary Connection: pulsatile versus steady flow experiments. *Med Sci Monit.* 2002;8:MT41-5.
39. Bove EL, de Leval MR, Migliavacca F, Guadagni G and Dubini G. Computational fluid dynamics in the evaluation of hemodynamic performance of cavopulmonary connections after the Norwood procedure for hypoplastic left heart syndrome. *J Thorac Cardiovasc Surg.* 2003;126:1040-7.
40. Hsia TY, Migliavacca F, Pittaccio S, Radaelli A, Dubini G, Pennati G and de Leval M. Computational fluid dynamic study of flow optimization in realistic models of the total cavopulmonary connections. *J Surg Res.* 2004;116:305-13.
41. Liu Y, Pekkan K, Jones SC and Yoganathan AP. The effects of different mesh generation methods on computational fluid dynamic analysis and power loss assessment in total cavopulmonary connection. *J Biomech Eng.* 2004;126:594-603.
42. Pekkan K, Kitajima HD, de Zelicourt D, Forbess JM, Parks WJ, Fogel MA, Sharma S, Kanter KR, Frakes D and Yoganathan AP. Total cavopulmonary connection flow with functional left pulmonary artery stenosis: angioplasty and fenestration in vitro. *Circulation.* 2005;112:3264-71.
43. Moyle KR, Mallinson GD, Occleshaw CJ, Cowan BR and Gentles TL. Wall shear stress is the primary mechanism of energy loss in the Fontan connection. *Pediatr Cardiol.* 2006;27:309-15.
44. Orlando W, Shandas R and DeGroff C. Efficiency differences in computational simulations of the total cavo-pulmonary circulation with and without compliant vessel walls. *Comput Methods Programs Biomed.* 2006;81:220-7.
45. Marsden AL, Vignon-Clementel IE, Chan FP, Feinstein JA and Taylor CA. Effects of exercise and respiration on hemodynamic efficiency in CFD simulations of the total cavopulmonary connection. *Ann Biomed Eng.* 2007;35:250-63.
46. Whitehead KK, Pekkan K, Kitajima HD, Paridon SM, Yoganathan AP and Fogel MA. Nonlinear power loss during exercise in single-ventricle patients after the Fontan: insights from computational fluid dynamics. *Circulation.* 2007;116:1165-71.

47. Sundareswaran KS, Pekkan K, Dasi LP, Whitehead K, Sharma S, Kanter KR, Fogel MA and Yoganathan AP. The total cavopulmonary connection resistance: a significant impact on single ventricle hemodynamics at rest and exercise. *Am J Physiol Heart Circ Physiol*. 2008;295:H2427-35.
48. Itatani K, Miyaji K, Tomoyasu T, Nakahata Y, Ohara K, Takamoto S and Ishii M. Optimal conduit size of the extracardiac Fontan operation based on energy loss and flow stagnation. *Ann Thorac Surg*. 2009;88:565-72; discussion 572-3.
49. Marsden AL, Bernstein AJ, Reddy VM, Shadden SC, Spilker RL, Chan FP, Taylor CA and Feinstein JA. Evaluation of a novel Y-shaped extracardiac Fontan baffle using computational fluid dynamics. *J Thorac Cardiovasc Surg*. 2009;137:394-403 e2.
50. Marsden AL, Reddy VM, Shadden SC, Chan FP, Taylor CA and Feinstein JA. A new multiparameter approach to computational simulation for Fontan assessment and redesign. *Congenit Heart Dis*. 2010;5:104-17.
51. Baretta A, Corsini C, Yang W, Vignon-Clementel IE, Marsden AL, Feinstein JA, Hsia TY, Dubini G, Migliavacca F, Pennati G and Modeling of Congenital Hearts Alliance I. Virtual surgeries in patients with congenital heart disease: a multi-scale modelling test case. *Philos Trans A Math Phys Eng Sci*. 2011;369:4316-30.
52. Dasi LP, Whitehead K, Pekkan K, de Zelicourt D, Sundareswaran K, Kanter K, Fogel MA and Yoganathan AP. Pulmonary hepatic flow distribution in total cavopulmonary connections: extracardiac versus intracardiac. *J Thorac Cardiovasc Surg*. 2011;141:207-14.
53. Itatani K, Miyaji K, Nakahata Y, Ohara K, Takamoto S and Ishii M. The lower limit of the pulmonary artery index for the extracardiac Fontan circulation. *J Thorac Cardiovasc Surg*. 2011;142:127-35.
54. Haggerty CM, de Zelicourt DA, Restrepo M, Rossignac J, Spray TL, Kanter KR, Fogel MA and Yoganathan AP. Comparing pre- and post-operative Fontan hemodynamic simulations: implications for the reliability of surgical planning. *Ann Biomed Eng*. 2012;40:2639-51.
55. Khiabani RH, Restrepo M, Tang E, De Zelicourt D, Sotiropoulos F, Fogel M and Yoganathan AP. Effect of flow pulsatility on modeling the hemodynamics in the total cavopulmonary connection. *J Biomech*. 2012;45:2376-81.
56. Ding J, Liu Y and Wang F. Influence of bypass angles on extracardiac Fontan connections: a numerical study. *Int J Numer Method Biomed Eng*. 2013;29:351-62.
57. Haggerty CM, Kanter KR, Restrepo M, de Zelicourt DA, Parks WJ, Rossignac J, Fogel MA and Yoganathan AP. Simulating hemodynamics of the Fontan Y-graft based on patient-specific in vivo connections. *J Thorac Cardiovasc Surg*. 2013;145:663-70.
58. Kung E, Baretta A, Baker C, Arbia G, Biglino G, Corsini C, Schievano S, Vignon-Clementel IE, Dubini G, Pennati G, Taylor A, Dorfman A, Hlavacek AM, Marsden AL, Hsia TY, Migliavacca F and Modeling Of Congenital Hearts Alliance I. Predictive modeling of the virtual Hemi-Fontan operation for second stage single ventricle palliation: two patient-specific cases. *J Biomech*. 2013;46:423-9.
59. Bossers SS, Cibis M, Gijsen FJ, Schokking M, Strengers JL, Verhaart RF, Moelker A, Wentzel JJ and Helbing WA. Computational fluid dynamics in Fontan patients to evaluate power loss during simulated exercise. *Heart*. 2014;100:696-701.
60. Haggerty CM, Restrepo M, Tang E, de Zelicourt DA, Sundareswaran KS, Mirabella L, Bethel J, Whitehead KK, Fogel MA and Yoganathan AP. Fontan hemodynamics from 100 patient-specific cardiac magnetic resonance studies: a computational fluid dynamics analysis. *J Thorac Cardiovasc Surg*. 2014;148:1481-9.

61. Tang E, Restrepo M, Haggerty CM, Mirabella L, Bethel J, Whitehead KK, Fogel MA and Yoganathan AP. Geometric characterization of patient-specific total cavopulmonary connections and its relationship to hemodynamics. *JACC Cardiovasc Imaging*. 2014;7:215-24.
62. Haggerty CM, Whitehead KK, Bethel J, Fogel MA and Yoganathan AP. Relationship of single ventricle filling and preload to total cavopulmonary connection hemodynamics. *Ann Thorac Surg*. 2015;99:911-7.
63. Khiabani RH, Whitehead KK, Han D, Restrepo M, Tang E, Bethel J, Paridon SM, Fogel MA and Yoganathan AP. Exercise capacity in single-ventricle patients after Fontan correlates with haemodynamic energy loss in TCPC. *Heart*. 2015;101:139-43.
64. Restrepo M, Tang E, Haggerty CM, Khiabani RH, Mirabella L, Bethel J, Valente AM, Whitehead KK, McElhinney DB, Fogel MA and Yoganathan AP. Energetic implications of vessel growth and flow changes over time in Fontan patients. *Ann Thorac Surg*. 2015;99:163-70.
65. Trusty PM, Restrepo M, Kanter KR, Yoganathan AP, Fogel MA and Slesnick TC. A pulsatile hemodynamic evaluation of the commercially available bifurcated Y-graft Fontan modification and comparison with the lateral tunnel and extracardiac conduits. *J Thorac Cardiovasc Surg*. 2016;151:1529-36.
66. Tang E, Wei ZA, Whitehead KK, Khiabani RH, Restrepo M, Mirabella L, Bethel J, Paridon SM, Marino BS, Fogel MA and Yoganathan AP. Effect of Fontan geometry on exercise haemodynamics and its potential implications. *Heart*. 2017.
67. Wei ZA, Trusty PM, Tree M, Haggerty CM, Tang E, Fogel M and Yoganathan AP. Can time-averaged flow boundary conditions be used to meet the clinical timeline for Fontan surgical planning? *J Biomech*. 2017;50:172-179.
68. Sharma S, Ensley AE, Hopkins K, Chatzimavroudis GP, Healy TM, Tam VK, Kanter KR and Yoganathan AP. In vivo flow dynamics of the total cavopulmonary connection from three-dimensional multislice magnetic resonance imaging. *Ann Thorac Surg*. 2001;71:889-98.
69. Honda T, Itatani K, Takanashi M, Mineo E, Kitagawa A, Ando H, Kimura S, Nakahata Y, Oka N, Miyaji K and Ishii M. Quantitative evaluation of hemodynamics in the Fontan circulation: a cross-sectional study measuring energy loss in vivo. *Pediatr Cardiol*. 2014;35:361-7.
70. Cibis M, Jarvis K, Markl M, Rose M, Rigsby C, Barker AJ and Wentzel JJ. The effect of resolution on viscous dissipation measured with 4D flow MRI in patients with Fontan circulation: Evaluation using computational fluid dynamics. *J Biomech*. 2015;48:2984-9.
71. Ascuitto RJ, Kydon DW and Ross-Ascuitto NT. Pressure loss from flow energy dissipation: relevance to Fontan-type modifications. *Pediatr Cardiol*. 2001;22:110-5.
72. Sundareswaran KS, Haggerty CM, de Zelicourt D, Dasi LP, Pekkan K, Frakes DH, Powell AJ, Kanter KR, Fogel MA and Yoganathan AP. Visualization of flow structures in Fontan patients using 3-dimensional phase contrast magnetic resonance imaging. *J Thorac Cardiovasc Surg*. 2012;143:1108-16.
73. Goldstein BH, Connor CE, Gooding L and Rocchini AP. Relation of systemic venous return, pulmonary vascular resistance, and diastolic dysfunction to exercise capacity in patients with single ventricle receiving fontan palliation. *Am J Cardiol*. 2010;105:1169-75.
74. DeGroff CG, Carlton JD, Weinberg CE, Ellison MC, Shandas R and Valdes-Cruz L. Effect of vessel size on the flow efficiency of the total cavopulmonary connection: in vitro studies. *Pediatr Cardiol*. 2002;23:171-7.
75. Dasi LP, Krishnankuttyrema R, Kitajima HD, Pekkan K, Sundareswaran KS, Fogel M, Sharma S, Whitehead K, Kanter K and Yoganathan AP. Fontan hemodynamics: importance of pulmonary artery diameter. *J Thorac Cardiovasc Surg*. 2009;137:560-4.



76. de Zelicourt DA and Kurtcuoglu V. Patient-Specific Surgical Planning, Where Do We Stand? The Example of the Fontan Procedure. *Ann Biomed Eng.* 2016;44:174-86.
77. van Brakel TJ, Schoof PH, de Roo F, Nikkels PG, Evens FC and Haas F. High incidence of Dacron conduit stenosis for extracardiac Fontan procedure. *J Thorac Cardiovasc Surg.* 2014;147:1568-72.
78. Tang E, McElhinney DB, Restrepo M, Valente AM and Yoganathan AP. Haemodynamic impact of stent implantation for lateral tunnel Fontan stenosis: a patient-specific computational assessment. *Cardiol Young.* 2016;26:116-26.
79. Yang W, Vignon-Clementel IE, Troianowski G, Reddy VM, Feinstein JA and Marsden AL. Hepatic blood flow distribution and performance in conventional and novel Y-graft Fontan geometries: a case series computational fluid dynamics study. *J Thorac Cardiovasc Surg.* 2012;143:1086-97.
80. Salim MA, DiSessa TG, Arheart KL and Alpert BS. Contribution of superior vena caval flow to total cardiac output in children. A Doppler echocardiographic study. *Circulation.* 1995;92:1860-5.
81. Wei Z, Whitehead KK, Khiabani RH, Tree M, Tang E, Paridon SM, Fogel MA and Yoganathan AP. Respiratory Effects on Fontan Circulation During Rest and Exercise Using Real-Time Cardiac Magnetic Resonance Imaging. *Ann Thorac Surg.* 2016;101:1818-25.
82. Pedersen EM, Stenbog EV, Frund T, Houliand K, Kromann O, Sorensen KE, Emmertsen K and Hjortdal VE. Flow during exercise in the total cavopulmonary connection measured by magnetic resonance velocity mapping. *Heart.* 2002;87:554-8.
83. Soerensen DD, Pekkan K, Sundareswaran KS and Yoganathan AP. New power loss optimized Fontan connection evaluated by calculation of power loss using high resolution PC-MRI and CFD. *Conf Proc IEEE Eng Med Biol Soc.* 2004;2:1144-7.
84. Trusty PM, Wei Z, Tree M, Kanter KR, Fogel MA, Yoganathan AP and Slesnick TC. Local Hemodynamic Differences Between Commercially Available Y-Grafts and Traditional Fontan Baffles Under Simulated Exercise Conditions: Implications for Exercise Tolerance. *Cardiovasc Eng Technol.* 2017;8:390-399.
85. Desai K, Haggerty CM, Kanter KR, Rossignac J, Spray TL, Fogel MA and Yoganathan AP. Haemodynamic comparison of a novel flow-divider Optiflow geometry and a traditional total cavopulmonary connection. *Interact Cardiovasc Thorac Surg.* 2013;17:1-7.
86. Arbia G, Corsini C, Esmaily Moghadam M, Marsden AL, Migliavacca F, Pennati G, Hsia TY, Vignon-Clementel IE and Modeling Of Congenital Hearts Alliance I. Numerical blood flow simulation in surgical corrections: what do we need for an accurate analysis? *J Surg Res.* 2014;186:44-55.
87. Masters JC, Ketner M, Bleiweis MS, Mill M, Yoganathan A and Lucas CL. The effect of incorporating vessel compliance in a computational model of blood flow in a total cavopulmonary connection (TCPC) with caval centerline offset. *J Biomech Eng.* 2004;126:709-13.
88. Biglino G, Capelli C, Bruse J, Bosi GM, Taylor AM and Schievano S. Computational modelling for congenital heart disease: how far are we from clinical translation? *Heart.* 2017;103:98-103.
89. Tree M, Wei ZA, Trusty PM, Raghav V, Fogel M, Maher K and Yoganathan A. Using a Novel In Vitro Fontan Model and Condition-Specific Real-Time MRI Data to Examine Hemodynamic Effects of Respiration and Exercise. *Ann Biomed Eng.* 2018;46:135-147.
90. Roldan-Alzate A, Garcia-Rodriguez, S., Anagnostopoulos, P., Srinivasan, S., Francois, C. Kinetic energy efficiency of single ventricle and TCPC using 4D flow MRI. *Journal of cardiovascular magnetic resonance.* 2015;17.

91. Wei ZA, Tree M, Trusty PM, Wu W, Singh-Gryzbon S and Yoganathan A. The Advantages of Viscous Dissipation Rate over Simplified Power Loss as a Fontan Hemodynamic Metric. *Ann Biomed Eng.* 2017.
92. Sjoberg P, Heiberg E, Wingren P, Ramgren Johansson J, Malm T, Arheden H, Liuba P and Carlsson M. Decreased Diastolic Ventricular Kinetic Energy in Young Patients with Fontan Circulation Demonstrated by Four-Dimensional Cardiac Magnetic Resonance Imaging. *Pediatr Cardiol.* 2017;38:669-680.
93. Giardini A, Hager A, Pace Napoleone C and Picchio FM. Natural history of exercise capacity after the Fontan operation: a longitudinal study. *Ann Thorac Surg.* 2008;85:818-21.
94. Gewillig M and Brown SC. The Fontan circulation after 45 years: update in physiology. *Heart.* 2016;102:1081-6.
95. Naeije R and Chesler N. Pulmonary circulation at exercise. *Compr Physiol.* 2012;2:711-41.
96. Khiabani RH, Whitehead KK, Han D, Restrepo M, Tang E, Bethel J, Paridon SM, Fogel MA and Yoganathan AP. Does TCPC power loss really affect exercise capacity? *Heart.* 2015;101:575-6.
97. Cavalcanti S, Gnudi G, Masetti P, Ussia GP and Marcelletti CF. Analysis by mathematical model of haemodynamic data in the failing Fontan circulation. *Physiol Meas.* 2001;22:209-22.
98. Migliavacca F, Dubini G, Bove EL and de Leval MR. Computational fluid dynamics simulations in realistic 3-D geometries of the total cavopulmonary anastomosis: the influence of the inferior caval anastomosis. *J Biomech Eng.* 2003;125:805-13.
99. Hong H, Menon PG, Zhang H, Ye L, Zhu Z, Chen H and Liu J. Postsurgical comparison of pulsatile hemodynamics in five unique total cavopulmonary connections: identifying ideal connection strategies. *Ann Thorac Surg.* 2013;96:1398-404.
100. Sun Q, Liu J, Qian Y, Zhang H, Wang Q, Sun Y, Hong H and Liu J. Computational haemodynamic analysis of patient-specific virtual operations for total cavopulmonary connection with dual superior venae cavae. *Eur J Cardiothorac Surg.* 2014;45:564-9.

## Supplemental material

### Appendix A: Theoretical background and calculation of energy loss

Mechanical energy is the ability to transport a mass (i.e. blood) over a certain distance and, in the human circulation, consists of three forms: 1) pressure potential energy, which is expressed by the static pressure (e.g. the pressure measured during catheterization), 2) kinetic energy, which is the energy of a mass ( $m$ ) moving with a certain velocity ( $v$ ) and is expressed by the dynamic pressure, and 3) gravitational potential energy (hydrostatic pressure), which is the energy of a mass compared with another mass within a gravitational field, i.e. a blood particle in the superior vena cava (SVC) contains more gravitational energy than a blood particle in the IVC in upright position.<sup>1, 2</sup>

As derived from the principle of conservation of energy, Bernoulli's equation (Eq A.1) states that in an idealized, steady flow with no frictional forces, the energy entering a blood vessel equals the energy exiting a blood vessel. For example, when considering a blood pressure drop, this pressure (static pressure) drop must be accompanied by an increase in dynamic pressure (kinetic energy) or gravitational energy of equal amount.

$$\frac{1}{2}\rho v_1^2 + \rho gh_1 + P_1 = \frac{1}{2}\rho v_2^2 + \rho gh_2 + P_2 \quad (\text{Eq A.1})$$

where  $\frac{1}{2}\rho v^2$  = kinetic energy (dynamic pressure),  $\rho gh$  = gravitational energy (hydrostatic pressure) and  $P$  = pressure energy (static pressure).  $\rho$  = density,  $v$  = velocity,  $h$  = height and  $g$  = gravitational acceleration

Because the change in gravitational energy is considered negligible, its contribution is often ignored leading to the simplified Bernoulli equation (Eq A.2). Whether this is a valid assumption or not in the calculation of energy loss in the TCPC has been questioned<sup>3</sup>.

$$\frac{1}{2}\rho v_1^2 + P_1 = \frac{1}{2}\rho v_2^2 + P_2 \quad (\text{Eq A.2})$$

However, blood flow in the human circulation is non-idealized and mechanical energy can be irreversibly converted to thermal energy through viscous forces, a form of energy dissipation. Because of its irreversibility, this energy is lost.<sup>1</sup> If you consider a simplified example of a car engine, chemical energy (i.e. gasoline) is converted into heat (thermal energy), engine-sound (acoustic energy) and the desired movement of the car (kinetic energy). As the thermal and acoustic energy, which are formed because of frictional forces, cannot be converted back to useful energy, this energy is considered dissipated. The less energy is dissipated, the more efficient the system works.

Since an 'inviscid' fluid does not exist, it is important to realize that the Bernoulli equation is only valid in situations where the viscous (decelerating) forces are considered minimal

and therefore negligible compared with the inertial (accelerating) forces. This means that the Bernoulli equation is not valid in situations where this is not the case, such as long segments of narrow arteries, areas of turbulence or areas of flow separation (which are all associated with relevant viscous forces).

The amount of energy lost can be calculated according to the simplified control volume approach (Eq A.3) <sup>4</sup>, which states that energy loss is the difference between energy input and energy output over a specified volume:

$$\dot{E}_{\text{loss}} = \sum(P_{\text{total inlet}})Q_{\text{inlet}} - \sum(P_{\text{total outlet}})Q_{\text{outlet}}, \quad (\text{Eq A.3})$$

where  $P_{\text{total}} \cong P_{\text{static}} + \frac{1}{2}\rho v^2$ , with the inlet being IVC and SVC and the outlet being the right (RPA) and left pulmonary artery (LPA) and  $v = Q/A$ , with  $Q$ =blood flow and  $A$ =surface area.

This method is mostly being used in *in-vitro* experiments, as it only requires total pressure and velocity values at inlet and outlet sections.

The theoretical control volume approach (Eq A.4) <sup>4</sup> is commonly used in CFD studies, as it requires detailed velocity and pressure data over the entire inlet or outlet section, something that is only possible via CFD and not *in-vivo* or *in-vitro*.

$$\dot{E}_{\text{loss}} = - \int_{CS} [P_{\text{static}} + \frac{1}{2}\rho v_k v_k] v_i n_i dS \quad (\text{Eq A.4})$$

where  $CS$  is the control surface,  $v_i$  represent the components of the velocity vector,  $n_i$  represents the components of the outward surface normal vector of the control surfaces and  $dS$  is the differential surface area element on the control surface.

Calculating energy loss *in-vivo* with the simplified control volume approach (Eq A.3) would require invasive catheterization, as it requires both pressure and velocity data. Therefore, the viscous dissipation method has been developed <sup>5</sup> and successfully applied in the TCPC. <sup>4,6-9</sup> This method is based on the assumption that in laminar, Newtonian blood flow, all lost energy is the result from frictional (viscous) forces. These viscous forces, caused by fluid viscosity and the no-slip condition<sup>1</sup> (i.e blood immediately adjacent to the vessel wall is not flowing), irreversibly convert the kinetic energy of the blood flow to thermal energy. This loss can be calculated by using the viscous dissipation function ( $\phi_v$ ) in the Navier-Stokes energy equations (Eq A.5), a quantity that depends on the fluid viscosity and elements of the strain rate tensor.<sup>2, 10</sup> In other words, this function only uses velocity based gradients and does not require pressure data, which makes it very suitable for calculations of energy loss non-invasively obtained *in-vivo* with 4D MRI.<sup>8,9,11</sup>

$$\phi_v = 2 \left[ \left( \frac{\partial v_x}{\partial x} \right)^2 + \left( \frac{\partial v_y}{\partial y} \right)^2 + \left( \frac{\partial v_z}{\partial z} \right)^2 \right] + \left[ \frac{\partial v_y}{\partial x} + \frac{\partial v_x}{\partial y} \right]^2 + \left[ \frac{\partial v_z}{\partial y} + \frac{\partial v_y}{\partial z} \right]^2 + \left[ \frac{\partial v_x}{\partial z} + \frac{\partial v_z}{\partial x} \right]^2 - \frac{2}{3} \left[ \frac{\partial v_x}{\partial x} + \frac{\partial v_y}{\partial y} + \frac{\partial v_z}{\partial z} \right]^2 \quad (\text{Eq A.5})$$

where  $v_x$ ,  $v_y$  and  $v_z$  represent the three spatial velocity components of the volume element.

This formula calculates the velocity gradients between all the adjacent volume elements. A summation of these viscous dissipation values per volume element over the entire control volume provides the total viscous dissipation (energy loss (Watt), Eq 6) via:

$$\dot{E}_{\text{loss}} = \mu \sum_{i=1}^{\text{Number of voxels}} \phi_v V_i, \quad (\text{Eq A.6})$$

where  $\mu$  is the dynamic viscosity and  $V_i$  is the volume of each volume element (voxel).<sup>8</sup>

These three methods have been shown to have good agreement with each other, i.e. the trend in energy loss for a TCPC for different flow conditions or geometries is the same for these three methods, although absolute values will differ. The simplified control volume approach generally overestimates energy loss and the viscous dissipation method generally underestimates absolute energy loss, compared with the theoretical control volume approach as a reference.<sup>4, 6</sup>

Recently, Wei et al showed that the viscous dissipation method is theoretically the best and most accurate way to calculate energy loss in the TCPC and is recommended as the preferred hemodynamic parameter, because of a lack of limiting assumptions when compared with the simplified control volume method.<sup>12</sup>

As the dissipation method is completely based on velocity gradients, spatial resolution is of utmost importance and is generally the limiting factor in MRI derived velocity fields. Although this has a significant effect on absolute energy loss values, the relative performance of the TCPC between subjects remains intact, which makes comparing TCPC efficiency between patients who are scanned with the same resolution possible.<sup>8, 9</sup>

## Appendix B: Comparing energy loss

As energy loss in the TCPC is highly flow dependent<sup>13</sup>, it is not useful to compare absolute energy loss between patients with different flow characteristics. To put energy loss between patients in the context of pulmonary (PVR) and systemic vascular resistance (SVR), the resistance and resistance index<sup>14</sup> are two parameters which can be calculated via the obtained energy loss:

$$\Delta P_{\text{TCPC}} = \frac{\dot{E}_{\text{loss}}}{\text{CO}}, \quad (\text{Eq B.1})$$

where  $\Delta P_{\text{TCPC}}$  (head loss) is the energy loss based pressure drop over the TCPC and cardiac output (CO) equals  $Q_{\text{IVC}} + Q_{\text{SVC}}$ . Note, pressure drop is not equivalent to the difference in static pressure between inlet and outlet sections, as previously mentioned, but also incorporates the dynamic pressure (kinetic energy).

$$\text{Resistance} = \frac{\Delta P_{\text{TCPC}}}{\text{CO}} \quad (\text{Eq B.2})$$

$$\text{Resistance index} = \frac{\Delta P_{\text{TCPC}}}{\text{CI}}, \quad (\text{Eq B.3})$$

where CI=cardiac index in L/min/m<sup>2</sup>. Resistance is generally measured by cardiologists in Woods units (WU):  $1 \frac{\text{mmHg.L}}{\text{min}}$ .

Another parameter used to compare energy loss between patients is the indexed power loss (iPL), developed by Dasi et al. in 2008<sup>15</sup>, which is a flow and BSA independent parameter.

$$\text{iPL} = \frac{PL}{\rho Q^3 / \text{BSA}^2} \quad (\text{Eq B.4})$$

## Appendix C: Laminar versus turbulent flow

In the normal human circulation, blood flow is laminar. However, in pathological conditions, turbulent flow can occur and is characterized by random spatial and temporal alterations in the direction and magnitude of blood flow velocity and is a source of major energy loss.<sup>1</sup>

The Reynolds number, the ratio between inertial and viscous forces, can be calculated to determine if blood flow is in the laminar or turbulent regime via:

$$\text{Reynolds number} = \frac{\rho U D}{\mu}, \quad (\text{Eq C.1})$$

where  $\rho$  is the blood density,  $U$  is the mean velocity,  $D$  is the hydraulic diameter and  $\mu$  is the dynamic viscosity. Reynolds numbers <2300 are considered laminar. In the ECC and LT Fontan circulation, Reynolds numbers have been reported to be well within the laminar flow regime during rest and exercise.<sup>16</sup> However, blood flow in the transitional turbulent regime has also been described in a patient with an intra-atrial 'pouch-like' connection.<sup>17</sup> As can be derived from Equation C.1, turbulent flow is more likely to occur in Fontan connections with increased velocities or diameters.

## References

1. Akins CW, Travis B and Yoganathan AP. Energy loss for evaluating heart valve performance. *J Thorac Cardiovasc Surg.* 2008;136:820-833.
2. Bird RB. *Transport phenomena*. New York,: Wiley; 1960.
3. Grigioni M, D'Avenio G, Amodeo A and Di Donato RM. Power dissipation associated with surgical operations' hemodynamics: critical issues and application to the total cavopulmonary connection. *J Biomech.* 2006;39:1583-1594.
4. Ryu K, Healy TM, Ensley AE, Sharma S, Lucas C and Yoganathan AP. Importance of accurate geometry in the study of the total cavopulmonary connection: computational simulations and in vitro experiments. *Ann Biomed Eng.* 2001;29:844-853.
5. Healy TM, Lucas C and Yoganathan AP. Noninvasive fluid dynamic power loss assessments for total cavopulmonary connections using the viscous dissipation function: a feasibility study. *J Biomech Eng.* 2001;123:317-324.
6. Liu Y, Pekkan K, Jones SC and Yoganathan AP. The effects of different mesh generation methods on computational fluid dynamic analysis and power loss assessment in total cavopulmonary connection. *J Biomech Eng.* 2004;126:594-603.
7. Soerensen DD, Pekkan K, Sundareswaran KS and Yoganathan AP. New power loss optimized Fontan connection evaluated by calculation of power loss using high resolution PC-MRI and CFD. *Conf Proc IEEE Eng Med Biol Soc.* 2004;2:1144-1147.
8. Venkatachari AK, Halliburton SS, Setser RM, White RD and Chatzimavroudis GP. Noninvasive quantification of fluid mechanical energy losses in the total cavopulmonary connection with magnetic resonance phase velocity mapping. *Magn Reson Imaging.* 2007;25:101-109.
9. Cibis M, Jarvis K, Markl M, Rose M, Rigsby C, Barker AJ and Wentzel JJ. The effect of resolution on viscous dissipation measured with 4D flow MRI in patients with Fontan circulation: Evaluation using computational fluid dynamics. *J Biomech.* 2015;48:2984-2989.
10. Currie IG. *Fundamental mechanics of fluids*. 4th ed. Boca Raton, FL: Taylor & Francis; 2013.
11. Barker AJ, van Ooij P, Bandi K, Garcia J, Albaghdadi M, McCarthy P, Bonow RO, Carr J, Collins J, Malaisrie SC and Markl M. Viscous energy loss in the presence of abnormal aortic flow. *Magn Reson Med.* 2014;72:620-628.
12. Wei ZA, Tree M, Trusty PM, Wu W, Singh-Gryzbon S and Yoganathan A. The Advantages of Viscous Dissipation Rate over Simplified Power Loss as a Fontan Hemodynamic Metric. *Ann Biomed Eng.* 2018;46:404-416.
13. Whitehead KK, Pekkan K, Kitajima HD, Paridon SM, Yoganathan AP and Fogel MA. Nonlinear power loss during exercise in single-ventricle patients after the Fontan: insights from computational fluid dynamics. *Circulation.* 2007;116:165-171.
14. Sundareswaran KS, Pekkan K, Dasi LP, Whitehead K, Sharma S, Kanter KR, Fogel MA and Yoganathan AP. The total cavopulmonary connection resistance: a significant impact on single ventricle hemodynamics at rest and exercise. *Am J Physiol Heart Circ Physiol.* 2008;295:H2427-2435.
15. Dasi LP, Pekkan K, Kitajima HD and Yoganathan AP. Functional analysis of Fontan energy dissipation. *J Biomech.* 2008;41:2246-2252.
16. Bossers SS, Cibis M, Gijzen FJ, Schokking M, Strengers JL, Verhaart RF, Moelker A, Wentzel JJ and Helbing WA. Computational fluid dynamics in Fontan patients to evaluate power loss during simulated exercise. *Heart.* 2014;100:696-701.

17. Pekkan K, de Zelicourt D, Ge L, Sotiropoulos F, Frakes D, Fogel MA and Yoganathan AP. Physics-driven CFD modeling of complex anatomical cardiovascular flows-a TCPC case study. *Ann Biomed Eng.* 2005;33:284-300.



# 10

CHAPTER 10

# Non-uniform mixing of hepatic venous flow and inferior vena cava flow in the Fontan conduit

Rijnberg FM, van der Woude SFS, van Assen HC, Juffermans JF, Hazekamp MG, Jongbloed MRM, Kenjeres S, Lamb HJ, Westenberg JJM, Wentzel JJ, Roest AAW

# Abstract

## Background

Fontan patients require a balanced hepatic blood flow distribution (HFD) to prevent pulmonary arteriovenous malformations. Currently, HFD is quantified by tracking Fontan conduit flow, assuming hepatic venous (HV) flow to be uniformly distributed within the Fontan conduit. However, this assumption may be invalid leading to inaccuracies in HFD quantification with potential clinical impact. The aim of this study was to 1) assess mixing of HV flow and inferior vena caval (IVC) flow within the Fontan conduit and 2) quantify HFD by directly tracking HV flow and quantitatively compare results with the conventional approach.

## Methods

Patient-specific, time-resolved computational fluid dynamic models of 15 total cavopulmonary connections (TCPC) were generated, including the hepatic veins (HV) and subhepatic IVC. Mixing of HV and IVC flow, on a scale between 0 (no mixing) and 1 (perfect mixing), was assessed at the caudal and cranial Fontan conduit. HFD was quantified by tracking particles from the caudal ( $HFD_{\text{caudal conduit}}$ ) and cranial ( $HFD_{\text{cranial conduit}}$ ) conduit and from the hepatic veins ( $HFD_{\text{HV}}$ ).

## Results

HV flow was non-uniformly distributed at both the caudal (mean mixing  $0.66 \pm 0.13$ ) and cranial (mean  $0.79 \pm 0.11$ ) level within the Fontan conduit. On a cohort-level, differences in HFD between methods were significant but small;  $HFD_{\text{HV}}$  ( $51.0 \pm 20.6\%$ ) versus  $HFD_{\text{caudal conduit}}$  ( $48.2 \pm 21.9\%$ ,  $p=0.033$ ) or  $HFD_{\text{cranial conduit}}$  ( $48.0 \pm 21.9\%$ ,  $p=0.044$ ). However, individual absolute differences of 8.2-14.9% in HFD were observed in 4/15 patients.

## Conclusion

HV flow is non-uniformly distributed within the Fontan conduit. Substantial individual inaccuracies in HFD quantification were observed in a subset of patients with potential clinical impact.

## Introduction

The Fontan operation is the palliative procedure for single ventricle patients, in which both venae cavae are connected with the pulmonary arteries (PAs), also called the total cavopulmonary connection (TCPC). The TCPC needs to ensure a balanced hepatic venous flow distribution (HFD), containing an important hepatic factor, towards both lungs<sup>1</sup>. A lack of hepatic factor has been associated with the formation of pulmonary arteriovenous malformations in the affected lung, leading to progressive hypoxemia, cyanosis and exercise intolerance<sup>2</sup>.

In recent years, patient-specific platforms using a combination of computational fluid dynamics (CFD) and magnetic resonance imaging (MRI) are emerging as a valuable tool for clinicians for evaluating HFD and power loss<sup>3,4</sup>. In addition, these platforms allow for performing “virtual surgery”, by which multiple different TCPC geometries can be virtually created and associated blood flow can be predicted. Subsequently, the optimal TCPC geometry with minimal power loss and a balanced HFD can be determined guiding surgical and catheter-based interventions<sup>5,6</sup>.

HFD can be determined with particle tracing techniques using 4D flow MRI<sup>7-11</sup> or computational fluid dynamic models (CFD)<sup>12</sup>. Conventional HFD quantification methods track particles that are uniformly seeded within the Fontan conduit and determine the distribution of these particles towards both PAs. Therefore, this method relies on the unvalidated assumption that hepatic blood is uniformly distributed within the Fontan conduit<sup>13, 14</sup>. However, since blood flow is laminar in the inferior vena cava (IVC) and Fontan conduit, the mixing of hepatic blood with IVC blood might be less optimal than generally assumed. We hypothesized that there is a non-uniform distribution of hepatic venous flow in the Fontan conduit that affects the accuracy of the current HFD quantification approach. These inaccuracies have potential consequences for identification of patients with unbalanced HFD, or by affecting optimal TCPC model selection in virtual surgery platforms. The aim of this study was twofold: 1) to test the hypothesis of non-uniform hepatic blood distribution within the Fontan conduit by quantification of mixing between IVC and hepatic venous flow within the Fontan conduit, and 2) to quantify HFD from the level of the Fontan conduit (conventional method), as well as from the level of the hepatic veins (HVs, direct method).

## Methods

### Patient population

Fifteen Fontan patients were included that underwent MRI as part of a prospective study between November 2018-May 2019 at the Leiden University Medical Center. All patients >8 years old without contraindications for MRI were eligible for inclusion. Patient characteristics are provided in Table 1. The study was approved by the institutional review board of the hospital. Informed consent was obtained from all subjects and/or their guardians.

### Magnetic resonance imaging

MRI acquisitions details are provided in Supplementary Table 1. Transversal and sagittal stacks of static, respiratory-compensated 2D anatomic images were acquired for segmentation of the TCPC. Free-breathing, two-dimensional phase-contrast MRI (2D PC-MRI) with three-directional velocity encoding was acquired at the following locations: subhepatic IVC, Fontan conduit, superior vena cava (SVC), right (RPA) and left PAs (LPA). In this study, flow was quantified using the (clinically standard) through-plane velocity direction only (CAAS MR Solutions v5.1, Pie Medical Imaging, Maastricht, the Netherlands). Total hepatic venous flow was determined by subtracting IVC flow from Fontan conduit flow.

### 3D TCPC model creation

A detailed description of the TCPC segmentation and CFD analysis are provided in Supplementary Material 1. The TCPC was segmented using both sagittal and transversal stacks, covering the area between the subhepatic IVC, hepatic veins, SVC, RPA and LPA (ITK-SNAP<sup>15</sup>). Segmental branches were excluded, except for the right upper lobe branches. A 3D TCPC model was created, smoothed and centerlines were derived for each vessel (VMTK<sup>16</sup>).

### CFD simulations

All inlets and outlets of the 3D TCPC model were clipped perpendicular to the centerlines. Furthermore, vessel extensions were added to the entrances and exits of the model. Using these vessel extensions, the inflow velocity profiles at the entrances of the 3D TCPC model were fully developed and resembled the velocity profiles at those locations. After adding vessel extensions at all in- and outlets, the 3D TCPC models were meshed with 30 polyhedral elements across the average vessel diameter (range 0.4-0.5mm elements) in order to achieve mesh-independent results (ANSYS ICEM v17.1, Inc., Canonsburg, PA)<sup>17</sup>. All CFD simulations were performed using commercially available Fluent software (v17.1, ANSYS, Inc., Canonsburg, PA).

Time-resolved flowrates were prescribed with a parabolic velocity profile at the inlets. Total hepatic venous flow was divided over the multiple hepatic veins based on the ratio of their respective cross-sectional areas. Outlet boundary conditions were imposed based on the ratio of measured pulmonary flow distribution (RPA/LPA flow divided by the total PA flow)<sup>3</sup>. A rigid vessel wall was assumed and a no-slip condition prescribed. Blood flow was assumed to be laminar. A Carreau model was used to account for the non-Newtonian blood properties in the TCPC<sup>18</sup>.

### Quantification of mixing between IVC and Hepatic blood flow

A method to quantify mixing of hepatic and IVC blood flow within the Fontan conduit was developed based on the spatial distribution of both flows within the Fontan conduit using particle tracing (Paraview.org). A total of 7500 particles were released from the hepatic veins for each time-step during 5 cardiac cycles. The number of particles per hepatic vein was based on the ratio of their respective cross-sectional areas. The amount of particles released from the subhepatic IVC was based on the average flow ratio between the IVC and hepatic veins;  $7500 \times \frac{Q_{IVC}}{Q_{HV}}$ .

Particles were released from the HVs and IVC for each time-step during 5 cardiac cycles.

Pathlines, representing the trajectory each particle follows over time, were generated and transections with these pathlines were made at two cross-sections with the Fontan conduit: the caudal part of the Fontan conduit, just above the connection between the Fontan conduit with the IVC/HVs, and at the cranial part of the Fontan conduit, just below the connection with the PA (Figure 1A-C, Video 1). The ratio of IVC and HV pathline transections at each cross-section of the Fontan conduit were recorded for each time-step in the 5<sup>th</sup> cardiac cycle.

Subsequently, both caudal and cranial Fontan conduit cross-sections were manually subdivided in a right-left and anterior-posterior direction, resulting in four subsections: left-anterior, left-posterior, right-anterior and right-posterior (Figure 1B-C). The ratio of IVC and HV pathline transections was determined in each of the four subsections. Next, mixing (M) in each of the four subsections was determined for each time-phase of the cardiac cycle by comparing the ratios of IVC and HV pathline transections within the entire cross-section with the ratios of IVC and HV pathline transections within each of the four subsections, ranging from 0 (no mixing) to 1 (perfect mixing). A mixing of 0 indicates no mixing (only HV or IVC pathlines present in the subsection) and 1 indicates perfect mixing (the exact same ratio of HV and IVC pathlines in the subsection as in the entire cross-section). Furthermore, cardiac-cycle averaged mixing ( $M_{\text{average}}$ ) was determined for each subsection and for the entire cross-section. A detailed description of the mixing quantification method is provided in Supplementary material 2.

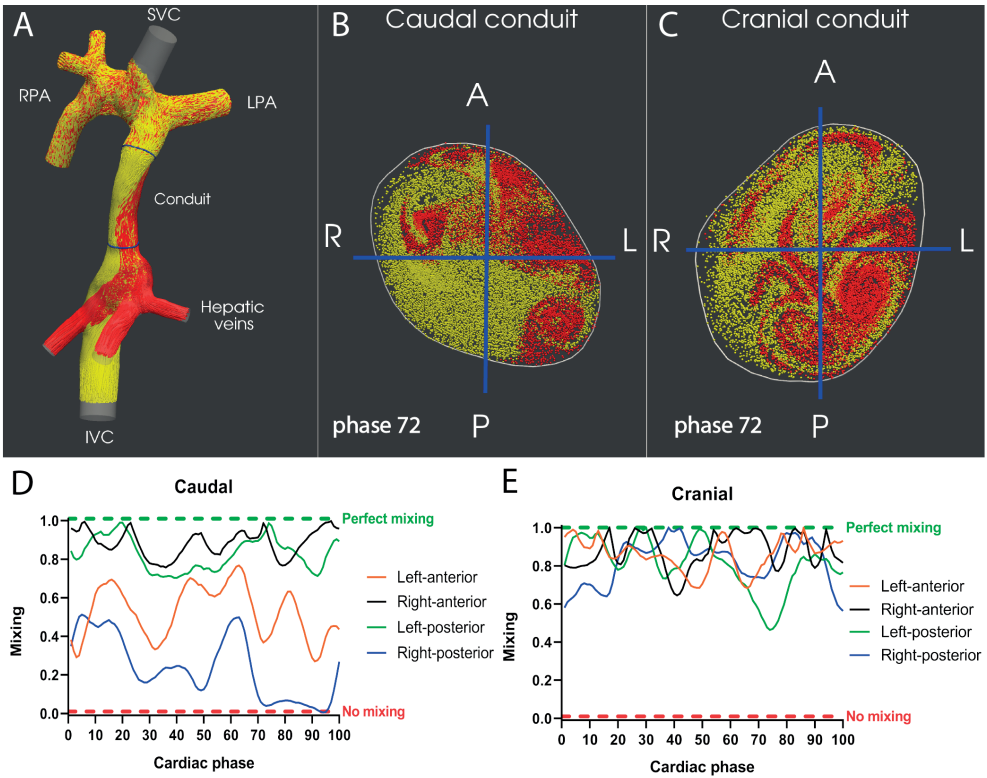


**Figure 1.** (A) Pathlines originating from the hepatic veins (HV, red) and inferior vena cava (IVC, yellow) are shown within the TCPC of a typical extracardiac conduit Fontan patient. Positions of the caudal and cranial cross-sections with the Fontan conduit are shown (blue). Of note, no pathlines were generated from the superior vena cava to allow for better visualization of the HV and IVC flow. (B-C) Transections with HV and IVC pathlines are shown for the caudal (B) and cranial (C) cross-sections for phase 72/100 of the cardiac cycle. The division into four subsections is indicated by blue lines. Note how a evidently non-uniform distribution of HV flow is present, most strikingly at the caudal part of the conduit, with almost no HV flow present in the right-posterior subsection. (D-E) Time-resolved mixing characteristics of HV and IVC flows are shown for the caudal and cranial cross-section of the conduit. At the caudal conduit, a relatively good mixing is present in the right-anterior and left-posterior subsections, with reduced mixing in the left-anterior and right-posterior segments. Note how almost no mixing is present at phase 72 in the right-posterior segment, consistent with the absence of HV flow in this subsection (B). (E) Significantly better mixing is present at the cranial part of the conduit, illustrated by a more uniform distribution of IVC and HV flow streams over the cross-section.

SVC/IVC; superior/inferior vena cava, LPA/RPA; left/right pulmonary artery, A; anterior, P; posterior, L/R; left/right

## HFD quantification

HFD was quantified using particle tracing<sup>7,13,19</sup>, by seeding 7500 particles from either the HVs (HFD<sub>HV</sub>: direct method) or from the level of one of the 2 cross-sections (HFD<sub>caudal conduit</sub> and HFD<sub>cranial conduit</sub>: conventional method, Figure 2). The 7500 particles were divided over the hepatic veins based on the ratio of their respective areas. Particles were released

for 100 time-steps (1 cardiac cycle) and particles arriving at the PAs were recorded for 500-1200 timesteps (5-12 cardiac cycles) to allow for sufficient transit time for particles to reach the PAs. HFD is defined as the ratio of particles exiting through the LPA with respect to the total number of particles reaching either PA<sup>13</sup>:

$$\text{HFD} = \frac{P_{\text{LPA}}}{P_{\text{RPA}} + P_{\text{LPA}}} * 100\%$$
, where P is the number of particles arriving in each PA, respectively.

## Statistical analysis

Mixing (M) of HV flow in the Fontan conduit was defined as follows: no mixing <0.1, poor mixing 0.1-0.3, mild mixing 0.3-0.5, moderate mixing 0.5-0.7, good mixing 0.7-0.9, uniform mixing >0.9. Bland-Altman plots and intraclass correlation (ICC) analysis were used to assess agreement between HFD methods. The mean absolute difference ( $\pm 1.96$  standard error of the mean) between methods was quantified to determine the absolute amount of which one HFD quantification method over- or underestimates the other method. All differences were reported in percentage points. Measurements were compared using a paired t-test.  $M_{\text{average}}$  between subsections was compared using a repeated measurements one-way ANOVA test with post-hoc analysis (Tukey). A p-value <0.05 was considered statistically significant. Continuous data were presented as mean $\pm$ SD. Data were analyzed with SPSS 25.0 and Prism 8.0.

## Results

Patient characteristics and MRI flow measurements are presented in Table 1.

### Mixing of IVC and HV flow

An evident streaming pattern of HV flow within the Fontan conduit was present resulting in non-uniform distribution of HV flow within the Fontan conduit, most evidently shown in the caudal part of the Fontan conduit (Figure 1A-B, Supplemental Video 1). This observation was also reflected by a significant lower cardiac-cycle averaged mixing ( $M_{\text{average}}$ ) in the caudal (moderate mixing, mean  $0.66 \pm 0.13$ ) compared to the cranial part of the Fontan conduit (good mixing, mean  $0.79 \pm 0.11$ ,  $p < 0.001$ ).  $M_{\text{average}}$  over the entire cross-section at both the caudal and cranial level of the Fontan conduit were significantly different from 0.9 (i.e. uniform mixing),  $p < 0.001$  and  $p = 0.012$ , respectively. The mixing of HV and IVC blood flows within the caudal and cranial part of the Fontan conduit for a typical extracardiac conduit Fontan patient is shown in Figure 1 and Video 1. The time-resolved mixing between HV and IVC flow in the four subsections at two different levels of the Fontan conduit is shown for a typical extracardiac Fontan patient (Figure 1D-E).



**Table 1.** Patient characteristics

Male/Female	9/6
BSA, m <sup>2</sup>	1.6 (0.2)
Age at MRI, years	18.2 (5.6)
Fontan type (ECC/LT)	14/1
Conduit size (16/18/20 millimeter)	9/4/1
Q <sub>IVC</sub> , L/min	3.0 (0.7)
Q <sub>HV</sub> , L/min	1.5 (0.6)
Contribution of Q <sub>HV</sub> to Q <sub>conduit</sub> (%)	32.7 (9.3)

Values are reported as mean (standard deviation). BSA; body surface area (Haycock), MRI; magnetic resonance imaging, ECC; extracardiac conduit, LT; lateral tunnel, Q; flowrate, IVC; inferior vena cava, HV; hepatic veins. L/min; liter per minute

When comparing  $M_{\text{average}}$  at the four subsections in the caudal cross-section,  $M_{\text{average}}$  at the right-posterior subsection was lowest, significantly lower compared to the right-anterior subsection ( $0.47 \pm 0.34$  vs  $0.76 \pm 0.20$ , respectively,  $p=0.03$ ). No significant differences between other caudal subsections (left-posterior  $0.68 \pm 0.29$ , left-anterior  $0.65 \pm 0.24$ ) were observed.  $M_{\text{average}}$  was significantly different from 0.9 (i.e. uniform mixing) for all caudal subsections (all  $p$ -values  $<0.025$ ). At the cranial level, no significant differences in  $M_{\text{average}}$  were found between the four subsections: right-anterior ( $0.85 \pm 0.13$ ), left-anterior ( $0.80 \pm 0.18$ ), right-posterior ( $0.75 \pm 0.23$ ) or left-posterior ( $0.73 \pm 0.19$ ).  $M_{\text{average}}$  was significantly different from 0.9 in the right and left posterior subsections ( $p=0.02$  and  $P=0.004$ , respectively), indicating non-uniform mixing in these segments, but not in the right and left anterior subsections ( $p=0.2$  and  $p=0.06$ , respectively).

## HFD analysis

The result of the HFD analysis and comparison between the three methods are presented in Table 2 and Figure 3. No significant differences were found between  $\text{HFD}_{\text{caudal conduit}}$  and  $\text{HFD}_{\text{cranial conduit}}$  ( $p=0.80$ ). However, when comparing the direct  $\text{HFD}_{\text{HV}}$  method with the conventional methods, significant differences were observed:  $\text{HFD}_{\text{HV}}$  ( $51.0 \pm 20.6\%$ ) versus  $\text{HFD}_{\text{caudal conduit}}$  ( $p=0.033$ ) as well as  $\text{HFD}_{\text{HV}}$  versus  $\text{HFD}_{\text{cranial conduit}}$  ( $p=0.044$ ). Although statistically significant, differences between the conventional and direct HFD quantification methods were relatively small, with differences  $<5\%$  in 8/15 and 11/15 using the  $\text{HFD}_{\text{caudal conduit}}$  and  $\text{HFD}_{\text{cranial conduit}}$  methods, respectively. However, in individual subjects differences as high as 8.2-14.9% were observed in 4/15 patients.

No significant correlation was found for the absolute difference in HFD between the direct and both conventional methods and  $M_{\text{average}}$  at the caudal or cranial conduit, respectively ( $r=0.32$ ,  $p=0.27$  and  $r=-0.06$ ,  $p=0.82$ , respectively). The 4 patients with highest absolute differences between methods did not have a significantly different HV to IVC flow ratio (mean ratio 0.50 vs 0.54,  $p=0.41$ ), pulsatility ( $(Q_{\text{max}} - Q_{\text{min}})/Q_{\text{mean}}$ , where  $Q$

is the flowrate ) of the IVC (mean 0.40 vs 0.41,  $P=0.66$ ) and conduit (mean 0.66 vs 0.53,  $p=0.41$ ) or HV to conduit percentage (mean 32% vs 35%,  $p=0.75$ ) compared to the 11 patients with smallest differences.

**Table 2.** Comparisons between HFD quantification methods

Comparisons	Paired t-test	Bland-Altman		Intraclass Correlation	Mean absolute difference
	P value	Mean difference	LoA	ICC	( $\pm 1.96$ SEM)
HFD <sub>HV</sub> vs HFD <sub>caudal tunnel</sub>	<b>0.033</b>	2.9	-6.3–12.0	0.97	4.6(3.1-6.0)
HFD <sub>HV</sub> vs HFD <sub>cranial tunnel</sub>	<b>0.044</b>	3.1	-7.4–13.6	0.96	4.4(2.2-6.5)
HFD <sub>caudal tunnel</sub> vs HFD <sub>cranial tunnel</sub>	0.80	0.2	-6.0–6.4	0.99	2.4(1.3-3.4)

HFD; hepatic flow distribution. SEM; standard error of the mean, LoA; limits of agreement, defined as the mean difference  $\pm 1.96$  standard deviations.

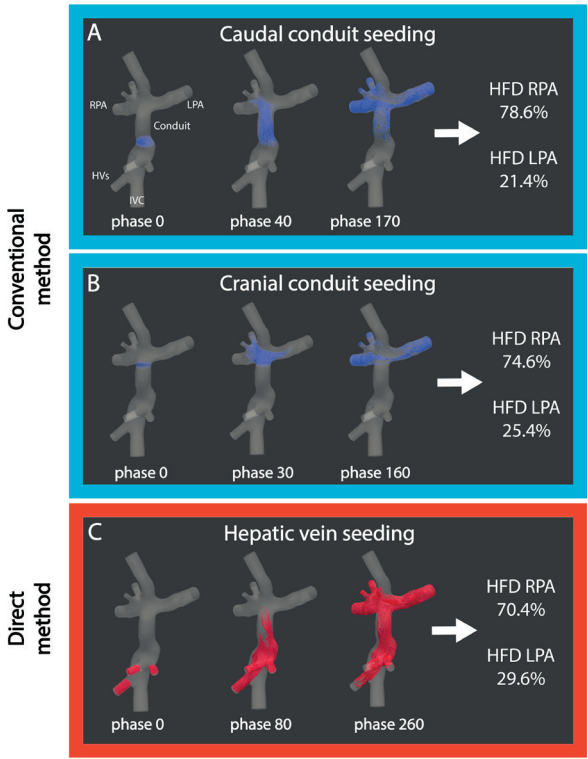


**Figure 2.** The three HFD quantification approaches are shown for a typical Fontan patient. Particles were uniformly seeded from the caudal or cranial conduit (conventional method) or directly from the hepatic veins (direct method). The starting position and the trajectory of these particles over time are shown for two cardiac phases. The percentage of particles arriving at each pulmonary artery were recorded representing the HFD.

IVC; inferior vena cava, HVs; hepatic veins, LPA/RPA; left/right pulmonary artery, HFD; hepatic flow distribution.

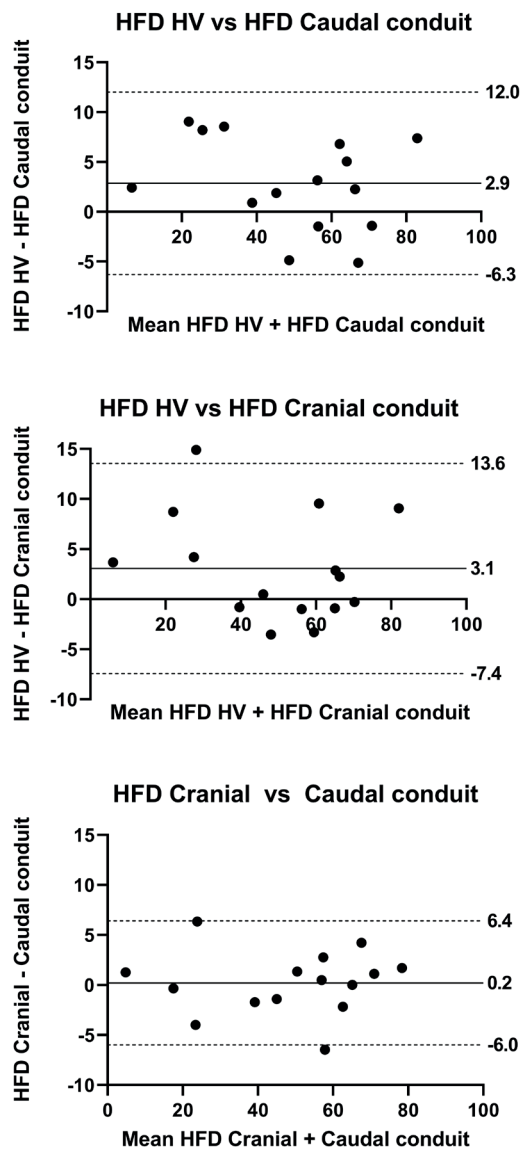


**Figure 3.** Bland-Altman plots comparing HFD measurements between the three different approaches. The mean difference + limits of agreement ( $\pm 1.96$  times the standard deviation) are shown in the plot.

## Comment

This study incorporates the hepatic veins into patient-specific CFD models of the TCPC in Fontan patients, in order to assess mixing of HV and IVC flow and to allow for HFD quantification by tracking particles directly from the HVs. Main findings show that hepatic venous flow is not uniformly distributed within the Fontan conduit. This lack of uniform distribution was most evidently present at the caudal part of the Fontan conduit (just distal of the entry of the HVs into the IVC) with significantly better mixing of HV and IVC flows at the cranial part of the conduit. Tracking particles from the caudal or cranial part of the Fontan conduit did not result in significant different HFD despite these different mixing characteristics. However, tracking particles directly from the HVs ( $HFD_{HV}$ ) was significantly different from both conventional HFD quantification methods (i.e. tracking Fontan conduit flow), although on a cohort-level differences were small. On an individual basis, however, differences of 8.2-14.9% in HFD were observed which may be of clinical importance.

HFD quantification is an important metric in the evaluation of the TCPC in Fontan patients, since there is compelling evidence for a strong association between a lack of HV flow towards the lung and the formation of pulmonary arteriovenous malformations<sup>2</sup>. Therefore, identification of an unbalanced HFD may indicate the need for intervention aiming to restore a more balanced HFD. Furthermore, when an intervention of the TCPC is considered, virtual surgery platforms offer the possibility to evaluate multiple different TCPC geometries<sup>1, 12, 20</sup>. Subsequently, the optimal geometry with minimal power loss while ensuring a balanced HFD can be selected<sup>6, 21, 22</sup>. The accuracy of the HFD quantification method itself, however, has not been studied.

The conventional approach for HFD quantification relies on the assumption that hepatic venous flow, theoretically taking up to approximately 38% of total Fontan conduit flow<sup>23</sup>, is uniformly distributed within the Fontan conduit and thus can be used interchangeably. This study showed that this assumption is not valid, most evident at the level just above the entry of the hepatic veins into the IVC. The HV flow and IVC flow demonstrate two different flow streams with only moderate mixing during the cardiac cycle. This can be explained by the fact that blood flow in the Fontan conduit is in general laminar with only minimal pulsatility along the cardiac cycle preventing thorough mixing of both flows. The right-posterior part of the caudal Fontan conduit showed lowest mixing of HV with IVC flow as the anatomy of the IVC and HVs likely resulted in less HV flow particularly in this segment. At the cranial side of the Fontan conduit, as both flows had more time to interact, significantly improved mixing was present but still non-uniform mixing was observed.

Therefore, using Fontan conduit flow as a surrogate of HV flow will introduce inaccuracies in HFD quantification. This study shows that on a cohort-level the anticipated inaccuracy is small and of minimal clinical relevance. Therefore, the fact that HV flow is not uniformly distributed in the Fontan conduit does in general not seem to make a significant difference in HFD quantification, with 95% of mean absolute differences expected to be <6.1-6.5% making previous obtained results on a cohort-level valid<sup>3, 20</sup>. Furthermore, results also indicated that when the conventional HFD quantification is used, starting position of the particles (from the caudal or cranial conduit) did not result in significantly different HFD, despite the difference in mixing characteristics.

Although differences were small on a cohort-level, it should be noted that on an individual basis, differences of 8.2-14.9% were observed in 4/15 patients which may have impact on patient-specific clinical decision making. For example, in the patient with the largest difference, HFD was only 20.7% by tracking cranial conduit flow, while HFD was 35.6% when directly tracking HV flow. Although the minimal amount of HFD to prevent the formation of pulmonary arteriovenous malformations is not clear, a minimum HFD of 30% towards a lung has been suggested to be clinical acceptable<sup>13, 22, 24</sup>. For this patient, therefore, the conventional method would imply insufficient HFD, while direct HV flow tracking shows sufficient HV flow towards the LPA. Since virtual surgery platforms are used for pre-interventional planning on an individual basis, incorporating hepatic veins into the patient-specific CFD models might have impact for at least some patients. As for the majority of patients the differences were small, it would be interesting to investigate if certain flow or geometric characteristics, which can show a wide variability at the level where the IVC and HVs join<sup>25</sup>, can help identify the patients with the largest inaccuracies that would benefit most from direct HFD quantification. Because of the limited number of patients this question could not be answered in this study. Larger numbers are needed in future studies to identify anatomical and/or flow characteristics to identify patients with important differences in direct and indirect HFD quantification.

## Limitations

Although this study reveals important, novel insights into the flow dynamics of HV and IVC flow within the Fontan conduit and its influence on HFD quantification, some limitations are present. Although the sample size is relatively small, significant differences between methods could be detected with considerable differences on a patient-specific level. Furthermore, no direct hepatic venous flow measurements were acquired which were considered clinically unfeasible, by requiring multiple extra survey scans to plan 3-6 extra 2D flow measurements in relatively small vessels. We assumed total hepatic venous flow to be distributed over the respective HVs by the ratio of their respective cross-sectional areas. Future studies should aim on obtaining direct measurements of HV flow in Fontan patients, for example using 4D flow MRI,

to further increase the accuracy of HV flow modelling in these patients. In addition, ECG-gated, free-breathing 2D PC-MRI was used as boundary conditions, which does not take respiration effects on hepatic flow into account. Previous studies have shown that hepatic venous flow can increase up to 3-fold during inspiration while having minimal effect on IVC flow<sup>23</sup>, which may influence HV streaming patterns and subsequent HFD quantification. Also, predominantly extracardiac conduit Fontan patients were included in this study, and possible different flow characteristics in lateral tunnel patients may provide different results. Furthermore, a relatively coarse assessment of mixing was performed by dividing the cross-section of the Fontan conduit in only 4 parts. Therefore, mixing on a smaller scale was not taken into account.

## Conclusion

In conclusion, hepatic venous flow is non-uniformly distributed within the Fontan conduit. Evident separate HV and IVC flow streaming patterns were present, most clearly just above entry of the HVs into the IVC. On a cohort-level, significant but small differences in HFD were observed when comparing direct (tracking hepatic venous flow) and conventional methods (tracking Fontan conduit flow). However, individual differences of 8.2-14.9% in HFD were observed in a subset of patients which may be of clinical importance by affecting accurate identification of patients with unbalanced HFD or by affecting optimal TCPC geometry selection when using virtual surgery platforms.

## References

1. Rijnberg FM, Hazekamp MG, Wentzel JJ, de Koning PJH, Westenberg JJM, Jongbloed MRM, Blom NA, Roest AAW. Energetics of Blood Flow in Cardiovascular Disease: Concept and Clinical Implications of Adverse Energetics in Patients With a Fontan Circulation. *Circulation* 2018;137(22):2393-2407.
2. Kavarana MN, Jones JA, Stroud RE, Bradley SM, Ikonomidis JS, Mukherjee R. Pulmonary arteriovenous malformations after the superior cavopulmonary shunt: mechanisms and clinical implications. *Expert Rev Cardiovasc Ther* 2014;12(6):703-13.
3. Haggerty CM, Restrepo M, Tang E, de Zelicourt DA, Sundareswaran KS, Mirabella L, Bethel J, Whitehead KK, Fogel MA, Yoganathan AP. Fontan hemodynamics from 100 patient-specific cardiac magnetic resonance studies: a computational fluid dynamics analysis. *J Thorac Cardiovasc Surg* 2014;148(4):1481-9.
4. Yang W, Chan FP, Reddy VM, Marsden AL, Feinstein JA. Flow simulations and validation for the first cohort of patients undergoing the Y-graft Fontan procedure. *J Thorac Cardiovasc Surg* 2015;149(1):247-55.
5. de Zelicourt DA, Marsden A, Fogel MA, Yoganathan AP. Imaging and patient-specific simulations for the Fontan surgery: current methodologies and clinical applications. *Prog Pediatr Cardiol* 2010;30(1-2):31-44.
6. Trusty PM, Slesnick TC, Wei ZA, Rossignac J, Kanter KR, Fogel MA, Yoganathan AP. Fontan Surgical Planning: Previous Accomplishments, Current Challenges, and Future Directions. *J Cardiovasc Transl Res* 2018;11(2):133-144.
7. Bachler P, Valverde I, Pinochet N, Nordmeyer S, Kuehne T, Crelier G, Tejos C, Irarrazaval P, Beerbaum P, Uribe S. Caval blood flow distribution in patients with Fontan circulation: quantification by using particle traces from 4D flow MR imaging. *Radiology* 2013;267(1):67-75.
8. Jarvis K, Schnell S, Barker AJ, Garcia J, Lorenz R, Rose M, Chowdhary V, Carr J, Robinson JD, Rigsby CK, Markl M. Evaluation of blood flow distribution asymmetry and vascular geometry in patients with Fontan circulation using 4-D flow MRI. *Pediatr Radiol* 2016;46(11):1507-19.
9. Bastkowski R, Bindermann R, Brockmeier K, Weiss K, Maintz D, Giese D. Respiration Dependency of Caval Blood Flow in Patients with Fontan Circulation: Quantification Using 5D Flow MRI. *Radiology: Cardiothoracic Imaging* 2019;1(4):e190005.
10. Rutkowski D, Medero R, Ruesink T, Roldan-Alzate A. Modeling Physiological Flow Variation in Fontan Models with 4d Flow Mri, Particle Image Velocimetry, and Arterial Spin Labeling. *J Biomech Eng* 2019.
11. Rutkowski DR, Barton G, Francois CJ, Bartlett HL, Anagnostopoulos PV, Roldan-Alzate A. Analysis of cavopulmonary and cardiac flow characteristics in fontan Patients: Comparison with healthy volunteers. *J Magn Reson Imaging* 2019;49(6):1786-1799.
12. Dasi LP, Whitehead K, Pekkan K, de Zelicourt D, Sundareswaran K, Kanter K, Fogel MA, Yoganathan AP. Pulmonary hepatic flow distribution in total cavopulmonary connections: extracardiac versus intracardiac. *J Thorac Cardiovasc Surg* 2011;141(1):207-14.
13. Trusty PM, Restrepo M, Kanter KR, Yoganathan AP, Fogel MA, Slesnick TC. A pulsatile hemodynamic evaluation of the commercially available bifurcated Y-graft Fontan modification and comparison with the lateral tunnel and extracardiac conduits. *J Thorac Cardiovasc Surg* 2016;151(6):1529-36.
14. Yang W, Feinstein JA, Shadden SC, Vignon-Clementel IE, Marsden AL. Optimization of a Y-graft design for improved hepatic flow distribution in the fontan circulation. *J Biomech Eng* 2013;135(1):011002.

15. Yushkevich PA, Piven J, Hazlett HC, Smith RG, Ho S, Gee JC, Gerig G. User-guided 3D active contour segmentation of anatomical structures: significantly improved efficiency and reliability. *Neuroimage* 2006;31(3):1116-28.
16. Antiga L, Piccinelli M, Botti L, Ene-Iordache B, Remuzzi A, Steinman DA. An image-based modeling framework for patient-specific computational hemodynamics. *Med Biol Eng Comput* 2008;46(11):1097-112.
17. Trusty PM, Wei Z, Sales M, Kanter KR, Fogel MA, Yoganathan AP, Slesnick TC. Y-graft modification to the Fontan procedure: Increasingly balanced flow over time. *J Thorac Cardiovasc Surg* 2019.
18. Wei Z, Singh-Gryzbon S, Trusty PM, Huddleston C, Zhang Y, Fogel MA, Veneziani A, Yoganathan AP. Non-Newtonian Effects on Patient-Specific Modeling of Fontan Hemodynamics. *Ann Biomed Eng* 2020.
19. Yang W, Vignon-Clementel IE, Troianowski G, Reddy VM, Feinstein JA, Marsden AL. Hepatic blood flow distribution and performance in conventional and novel Y-graft Fontan geometries: a case series computational fluid dynamics study. *J Thorac Cardiovasc Surg* 2012;143(5):1086-97.
20. Tang E, Restrepo M, Haggerty CM, Mirabella L, Bethel J, Whitehead KK, Fogel MA, Yoganathan AP. Geometric characterization of patient-specific total cavopulmonary connections and its relationship to hemodynamics. *JACC Cardiovasc Imaging* 2014;7(3):215-24.
21. Slesnick TC, Yoganathan AP. Computational modeling of Fontan physiology: at the crossroads of pediatric cardiology and biomedical engineering. *Int J Cardiovasc Imaging* 2014;30(6):1073-84.
22. Sundareswaran KS, de Zelicourt D, Sharma S, Kanter KR, Spray TL, Rossignac J, Sotiropoulos F, Fogel MA, Yoganathan AP. Correction of pulmonary arteriovenous malformation using image-based surgical planning. *JACC Cardiovasc Imaging* 2009;2(8):1024-30.
23. Hsia TY, Khambadkone S, Redington AN, Migliavacca F, Deanfield JE, de Leval MR. Effects of respiration and gravity on infradiaphragmatic venous flow in normal and Fontan patients. *Circulation* 2000;102(19 Suppl 3):III148-53.
24. Wei ZA, Trusty PM, Tree M, Haggerty CM, Tang E, Fogel M, Yoganathan AP. Can time-averaged flow boundary conditions be used to meet the clinical timeline for Fontan surgical planning? *J Biomech* 2017;50:172-179.
25. Rijnberg FM, Elbaz MSM, Westenberg JJM, Kamphuis VP, Helbing WA, Kroft LJ, Blom NA, Hazekamp MG, Roest AAW. Four-dimensional flow magnetic resonance imaging-derived blood flow energetics of the inferior vena cava-to-extracardiac conduit junction in Fontan patients. *Eur J Cardiothorac Surg* 2019;55(6):1202-1210.



## Supplementary materials

**Supplemental table 1.** MRI details of TCPC anatomic and velocity acquisitions

MRI details	2D transversal and sagittal stacks	2D PC-MRI
Slice thickness (mm)	5, 2.5 overlap	5
Acquired in-plane spatial resolution (mm)	1.76x1.74	1.5 x 1.5
Reconstructed in-plane spatial resolution (mm)	0.9 x 0.9 mm	0.6 x 0.6
Acquired temporal resolution (ms)	-	41.0 (12.2)
Nr of phases per cardiac cycle	-	25-30
ECG-gating	-	retrospective
Respiratory compensation	navigator	-
Acceleration methods	SENSE factor 1.5	Segmentation factor 1-2, SENSE factor 1.4

All MRI examinations were performed on a 3T Philips MRI scanner (Ingenia, Philips Healthcare, Best, the Netherlands).

*mm; millimetre, ECG; electrocardiogram, PC-MRI; phase contrast magnetic resonance imaging*

## Supplementary material 1

### 3D reconstruction of the TCPC

In order to perform CFD, a 3D reconstruction of the TCPC is required. As a first step, automatic, rigid registration was performed of the transversal and sagittal anatomic MRI stacks to correct for possible spatial misalignment between both acquisitions (ITK-SNAP). Images were interpolated (linear) and the TCPC was subsequently segmented on both views using a semi-automatic, active contour method with manual adjustment. The segmented TCPC covered the area between the subhepatic IVC, hepatic veins, SVC, RPA and LPA. Segmental branches were excluded, except for the right upper lobe branches. A 3D TCPC model was reconstructed and smoothed using a non-shrinking Taubin filter (500 iterations, Passband 0.05), and centerlines were derived for each vessel (VMTK).

### CFD simulations

All in- and outlets of the 3D TCPC model were clipped perpendicular to the centerlines and vessel extensions were added. The hepatic veins were clipped close to the connection with the IVC and most often included a right, middle and left hepatic vein. In case of hepatic vein subbranching close to the connection with the IVC, the hepatic veins were clipped more away from the IVC into separate subbranches. In this way, the diameter

or inflow angle of the hepatic vein into the IVC was consolidated. After performance of a mesh-independence study, the TCPC geometries were meshed with 30 polyhedral elements across the average vessel diameter (range 0.4-0.5mm elements) in order to achieve mesh-independent results, including a four prism layer at the vessel walls (ANSYS ICEM CFD v17.1, ANSYS, Inc., Canonsburg, PA). The total number of elements ranged from 1.5 to 2.7 million. All CFD simulations were performed using commercially available Fluent software (v17.1, ANSYS, Inc., Canonsburg, PA).

Time-resolved flowrates were prescribed with a parabolic velocity profile at the inlets. Total hepatic venous flow was divided over the multiple hepatic veins on the basis of the ratio of their respective cross-sectional areas. Outlet boundary conditions were imposed based on the ratio of the pulmonary flow distribution (total RPA/total LPA flow divided by the total PA flow). The right pulmonary flow distribution was divided over the RPA branches based on their respective cross-sectional areas.<sup>1</sup> In case RPA flow was measured distal to the branch towards the right upper lobe, firstly flow towards the right upper lobe was calculated based on the ratio of the cross sectional area of the distal RPA and right upper lobe branch. In these cases, total RPA flow was determined by the sum of the distal RPA flow and calculated flow towards the right upper lobe branch. A rigid vessel wall was assumed and a no-slip condition prescribed. Blood flow was assumed to be laminar. The blood was considered as an incompressible fluid with a density of 1060 kg/m<sup>3</sup>. A Carreau model was used to account for the non-Newtonian blood properties in the TCPC. The convergence criteria was set to 10<sup>-4</sup>. Unsteady CFD simulations were performed for 7 cardiac cycles, simulating 1000 time-steps per cycle. The results of the last 4 cycles were used for the hepatic blood flow mixing and HFD analysis.

## Reference

<sup>1</sup> Haggerty CM, Restrepo M, Tang E, de Zelicourt DA, Sundareswaran KS, Mirabella L, Bethel J, Whitehead KK, Fogel MA, Yoganathan AP. Fontan hemodynamics from 100 patient-specific cardiac magnetic resonance studies: a computational fluid dynamics analysis. *J Thorac Cardiovasc Surg* 2014;148(4):1481-9.

## Supplementary material 2

### Quantification of mixing between IVC and Hepatic blood flow

A method to quantify mixing of hepatic and IVC blood flow within the Fontan conduit was developed based on the spatial distribution of both flows using particle tracing

(Paraview.org). A total of 7500 particles were released from the hepatic veins for each time-step during 5 cardiac cycles. The number of particles per hepatic vein was based on the ratio of their respective cross-sectional areas. The amount of particles released from the subhepatic IVC was based on the average flow ratio between the IVC and hepatic veins;  $7500 \times \frac{Q_{IVC}}{Q_{HV}}$ .

Pathlines, representing the trajectory each particle follows over time, were generated and transections with these pathlines were made at two cross-sections with the Fontan conduit, perpendicular to its centerline: the caudal part of the Fontan conduit, just above the connection between the Fontan conduit with the IVC/HVs, and at the cranial part of the Fontan conduit, just below the connection with the PA (Figure 1A-C, Video 1). IVC and HV pathline transections at each cross-section of the Fontan conduit were recorded for each time-step in the 5<sup>th</sup> cardiac cycle. The ideal mixing of HV and IVC blood flow was determined by the ratio between the number of IVC and HV pathlines for each time-step at both positions in the Fontan conduit (ideal mixing ratio HV:  $R_{\text{mixing\_HV}}$  and ideal mixing ratio IVC:  $R_{\text{mixing\_IVC}}$ ):

$$(1) \text{ Ideal mixing ratio HV, } R_{\text{mixing\_HV}}: \frac{P_{HV}}{P_{\text{total}}}, \in [0,1]$$

$$(2) \text{ Ideal mixing ratio IVC, } R_{\text{mixing\_IVC}}: \frac{P_{IVC}}{P_{\text{total}}}, \in [0,1]$$

where  $P_{HV}$ = number of HV pathlines in the entire cross-section,  $P_{IVC}$ = number of IVC pathlines in the entire cross-section,  $P_{\text{total}} = P_{HV} + P_{IVC}$ ;  $R_{\text{mixing\_HV}} = 1 - R_{\text{mixing\_IVC}}$ .

Subsequently, both caudal and cranial Fontan conduit cross-sections were manually subdivided in a right-left and anterior-posterior direction, resulting in four sections: left-anterior, left-posterior, right-anterior and right-posterior (Figure 1B-C). The mixing of HV and IVC blood flow within each of these four sections was quantified as follows:

$$(3) \text{ Measured mixing ratio HV in each section, } R_{\text{mixing\_HV}}^*: \frac{P_{HV}^*}{P_{\text{total}}^*}, \in [0,1]$$

$$(4) \text{ Measured mixing ratio IVC in each section, } R_{\text{mixing\_IVC}}^*: \frac{P_{IVC}^*}{P_{\text{total}}^*}, \in [0,1]$$

where,  $P_{HV}^*$ = number of HV pathlines in the section,  $P_{IVC}^*$ = number of IVC pathlines in the section,  $P_{\text{total}}^* = P_{HV}^* + P_{IVC}^*$ ,  $R_{\text{mixing\_HV}}^* = 1 - R_{\text{mixing\_IVC}}^*$

The relative mixing ratio in each section, defined as the ratio between the ideal (based on the entire cross-section) and measured mixing ratio (within each section), was determined as follows:

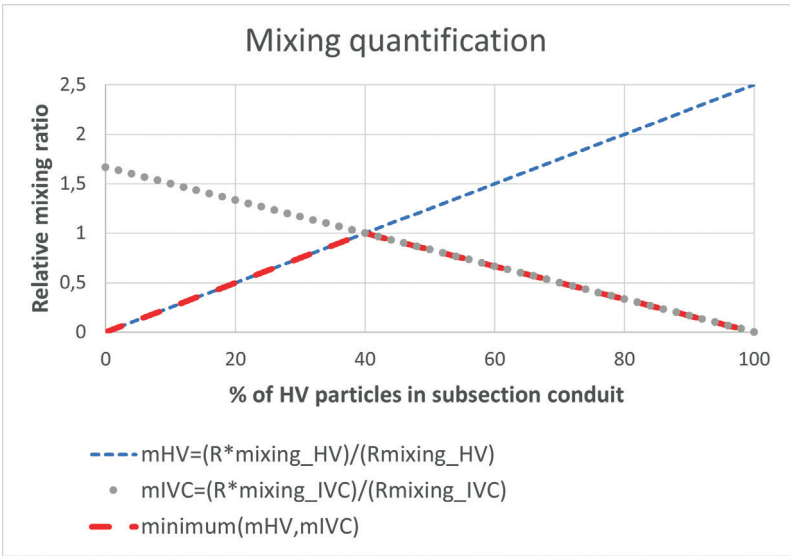
$$(5) \text{ Relative mixing ratio HV, } m_{HV}: m_{HV} = \frac{R^*_{\text{mixing\_HV}}}{R_{\text{mixing\_HV}}}$$

$$(6) \text{ Relative mixing ratio IVC, } m_{IVC}: m_{IVC} = \frac{R^*_{\text{mixing\_IVC}}}{R_{\text{mixing\_IVC}}}$$

Finally, HV and IVC blood flow mixing (M) in each section was defined as the minimal value of relative mixing ratios (Supplemental Figure 1):

$$(7) \text{ Mixing (M) in each section} = \min(m_{HV}, m_{IVC}) \in [0,1]$$

A mixing (M) of 0 indicates no mixing (only HV or IVC pathlines present in the section) and 1 indicates perfect mixing (the exact same ratio of HV and IVC pathlines in the section as in the entire cross-section (ideal mixing ratio)). A mixing value between 0 and 1, e.g. 0.4, can be interpreted as 60% less pathlines, either HV or IVC, are present in the section as expected based on the ideal mixing ratio. Therefore, this mixing parameter can quantify and visualize mixing characteristics within each of the four sections in the different levels of the Fontan conduit for each time-step in the cardiac cycle (Figure 1D-E). However, this mixing parameter cannot distinguish whether poor mixing is caused by an underrepresentation of HV or IVC blood flow in a section, which might change during the cardiac cycle (i.e. poor mixing in a section can be due to underrepresentation of HV flow in one phase but due to underrepresentation of IVC flow in another phase, leading to improved mixing in that section when averaged over time). Therefore, cardiac-cycle averaged mixing ( $M_{\text{average}}$ ) was determined for each section by using the average number of HV and IVC pathlines present during the cardiac cycle (i.e. taking the sum of IVC and HV pathlines in each section for each phase in the cardiac cycle divided by the total number of phases).  $M_{\text{average}}$  per section was weighted by the area of the section (area section/total area cross-section) and summed to obtain  $M_{\text{average}}$  for the entire cross-section.



**Supplemental Figure 1.** The graph shows an example of the calculation of the mixing between hepatic venous blood (HV) and inferior vena caval blood (IVC). In this example, the ideal mixing ratio ( $R_{mixing\_HV}$ ) for the HV was 0.4 and the ideal mixing ratio for the IVC ( $R_{mixing\_IVC}$ ) was 0.6. As noted from the graph, when the measured mixing ratio for the HV in a section of the conduit ( $R * mixing\_HV$ ) is also 0.4 (the ideal case), then the relative mixing ratio mHV (i.e. the ratio between the measured and ideal mixing ratio) is 1. When  $R * mixing\_HV$  is larger than 0.4 (i.e. more HV blood is present in the section than would be expected from the ratio of HV and IVC blood within the entire cross-section, which is suboptimal mixing), mHV will be larger than 1 but mIVC will be smaller than 1 (because less IVC blood will be present in that section than expected). Therefore, to determine the mixing of HV and IVC flow on a scale between 0 and 1, the minimum of mHV and mIVC is taken. As a result, a mixing of 0.7 indicates that 30% less HV or IVC pathlines were present in a certain subsection compared to what would be expected from the ratio of IVC and HV pathlines in the entire cross-section.



# CHAPTER 11



# Hemodynamic performance of 16-20mm extracardiac conduits in adolescent Fontan patients

Friso M. Rijnberg, Luca van 't Hul, Mark G. Hazekamp, Pieter J. van den Boogaard, Joe F. Juffermans, Hildo J. Lamb, Covadonga Terol Espinosa de Los Monteros, Lucia J.M. Kroft, Sasa Kenjeres, Saskia le Cessie, Monique R.M. Jongbloed, Jos J.M. Westenberg, Arno A.W. Roest, Jolanda J. Wentzel



# Abstract

## Objective

The synthetic extracardiac conduit used for the completion of the Fontan operation in single ventricle patients lacks growth potential and adequacy of 16-20mm conduits for adult Fontan patients remains unknown. This study aims to determine total cavopulmonary connection (TCPC) hemodynamics using computational fluid dynamics (CFD) in adolescent Fontan patients at rest and during simulated exercise and to assess the relationship between conduit size and hemodynamics.

## Methods

Patient-specific MRI-based CFD models of the TCPC were performed in 51 extracardiac Fontan patients (median age 16.2 years, Q1-Q3 14.0-18.2) with 16-20mm conduits. Power loss, pressure gradient and normalized resistance were quantified in rest and during simulated exercise, separated into inspiration and expiration. The cross-sectional area (CSA, mean and minimal) of the TCPC vessels were determined and normalized for vessel-specific flow rate ( $\text{mm}^2/\text{L}/\text{min}$ ). Peak (predicted)  $\text{VO}_2$  was assessed.

## Results

The normalized conduit CSA<sub>mean</sub> was a median of 35-73% smaller compared to other TCPC vessels (all  $P < 0.001$ ). All CFD hemodynamics significantly increased from rest to simulated exercise (all  $p < 0.001$ ) and were higher during inspiration compared to expiration ( $p < 0.001$ ). A moderate-strong inverse non-linear relationship was present between normalized conduit CSA<sub>mean</sub> and CFD hemodynamics in rest and exercise. Pressure gradients of  $\geq 1.0$  at rest and  $\geq 3.0\text{mmHg}$  during simulated exercise were observed in patients with a conduit  $\leq 45\text{mm}^2/\text{L}/\text{min}$ . Normalized TCPC resistance weakly correlated with (predicted) peak  $\text{VO}_2$ .

## Conclusions

Extracardiac conduits of 16-20mm have become relatively undersized in adolescent Fontan patients, with most adverse hemodynamics observed in patients with a conduit  $\leq 45\text{mm}^2/\text{L}/\text{min}$  and favorable hemodynamics in patients with a conduit size  $\geq 125\text{mm}^2/\text{L}/\text{min}$ .

## Introduction

Efficient flow is important in cardiology, and especially the Fontan circulation is dependent on optimal flow characteristics. The Fontan procedure or total cavopulmonary connection (TCPC) is the palliative treatment for children with a univentricular heart defect, by connecting the systemic venous return directly with the pulmonary arteries (PAs). Most centers nowadays use an extracardiac Goretex conduit of 16-20mm to connect the inferior vena cava with the PA at the age of 2-4 years old.(1) However, the synthetic extracardiac conduit lacks growth potential and it is currently unknown if 16,18 and 20mm conduits remain adequately sized for adult Fontan patients.

The Fontan circulation is characterized by chronically elevated central venous pressure (CVP) and reduced preload and thereby cardiac output.(2) Efficient TCPC blood flow is important to keep the elevation in CVP and reduction in preload to a minimum.(3,4) Small conduits are an important factor of increased TCPC resistance and should be avoided.(5) Chronic venous hypertension and reduction in preload lead to important morbidity, including liver fibrosis and reduced exercise capacity.(1)

Recently, important blood flow accelerations were observed from the subhepatic inferior vena cava (IVC) towards the conduit 13 years after Fontan completion, indicating that 16 to 20mm conduits had become relatively undersized for adolescent Fontan patients.(6) However, the hemodynamic consequences of undersized conduits in terms of pressure gradients and TCPC resistance at rest and during simulated exercise were not determined. Comprehensive assessment of the state of the Fontan circulation, one of the current gaps in knowledge of the Fontan physiology, is important for evaluation of the current surgical practice of Fontan completion and to optimize management of the expanding group of grown-up Fontan patients.(1) Therefore, the aim of this study is to determine TCPC hemodynamics using computational fluid dynamics (CFD) in a cohort of teenage and adolescent Fontan patients with 16 to 20mm conduits at rest and during simulated exercise and to assess the relationship between conduit size and TCPC hemodynamics.

## Methods

### Study population

Fontan patients with an extracardiac Goretex conduit prospectively underwent magnetic resonance imaging (MRI) examination between 2018-2021 at the Leiden University Medical Center, Leiden, the Netherlands. All patients >8 years old without

contraindications for MRI were eligible for inclusion. The study was approved by the medical ethical review committee of the hospital (P18.024). Written informed consent was obtained from all patients and/or their parents.

### **Cardiopulmonary exercise testing**

Cardiopulmonary exercise testing (CPET) was performed using a continuous incremental bicycle protocol. Peak VO<sub>2</sub> (ml/kg/min) and predicted peak VO<sub>2</sub> (%) were determined in all patients with a respiratory exchange ratio >1.0.

### **Magnetic resonance imaging**

Anatomical and two-dimensional (2D) real-time flow MRI acquisition details are presented in Supplemental Table 1. Real-time 2D flow MRI measurements were obtained at the subhepatic inferior vena cava (IVC, below entry of the hepatic veins, HVs), at the extracardiac conduit and at the superior vena cava (SVC). HV flow was determined indirectly by subtracting IVC flow from conduit flow. Flow measurements consisted of 250 real-time (non electrocardiogram-gated) flow acquisitions with continuously monitoring of the respiratory signal using an air-filled abdominal belt. The respiratory signal was used to divide the flow signal into inspiration and expiration phases as previously described.(6)

A three-dimensional (3D) model of the TCPC was created based on lumen segmentation on respiratory-navigator gated sagittal and transversal 2D anatomical stacks. The 3D model included the area between the subhepatic IVC, HVs, SVC and RPA (including the right upper lobe branches) and LPA up to the level of the segmental branches (ITK-SNAP(7)). The TCPC model was smoothed, centerlines were derived and vessel extensions were added at all inlets and outlets.(8)

### **Geometry analysis**

The TCPC was automatically divided into standardized segments (conduit, SVC, RPA (distal to right upper lobe branch) and LPA) as previously described.(9) The mean and minimum CSA of these segments were determined perpendicular to the centerline at 1mm intervals. The CSA of the inlet extensions were reported for the subhepatic IVC and HVs since the contribution of these vessels to the TCPC volume was minimal. The CSA was normalized for the vessel-specific average flow rate (mm<sup>2</sup>/L/min) as a marker of functional vessel CSA. Ideally, an optimally sized conduit in Fontan patients results in minimal energy loss and minimal flow stasis. Both of these factors are dependent on the ratio between conduit CSA and the amount of conduit flow which are captured in the normalized conduit CSA<sub>mean</sub> parameter.

In addition, the change in measured conduit  $CSA_{\text{mean}}$  versus theoretical implanted conduit  $CSA_{\text{mean}}$  was reported (16mm=201mm<sup>2</sup>, 18mm=254mm<sup>2</sup> and 20mm=314mm<sup>2</sup>).

### Computational Fluid Dynamics

The 3D TCPC model was meshed with 30 polyhedral elements across the average vessel diameter (0.35-0.45mm elements) with four prism layers at the wall in order to achieve mesh-independent results (ANSYS ICEM v17.1, Inc., Canonsburg, PA). All CFD simulations were performed using commercially available Fluent software (v17.1, ANSYS, Inc., Canonsburg, PA). Respiratory cycle-resolved flowrates were prescribed at the inlets using a parabolic velocity profile. Total HV flow was divided over the individual HVs based on the ratio of their respective CSAs. Constant outflow ratios at the PAs were imposed as the outlet boundary condition and subdivided over side branches based on their respective CSAs.(10) The outflow ratio was determined from ECG-gated 2D flow MRI measurements since 2D real-time flow measurements were not performed in the PAs. A rigid vessel wall was assumed and a no-slip condition prescribed. Blood flow was assumed to be laminar. A Carreau model was used to account for the non-Newtonian blood properties in the TCPC.(11)

### Exercise condition

To simulate the effect of increased flow during exercise, resting flow rates were adapted according to a study by Wei et al, in which 2D real-time flow MRI measurements were obtained during supine lower-leg exercise.(12) The total duration of the respiratory cycle was decreased with a factor of 1.6, the inspiratory fraction (inspiratory time vs total respiration time) was increased with a factor of 1.17(13) and time-resolved flow rates were increased by a factor of 2.44 (both subhepatic IVC and HVs) and 1.67 (SVC). The resting PA outflow ratios were assumed to remain the same during exercise.(14)

## Hemodynamic parameters

### Energetics

All parameters were reported during inspiration, expiration and during the entire respiratory cycle. Power loss (PL, in milliwatt, mW) was determined using the viscous dissipation rate method (15). Power loss based pressure gradient (mmHg) from the inlets towards the outlets was determined as follows(10):

$$\Delta P_{\text{TCPC}} = \frac{PL}{Q_s},$$

where PL and  $Q_s$  are the total power loss and the total systemic venous return in the corresponding respiratory phase.

The resistance normalized for body surface area (BSA) (in mmHg/L/min/m<sup>2</sup>) was determined as follows(10):

$$\text{Normalized resistance} = \frac{\Delta P_{\text{TCPC}}}{\frac{Q_s}{\text{BSA}}}.$$

### Flow stagnation volume

Flow stagnation volume (volume of cells with a velocity <0.01 m/s(16)) was determined in a subset of 15 patients as a marker of thrombosis risk; 5 patients per implanted conduit size (16, 18 and 20mm) matched on average conduit flow rate (range 2.2-4.6 L/min, Supplemental Figure 1). The minimal (at peak flow during inspiration) and maximal flow stagnation volume (at lowest flow during expiration) was determined in the entire TCPC and in the conduit only by manually isolating the conduit from the TCPC (Paraview.org). The minimal flow stagnation is of particular clinical interest, as this is the volume of blood in the TCPC that remains stagnated during the entire respiratory cycle. The volume of cells with a velocity magnitude of 0.00 m/s was excluded from the flow stagnation volume to not take the mesh cells with zero velocity at the vessel wall (no slip condition) into account.

### Statistical analysis

Data were presented as median (Q1-Q3) or mean (standard deviation). Correlation analysis was performed using Pearson (r) or Spearman (ρ) correlation (weak 0.3-0.5, moderate 0.5-0.7, strong ≥0.7-0.9 and very strong >0.9). Comparison of parameters between respiratory phases were performed using the Friedman test (adjusted for multiple comparisons using Bonferroni). The non-linear relationship between CFD derived energetics and normalized conduit CSA was analyzed using linear regression after log transformation of both the dependent and independent parameters (power curve). A p-value <0.05 was considered statistically significant. Data were analyzed with SPSS 25.0 (IBM Corp., Armonk, NY, USA) and Graphpad Prism 8.0 (GraphPad Software, La Jolla, California, USA).

## Results

Sixty-five sequential patients underwent MRI examination during the study period. Fourteen/65 patients were excluded because of incomplete 2D real-time MRI flow data (n=7), central device related artefacts (n=3) or patients with a lateral tunnel Fontan connection (n=4), resulting in 51 patients that were included in this study. Patient characteristics are reported in Table 1. All patients were recruited from the outpatient clinic and were in relatively good clinical condition (NYHA class I-II). CPET was performed

in 46/51 patients, with 40 patients reaching maximal effort (median time between CPET and MRI 0 days (Q1-Q3 -6-0 days).

**Table 1.** Patient characteristics

Male/Female, n	24/27
<b>Primary diagnosis, n (%)</b>	
- TA	12 (24)
- HLHS	9 (17)
- DILV + TGA	10 (20)
- DORV	6 (11)
- uAVSD	3 (6)
- ccTGA	4 (8)
- PA + IVS	2 (4)
- Other	5 (10)
<b>Dominant ventricle</b>	
Left, n (%)	30 (59)
Right, n (%)	16 (31)
Biventricular/indeterminate, n (%)	5 (10)
<b>Characteristics at Fontan procedure</b>	
Age at Fontan, years	3.3 (2.7-3.9)
Height, cm	98 (92-102)
Weight, kg	14 (13-16)
BSA, m <sup>2</sup>	0.63 (0.58-0.67)
Implanted conduit size (16/18/20mm), n	27/18/6
Fenestration, n(%)	31 (61)
<b>Characteristics at time of MRI</b>	
Age at MRI, years	16.2 (14.0-18.2)
Height, cm	168 (163-175)
Weight, kg	59 (50-66)
BSA, m <sup>2</sup>	1.66 (1.52-1.76)
Time between Fontan and MRI, years	13.1 (10.4-15.8)
NYHA-class I-II, n (%)	51 (100)
<b>Cardiopulmonary exercise testing</b>	
RER	1.11 (1.05-1.17)
Peak Watt	120 (105-150)
Peak heart rate	173 (164-184)
Peak predicted heart rate, %	94 (86-101)
Peak VO <sub>2</sub> , ml/kg/min	27.1 (22.4-30.0)
Peak predicted VO <sub>2</sub> , %	55 (47-65)

Values are reported as median (Q1-Q3) unless otherwise specified. TA; tricuspid atresia, HLHS; hypoplastic left heart syndrome, DILV; double inlet left ventricle, (cc)TGA; (congenital corrected) transposition of the great arteries, DORV; double outlet right ventricle, uAVSD; unbalanced atrioventricular septal defect, PA+IVS; pulmonary atresia with intact ventricular septum, RER; respiratory exchange ratio

## Geometry and flow

Vessel CSA of the different segments of the TCPC are reported in Table 2. Absolute measured conduit CSA<sub>mean</sub> was 100% (Q1-Q3 94-105), 95% (Q1-Q3 90-106) and 95% (Q1-Q3 72-105) of theoretical implanted conduit size in patients with 16,18 and 20mm conduits, respectively (p=0.42). The conduit CSA<sub>mean</sub> normalized for conduit flow rate was significantly smaller compared to the normalized vessel CSA<sub>mean</sub> of all other vessels (all P<0.001); a median 56,73 and 64% smaller compared to the subhepatic IVC, HVs and SVC, respectively, and 40 and 35% smaller compared to the LPA and RPA, respectively.

**Table 2.** Flow and geometry characteristics

	Flow (L/min)			Geometry		
	Average respiratory cycle	Inspiration	Expiration	Absolute CSA <sub>mean</sub> (mm <sup>2</sup> )	Absolute CSA <sub>min</sub> (mm <sup>2</sup> )	Normalized CSA <sub>mean</sub> (mm <sup>2</sup> /L/min)
Conduit	3.3 (2.5-4.0)	4.5 (3.7-5.3)	2.6 (1.9-3.3)	217 (199-249)	196 (182-230)	65 (54-90)
IVC	1.8 (1.5-2.2)	2.0 (1.6-2.4)	1.7 (1.3-2.1)	263 (222-303)	-	147 (122-170)
HVs	1.5 (1.0-1.8)	2.5 (1.8-3.0)	0.7 (0.5-1.2)	347 (303-405)	-	243 (183-352)
SVC	1.3 (1.0-1.6)	1.5 (1.2-1.8)	1.2 (1.0-1.5)	214 (192-262)	193 (165-224)	180 (133-216)
LPA	1.9 (1.3-2.3)	2.5 (1.7-2.9)	1.5 (1.1-1.9)	186 (150-236)	149 (109-192)	108 (89-153)
RPA (distal to RUL branch)	1.9 (1.5-2.3)	2.5 (2.0-2.8)	1.5 (1.1-1.8)	201 (167-231)	181 (134-215)	100 (84-136)

CSA; cross-sectional area, IVC/SVC; inferior/superior vena cava, RPA/LPA; right/left pulmonary artery, HV; hepatic veins, mm; millimeter, L/min; liter/minute

Total systemic venous return during the entire respiratory cycle was 4.5 (Q1-Q3 3.8-5.5) L/min in rest, increasing to 10.8 (Q1-Q3 8.4-12.5) L/min during simulated exercise. Flow rates during inspiration and expiration in the TCPC are reported in Table 2. Flow rates in all vessels were lowest during expiration and highest during inspiration (all P<0.001), most predominantly in the HVs (Table 2). Mean conduit flow during the entire respiratory cycle positively correlated with BSA, but considerable variability in flow rates was observed (Figure 1).

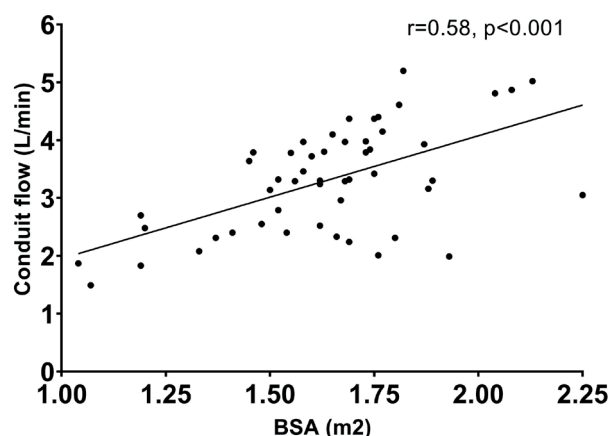


**Figure 1.** A moderate positive correlation is present between BSA and mean conduit flow rate along the entire respiratory cycle. The linear regression line is shown.

*BSA; body surface area (Haycock).*

**Energetics**

CFD derived energetics along the respiratory cycle are reported in Table 3, both for resting and simulated exercise conditions. No significant difference in energetics was present between gender.

***Inspiration vs expiration***

During rest, mean power loss was higher during inspiration (median 10.5mW, Q1-Q3 6.5-14.2) compared to expiration (3.7mW, Q1-Q3 2.5-6.3,  $p<0.001$ ). Furthermore, the median pressure gradient was higher during inspiration (0.8mmHg, Q1-Q3 0.6-1.0) compared to expiration (0.5mmHg, Q1-Q3 0.4-0.7). No significant difference was present in normalized resistance between inspiration and expiration (Table 3).

***Rest vs simulated exercise***

Power loss, pressure gradient and normalized resistance all significantly increased from resting to simulated exercise conditions (all  $p<0.001$ , Table 3), most pronounced during inspiration for power loss and pressure gradient. From rest to exercise, the respiratory-cycle averaged power loss increased with a median factor of 6.9 (Q1-Q3 6.2-7.7), the pressure gradient increased with a factor of 3.0 (Q1-Q3 2.7-3.4) and the normalized resistance increased with a factor of 1.3 (Q1-Q3 1.2-1.5).



**Table 3.** Computational fluid dynamics results

<b>Energetics</b>	<b>Resting conditions</b>			<b>Exercise conditions</b>		
	<b>Average</b>	<b>Inspiration</b>	<b>Expiration</b>	<b>Average</b>	<b>Inspiration</b>	<b>Expiration</b>
Power loss, mW	6.8 (4.1-9.8)†,‡	10.5 (6.5-14.2)‡,§	3.7 (2.5-6.3)†,§	48.6 (27.4-70.5)†,‡	61.0 (33.5-86.3)‡,§	38.6 (19.0-57.6)†,§
Pressure gradient, mmHg	0.7 (0.5-0.8)†,‡	0.8 (0.6-1.0)‡,§	0.5 (0.4-0.7)†,§	2.0 (1.4-2.6)†,‡	2.3 (1.5-2.8)‡,§	1.8 (1.2-2.3)†,§
Normalized resistance, mmHg/L/min/m <sup>2</sup>	0.23 (0.18-0.28)†,‡	0.21 (0.15-0.28)§	0.22 (0.18-0.27)§	0.29 (0.22-0.42)‡	0.29 (0.21-0.41)‡	0.29 (0.21-0.41)†,§
<b>Thrombosis marker (n=15)</b>	<b>Minimum (inspiration)</b>	<b>Maximum (expiration)</b>		<b>Minimum (inspiration)</b>	<b>Maximum (expiration)</b>	
Flow stagnation entire TCPC, %	1.2 (0.7-1.8)	6.2 (4.8-8.0)		0.4 (0.2-0.7)	1.5 (0.8-2.2)	
Flow stagnation conduit, %	0.0 (0.0-0.0)	0.5 (0.2-1.2)		0.0 (0.0-0.0)	0.0 (0.0-0.0)	

P-value <0.05 compared to inspiration†, expiration‡ or the entire respiratory cycle§. mW; miliwatt, mmHg; millimeter mercury, L/min; liter/minute

A moderate-strong inverse non-linear relationship was present between normalized conduit  $CSA_{mean}$  and power loss, pressure gradient and normalized resistance, both in rest and simulated exercise conditions (Figure 2). As derived from the regression curves in Figure 2B, a normalized conduit  $CSA_{mean}$  of  $\leq 45 \text{ mm}^2/\text{L/min}$  corresponded to a median pressure gradient of  $\geq 1.0$  at rest and  $\geq 3.0$  during simulated exercise. A normalized conduit  $CSA_{mean}$  of  $\geq 125 \text{ mm}^2/\text{L/min}$  corresponded to a pressure gradient of  $\leq 1.0 \text{ mmHg}$  during both rest and simulated exercise. An example of streamline blood flow visualization and power loss heatmaps in two Fontan patients with a small and relatively large normalized conduit  $CSA_{mean}$  are illustrated in Figure 3. Pathline blood flow visualization during two respiratory cycles during resting and simulated exercise conditions are shown in Video 1&2.

Furthermore, a negative correlation was present between normalized conduit  $CSA_{mean}$  and the relative rest-to-exercise increase in power loss ( $\rho = -0.63$ ,  $p < 0.001$ ), pressure gradient ( $\rho = -0.59$ ,  $p < 0.001$ ) and normalized resistance ( $\rho = -0.50$ ,  $p < 0.001$ ), indicating strongest increases in patients with smallest conduits.

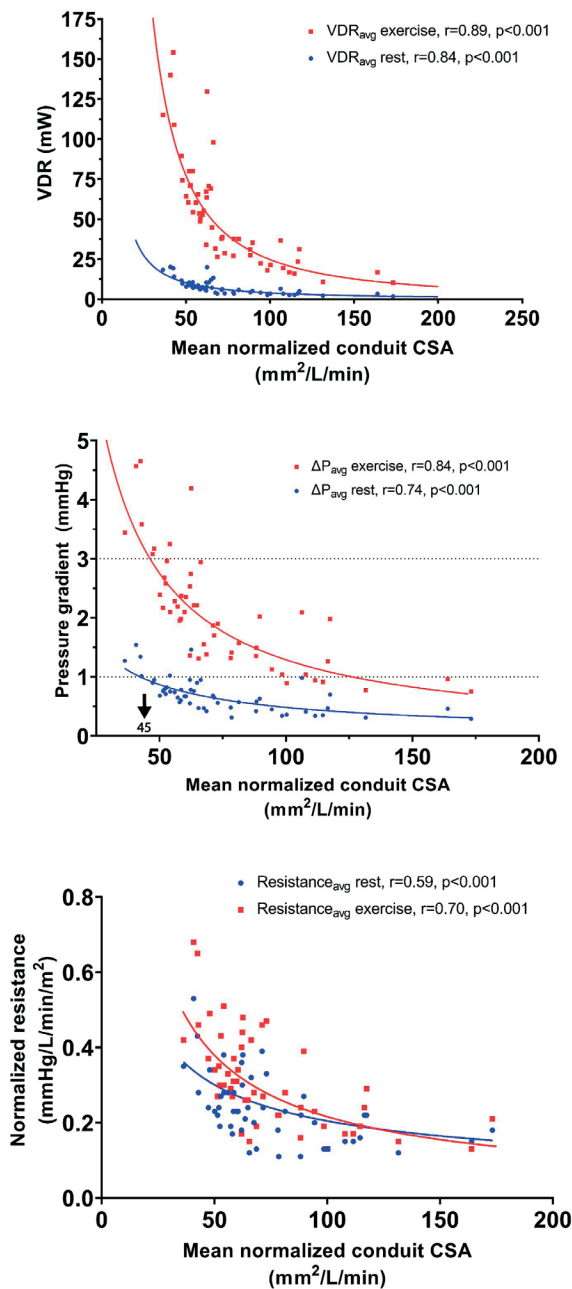


**Figure 2.** A moderate to strong inverse non-linear relationship is present between power loss (upper panel), pressure gradient (middle panel) and normalized resistance (lower panel) with normalized conduit cross sectional area, during both rest (blue) and simulated exercise (red). One significant outlier of normalized TCPC resistance was excluded from the analysis.

CSA; cross-sectional area, mW; milliwatt.

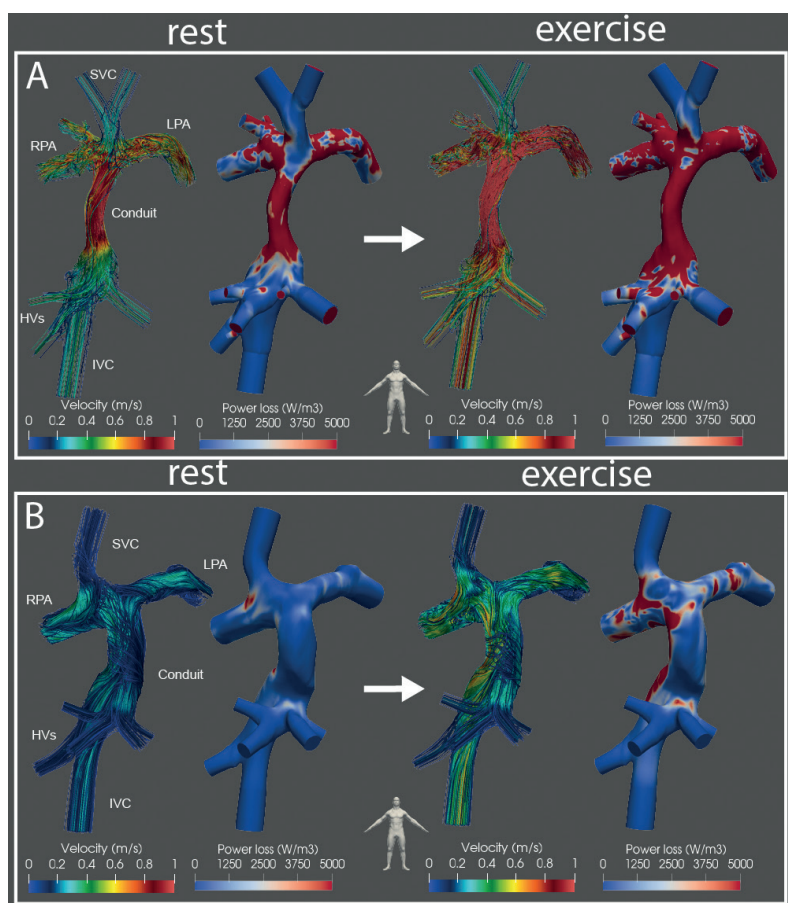


**Figure 3.** Velocity-colored streamline representation and power loss heatmaps of blood flow in the TCPC during peak inspiration is shown for 2 Fontan patients with a relatively small (A) and large (B) normalized conduit  $CSA_{mean}$ . Note the strong increase in blood flow velocity and power loss at the junction between the IVC/HVs and the extracardiac conduit extending into the PAs in patient A, indicating the presence of an functionally undersized conduit.

**Patient A.** 16yr, BSA 1.82m<sup>2</sup>, 16mm implanted conduit, mean conduit flow respiratory cycle 5.2 L/min, normalized conduit  $CSA_{mean}$  36mm<sup>2</sup>/L/min. CFD energetics (rest/exercise): Power loss 18.3/115.1mW, pressure drop 1.3/3.4mmHg, normalized resistance 0.35/0.41 mmHg/L/min/m<sup>2</sup>.

**Patient B.** 16yr, BSA 1.76m<sup>2</sup>, 18mm implanted conduit, mean conduit flow respiratory cycle 2.0 L/min, normalized conduit  $CSA_{mean}$  173mm<sup>2</sup>/L/min. CFD energetics (rest/exercise): Power loss 1.7/10.3mW, pressure drop 0.3/0.8mmHg, normalized resistance 0.18/0.21 mmHg/L/min/m<sup>2</sup>.

A weak negative correlation was present between normalized resistance of the TCPC and peak VO<sub>2</sub> during both rest ( $r=-0.41$ ,  $p=0.009$ ) and during simulated exercise ( $r=-0.37$ ,  $p=0.020$ ). Normalized resistance correlated with predicted peak VO<sub>2</sub> during rest ( $r=-0.36$ ,  $p=0.024$ ) and during simulated exercise ( $r=-0.37$ ,  $p=0.020$ , Figure 4). No

correlation was found between power loss or pressure gradient and peak VO2 ( $r=-0.25$ ,  $p=0.10$  for both power loss and pressure gradient).

**Flow stagnation volume**

Maximal flow stagnation volume (expiration) in rest in the entire TCPC was 6.2% (Q1-Q3 4.8-8.0) of the total volume. Minimal flow stagnation (inspiration) was significantly smaller (median 1.2%, Q1-Q3 0.7-1.8,  $p<0.001$ ) due to the increase in flow during inspiration (Table 3). Increased flow during simulated exercise further reduced maximal (median 1.5%, Q1-Q3 0.8-2.2) and minimal (median 0.4%, Q1-Q3 0.2-0.7) flow stagnation volume. Both minimal and maximal flow stagnation volume in the conduit only were absent/negligible (Table 3). No significant differences in flow stagnation volume in the conduit were found between patients with implanted 16,18 and 20mm conduit sizes.

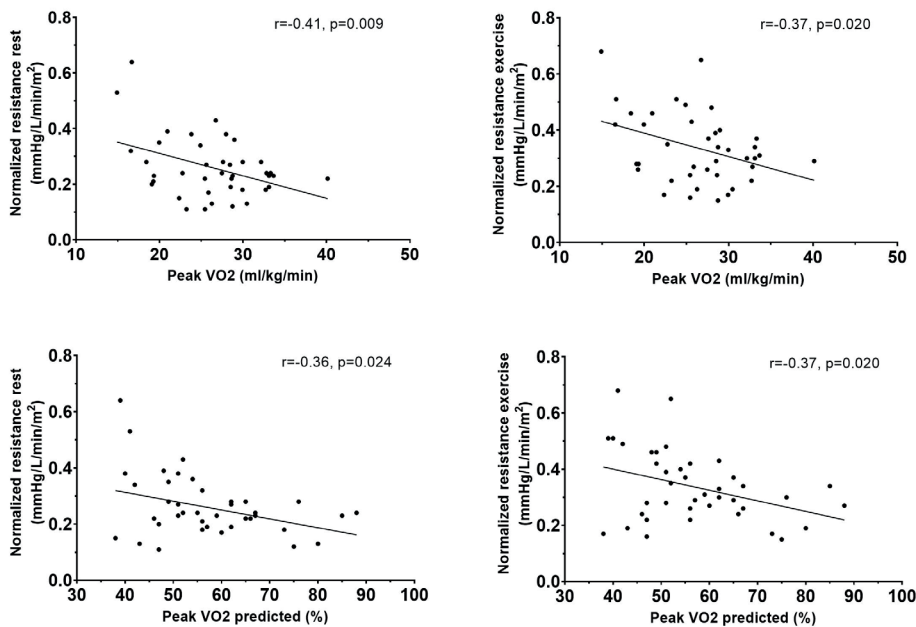


**Figure 4.** A weak inverse linear correlation is observed between normalized resistance of the TCPC and peak VO2 (upper panels) and predicted peak VO2 (lower panels) in rest (left panels) and during simulated exercise (right panels).

## Discussion

This study shows that extracardiac conduits of 16 to 20mm have become undersized for teenage and adolescent Fontan patients on average 13 years after Fontan completion. Main results are a significantly smaller normalized conduit  $CSA_{mean}$  compared to the other TCPC vessels. Furthermore, pressure gradients and resistance in the TCPC increased non-linearly with decreasing normalized conduit CSA. Finally, a weak correlation was observed between TCPC resistance and peak  $VO_2$ . Especially patients with a normalized conduit  $CSA_{mean} \leq 45 \text{ mm}^2/\text{L/min}$  showed important pressure gradients in the TCPC, most pronounced during simulated exercise, and may require close monitoring for Fontan failure. In patients with a univentricular heart defect, the Fontan procedure is the palliative treatment of choice. The current recommendation is to implant a slightly oversized (16 to 20mm extracardiac Goretex conduit) in children at the age of 2-4 years, thereby aiming to avoid somatic overgrowth necessitating reintervention.(1,17) However, optimal conduit size for adult Fontan patients remains elusive mainly because no clear definition is present to describe conduit adequacy. Recently, our group observed important velocity accelerations from the subhepatic IVC towards the conduit indicating that these conduits have become too small.(6,18) The current study adds important information by assessment of the functional conduit size to describe conduit adequacy: conduit  $CSA_{mean}$  normalized for conduit flow rate, and by characterizing the hemodynamic performance of the TCPC using CFD at rest and during simulated exercise. Of note, in the absence of a distinct conduit stenosis, functional conduit size can be easily obtained from a 2D flow measurement at the level of the conduit which is part of standard Fontan MRI protocols.

### Conduit adequacy

In our cohort of on average 16 year old patients with a median conduit flow rate of 3.3 L/min, a median normalized conduit CSA of  $65 \text{ mm}^2/\text{L/min}$  was present, significantly smaller compared to the other vessels in the TCPC. For comparison, Itatani et al. recommended the use of 16-18mm conduits (conduit CSA of  $201\text{-}254 \text{ mm}^2$ ) for Fontan completion using CFD models based on 36 months old children with an average conduit flow rate of approximately 0.85 L/min in rest.(16) This would correspond to a normalized conduit  $CSA_{mean}$  of approximately  $240\text{-}300 \text{ mm}^2/\text{L/min}$ . In addition, flow stagnation was absent or negligible in both the entire TCPC and in the conduit only in our cohort, further emphasizing that blood flow stasis caused by oversizing is not a relevant problem anymore in 16-20mm conduits when reaching the adolescent age. However, other factors associated with thrombus formation such as high shear flows may become increased by undersized conduits and is subject to future research.(19)

To assess the hemodynamic consequence of the reduced normalized conduit  $CSA_{mean}$ , we used CFD modelling in rest and during simulated exercise for the quantification

of the power loss based pressure gradient and resistance of the TCPC.(10) The ability to simulate blood flow during exercise is one great advantage of CFD compared to conventional diagnostics such as catheterization, which is usually only limited to resting conditions.(20) Main results of the CFD analysis showed a strong inverse non-linear correlation between normalized conduit  $CSA_{mean}$  and pressure gradients, reaching  $\geq 1\text{mmHg}$  in rest and  $\geq 3\text{mmHg}$  during simulated exercise in patients with a conduit  $\leq 45\text{mm}^2/\text{L}/\text{min}$ . Especially during inspiration in exercise, pressure gradients in the order of  $5\text{mmHg}$  were observed in patients with smallest functional conduit sizes. Additionally, patients with smallest functional conduit sizes showed a higher increase in energetics from rest-to-exercise than patients with larger functional conduits. Importantly, the use of CFD simulated exercise showed that in patients with a conduit CSA of  $45\text{-}125\text{mm}^2/\text{L}/\text{min}$ , pressure gradients were relatively low ( $<1\text{mmHg}$ ) in rest, but significantly increased during simulated exercise to values of  $1\text{-}3\text{mmHg}$  which may be of clinical significance. This data therefore emphasizes the current drawbacks of evaluating TCPC hemodynamics using catheterization in rest, as small pressure gradients in rest may mask important pressure gradients during exercise.(21)

Currently, no cut-off values for clinically relevant pressure gradients in the TCPC are defined that may indicate the need for intervention, but catheterization derived pressure gradients as low as  $1\text{mmHg}$  may already be an indication of clinically relevant Fontan pathway obstruction.(22) Our data indicate that patients with a conduit  $\leq 45\text{mm}^2/\text{L}/\text{min}$  may require close monitoring, as further decline in functional conduit size is expected to lead to a non-linear increase in pressure gradient and resistance. A recent study showed that dilatation of the conduit significantly improved hemodynamics, but will depend on the increase in conduit CSA that can be accomplished.(23) On the other hand, pressure gradients in the TCPC were relatively small in the majority of patients and the expected reduction in pressure gradients associated with conduit replacement may be insufficient to justify the risk of reoperation. It should also be noted that our study cohort represented patients in overall good clinical condition without any signs of Fontan failure. However, the chronic adverse effects of decreasing flow efficiency and subsequent elevation in CVP and/or gradual decrease in preload may take more time to become clinically apparent.

## Relevance for surgical strategy

The results of our study raise concern that the current surgical strategy may lead to suboptimal hemodynamics of the Fontan circulation for both young children and adolescent Fontan patients. In young children, oversizing increases thrombosis risk and also lead to increased energy losses(16,24,25), while in adolescent Fontan patients these conduits become undersized. Favorable hemodynamics (pressure gradient  $<1\text{mmHg}$  during both rest and exercise) were observed in patients with a conduit CSA

of  $\geq 125 \text{ mm}^2/\text{L}/\text{min}$ . This corresponds to conduit sizes of between  $375 \text{ mm}^2$  (i.e.  $\pm 22 \text{ mm}$ ) and  $625 \text{ mm}^2$  ( $\pm 28 \text{ mm}$ ) for patients with 3-5 L/min conduit flow. These values would be in line with suprahepatic IVC diameters observed in healthy persons(26), and with Fontan tunnel CSA ( $420\text{-}580 \text{ mm}^2$ , i.e. 23-27 mm) observed in 10-15 year old Fontan patients with a lateral tunnel.(6,27,28) However, implanting larger conduit sizes at the initial Fontan operation is not feasible due to anatomical constraints and the increased risk of conduit thrombosis.(16,24) Based on our observations, in our opinion alternative surgical strategies should be explored such as implanting other, non-rigid materials to optimize future hemodynamics, including dilatable ePTFE grafts (PECA labs) and stress the need for tissue-engineered grafts with growth potential.(29)

## Limitations

Flow rates were modelled with respect to the respiratory cycle, ignoring the effect of the cardiac cycle on flow rates. However, since flow pulsatility is almost entirely related to the respiratory cycle(30,31), inaccuracies are likely small. No patient-specific exercise flow data was available necessitating the use of adapted cohort averaged increases in flow from rest to exercise. However, a previous study found an increase in CVP from 9 towards 20 mmHg during lower leg exercise and TCPC pressure gradients of 3-5 mmHg found in our study in patients with smallest conduits are in line with the rise seen in CVP from rest to exercise.(32) The measured conduit  $\text{CSA}_{\text{mean}}$  exceeded the theoretical conduit CSA in some patients and this overestimation is most likely related to the resolution of the MRI acquisitions. Lastly, the potential improvement in TCPC hemodynamics with larger conduits was not studied and could only be indirectly determined from the curves in Figure 2. CFD models using virtual surgery could be useful to validate the improvement in TCPC hemodynamics with implantation of larger conduit sizes.

## Conclusions

Extracardiac conduits of 16 to 20 mm have become relatively undersized in teenage and adolescent Fontan patients. Pressure gradients and resistance in the TCPC increased non-linearly with decreasing normalized conduit CSA and a weak correlation was observed between normalized TCPC resistance and peak  $\text{VO}_2$ . Patients with a conduit  $\leq 45 \text{ mm}^2/\text{L}/\text{min}$  showed important pressure gradients in the TCPC, most predominantly during simulated exercise, and may require close monitoring for worsening of Fontan pathway obstruction. Furthermore, these observations question the long-term efficacy of the current surgical Fontan approach using 16-20 mm conduits and alternative surgical strategies should be explored to optimize future hemodynamics in adult Fontan patients.

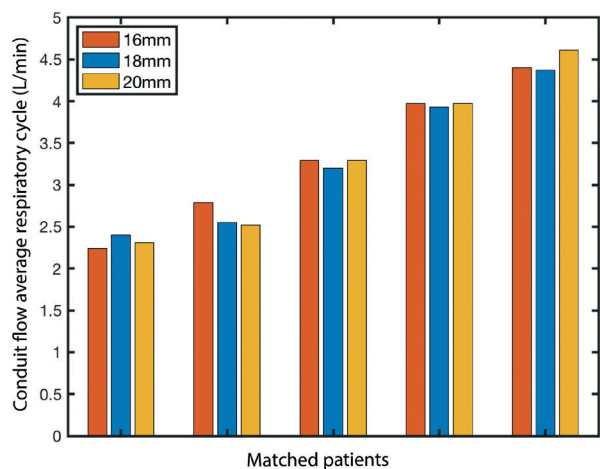
## References

1. Rychik J, Atz AM, Celermajer DS et al. Evaluation and Management of the Child and Adult With Fontan Circulation: A Scientific Statement From the American Heart Association. *Circulation* 2019.
2. Gewillig M, Brown SC. The Fontan circulation after 45 years: update in physiology. *Heart* 2016;102:1081-6.
3. Rijnberg FM, Hazekamp MG, Wentzel JJ et al. Energetics of Blood Flow in Cardiovascular Disease: Concept and Clinical Implications of Adverse Energetics in Patients With a Fontan Circulation. *Circulation* 2018;137:2393-2407.
4. Sundareswaran KS, Pekkan K, Dasi LP et al. The total cavopulmonary connection resistance: a significant impact on single ventricle hemodynamics at rest and exercise. *Am J Physiol Heart Circ Physiol* 2008;295:H2427-35.
5. Tang E, Restrepo M, Haggerty CM et al. Geometric characterization of patient-specific total cavopulmonary connections and its relationship to hemodynamics. *JACC Cardiovasc Imaging* 2014;7:215-24.
6. Rijnberg FM, van der Woude SFS, Hazekamp MG et al. Extracardiac conduit adequacy along the respiratory cycle in adolescent Fontan patients. *European Journal of Cardio-Thoracic Surgery* 2021.
7. Yushkevich PA, Gerig G. ITK-SNAP: An Intractive Medical Image Segmentation Tool to Meet the Need for Expert-Guided Segmentation of Complex Medical Images. *IEEE Pulse* 2017;8:54-57.
8. Antiga L, Piccinelli M, Botti L, Ene-Iordache B, Remuzzi A, Steinman DA. An image-based modeling framework for patient-specific computational hemodynamics. *Med Biol Eng Comput* 2008;46:1097-112.
9. Rijnberg FM, Juffermans JF, Hazekamp MG et al. Segmental assessment of blood flow efficiency in the total cavopulmonary connection using 4D flow MRI: vortical flow is associated with increased viscous energy loss. *European Heart Journal Open* 2021.
10. Haggerty CM, Restrepo M, Tang E et al. Fontan hemodynamics from 100 patient-specific cardiac magnetic resonance studies: a computational fluid dynamics analysis. *J Thorac Cardiovasc Surg* 2014;148:1481-9.
11. Wei Z, Singh-Gryzbon S, Trusty PM et al. Non-Newtonian Effects on Patient-Specific Modeling of Fontan Hemodynamics. *Ann Biomed Eng* 2020;48:2204-2217.
12. Wei Z, Whitehead KK, Khiabani RH et al. Respiratory Effects on Fontan Circulation During Rest and Exercise Using Real-Time Cardiac Magnetic Resonance Imaging. *Ann Thorac Surg* 2016;101:1818-25.
13. Hjortdal VE, Emmertsen K, Stenbog E et al. Effects of exercise and respiration on blood flow in total cavopulmonary connection: a real-time magnetic resonance flow study. *Circulation* 2003;108:1227-31.
14. Khiabani RH, Whitehead KK, Han D et al. Exercise capacity in single-ventricle patients after Fontan correlates with haemodynamic energy loss in TCPC. *Heart* 2015;101:139-43.
15. Wei ZA, Tree M, Trusty PM, Wu W, Singh-Gryzbon S, Yoganathan A. The Advantages of Viscous Dissipation Rate over Simplified Power Loss as a Fontan Hemodynamic Metric. *Ann Biomed Eng* 2018;46:404-416.
16. Itatani K, Miyaji K, Tomoyasu T et al. Optimal conduit size of the extracardiac Fontan operation based on energy loss and flow stagnation. *Ann Thorac Surg* 2009;88:565-72; discussion 572-3.



17. Daley M, d'Udekem Y. The optimal Fontan operation: Lateral tunnel or extracardiac conduit? *J Thorac Cardiovasc Surg* 2020.
18. Rijnberg FM, van Assen HC, Hazekamp MG, Roest AAW, Westenberg JJM. Hemodynamic Consequences of an Undersized Extracardiac Conduit in an Adult Fontan Patient Revealed by 4-Dimensional Flow Magnetic Resonance Imaging. *Circ Cardiovasc Imaging* 2021;14:e012612.
19. van Rooij BJM, Zavodszky G, Azizi Tarksalooyeh VW, Hoekstra AG. Identifying the start of a platelet aggregate by the shear rate and the cell-depleted layer. *J R Soc Interface* 2019;16:20190148.
20. Whitehead KK, Pekkan K, Kitajima HD, Paridon SM, Yoganathan AP, Fogel MA. Nonlinear power loss during exercise in single-ventricle patients after the Fontan: insights from computational fluid dynamics. *Circulation* 2007;116:1165-71.
21. Shachar GB, Fuhrman BP, Wang Y, Lucas RV, Lock JE. Rest and exercise hemodynamics after the Fontan procedure. *Circulation* 1982;65:1043-1048.
22. Alsaied T, Rathod RH, Aboulhosn JA et al. Reaching consensus for unified medical language in Fontan care. *ESC Heart Fail* 2021.
23. Hagler DJ, Miranda WR, Haggerty BJ et al. Fate of the Fontan connection: Mechanisms of stenosis and management. *Congenit Heart Dis* 2019;14:571-581.
24. Alexi-Meskishvili V, Ovroutski S, Ewert P et al. Optimal conduit size for extracardiac Fontan operation. *Eur J Cardiothorac Surg* 2000;18:690-5.
25. Ascuitto RJ, Kydon DW, Ross-Ascuitto NT. Pressure loss from flow energy dissipation: relevance to Fontan-type modifications. *Pediatr Cardiol* 2001;22:110-5.
26. Ettinger E. Angiocardiographic measurement of the cardiac segment of the inferior vena cava in health and in cardiovascular disease. *Circulation* 1962;26:508-15.
27. Bossers SS, Cibis M, Gijzen FJ et al. Computational fluid dynamics in Fontan patients to evaluate power loss during simulated exercise. *Heart* 2014;100:696-701.
28. Restrepo M, Mirabella L, Tang E et al. Fontan pathway growth: a quantitative evaluation of lateral tunnel and extracardiac cavopulmonary connections using serial cardiac magnetic resonance. *Ann Thorac Surg* 2014;97:916-22.
29. Szafron JM, Ramachandra AB, Breuer CK, Marsden AL, Humphrey JD. Optimization of Tissue-Engineered Vascular Graft Design Using Computational Modeling. *Tissue Eng Part C Methods* 2019;25:561-570.
30. Gabbert DD, Hart C, Jerosch-Herold M et al. Heart beat but not respiration is the main driving force of the systemic venous return in the Fontan circulation. *Sci Rep* 2019;9:2034.
31. van der Woude SFS, Rijnberg FM, Hazekamp MG et al. The Influence of Respiration on Blood Flow in the Fontan Circulation: Insights for Imaging-Based Clinical Evaluation of the Total Cavopulmonary Connection. *Front Cardiovasc Med* 2021;8:683849.
32. Van De Bruaene A, La Gerche A, Claessen G et al. Sildenafil improves exercise hemodynamics in Fontan patients. *Circ Cardiovasc Imaging* 2014;7:265-73.

Supplementary materials



**Supplemental Figure 1.** Fifteen patients with 16,18 and 20mm conduits were matched based on average conduit flow rate along the respiratory cycle.

**Supplemental table 1.** MRI details of TCPC anatomic and velocity acquisitions

MRI details	2D transversal and sagittal stacks	2D realtime PC-MRI
Slice thickness (mm)	5, 2.5 overlap	6
Acquired in-plane spatial resolution (mm)	1.8x1.7	2.5 x 2.5
Reconstructed in-plane spatial resolution (mm)	0.9 x 0.9 mm	1.1 x 1.1
Acquired temporal resolution (ms)	-	63-67ms
Nr of samples	-	250
Respiratory compensation	navigator	-
Acceleration methods	SENSE factor 1.5	SENSE factor 3, EPI 11

All MRI examinations were performed on a 3T Philips MRI scanner (Ingenia, Philips Healthcare, Best, the Netherlands). mm; millimetre, PC-MRI; phase contrast magnetic resonance imaging, EPI; echo planar imaging

# CHAPTER 12

# 12

## Summary and future perspectives



## Introduction

Cardiology is flow<sup>1</sup>, and especially Fontan patients are characterized by profound alterations in flow physiology. Since no subpulmonary ventricle is present to sustain the pulmonary circulation, the interplay between pressure, flow and resistance in the Fontan pathway and pulmonary circulation is vulnerable with only a small margin for suboptimal hemodynamics. In analogy with Ohm's law, pulmonary blood flow in Fontan patients is determined by the relation between perfusion pressure, i.e. the difference between the central venous pressure and atrial pressure, and blood flow resistance, including the resistance in the total cavopulmonary connection (TCPC) and in the pulmonary vascular bed. Since central venous pressure is ideally as low as possible to avoid end-organ complications (i.e. liver fibrosis)<sup>2</sup>, perfusion pressure is only limited and therefore achievement of minimal resistance in the TCPC and pulmonary vascular bed becomes critical.

In this thesis, the main focus is placed on the evaluation of blood flow efficiency in the TCPC, the area between the inferior vena cava, liver veins, superior vena cava and both pulmonary arteries, using 4D flow MRI and patient-specific computational fluid dynamic models. This area is of particular interest as it is surgically created and therefore identification of adverse TCPC characteristics and associated flow inefficiencies can potentially lead to improvement of surgical approach or may be amenable to optimization with reintervention.

## Part I: Long term outcome after the Fontan procedure

In **chapter 2**, the long-term outcome of univentricular patients that underwent the Fontan operation in the Center for Congenital Heart Disease Amsterdam-Leiden between 1972-2016 is reported (median follow up 11.9, IQR 7.6-17.5 years). A total of 277 patients were included, of which 72 atriopulmonary connections/Björk modifications (right atrium to right ventricle conduit), 42 lateral tunnels and 163 extracardiac conduits. Operative mortality decreased over time to 1.2% in our most recent patientgroup with an extracardiac conduit. Longest survival estimates were 31% at 35 years for atriopulmonary connection/Björk patients, 87% at 20 years for lateral tunnel patients and 99% at 15 years for extracardiac conduit Fontan patients. It is now estimated that univentricular patients operated on today will have a 85% survival rate at 30 years after Fontan completion<sup>3</sup>, illustrating the tremendous improvement in long-term survival of Fontan patients. However, the majority of Fontan patients are faced with significant morbidity over time. In our cohort, freedom from Fontan related morbidity (Fontan failure, tachy- and bradyarrhythmia or thromboembolic/neurological events) was only

19% at 20 years in the APC/Björk group, 59% at 15 years in the lateral tunnel group and 77% at 15 years in the extracardiac conduit group. Importantly, a continuous attrition rate was present illustrating the long-term vulnerability of the Fontan circulation physiology. In particular the occurrence of tachyarrhythmias was associated with increased risk on Fontan failure (HR 2.6) and thromboembolic and/or neurological events (HR 3.6). Tachyarrhythmias can result in quick hemodynamic deterioration with increases in central venous pressure and is poorly tolerated.<sup>4</sup>

One of the early goals in single ventricle management is to obtain an unobstructed systemic outflow tract when present. In **chapter 3** long-term results of direct relief of systemic outflow tract obstruction in univentricular patients with unrestrictive pulmonary blood flow are reported, a challenging population with unknown optimal surgical strategy. In these patients, systemic blood flow needs to pass through a ventricular septal defect into a rudimentary subaortic outlet chamber and this path can become obstructed and can be directly (VSD  $\pm$  subaortic chamber enlargement) or indirectly relieved (e.g. by means of DKS or Norwood). In our experience with 23 children between 1989-2016, direct relief of subaortic stenosis resulted in a relative high reobstruction rate (30%) and patch (pseudo)aneurysm formation (50%), but low pacemaker implantation rate (4%) with the majority of patients reaching successful Fontan completion (86%). Therefore, this method could be a good and relatively simple method in selected patients for relief of subaortic stenosis, and especially in patients with neonatal subaortic stenosis it may defer neonatal Norwood/DKS to a later stage if necessary with potential better outcome.

While the outcome of the different surgical techniques reported in chapter 2 represent different surgical eras with improvement in medical care over time, avoiding a dilated right atrium that is prone to flow inefficiencies, thrombus formation and tachyarrhythmias will have significantly contributed to the improved outcome observed with contemporary Fontan techniques.<sup>5</sup> In order to further improve long-term outcome and freedom from important morbidity, a better understanding of the Fontan physiology and better characterization of the state of the Fontan circulation during follow-up are needed. The goal in part II and III of this thesis was to evaluate the role of TCPC blood flow efficiency using state-of-the-art flow imaging modalities in contemporary Fontan patients and investigate the relationship between adverse TCPC flow efficiency with outcome.

## Part II: In vivo blood flow dynamics of the Fontan circulation

In this part of the thesis, blood flow in the TCPC is prospectively evaluated using multiple different MRI sequences including 2D flow MRI, real-time 2D flow MRI and 4D flow MRI. Firstly, in **chapter 4**, the influence of the cardiac cycle and respiratory cycle on flow dynamics in the Fontan circulation is reviewed. Since no subpulmonary ventricle is present in Fontan patients, driving pressure for pulmonary blood flow is limited making TCPC blood flow dynamics strongly influenced by minor intrathoracic pressure changes during respiration. Respiration is thus often considered as an important “pump” for forward pulmonary blood flow, as negative intrathoracic pressures during inspiration can suck blood towards the lungs. Recent research, however, indicates that respiration indeed leads to flow pulsatility, but does not lead to a net increase in pulmonary blood flow.<sup>6,7</sup> On the other hand, blood flow pulsatility along the cardiac cycle is minimal but is the main driver for net forward flow. In other words, the increase in blood flow during inspiration is largely countered by a decrease in pulmonary blood flow during expiration and thereby does not significantly influence net forward flow. Most conventional phase-contrast MRI flow sequences, including 4D flow MRI, use ECG-gated data (i.e. focus on the cardiac cycle) and thereby fully miss the flow dynamics during respiration.

Since cardiac pulsatility is only minimal, a novel non ECG-gated 3D flow MRI sequence is developed and introduced in **chapter 5**. 3D flow MRI allows for the acquisition of cardiac-cycle averaged flow rates and flow derived parameters and measurements were compared with conventional ECG-gated 2D and 4D flow MRI. Main results show that 3D flow MRI showed good-excellent agreement for multiple different flow parameters (e.g. flow rates, pulmonary flow distribution, systemic to pulmonary collateral flow) with 2D and 4D flow MRI. Furthermore, almost identical three-dimensional flow patterns were captured using 3D flow MRI compared to 4D flow MRI. Importantly, a ten-fold reduction in scan time was achieved (1.6 minutes for 3D flow vs 16 minutes for 4D flow) while achieving a significantly higher image quality. Long scanning times are currently one of the drawbacks of 4D flow MRI and 3D flow MRI may therefore lead to a better widespread clinical applicability of three-dimensional flow imaging in Fontan patients.

With 4D flow MRI, three-dimensional blood flow patterns can not only be visualized, but also allows for quantification of flow related hemodynamic parameters that provides insight in areas with adverse flow efficiency. **Chapter 6** evaluates 4D flow MRI derived energetics in different segments of the TCPC. In order to systematically evaluate blood flow in the TCPC with 4D flow MRI in a cohort of Fontan patients, a semi-automatic segmental analysis approach is developed to allow for evaluation of flow energetics in standardized segments of the TCPC. The Fontan conduit and the left pulmonary artery were the segments with most adverse energetics, indicating potential room for



improvement with targeted intervention in particularly these segments. A significant inverse correlation was observed between conduit cross-sectional area (CSA) and viscous energy loss rate, indicating the importance of conduit size for flow efficiency. Vortical flow patterns were observed in the Fontan confluence and LPA in 25-46% of patients and was associated with significantly increased viscous energy loss rate in these segments. Interestingly, patients with vortical flow in the pulmonary artery had a significantly larger cross-sectional area compared to patients without vortical flow, indicating that pulmonary artery CSA alone does not fully characterize the hemodynamic resistance for pulmonary blood flow. This illustrates how relevant information can be acquired with 4D flow imaging in Fontan patients that are not captured with conventional diagnostic modalities.

The second paper in this chapter focused on the evaluation of blood flow patterns and related energetics in the area between the inferior vena cava and the junction with the extracardiac conduit. A high heterogeneity in geometry and related flow patterns was observed, including patients with a relatively straight connection with minimal flow disturbance and low viscous energy loss, patients with evident inferior vena cava to extracardiac conduit mismatch due to undersized conduits, and patients with distorted connections leading to adverse flow patterns associated with elevated energy losses.

The third paper in this chapter shows how evaluation of TCPC blood flow with 4D flow MRI can gain important insights that are not appreciated with conventional imaging modalities. This case shows how the presence of a remnant pulmonary trunk leads to adverse helical flow patterns which were associated with elevated viscous energy losses, more than a third of total energy loss in the TCPC. Importantly, this can simply be avoided by removing the pulmonary trunk at time of Glenn or Fontan operation.

In **chapter 7**, a case-report highlights that a 16mm Goretex conduit, implanted at 3 years of age, becomes undersized at adult age resulting in significant flow accelerations from the inferior vena cava towards the conduit. Secondly, flow penetration into the superior vena cava was observed leading to local vessel dilatation. The areas of flow acceleration were associated with increased viscous energy loss rate and wall shear stress, indicating reduced flow efficiency.

While 4D flow MRI evaluation of the Fontan pathway in previous chapters provided insights that conventionally implanted conduits can become undersized in older Fontan patients, the influence of respiration on flow dynamics can not be evaluated with 4D flow. Since respiration strongly influences flow pulsatility as shown in Chapter 4, evaluation of flow characteristics during both inspiration (phase with highest flow) and expiration (phase with lowest flow) is important to properly evaluate conduit

adequacy. 2D real-time flow MRI was used in the second paper in chapter 7 to assess blood flow dynamics in both inspiration and expiration in 50 patients with 16-20mm extracardiac conduits. In a cohort of on average 17 year old children (13 years after Fontan completion), significant blood flow accelerations were observed from the IVC towards the conduit, significantly increasing during inspiration but already present during expiration. Predominantly hepatic venous flow increased during inspiration, explaining most of the respiratory derived pulsatility observed in the Fontan conduit. The influence of respiration on blood flow in the inferior and superior vena cava was only minimal. The normalized IVC-conduit velocity mismatch factor during expiration and the entire respiratory cycle inversely correlated to peak VO<sub>2</sub>. Therefore, this study indicates that 16-20mm conduits have become relatively undersized for older Fontan patients raising concerns on the current surgical approach of implanting rigid 16-20mm Gore-Tex conduits in young children.

In **chapter 8**, the relationship between 4D flow MRI derived energetics in the TCPC and clinical outcome, e.g. exercise capacity and level of liver fibrosis, was assessed. Sixty-two patients were prospectively evaluated using a comprehensive imaging protocol including 4D flow MRI and multiparametric liver imaging, including iron-corrected T1 mapping as a marker of liver fibrosis/venous congestion. Patients underwent exercise bicycle testing on the same day of MRI or within 6 months from MRI to quantify maximal exercise capacity. Main results showed that kinetic energy and viscous energy loss rate in the entire TCPC positively correlated to liver cT1 values and negatively correlated with peak (predicted) VO<sub>2</sub>, while conventional parameters such as ventricular ejection fraction and cardiac index did not. Segmental analysis again indicated that the most adverse flow energetics were found in the Fontan tunnel and left pulmonary artery, reproducing the results found in the study presented in chapter 6. This study therefore showed that 4D flow MRI is a promising, non-invasive screening tool for (early) identification of patients with adverse TCPC flow efficiency that is associated with reduced exercise capacity and increased levels of liver fibrosis/venous congestion.

Thus, part II of this thesis illustrates the great heterogeneity in 4D flow MRI derived flow patterns and related flow energetics, with correlations between adverse energetics and outcome. While multiple areas with reduced flow efficiency are identified, the size of currently used extracardiac conduits are an important factor for suboptimal energetics. In part III of this thesis, the adequacy of the extracardiac conduit is evaluated in further detail in rest and during simulated exercise by determining blood flow dynamics using computational fluid dynamics (CFD).

## Part III: Computational fluid dynamics of the Fontan circulation

In **chapter 9**, the role of evaluating blood flow energetics in cardiovascular disease is reviewed, with a focus on the surgical and (patho)physiological insights that have been obtained by investigating fluid dynamics in the TCPC using CFD modelling. Important insights in the role of TCPC geometry on flow efficiency and hepatic flow distribution are covered. An optimal TCPC must distribute systemic venous blood flow to the lungs as efficient as possible, while ensuring balanced distribution of hepatic venous flow towards both lungs to avoid pulmonary arteriovenous malformations. In **chapter 10** the assumption of uniform distribution of hepatic venous flow inside the extracardiac conduit is tested by determining mixing characteristics between inferior vena cava and hepatic venous blood with patient-specific CFD models and to assess differences in hepatic flow distribution using indirect (tracking conduit flow) and direct (tracking hepatic venous flow) particle tracing techniques. Main results show that hepatic venous blood is not fully mixed with IVC blood flow leading to potential inaccuracies in quantification of hepatic blood flow distribution.

An important advantage of CFD modelling compared to in vivo 4D flow MRI imaging of blood flow in the TCPC is the ability to study the effect of different flow conditions. In **chapter 11**, the hemodynamic performance of 16-20mm extracardiac conduits was studied during both resting conditions and simulated exercise conditions using patient-specific CFD models in 51 patients to further investigate the hemodynamic relevance of the findings in chapter 7. From these models, viscous energy loss rate, pressure gradients in the TCPC and resistance were quantified and vessel cross-sectional area was determined. The functional conduit size was introduced to describe conduit adequacy (CSA normalized for flow). Main results showed that the functional cross-sectional area of the conduit was on average 35-73% smaller compared to the other vessels in the TCPC, indicating the relative undersizing of 16-20mm conduits in these patients. A moderate-strong inverse non-linear relationship was present between normalized conduit CSA and CFD hemodynamics in both rest and exercise. Pressure gradients of  $\geq 1.0$  at rest and  $\geq 3.0$  during simulated exercise were observed in patients with a conduit  $\leq 45 \text{ mm}^2/\text{L/min}$ . Furthermore, a negative correlation was present between normalized conduit CSA and the relative rest-to-exercise increase in hemodynamics, indicating strongest increases in patients with smallest conduits. Normalized TCPC resistance weakly correlated with (predicted) peak  $\text{VO}_2$ . Flow stagnation volume in the entire TCPC and in the conduit only was only minimal, also during expiration, furthermore illustrating that currently used conduit sizes become undersized. These results therefore highlight the importance of adequately sized conduits for optimal hemodynamics and

implicates that alternative surgical strategies should be explored to optimize adult TCPC hemodynamics.

Thus, CFD modelling in Fontan patients provides relevant insights in the functioning of the TCPC during different flow conditions. The modelling of exercise flow dynamics illustrated the difference in pressure gradients from rest to exercise. Measurement of relatively low pressure gradients in rest, as conventionally is done during catheterization, does not necessarily mean the presence of an unobstructed TCPC, as pressure gradients during exercise may significantly rise in a subset of patients.

## General conclusion

Long-term survival for univentricular heart patients with a Fontan circulation is nowadays excellent, with the majority of patients expecting to reach adulthood. Nevertheless, a general attrition rate remains present and the majority of Fontan patients will be faced with significant morbidity. However, no Fontan patient is the same and there is a need for better understanding which patients will do worse, ideally by (early) identification of adverse factors that can be optimized. In this thesis, the role of flow efficiency in the TCPC was thoroughly investigated leading to multiple new insights. A novel three-dimensional blood flow MR sequence (3D flow MRI) was developed and shown to be superior to conventional 2D and 4D flow MRI sequences which could potentially lead to a more widespread use. Adverse flow patterns associated with reduced flow efficiency were shown at multiple areas within the TCPC which were related to adverse energetics. Increased 4D flow MRI derived energetics in turn are associated with reduced exercise capacity and increased levels of liver fibrosis/venous congestion. A focus on conduit size adequacy demonstrated that the currently used 16-20mm extracardiac conduits become undersized for teenage and adolescent Fontan patients. Undersized conduits proved to be an important factor leading to reduced flow efficiency, especially during exercise conditions. Achievement of optimal blood flow in Fontan patients may ultimately lead to improved long-term outcome.

## Future perspectives

The ultimate solution for Fontan patients would be the incorporation of a subpulmonary power source allowing for the chronic reversal of the deleterious effects of the Fontan physiology. Until then, achieving an optimal Fontan circulation with minimal energy loss remains important to maximally utilize available energy with low CVP and maximal forward flow. To achieve this, the construction of the TCPC should be optimal and

blood flow efficiency should be regularly evaluated during follow-up in order to detect (subclinical) complications that can be optimized by intervention.

### **TCPC construction: the extracardiac conduit**

Implantation of rigid conduits in young children leads to suboptimal hemodynamics in adult Fontan patients, as shown in this thesis. The current “one-size-fits all” approach is suboptimal, and ideal conduit size will be patient-specific and predominantly depend on conduit flow rate. Future efforts should focus on developing different conduit materials that either allow for growth (e.g. tissue engineered conduits) or can be (serially) dilated to match the increasing flow rates during growth of the patient, and eventually replace the implantation of rigid Gore-Tex conduits.

The “ideal” conduit size based on CFD-derived hemodynamics studied in chapter 11 is expected to be around 125mm<sup>2</sup>/L/min conduit flow, indicating ideal conduit diameters of 22 (3 L/min conduit flow) to 28mm (5 L/min conduit flow) for older Fontan patients. Future studies using “virtual surgery”, in which the conduit can be enlarged on the computer and subsequently the effect on blood flow can be modelled, should verify if these sizes result in optimal hemodynamic performance.

### **Extracardiac conduit vs lateral tunnel**

While we included predominantly Fontan patients with an extracardiac Goretex conduit, blood flow in patients with a lateral Fontan tunnel showed profound differences. In contrast to relatively undersized conduits observed in the extracardiac patients, the limited amount of lateral tunnel patients scanned in our study often showed dilated lateral tunnels with low velocities (Figure 1). A head-to-head comparison of fluid dynamics between lateral tunnel and extracardiac conduits in older Fontan patients would be of interest for future study.

### **Flow imaging**

Incorporation of respiration in 4D flow MRI, so-called 5D flow MRI (three-directional velocity encoding, along both the cardiac and respiratory cycle), is being developed and could lead to more detailed evaluation of blood flow.<sup>8</sup> However, cardiac-cycle averaged 3D flow MRI, as introduced in this thesis, may offer sufficient information for clinicians to evaluate TCPC performance in a fraction of scanning time. The short scan time of 3D flow MRI provides room for further scan optimization, e.g. increased spatial resolution with multiple signal averages. Achievement of high resolution with relatively short scan times could lead to a more widespread application of 3D flow MRI in younger children with small vessels and is subject to future research. Furthermore, comparison of advanced energetic parameters between 4D and 3D flow would be of interest.

Also serial assessment of 4D or 3D flow in Fontan patients would provide additional insights how flow patterns, energetics and TCPC geometry develop over time and how these changes relate to changes in outcome (i.e. exercise capacity or liver fibrosis).

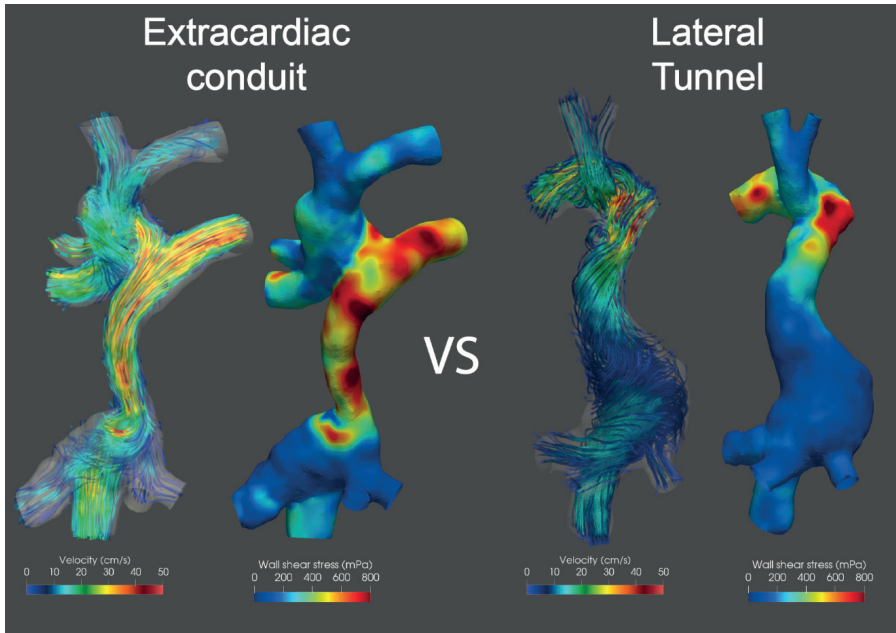


**Figure 1:** Streamlines of blood flow velocity and wall shear stress heatmaps are shown for a Fontan patient with an extracardiac conduit and a lateral tunnel. A relatively undersized Fontan conduit with high wall shear stress is often observed in patients with an extracardiac conduit, while patients with a lateral tunnel can have dilated Fontan tunnels with low velocities and low wall shear stresses.

### Atrio-ventricular valve regurgitation

Besides the role of inefficiencies at the TCPC, atrioventricular valve regurgitation may also importantly influence the hemodynamics of the Fontan circulation by raising atrial pressures. Elevated atrial pressures will lead to an elevated CVP or to reduced blood flow, thereby potentially leading to adverse outcome. Although the presence of important regurgitation is a well known risk factor for Fontan failure<sup>9</sup>, the long-term effects of mild-to-moderate regurgitation that is often observed during follow-up is not known and could be another area of relevant suboptimal hemodynamics that should be investigated and could potentially be optimized.

## References

1. Richter Y and Edelman ER. Cardiology is flow. *Circulation*. 2006;113:2679-82.
2. Emamaullee J, Zaidi AN, Schiano T, Kahn J, Valentino PL, Hofer RE, Taner T, Wald JW, Olthoff KM, Bucuvalas J and Fischer R. Fontan-Associated Liver Disease: Screening, Management, and Transplant Considerations. *Circulation*. 2020;142:591-604.
3. Rychik J, Atz AM, Celermajer DS, Deal BJ, Gatzoulis MA, Gewillig MH, Hsia TY, Hsu DT, Kovacs AH, McCrindle BW, Newburger JW, Pike NA, Rodefeld M, Rosenthal DN, Schumacher KR, Marino BS, Stout K, Veldtman G, Younoszai AK, d'Udekem Y, American Heart Association Council on Cardiovascular Disease in the Y, Council on C and Stroke N. Evaluation and Management of the Child and Adult With Fontan Circulation: A Scientific Statement From the American Heart Association. *Circulation*. 2019.
4. Ohuchi H, Miyazaki A, Watanabe T, Yamada O, Yagihara T and Echigo S. Hemodynamic deterioration during simulated supraventricular tachycardia in patients after the Fontan operation. *Int J Cardiol*. 2007;117:381-7.
5. de Leval MR, Kilner P, Gewillig M and Bull C. Total cavopulmonary connection: a logical alternative to atriopulmonary connection for complex Fontan operations. Experimental studies and early clinical experience. *J Thorac Cardiovasc Surg*. 1988;96:682-95.
6. Wei Z, Whitehead KK, Khiabani RH, Tree M, Tang E, Paridon SM, Fogel MA and Yoganathan AP. Respiratory Effects on Fontan Circulation During Rest and Exercise Using Real-Time Cardiac Magnetic Resonance Imaging. *Ann Thorac Surg*. 2016;101:1818-25.
7. Gabbert DD, Hart C, Jerosch-Herold M, Wegner P, Salehi Ravesh M, Voges I, Kristo I, Bulushi AAL, Scheewe J, Kheradvar A, Kramer HH and Rickers C. Heart beat but not respiration is the main driving force of the systemic venous return in the Fontan circulation. *Sci Rep*. 2019;9:2034.
8. Bastkowski R, Bindermann R, Brockmeier K, Weiss K, Maintz D and Giese D. Respiration Dependency of Caval Blood Flow in Patients with Fontan Circulation: Quantification Using 5D Flow MRI. *Radiology: Cardiothoracic Imaging*. 2019;1:e190005.
9. King G, Ayer J, Celermajer D, Zentner D, Justo R, Disney P, Zannino D and d'Udekem Y. Atrioventricular Valve Failure in Fontan and Palliation. *Journal of the American College of Cardiology*. 2019;73:810-822.





# CHAPTER 13

# 13

# Dutch summary

Nederlandse samenvatting



## Introductie

Cardiologie is flow<sup>1</sup>, en vooral patiënten met een Fontan circulatie worden gekenmerkt door belangrijke veranderingen in de bloedstroming. Omdat er geen subpulmonale ventrikel meer aanwezig is die de circulatie richting de longen verzorgd, is de wisselwerking tussen druk, bloedstroom en weerstand in het Fontan traject en de longcirculatie kwetsbaar, met slechts een kleine marge voor suboptimale hemodynamiek. In analogie met de wet van Ohm wordt de longcirculatie bij Fontan patiënten bepaald door de relatie tussen de perfusiedruk, dat wil zeggen het verschil tussen de centrale veneuze druk en de atriale druk, en de weerstand van de bloedstroom in de totale cavopulmonale connectie (TCPC) en in het longvaatbed. Omdat de centrale veneuze druk idealiter zo laag mogelijk is om eindorgaancomplicaties (e.g. leverfibrose)<sup>2</sup> te voorkomen, is de perfusiedruk slechts beperkt. Om deze reden is het bereiken van minimale weerstand in de TCPC en het longvaatbed van cruciaal belang om een adequate bloedstroming te bereiken.

In dit proefschrift wordt de belangrijkste focus gelegd op de evaluatie van de bloedstroming efficiëntie in de TCPC, het gebied tussen de onderste holle ader, leveraders, bovenste holle ader en beide longslagaders, met behulp van 4D flow MRI en patiënt-specifieke computer simulatie modellen (computational fluid dynamic modellen). De TCPC is een klinisch interessant gebied omdat het chirurgisch wordt aangelegd en daarom kan de identificatie van ongunstige TCPC kenmerken en de daarmee samenhangende inefficiënte bloedstroming potentieel leiden tot verbeteringen in de chirurgische techniek. Tevens kan de TCPC mogelijk geoptimaliseerd worden middels (cathether) reïnterventie.

## Deel I: Langetermijn resultaat na de Fontan procedure

In **hoofdstuk 2** wordt de lange termijn uitkomst gerapporteerd van patiënten met een eenkamerhart die de Fontan operatie ondergingen in het Centrum voor Congenitale Hartziekten Amsterdam-Leiden (CAHAL) tussen 1972-2016 (mediane follow-up 11,9 jaar, IQR 7,6-17,5 jaar). In totaal werden 277 patiënten geïnccludeerd, waarvan 72 atriopulmonale verbindingen (APC)/Björk-modificaties (rechteratrium naar rechterventrikel conduit), 42 laterale tunnels en 163 extracardiale conduits. De operatieve mortaliteit daalde in de loop van de tijd tot 1,2% bij onze meest recente patiëntengroep met een extracardiale conduit. De lange termijn overleving was 31% na 35 jaar voor patiënten met een atriopulmonale connectie/Björk, 87% na 20 jaar voor patiënten met een laterale tunnel en 99% na 15 jaar voor Fontan patiënten met een extracardiale conduit. Er wordt nu geschat dat 85% van de patiënten met een

eenkamerhart die nu geopereerd wordt nog in leven zal zijn 30 jaar na de Fontan operatie, wat de enorme verbetering in de lange termijn overleving van Fontan patiënten illustreert<sup>3</sup>. De meerderheid van de Fontan patiënten wordt echter in de loop van de tijd geconfronteerd met belangrijke complicaties. In ons cohort was de afwezigheid van Fontan-gerelateerde morbiditeit (Fontan-falen, tachy- en bradyaritmie of trombo-embolische/neurologische complicaties) slechts 19% op 20-jarige leeftijd in de APC/Björk-groep, 59% op 15-jarige leeftijd in de laterale tunnelgroep en 77% op 15-jarige leeftijd in de extracardiale conduit groep. Met name het optreden van tachyaritmieën ging gepaard met een verhoogd risico op Fontan-falen (hazard ratio 2,6) en trombo-embolische en/of neurologische voorvallen (hazard ratio 3,6). Tachyaritmieën kunnen resulteren in een snelle hemodynamische verslechtering met toename van de centrale veneuze druk en worden in deze patiëntengroep slecht verdragen.<sup>4</sup>

Het verkrijgen van een ongeobstrueerde ventriculaire uitstroombaan, indien een obstructie aanwezig is, is een belangrijk doel in het management van patiënten met een eenkamerhart. In **hoofdstuk 3** worden de lange termijn resultaten gerapporteerd van directe opheffing van ventriculaire uitstroombaan obstructie. Bij deze patiënten moet het bloed door een ventriculair septumdefect (VSD) naar een rudimentaire subaortaal ventrikel stromen en dit pad kan obstructief worden. Dit betreft een zeldzame en lastig te managen patiëntengroep met een onbekende optimale chirurgische strategie. Deze obstructie kan direct (VSD vergroten ± vergroten van het subaortale ventrikel) of indirect worden opgeheven (e.g. Damus-Kaye-Stansel (DKS) of Norwood). In onze ervaring met 23 kinderen tussen 1989 en 2016 resulteerde directe verlichting van de subaortale obstructie in een relatief hoog percentage reobstructie (30%) en vorming van (pseudo) aneurysma's ter plaatse van het geaugmenteerde ventrikel (50%), maar was er een laag risico op een atrioventriculair block waarvoor pacemaker implantatie noodzakelijk was (4%). Tevens onderging de meerderheid van de patiënten een succesvolle Fontan operatie (86%). Deze methode zou derhalve bij geselecteerde patiënten een goede en relatief eenvoudige methode kunnen zijn voor het opheffen van de subaortale obstructie, en vooral bij patiënten met neonatale subaortale obstructie kan het een neonatale Norwood/DKS, indien noodzakelijk, uitstellen naar een later stadium met mogelijk betere resultaten.

Hoewel de lange termijn uitkomsten van de verschillende chirurgische technieken die in hoofdstuk 2 worden beschreven ook verschillende chirurgische tijdperken vertegenwoordigen waarin de medische zorg in de loop der tijd is verbeterd, zal het vermijden van een verwijd rechter atrium en daaraan gerelateerde inefficiënte bloedstroming, thrombusvorming en tachyaritmieën aanzienlijk hebben bijgedragen aan de verbeterde uitkomst van hedendaagse Fontan patiënten ten opzichte van de patiënten met een atriopulmonale verbinding.<sup>5</sup> Om de lange termijn uitkomsten

verder te verbeteren is een beter begrip van de Fontan fysiologie noodzakelijk en is het belangrijk de hemodynamische staat van de Fontan circulatie gedurende follow-up goed in kaart te brengen om potentiële afwijkingen vroegtijdig op te sporen. Het doel in **deel II en III** van dit proefschrift was om de rol van bloedstromingsefficiëntie in de TCPC te evalueren met behulp van geavanceerde flow-imaging technieken en om de relatie tussen de aanwezigheid van ongunstige, inefficiënte TCPC bloedstroompatronen en klinische uitkomsten te onderzoeken.

## Deel II: In vivo hemodynamiek in de Fontan circulatie

In dit deel van het proefschrift wordt de bloedstroming in de TCPC prospectief geëvalueerd met behulp van meerdere verschillende MRI sequenties, waaronder 2D flow MRI, real-time 2D flow MRI en 4D flow MRI. In **hoofdstuk 4** wordt de invloed van respectievelijk de hartcyclus en de ademhalingscyclus op de bloedstroming in de Fontan circulatie besproken. Omdat er bij Fontan patiënten geen subpulmonale ventrikel aanwezig is welke actief het bloed richting de longen pompt, is de perfusie druk voor de longcirculatie beperkt. Als gevolg hiervan wordt de pulmonale bloedstroming sterk beïnvloed door kleine intrathoracale drukveranderingen tijdens de ademhaling. De ademhaling wordt daarom vaak beschouwd als een belangrijke “pomp” om voorwaartse pulmonale bloedstroom te bewerkstelligen, waarbij de negatieve intrathoracale druk tijdens het inademen bloed richting de longen zuigt. Recent onderzoek laat echter zien dat ademhaling inderdaad leidt tot pulsatie van de bloedstroming richting de longen, maar niet leidt tot een netto toename van de bloedstroming naar de longen.<sup>6,7</sup> Daarentegen is de pulsatie van de bloedstroming gedurende de hartcyclus minimaal, maar wel de belangrijkste factor voor de netto hoeveelheid bloedstroom richting de longen. Met andere woorden, de toename van de bloedstroom tijdens inademing wordt grotendeels gecompenseerd door een afname van de bloedstroom tijdens de uitademing en heeft daardoor geen significante invloed op de absolute hoeveelheid bloed die richting de longen stroomt. De meeste conventionele MRI technieken om bloedstroming te meten, inclusief 4D flow MRI, meten de bloedstroming gedurende de hartcyclus en missen daardoor volledig de bloedstromingsdynamiek tijdens de ademhaling.

Vanwege de minimale pulsatiliteit in de TCPC gedurende de hartcyclus hebben we een nieuwe 3D flow MRI techniek ontwikkeld en geïntroduceerd in **hoofdstuk 5**. Met 3D flow MRI kunnen de gemiddelde bloedstroomsnelheden gedurende een hartcyclus verkregen worden. Meerdere van bloedstroom afgeleide hemodynamische parameters werden vergeleken met conventionele 2D- en 4D flow MRI. De belangrijkste resultaten laten zien dat 3D flow MRI een goede tot uitstekende correlatie toonde voor

meerdere verschillende parameters (e.g. bloedstroomsnelheden, systemische naar pulmonale collaterale flow, pulmonale bloedstroom verdeling) met conventionele 2D- en 4D flow MRI technieken. Bovendien werden vrijwel identieke driedimensionale stromingspatronen vastgelegd met behulp van 3D flow MRI vergeleken met 4D flow MRI. 3D flow MRI scans waren echter tienmaal zo snel (1,6 minuten voor 3D flow MRI versus 16 minuten voor 4D flow MRI), terwijl een aanzienlijk hogere beeldkwaliteit werd bereikt. Lange scantijden zijn momenteel een van de nadelen van 4D flow MRI en 3D flow MRI kan daarom leiden tot een betere klinische toepasbaarheid van driedimensionale beeldvorming van de bloedstroming bij Fontan patiënten.

Met 4D flow MRI kunnen driedimensionale bloedstroompatronen niet alleen worden gevisualiseerd, maar kunnen ook bloedstroom gerelateerde hemodynamische parameters worden gekwantificeerd, zoals de kinetische energie, viskeus energieverlies en vorticeit. Hiermee kunnen gebieden met een abnormale, ongunstige flow efficiëntie inzichtelijk gemaakt worden. In **Hoofdstuk 6** wordt gekeken naar van 4D flow MRI afgeleide hemodynamische parameters in verschillende segmenten van de TCPC. Om deze 4D flow MRI hemodynamische parameters in de TCPC systematisch te kunnen evalueren en vergelijken in een cohort Fontan patiënten is er een semi-automatische segmentele analyse methode ontwikkeld. Resultaten laten zien dat het Fontan conduit en de linker longslagader de TCPC segmenten waren met de meest ongunstige hemodynamische parameters en interventie gericht op deze segmenten kan dan ook potentieel voor verbeterde bloedstroom efficiëntie zorgen. Er werd een significante correlatie waargenomen tussen een kleiner dwarsdoorsnede oppervlak van het Fontan conduit en toegenomen energieverlies in de bloedstroming aldaar, wat het belang van een adequate maat conduit op bloedstroom efficiëntie onderstreept. Een vortex in de bloedstroming werd waargenomen in het centrale gedeelte van de TCPC en in de linker longslagader bij 25-46% van de patiënten en de aanwezigheid van een vortex ging gepaard met een verhoogd energieverlies in deze segmenten. Interessant is dat patiënten met een vortex in de longslagader een significant groter dwarsdoorsnede oppervlak hadden van deze longslagader vergeleken met patiënten zonder vortex. Dit geeft aan dat de dwarsdoorsnede oppervlakte van de longslagader alleen de hemodynamische weerstand voor de bloedstroming richting de longen niet volledig karakteriseert. Dit laat zien hoe relevante informatie kan worden verkregen met 4D flow MRI bij Fontan patiënten die niet kan worden verkregen met conventionele diagnostische modaliteiten.

Het tweede artikel in **hoofdstuk 6** focust zich op de evaluatie van bloedstroompatronen en gerelateerde hemodynamische parameters in het gebied tussen de onderste holle ader en de connectie met het extracardiale conduit. Er werd een grote heterogeniteit in geometrie en gerelateerde bloedstroompatronen waargenomen in dit gebied,

waaronder patiënten met een relatief rechte verbinding met minimale verstoring in de bloedstroming met lage energieverliezen. Bij een deel van de patiënten was er echter sprake van een duidelijke mismatch tussen de onderste holle ader en het extracardiale conduit als gevolg van een te klein conduit of was deze connectie vervormd, wat in beide gevallen resulteerde in ongunstige bloedstroompatronen met verhoogde energieverliezen.

Het derde artikel laat een voorbeeld zien waarin evaluatie van de bloedstroming in de TCPC met 4D flow MRI belangrijke inzichten kan opleveren die niet verkregen werden met conventionele beeldvorming. Dit case-report toont hoe de aanwezigheid van een overgebleven truncus pulmonalis leidt tot een tornado-achtige, spiraalvormige bloedstroming aldaar die gepaard gaat met een verhoogd energieverlies. Meer dan een derde van het totale energieverlies in de TCPC vindt plaats binnen deze gedilateerde truncus pulmonalis. Belangrijk is dat dit eenvoudig kan worden voorkomen door de truncus pulmonalis te verwijderen of te clippen tijdens de Glenn- of Fontan operatie.

In **hoofdstuk 7** wordt in een case-report aangetoond dat een 16mm Goretex conduit, geïmplantéerd op 3-jarige leeftijd, te klein is geworden op volwassen leeftijd aangezien er een belangrijke stroomversnelling vanuit de onderste holle ader richting het Fontan conduit plaats vindt. Ten tweede toont 4D flow MRI analyse aan dat deze bloedstroomversnelling vanuit het conduit tot in de bovenste holle ader reikte en resulteerde in verwijding van de bovenste holle ader ter plaatse. De gebieden met stroomversnelling waren geassocieerd met een verhoogde wall shear stress en viskeus energieverlies wijzend op een minder efficiënte bloedstroming.

Hoewel 4D flow MRI analyse van de Fontan circulatie in eerdere hoofdstukken het inzicht gaf dat conventioneel geïmplanteerde conduits te klein kunnen worden voor oudere Fontan patiënten, kan de invloed van ademhaling op de bloedstroming niet worden geëvalueerd met 4D flow MRI. Aangezien de ademhaling de pulsatiliteit van de bloedstroming sterk beïnvloedt, zoals beschreven in hoofdstuk 4, is de evaluatie van de bloedstroming tijdens zowel inademing (fase met de hoogste flow) als uitademing (fase met de laagste flow) belangrijk om de maat van het Fontan conduit te kunnen beoordelen. In het tweede artikel in **hoofdstuk 7** werd 2D real-time flow MRI gebruikt om de bloedstroming te beoordelen tijdens zowel in- als uitademing bij 50 patiënten met 16-20 mm extracardiale conduits. In een cohort van gemiddeld 17 jaar oude patiënten (13 jaar na voltooiing van de Fontan circulatie) werden wederom significante stroomversnellingen waargenomen vanuit de onderste holle ader naar het extracardiale conduit. Deze stroomversnellingen namen significant toe tijdens inademing maar waren ook al aanwezig tijdens uitademing. Hoofdzakelijk bloedstroming uit de leveraders nam toe tijdens inademing en verklaarde verreweg het grootste deel van



de door ademhaling veroorzaakte pulsatiliteit in het Fontan conduit. De invloed van ademhaling op de bloedstroom in de onderste en bovenste holle ader was minimaal. De factor in snelheidstoename van bloedstroming in het Fontan conduit ten opzichte van de onderste holle ader tijdens uitademing en tijdens de gehele ademhalingscyclus correleerde omgekeerd evenredig met de  $VO_2$  max. Deze studie laat derhalve zien dat 16-20mm conduits relatief te klein zijn geworden voor oudere Fontan patiënten, wat zorgen oproept over de huidige chirurgische strategie van het implanteren van rigide 16-20mm Goretex conduits bij jonge kinderen.

In **hoofdstuk 8** werd de relatie tussen van 4D flow MRI afgeleide hemodynamische parameters in de TCPC en klinische uitkomsten onderzocht, zoals het inspanningsvermogen en de mate van leverfibrose. Hiervoor werden 62 patiënten prospectief geëvalueerd middels o.a. 4D flow MRI en een MRI van de lever, inclusief T1-mapping van de lever als marker voor leverfibrose/veneuze stuwings. De inspanningscapaciteit werd getest middels een fietstest op de dag van de MRI of binnen 6 maanden rondom de MRI, waaruit onder andere de  $VO_2$  max werd bepaald als maat van maximale inspanningscapaciteit. De belangrijkste resultaten toonden aan dat kinetische energie en energieverlies in de bloedstroming in de TCPC positief gecorreleerd waren met lever T1-waarden (lever fibrose/veneuze congestie) en negatief gecorreleerd waren met de  $VO_2$  max, terwijl conventionele parameters zoals ventriculaire ejectiefractie en cardiale output geen correlaties lieten zien. Segmentale TCPC analyse gaf opnieuw aan dat de meest ongunstige bloedstroming werd gevonden in het Fontan conduit en de linkerlongslagader. Deze studie laat zien dat 4D flow MRI en afgeleide hemodynamische parameters dus veelbelovende, niet-invasieve screeningsmethode zijn voor (vroeg) identificatie van patiënten met een verminderde efficiëntie van bloedstroming in de TCPC, wat geassocieerd is met een verminderde inspanningscapaciteit en verhoogde mate van leverfibrose/veneuze congestie.

Deel II van dit proefschrift illustreert derhalve de grote heterogeniteit in bloedstroompatronen en bloedstroom gerelateerde hemodynamische parameters in de TCPC in een cohort Fontan patiënten, waarbij correlaties werden aangetoond tussen ongunstige bloedstroming en klinische uitkomsten. Terwijl meerdere gebieden met minder efficiënte flow werden geïdentificeerd, is de grootte van momenteel gebruikte extracardiale conduits een belangrijke factor voor suboptimale hemodynamiek. In deel III van dit proefschrift wordt de hemodynamiek van het extracardiale conduit in detail bestudeerd in rust en tijdens inspanning door gebruik te maken van geavanceerde computer simulatie modellen (computational fluid dynamic modelling).

## Deel III: Computational fluid dynamics in de Fontan circulatie

In **hoofdstuk 9** wordt de rol van het evalueren van bloedstroom energetica in cardiovasculaire aandoeningen besproken, met een focus op de chirurgische en (patho)fysiologische inzichten die zijn verkregen door de vloeistofdynamica in de TCPC te onderzoeken met behulp van Computational Fluid Dynamic (CFD) modellering. Belangrijke inzichten in de rol van de TCPC geometrie op een efficiënte bloedstroming en verdeling van lever veneus bloed richting beide longen worden behandeld. Een optimale TCPC moet immers niet alleen het systemische veneuze bloed zo efficiënt mogelijk naar de longen leiden, er dient tevens een evenwichtige verdeling van lever veneus bloed richting beide longen te zijn om pulmonale arterioveneuze malformaties te vermijden. In **hoofdstuk 10** wordt de aanname dat veneus bloed uit de lever uniform verdeeld is in de bloedstroom ter hoogte van het extracardiale conduit getest door de menging tussen bloed uit de onderste holle ader en uit de lever aders te bestuderen. Met behulp van patiënt-specifieke CFD modellen wordt gekeken naar verschillen in de verdeling van lever veneus bloed wanneer men bloed deeltjes loslaat en volgt vanuit het extracardiale conduit (indirecte methode), waarbij wordt uitgegaan van een uniforme verdeling van lever veneus bloed, of direct vanuit de lever aders (directe methode). De belangrijkste resultaten tonen aan dat bloed uit de lever aders niet volledig mengt met de bloedstroom afkomstig uit de onderste holle ader, wat kan leiden tot onnauwkeurigheden bij de kwantificering van de verdeling van lever veneus bloed naar de longen wanneer men deze op de conventionele indirecte methode berekent.

Een belangrijk voordeel van CFD modellering ten opzichte van in vivo 4D flow MRI beeldvorming van de bloedstroom in de TCPC is de mogelijkheid om het effect van verschillende fysiologische omstandigheden te bestuderen. In **hoofdstuk 11** werd de hemodynamiek van de TCPC met 16-20mm extracardiale conduits tijdens zowel rust als gesimuleerde inspanning bestudeerd met behulp van patiënt-specifieke CFD modellen in 51 patiënten. Middels deze CFD modellen werd onderzocht wat de hemodynamische relevantie van de bevindingen in hoofdstuk 7 zijn door de bloedstroming binnen de TCPC te simuleren en hieruit energieverlies, drukgradiënten en weerstand te bepalen. Tevens werd de dwarsdoorsnede oppervlakte van de verschillende vaten in de TCPC bepaald. De functionele conduit maat werd geïntroduceerd (dwarsdoorsnede oppervlakte van het conduit gecorrigeerd voor flow) als parameter om de geschiktheid van de maat van het geïmplanteerde conduit voor de hoeveelheid flow in een patiënt te beschrijven. De functionele conduit maat was gemiddeld 35-73% kleiner in vergelijking met de andere vaten in de TCPC, wat er wederom op wijst dat 16-20mm conduits relatief te klein zijn geworden voor Fontan patiënten van gemiddeld 16 jaar oud. Tevens was er een omgekeerde niet-lineaire correlatie aanwezig tussen de functionele conduit maat en de van CFD afgeleide hemodynamische parameters, zowel in rust als bij inspanning.

Drukgradiënten van  $\geq 1,0$  mmHg in rust en  $\geq 3,0$  mmHg tijdens gesimuleerde inspanning werden waargenomen bij patiënten met een conduit  $\leq 45$  mm<sup>2</sup>/L/min. Bovendien was er een negatieve correlatie tussen de functionele conduit maat en de relatieve toename van de hemodynamische parameters van rust naar inspanning, wat wijst op de sterkste toenames bij patiënten met de kleinste conduits. De weerstand in de TCPC toonde een zwakke correlatie met VO<sub>2</sub> max. Het gedeelte van de bloedstroming dat stagneert (snelheid  $< 1$  cm/s) in de gehele TCPC en in het conduit specifiek was minimaal, zelfs tijdens de uitademing. Dit illustreert dat de momenteel gebruikte conduit maten relatief te klein zijn geworden voor oudere Fontan patiënten. Deze studie benadrukt daarom het belang van een adequate maat van het Fontan conduit om optimale hemodynamica in de TCPC te bewerkstelligen. Alternatieve chirurgische strategieën moeten worden onderzocht om de hemodynamiek van de TCPC in volwassen Fontan patiënten te optimaliseren.

CFD modellering bij Fontan patiënten biedt derhalve relevante inzichten in het functioneren van de TCPC tijdens zowel rust als tijdens gesimuleerde inspanning. Het meten van relatief lage drukgradiënten in rust, zoals conventioneel wordt gedaan tijdens een hartkatheterisatie, betekent niet noodzakelijk dat er sprake is van een ongeobstrueerde TCPC, aangezien drukgradiënten tijdens inspanning significant kunnen stijgen bij een deel van de patiënten.

## Conclusie

De langetermijnoverleving voor patiënten met een univentriculair hart en een Fontan circulatie is tegenwoordig uitstekend, waarbij de meerderheid van de patiënten de volwassen leeftijd bereikt. Desondanks blijft het een fragiel evenwicht en zal de meerderheid van de Fontan patiënten op termijn te maken krijgen met complicaties. Geen enkele Fontan patiënt is echter hetzelfde en is er behoefte aan een beter begrip waarom sommige patiënten het op termijn slechter doen, idealiter door (vroeg) identificatie van nadelige factoren die kunnen worden geoptimaliseerd. In dit proefschrift werd de rol van efficiëntie van de bloedstroming in de TCPC in detail onderzocht, wat leidde tot meerdere nieuwe inzichten. Een nieuwe, snelle 3D flow MRI scan werd ontwikkeld en bleek superieur te zijn aan de conventionele 2D- en 4D flow MRI scans wat mogelijk kan leiden tot een snellere toepassing in de klinische praktijk. Abnormale flowpatronen werden aangetoond op meerdere plaatsen binnen de TCPC en waren geassocieerd met ongunstige van 4D flow MRI afgeleide hemodynamische parameters. Deze hemodynamische parameters waren geassocieerd met een verminderde inspanningscapaciteit en een verhoogde mate van leverfibrose/veneuze congestie. Een gedetailleerde analyse van de bloedstroming in de TCPC toonde aan dat

de momenteel gebruikte 16-20mm extracardiale conduits relatief te klein worden voor tiener- en jong volwassen Fontan patiënten. Te kleine conduits bleken een belangrijke factor te zijn voor minder efficiënte bloedstroming in de TCPC, vooral tijdens inspanning. Het bereiken van optimale, efficiënte bloedstroming in de TCPC zou uiteindelijk kunnen leiden tot verbeterde langetermijn uitkomsten in deze patiëntengroep.

## Toekomstperspectief

De ultieme oplossing voor Fontan patiënten zou het implanteren van een subpulmonale pomp zijn, maar klinische toepassing van een dergelijke oplossing is nog niet in zicht. Tot die tijd blijft het belangrijk om een optimale Fontan circulatie te bereiken en te behouden met minimaal energieverlies, zodat de beschikbare energie maximaal wordt benut. Om dit te bereiken is een optimale TCPC essentieel en is het belangrijk om het functioneren van de TCPC tijdens follow-up regelmatig te evalueren om (subklinische) complicaties op te sporen die potentieel kunnen worden geoptimaliseerd door interventie.

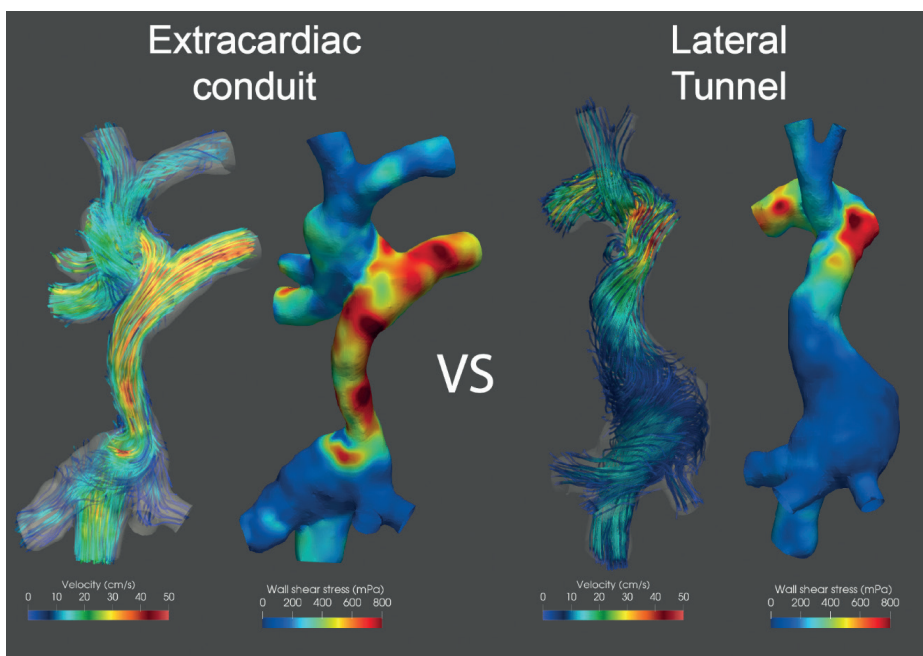
### Aanleggen van de TCPC: het extracardiale conduit

Implantatie van rigide conduits bij jonge kinderen leidt tot suboptimale hemodynamiek bij volwassen Fontan patiënten, zoals aangetoond in dit proefschrift. De huidige “one-size-fits-all” benadering is suboptimaal, en de ideale conduit maat zal patiënt-specifiek zijn en voornamelijk afhangen van de hoeveelheid bloed die door het conduit moet stromen. Toekomstig onderzoek moet gericht zijn op de ontwikkeling en toepassing van andere conduit materialen die ofwel kunnen meegroeien met de patient (bijv. tissue-engineered conduits) of die (serieel) gedilateerd kunnen worden. Uiteindelijk moeten in de toekomst conduits van dit soort materialen in plaats van rigide Goretex conduits geïmplant worden om te kleine conduits op volwassen leeftijd te voorkomen.

De “ideale” conduit maat, gebaseerd op van CFD afgeleide hemodynamische parameters zoals bestudeerd in hoofdstuk 11, wordt verwacht rond de  $125\text{mm}^2/\text{L}/\text{min}$  conduit flow. Dit betekent dat de ideale maat van het conduit voor volwassen patiënten ligt tussen 22mm (3 L/min flow in het conduit) en 28mm (5 L/min flow in het conduit). Middels “virtuele chirurgie”, waarin het conduit met de computer kan worden vergroot en vervolgens het effect op de bloedstroom kan worden gesimuleerd, moet geverifieerd worden of deze maten resulteren in optimale hemodynamiek.

## Extracardiale conduit versus laterale tunnel

Hoewel we voornamelijk Fontan patiënten met een extracardiale Goretex conduit hebben geïncubeerd, lieten patiënten met een laterale tunnel aanzienlijke verschillen in bloedstroming zien. In tegenstelling tot de relatief te kleine conduits die werden waargenomen bij patiënten met een extracardiaal conduit, vertoonden patiënten met een laterale tunnel vaak verwijde laterale tunnels met lage snelheden (Figuur 1). Een directe vergelijking van de hemodynamiek tussen laterale tunnels en extracardiale conduits bij oudere Fontan patiënten zou dan ook interessant zijn voor toekomstig onderzoek.



**Figuur 1:** Snelheid van de bloedstroming en wall shear stress heatmaps worden getoond in een Fontan patiënt met een extracardiale conduit (links) en een Fontan patiënt met een laterale tunnel (rechts). Een relatief te klein conduit wordt vaak gezien in patiënten met een extracardiale Fontan conduit, resulterend in toegenomen snelheid en wall shear stress ter plaatse van het conduit. Patiënten met een laterale tunnel hebben echter vaak een aneurysmatische Fontan tunnel met lage snelheden en lage wall shear stress.

## Beeldvorming van bloedstroming

De incorporatie van ademhaling in 4D flow MRI, ook wel 5D flow MRI (driedimensionale bloedstroomsnelheid langs de cardiale- en ademhalingscyclus), wordt ontwikkeld en zou kunnen leiden tot een nog gedetailleerdere evaluatie van de bloedstroom dynamiek.<sup>8</sup> Daarentegen kan 3D flow MRI welke over de cardiale cyclus gemiddelde bloedstroming meet, zoals geïntroduceerd in dit proefschrift, voldoende informatie

bieden voor klinici om de prestaties van de TCPC in een fractie van de scan tijd te beoordelen. De korte scantijd van 3D flow MRI biedt ruimte voor verdere optimalisatie van de scan zoals bijvoorbeeld het verbeteren van de resolutie. Een hogere resolutie kan van pas komen bij het gebruik van beeldvorming van bloedstroming in jonge kinderen met kleine bloedvaten. Bovendien zou een vergelijking van de geavanceerde energie parameters tussen 4D- en 3D flow MRI interessant zijn voor toekomstig onderzoek.

Ook seriële beoordeling van 4D- of 3D flow MRI bij Fontan patiënten kan inzicht bieden in hoe bloedstroompatronen, van bloedstroom afgeleide hemodynamische parameters en TCPC geometrie zich in de loop van de tijd ontwikkelen en hoe deze veranderingen verband houden met de langetermijnuitkomst (e.g. inspanningscapaciteit of leverfibrose).

### **Atrioventriculaire kleplekkage**

Naast de rol van bloedstromingsefficiëntie in de TCPC kan atrioventriculaire kleplekkage ook een belangrijke invloed hebben op de hemodynamiek van de Fontan circulatie door verhoging van de atriale druk. Verhoogde atriale drukken zullen leiden tot ofwel een verhoogde centraal veneuze druk danwel zorgen voor een afname van de bloedstroom met mogelijk negatieve gevolgen voor de lange termijn uitkomst. Hoewel de aanwezigheid van een significante atrioventriculaire kleplekkage een bekende risicofactor is voor Fontan falen<sup>9</sup>, is het langetermijneffect van milde tot matige lekkage, welke vaak wordt waargenomen tijdens follow-up, niet bekend. Atrioventriculaire kleplekkage zou derhalve een ander relevant gebied van suboptimale hemodynamiek binnen de Fontan circulatie kunnen zijn dat potentieel kan worden geoptimaliseerd.

## References

1. Richter Y and Edelman ER. Cardiology is flow. *Circulation*. 2006;113:2679-82.
2. Emamaullee J, Zaidi AN, Schiano T, Kahn J, Valentino PL, Hofer RE, Taner T, Wald JW, Olthoff KM, Bucuvalas J and Fischer R. Fontan-Associated Liver Disease: Screening, Management, and Transplant Considerations. *Circulation*. 2020;142:591-604.
3. Rychik J, Atz AM, Celermajer DS, Deal BJ, Gatzoulis MA, Gewillig MH, Hsia TY, Hsu DT, Kovacs AH, McCrindle BW, Newburger JW, Pike NA, Rodefeld M, Rosenthal DN, Schumacher KR, Marino BS, Stout K, Veldtman G, Younoszai AK, d'Udekem Y, American Heart Association Council on Cardiovascular Disease in the Y, Council on C and Stroke N. Evaluation and Management of the Child and Adult With Fontan Circulation: A Scientific Statement From the American Heart Association. *Circulation*. 2019.
4. Ohuchi H, Miyazaki A, Watanabe T, Yamada O, Yagihara T and Echigo S. Hemodynamic deterioration during simulated supraventricular tachycardia in patients after the Fontan operation. *Int J Cardiol*. 2007;117:381-7.
5. de Leval MR, Kilner P, Gewillig M and Bull C. Total cavopulmonary connection: a logical alternative to atriopulmonary connection for complex Fontan operations. Experimental studies and early clinical experience. *J Thorac Cardiovasc Surg*. 1988;96:682-95.
6. Wei Z, Whitehead KK, Khiabani RH, Tree M, Tang E, Paridon SM, Fogel MA and Yoganathan AP. Respiratory Effects on Fontan Circulation During Rest and Exercise Using Real-Time Cardiac Magnetic Resonance Imaging. *Ann Thorac Surg*. 2016;101:1818-25.
7. Gabbert DD, Hart C, Jerosch-Herold M, Wegner P, Salehi Ravesh M, Voges I, Kristo I, Bulushi AAL, Scheewe J, Kheradvar A, Kramer HH and Rickers C. Heart beat but not respiration is the main driving force of the systemic venous return in the Fontan circulation. *Sci Rep*. 2019;9:2034.
8. Bastkowski R, Bindermann R, Brockmeier K, Weiss K, Maintz D and Giese D. Respiration Dependency of Caval Blood Flow in Patients with Fontan Circulation: Quantification Using 5D Flow MRI. *Radiology: Cardiothoracic Imaging*. 2019;1:e190005.
9. King G, Ayer J, Celermajer D, Zentner D, Justo R, Disney P, Zannino D and d'Udekem Y. Atrioventricular Valve Failure in Fontan and Palliation. *Journal of the American College of Cardiology*. 2019;73:810-822.







# APPENDICES



## List of Publications

**Rijnberg FM**, Butler CR, Bieli C, Kumar S, Nouraei R, Asto J, et al. Aortopexy for the treatment of tracheobronchomalacia in 100 children: a 10-year single-centre experience. *European Journal of CardioThoracic Surgery*. 2018.

**Rijnberg FM**, Butler CR, Speggorin S, Fierens A, Wallis C, Nouraei R, et al. The influence of stents on microbial colonization of the airway in children after slide tracheoplasty: a 14-year single-center experience. *Pediatric Pulmonology*. 2015

Butler CR, Speggorin S, **Rijnberg FM**, Roebuck DJ, Muthialu N, Hewitt RJ, et al. Outcomes of slide tracheoplasty in 101 children: a 17-year single-center experience. *Journal of Thoracic and Cardiovascular Surgery*. 2014

**Rijnberg FM**, Butler Cr et al. Aortopexy for the treatment of tracheobronchomalacia in children. *Multimedia Manual Cardiothoracic Surgery*. 2020

**Rijnberg FM**, Hazekamp MG, Wentzel JJ, de Koning PJH, Westenberg JJM, Jongbloed MRM, et al. Energetics of Blood Flow in Cardiovascular Disease: Concept and Clinical Implications of Adverse Energetics in Patients With a Fontan Circulation. *Circulation*. 2018

**Rijnberg FM**, van Assen HC, Hazekamp MG, Roest AAW: Tornado-like flow in the Fontan circulation: insights from quantification and visualization of viscous energy loss rate using 4D flow MRI. *European Heart Journal*. 2019

**Rijnberg FM**, Sojak V, Blom NA, Hazekamp MG. Long-term outcome of direct relief of subaortic stenosis in single ventricle patients. *World journal of pediatric and congenital heart surgery*. 2018

**Rijnberg FM**, Blom NA, Sojak V, Bruggemans EF, Kuipers IM, Rammeloo LAJ, Jongbloed MRM, Bouma BJ, Hazekamp MG. 45-year experience with the Fontan procedure: tachyarrhythmia is an important predictor of late adverse outcome. *Interactive journal cardiovascular and Thoracic surgery*. 2019

**Rijnberg FM**, Elbaz MSM, Blom NA, Westenberg JW, Kroft LJ, Kamphuis V, Helbing WA, Hazekamp MG, Roest AAW. 4D flow MRI blood flow energetics of the inferior vena cava-to-extracardiac conduit junction in Fontan patients. *European Journal of Cardiothoracic Surgery*. 2019

**Rijnberg FM**, van Assen HC, Juffermans JF, Kroft LJM, van den Boogaard PJ, de Koning PJH, Hazekamp MG, van der Woude SFS, Warmerdam EG, Leiner T, Grotenhuis HB, Goeman JJ, Lamb HJ, Roest AAW, Westenberg JJM. Reduced scan time and superior image quality with 3D flow MRI compared to 4D flow MRI for hemodynamic evaluation of the Fontan pathway. *Scientific Reports*. 2021

**Rijnberg FM**, van der Woude SFS, van Assen HC, Juffermans JF, Hazekamp MG, Jongbloed MRM, Kenjeres S, Lamb HJ, Westenberg JJM, Wentzel JJ, Roest AAW. Non-uniform mixing of hepatic venous flow and inferior vena cava flow in the Fontan conduit. *Journal of the Royal Society Interface*. 2021

**Rijnberg FM**, Juffermans JF, Hazekamp MG, Helbing WA, Lamb HJ, Roest AAW, Westenberg JJM, van Assen HC. Segmental assessment of blood flow efficiency in the total cavopulmonary connection using 4D flow MRI: vortical flow is associated with increased viscous energy loss. *European Heart Journal open*. 2021.

van der Woude SFS, **Rijnberg FM (shared first author)**, Hazekamp MG, Jongbloed MRM, Kenjeres S, Lamb HJ, Westenberg JJM, Roest AAW, Wentzel JJ. The influence of respiration on blood flow in the Fontan circulation: insights for imaging-based clinical evaluation of the total cavopulmonary connection. *Frontiers Cardiovascular medicine, subsection pediatric cardiology*. 2021.

**Rijnberg FM**, van Assen HC, Hazekamp MG, Roest AAW, Westenberg JJM. Hemodynamic consequences of an undersized extracardiac conduit in an adult Fontan patient revealed by 4D flow MRI. *Circulation Cardiovascular imaging*. 2021.

**Rijnberg FM**, van der Woude SFS, Hazekamp MG, van den Boogaard PJ, Lamb HJ, Terol Espinosa de Los Monteros C, Kroft LJM, Kenjeres S, Karim T, Jongbloed MRM, Westenberg JJM, Wentzel JJ, Roest AAW. Extracardiac conduit adequacy along the respiratory cycle in adolescent Fontan patients. *European Journal of Cardiothoracic Surgery*. 2021.

**Rijnberg FM**, van t' Hul L, Hazekamp MG, van den Boogaard PJ, Juffermans JF, Lamb HJ, Terol Espinosa de Los Monteros C, Kroft LJM, Kenjeres S, le Cessie S, Jongbloed MRM, Westenberg JJM, Roest AAW, Wentzel JJ. Hemodynamic performance of 16-20mm extracardiac Goretex conduits in adolescent Fontan patients at rest and during simulated exercise. *European Journal of Cardiothoracic Surgery*. 2022

**Rijnberg FM**, Westenberg JJM, van Assen HC, Juffermans JF, Kroft LJM, van den Boogaard PJ, Terol Espinosa de los Monteros C, Warmerdam E, Leiner T, Grotenhuis HB, Jongbloed MRM, Hazekamp MG, Roest AAW, Lamb HJ. 4D flow MRI derived energetics

in the Fontan circulation correlate with exercise capacity and MR-derived liver fibrosis/congestion. *Journal of Cardiovascular Magnetic Resonance*. 2022

Arrigoni SC, IJsselhof R, Postmus D, Vonk JM, François K, Bové T, Hazekamp MG, **Rijnberg FM**, Meyns B, van Puyvelde J, Poncelet AJ, de Beco G, van de Woestijne PC, Bogers AJJC, Schoof PH, Ebels T. Long-term outcomes of atrioventricular septal defect and single ventricle: A multicenter study. *Journal of Thoracic and Cardiovascular Surgery*. 2021

Van den Eynde J, Bartelse S, **Rijnberg FM**, Kutty S, Jongbloed MRM, de Bruin C, Hazekamp MG, Le Cessie S, Roest AAW. Somatic growth in single ventricle patients: A systematic review and meta-analysis. *Acta Paediatrica*. 2023

Roos PR, **Rijnberg FM**, Westenberg JJM, Lamb HJ. Particle Tracing Based on 4D Flow Magnetic Resonance Imaging: A Systematic Review into Methods, Applications, and Current Developments. *Journal of Magnetic Resonance Imaging*. 2023

Hut T, Roest AAW, Gaillard D, Hazekamp M, van den Boogaard P, Lamb HJ, Kroft LJM, Jongbloed MRM, Westenberg JJM, Wentzel JJ, **Rijnberg FM (shared last author)**, Kenjeres S. Virtual surgery to predict optimized conduit size for adult fontan patients with 16mm conduits. *Interdisciplinary Cardiovascular and Thoracic Surgery*. 2023

Warmerdam EG, Westenberg JJM, Voskuil M, **Rijnberg FM**, Roest AAW, Lamb HJ, van Wijk B, Sieswerda GT, Doevendans PA, Ter Heide H, Krings GJ, Leiner T, Grotenhuis HB. Comparison of Four-Dimensional Flow MRI, Two-Dimensional Phase-Contrast MRI and Echocardiography in Transposition of the Great Arteries. *Pediatric Cardiology*. 2023

Van den Eynde J, Westenberg JJM, Hazekamp MG, Lamb HJ, Jongbloed MRM, Wentzel JJ, Kenjeres S, Dekkers IA, van de Bruaene A, **Rijnberg FM (shared last author)**, Roest AAW. Non-Invasive Cardiovascular Magnetic Resonance-Derived Fontan Hemodynamics Are Associated With Reduced Kidney Function But Not Albuminuria. Submitted

## **Grants and Awards**

**2019:** Personal Grant Dutch Heart Foundation (Dekkerbeurs)

**2019:** Best oral presentation Dutch association for Thoracic surgery

**2020:** Travel award Society of Cardiovascular Magnetic Resonance, 2020, Orlando

**2021:** Young Investigator Award Congenital European Association of CardioThoracic Surgery annual meeting 2021, Barcelona

**2021:** Best oral presentation 12<sup>th</sup> Rembrandt symposium

## Curriculum Vitae

Friso Matthijs Rijnberg was born on 30 September 1990 in Rotterdam, the Netherlands. After graduating secondary school (Stedelijk Gymnasium Arnhem) in 2008, he started to study medicine at the Leiden University in 2008. During his study he did a clinical internship at the Department of Otorhinolaryngology – Head and Neck surgery at the Groote Schuur Hospital, Cape Town, South Africa. From October 2011 to April 2012 he completed a research internship on the subject congenital long-segmental tracheal stenosis in children at the renowned Great Ormond Street Hospital in London, United Kingdom, under supervision of pediatric cardiothoracic surgeon Prof. dr. Martin Elliott. Due to this internship he became interested in cardiothoracic surgery and congenital heart disease in particular. He got in contact with prof. dr. Mark Hazekamp, pediatric cardiothoracic surgeon Leiden University Medical Center (LUMC), and the early foundations for this PhD about the Fontan circulation were made. He obtained his medical degree in December 2015. From March 2016 to July 2017 he worked as a resident at the department of Cardiothoracic Surgery at the LUMC. From July 2017 to September 2021 he worked as a PhD Candidate on the work presented in this thesis (supervision of prof. dr. M.G. Hazekamp, department of Cardiothoracic surgery, Dr. A.A.W. Roest, department of Pediatric Cardiology and Dr. ir. J.J.M. Westenberg, department of Radiology, LUMC), including the analysis of blood flow in the Fontan circulation using four-dimensional flow MRI (VELOCITY project, funded by Stichting Hartekind). In 2019 he received a personal Dekker grant by the Dutch Heart Foundation which allowed him to expand the research on the Fontan circulation with computational fluid dynamic modelling and virtual surgery under supervision of Prof. dr. S. Kenjeres, department of Chemical Engineering, TU Delft and Dr. ir. J.J. Wentzel, department of Cardiology, Biomechanical Engineering, Erasmus Medical Center, Rotterdam. In October 2021 he started his training in Cardiothoracic surgery at the LUMC.



## Dankwoord

Veel dank voor de vruchtbare samenwerking tussen de afdelingen (kinder)cardiologie, radiologie, cardiothoracale chirurgie en de engineering afdelingen in Delft en Rotterdam, het was een zeer inspirerend en leerzaam project. Grote dank aan alle betrokken medewerkers van de radiologie, zonder wie een “imaging” proefschrift onmogelijk zou zijn.

Ik dank alle patiënten, in het bijzonder alle kinderen en hun ouders, voor de bereidheid de 1.5 uur durende MRI-scans te trotseren. Alle betrokken collega's binnen het CAHAL, van de Holter/fietstest kamers, uit het UMC Utrecht, dank voor de fijne samenwerking. Alle vrijwilligers, familie en vrienden die 2 uur in de MRI-scanner hebben gelegen, jullie hart is groot.

Daarnaast dank ik een aantal mensen in het bijzonder:

Allereerst mijn promotor, prof. dr. M.G. Hazekamp, beste Mark, samen met een zak varkensorganen, tuinslangen en een compressor in je garage klussen om een idee te onderzoeken zal ik niet snel vergeten. Het samen filosoferen over problemen en mogelijke out-of-the-box oplossingen waardeer ik enorm.

Mijn co-promotor, dr. A.A.W. Roest, beste Arno, niet alleen je aanstekelijke enthousiasme en positiviteit, maar ook je wetenschappelijke kijk op problemen waren enorm waardevol. Met verwondering samen naar nieuwe bevindingen kijken en de daaropvolgende lange discussies over nieuwe concepten heeft mij altijd enthousiast gehouden.

Mijn co-promotor, dr. ir. J.J.M. Westenberg, beste Jos, de passie en toewijding waarmee jij je hebt ingezet voor dit MRI-onderzoek is ongelooflijk. Al balancerend op de grens van de MRI-scanner, en geregeld er net over, zijn we veel te weten gekomen over de Fontan circulatie, dank voor alles.

Pieter van den Boogaard, beste Pieter, dank voor al die dagen dat je als scanbuddy mij hebt geholpen. Jouw rust en kennis hebben ons door de vele MRI-crashes geloodst.

Dr. ir. H.C. van Assen, Joe Juffermans, beste Hans en Joe, dank voor de gezellige tijd en hulp bij ontwikkeling van de analyse tools, ik heb veel met jullie gelachen.

Prof. dr. H.J. Lamb, beste Hildo, dank voor alle mogelijkheden voor het uitvoeren van dit onderzoek binnen de radiologie en het CVIG.

Dr. L.J.M. Kroft, beste Lucia, dank voor de fijne samenwerking en je klinische input.

Dr. ir. J.J. Wentzel en prof. dr. ir. S. Kenjeres, beste Jolanda en Sasa, jullie kijk als engineer op de Fontan circulatie is waardevol en zeer leerzaam. Veel dank voor jullie enthousiasme en tijd voor het begeleiden van talloze getalenteerde studenten.

Séline, Luca, Duco, Tawab, Tjerry, Rosemary en alle andere studenten, dank voor jullie enthousiasme en inzet. Een simpele arts leren werken met MATLAB en CFD simulatie modellen is een prestatie op zich.

Ron Slagter, dank voor de vele prachtige figuren.

Prof. dr. N.A. Blom, beste Nico, dank voor de fijne samenwerking. Het uitzoeken van de lange-termijn follow-up was een hels karwei en je klinische input hierbij werd gewaardeerd.

Prof. dr. M.R.M. Jongbloed, beste Monique, dank voor je hulp bij het rekruteren van patiënten en je klinische input.

Mijn opleider, prof. dr. R.J.M. Klautz, beste Robert, dank voor het gestelde vertrouwen in mij. Het is een voorrecht om het vak cardiothoracale chirurgie in Leiden te mogen leren.

Prof. dr. J. Braun, beste Jerry, jouw vermogen om altijd kritisch en scherp te zijn en de gesprekken over hoe zaken fysiologisch in elkaar steken waardeer ik enorm. Wegkomen met een half verhaal is onmogelijk.

Alle stafleden van de afdeling Thoraxchirurgie, assistenten, PA's en overige collegae, dank voor de fijne samenwerking, het is een bijzondere werkomgeving en ik voel me bevoorrecht dit als werk te mogen doen.

Prof. dr. A.F. Cohen, beste Adam, op een aantal sleutelmomenten aan het begin van mijn carrière ben je er voor mij geweest. Je hebt mijn toekomstige carrière als cardiothoracaal chirurg mede vorm gegeven. Veel dank daarvoor.

Prof. dr. M.J. Elliott, my time at Great Ormond Street Hospital was fantastic and inspired me to pursue a career in cardiothoracic surgery and got me interested in congenital heart disease. I'm very grateful to you and the entire team at GOSH.

Lieve vrienden, dank voor de gewenste afleiding tijdens dit promotieonderzoek. Samen trainen voor een zware fietstocht in de Alpen was een hoogtepunt.

Lieve schoonzussen, beste zwagers, lieve Alexandra, beste Karel, lieve Marjo en Fer, dank voor jullie betrokkenheid.

Lieve Nynke, Dolf en Marnix, onze band is sterk. Dolf, ik ben trots dat je mijn paranimf bent.

Lieve pap en mam, aan jullie heb ik veel te danken. Jullie betekenen veel voor me.

Lieve Elise, ik heb veel bewondering voor je en ik ben je veel dank verschuldigd voor de afgelopen jaren. Een promotieonderzoek en het leven als thoraxchirurg in spé zijn vaak veeleisend, maar desondanks ben je er altijd, onvoorwaardelijk, voor mij en onze kinderen en steun je alle keuzes die dit leven met zich meebrengt. De oprechte trots en glundering waarmee je aangaf mijn paranimf te willen zijn doet me veel. Jij en de kinderen betekenen alles voor me.

Lieve Emilie en Hugo, jullie komst maakt alles zoveel mooier. Jullie lieve, ontwapenende persoonsjes zijn magisch.



